The Dissertation Committee for Di Zhu Certifies that this is the approved version of the following dissertation:

Simultaneous Phase-Stability/-Split Computation for Multiphase Oil-Displacement Simulation

Committee:

Ryosuke Okuno, Supervisor

Kishore Mohanty

Mojdeh Delshad

David DiCarlo

Huazhou Li

Simultaneous Phase-Stability/-Split Computation for Multiphase Oil-Displacement Simulation

by

Di Zhu

Dissertation

Presented to the Faculty of the Graduate School of

The University of Texas at Austin

in Partial Fulfillment

of the Requirements

for the Degree of

Doctor of Philosophy

The University of Texas at Austin

December 2017

Dedication

To my parents, Jianjun Zhu and Zhangfeng Sun,

To my husband, Zhenyu Guo,

for their endless love, support and encouragement.

Acknowledgements

It is impossible to complete this dissertation without the help from a number of people. First of all, I would like to express my sincerest gratitude to my supervisor, Dr. Ryosuke Okuno for his inspiration, encouragement, and guidance throughout my study at The University of Texas at Austin and the University of Alberta. His friendly character and professional supervision have made my study at the University of Texas at Austin fruitful and enjoyable. I would also like to thank my dissertation committee members, Dr. Kishore Mohanty, Dr. Mojdeh Delshad, Dr. David DiCarlo, and Dr. Huazhou Li, for taking time to review my dissertation and providing me with valuable feedback and comments.

I would like to thank my colleagues for their support in my studies and life at the University of Texas at Austin and the University of Alberta: Chandra Shekhar, Kwang Hoon Baek, Dr. Francisco J. Arguelles Vivas, Jianyi Gao, Kai Sheng, Dr. Arun Venkat Venkatramani, and Mingyuan Wang. I also would like to express my gratitude to the following friends for their friendship and help, which gave me a wonderful life with numerous good memories during my Ph.D. studies: Dr. Wenlong Jia, Zhe Liu, Mo Zhang, Ningyu Wang, Yu Leng, and Min Zhang.

Finally, thank you to my parents, Jianjun Zhu and Zhangfeng Sun, for their endless love, encouragement, and support. My special gratitude is to my husband Zhenyu Guo for his love, understanding and encouragement all the time in my life.

Simultaneous Phase-Stability/-Split Computation for Multiphase Oil-Displacement Simulation

Di Zhu, Ph.D.

The University of Texas at Austin, 2017

Supervisor: Ryosuke Okuno

Solvent injection is a widely used method for enhanced oil recovery. Phase behavior of reservoir-oil/injection-gas mixtures should be effectively used for successful implementation of solvent injection. Complex phase behavior involving three hydrocarbon phases has been observed for many solvent injection processes at temperatures typically below 120°F. Well-known examples are CO_2 injection for West Texas oils and enriched gas injection for Alaskan viscous oils, for which the multiphase behavior consisted of the oleic, solvent-rich liquid, and gaseous phases.

Such multiphase behavior makes it challenging to study details of solvent injection. Firstly, it is computationally difficult to robustly solve for multiphase behavior using an equation of state. Secondly, how the interplay between multiphase flow and multiphase behavior affects oil displacement is much more involved than the traditional gas injection problem with only two hydrocarbon phases. This research is concerned with two main technical challenges in multiphase behavior modeling for solvent injection: robust multiphase flash calculation, and quantification of the miscibility development through three-hydrocarbon-phase flow.

In the initial part of this dissertation, a novel algorithm is presented for multiphase isobaric isothermal flash. The formulation is derived from global minimization of the

Gibbs free energy using the tangent plane defined at an equilibrium phase composition at a specified temperature and pressure. The new algorithm solves for two groups of stationary points of the tangent-plane-distance (TPD) function: tangent and non-tangent stationary points of the TPD function. Equilibrium phases, at which the Gibbs free energy is tangent to the TPD function, are found as a subset of the solution.

Unlike the traditional flash algorithms, the new algorithm does not require finding false solutions for robust multiphase flash. The advantage of the new algorithm in terms of robustness is shown to be more pronounced for more complex phase behavior, for which multiple local minima of the TPD function are present. It can be robustly initialized even when no K value correlation is available for the fluid of interest; e.g., multiphase behavior involving a solvent-rich liquid phase.

The final part of this dissertation presents a straightforward application of a mass conservation equation to explain and quantify the local oil displacement efficiency in three-hydrocarbon-phase flow. Mass conservation dictates how components must partition into phases upon a multiphase transition (e.g., between two and three phases) in multiphase convective flow. Detailed analysis of multiphase compositional flow equations leads to the distance parameter that quantifies the level of the miscibility developed between a displaced phase and a displacing phase in the presence of other immiscible phases. This distance parameter becomes zero when multicontact miscibility is developed, for example, between the oleic and solvent-rich liquid phases in the presence of the gaseous phase in low-temperature CO_2 flooding.

However, the application of the distance parameter is complicated when a composition path is calculated by using the equation-of-state compositional formulation that takes into account volume change on mixing. In such an application, the mapping of the distance parameter from volume space to composition space was performed, which

made the calculated distance parameter less accurate near a displacement front where the solvent concentration rapidly changes.

In this research, the distance parameter is applied directly in volume space for a given composition path. This is a more direct and accurate way to validate the utility of the distance parameter to quantify the local displacement efficiency in three-phase flow. A composition path in three-phase oil displacement is obtained by numerically solving 1-D convective compositional flow equations with no volume change on mixing in this research. The new flash algorithm mentioned above is implemented in this in-house slim-tube simulator. In case studies based on experimental data, the distance parameter is shown to successfully quantify the local oil displacement efficiency in three-phase flow. It properly captures the effects of numerical dispersion and relative permeability on the development of multicontact miscibility. This is because the distance parameter is derived by a simple rearrangement of the weak form of a compositional flow equation.

Table of Contents

List of Tables

List of Figures

xviii

CHAPTER 1: Introduction

This chapter describes the types of problems to be addressed in this dissertation. The objectives of this research are then listed. An outline of the dissertation is given at last.

1.1 STATEMENT OF THE PROBLEM

Solvent injection is a widely used method for enhanced oil recovery (Orr 2007, Lake 2014). It has been successfully applied to a variety of oil reservoirs in Alaska (McGuire et al. 2001), Canada (Malik and Islam 2000), and West Texas (Stein et al. 1992, Tanner et al. 1992).

The main mechanism for oil recovery by solvent injection is the miscibility development caused by multiple contacts between the injected solvent and reservoir oil. The interaction of flow and multiphase behavior can be complicated in such a process. Multiple phases, such as solvent-rich liquid phase (L_2), oleic phase (L_1) and gaseous phase (V), have been observed and reported in the literature for oil displacements by CO_2 or enriched gas at low reservoir temperatures typically below 120°F. More complicated situations can occur when asphaltene-induced emulsion occurs in the presence of oil-field brine.

One important design parameter in gas injection is minimum miscibility pressure (MMP). Thermodynamic MMP was theoretically defined as the minimum displacement pressure at which complete miscibility along a composition path from the injection gas to the reservoir oil is developed in absence of dispersion (Okuno 2009). For the traditional oil displacement involving only two hydrocarbon phases (i.e., L_1 and V phases), MMP is the pressure at which any of the key tie lines becomes zero length for a given

composition path and reservoir temperature. At such an MMP, a homogeneous phase is formed through the interplay between flow and phase behavior at a given time and space in oil displacement. Therefore, the MMP so defined is called "thermodynamic MMP", which is independent of fractional flow.

One proposal was recently made by Li et al. (2015) for estimation of MMP for three-hydrocarbon-phase flow. Their method is an extension of the mixing-cell method originally developed for two-phase flow by Ahmadi and Johns (2011). In their methods, tie line lengths were tracked to quantify if a miscibility was achieved at any of the key tie lines (Ahmadi and Johns 2011, Li et al. 2015). However, one of the main assumptions used in Li et al. (2015) is that fluid flow is independent of relative permeabilities, searching for a thermodynamic MMP. Three-phase mobilities cannot be rigorously modeled in their method. No report has been published that shows the development of a complete miscibility (or a homogeneous phase) through three-phase flow.

Okuno and Xu (2014ab) investigated the efficiency of local oil displacement by solvent with three-phase flow. They derived the mass conservation equation for multiphase transitions in 1-D convective flow, which dictates how components must be redistributed upon a phase transition. Then, they developed a parameter that quantifies the displacement efficiency of a displaced phase by a displacing phase in the presence of other phases. The parameter was called the distance parameter, which tends to zero as multicontact miscibility between the displacing and displaced phases is approached. They showed the application of their distance parameter to simulation results for low-temperature gas floods using UTCOMP, an EOS-based multicomponent multiphase compositional reservoir simulator developed at the University of Texas at Austin. Because composition paths were obtained by 1D simulations with UTCOMP, they had to

convert the original distance parameter, which was based on volume, to the composition-based distance parameter. This conversion required finding the intersection between a tie line and a tie triangle in composition space. This mapping from volume to composition was considered to cause less accurate calculation of the distance parameter at the leading edge of a three-phase region, where the solvent concentration rapidly changed. Details of the derivation and the volume-composition mapping for their distance parameters will be presented in chapters 2 and 5 in this dissertation. In Chapter 5, a remedy will be presented to make the calculation of distance parameters more direct and reliable for quantification of the efficiency of local oil displacement in three-phase flow.

Note that the multicontact miscibility in this research is concerned with the one developed between a displaced phase and a displacing phase in 1-D oil displacement by solvent. This is in general different from the multicontact miscibility that has been studied in the context of thermodynamic MMP involving no fractional flow in its definition. Their meanings become identical only when one hydrocarbon phase is displaced by another hydrocarbon phase with no other phases (e.g., oil being displaced by miscible gas).

Robust solution of multiphase flash problems is important for finding a composition path through multiphase regions for solvent injection. Numerical simulation of solvent injection involves a large number of phase-stability/-split calculations for every grid block at each time step. Reliability and efficiency of the numerical flow simulation depend significantly on the algorithms used for phase equilibrium calculations. In the traditional flash algorithms, phase stability and phase split calculations are performed in sequence, where the phase stability calculation indicates whether phase splitting may reduce the total Gibbs free energy. If so, phase-

split calculation solves for intensive and extensive properties of the resulting equilibrium phases. Phase stability test is often difficult for more than two phases, since multiple local minima of the tangent-plane-distance (TPD) function exist. It is difficult to ensure location of all stationary points of the TPD function by use of the traditional algorithms. Phase split calculation for more than three phases is also problematic with the traditional algorithms. Achievement of the global minimum of the Gibb free energy (GFE) relies significantly on the initial estimates used; however, they are not always available from the current stability test algorithms. These are especially true for miscible solvent injection simulations, as phase equilibrium calculations are performed in near critical regions, at which false solution and/or non-convergence can often occur with the traditional algorithms. A new algorithm will be developed for robust multiphase flash in this dissertation.

1.2 RESEARCH OBJECTIVES

Understanding oil displacements involving multiple phases in solvent injection requires detailed knowledge of complex multiphase behaviors between reservoir oils and injection gas. Quantification of displacement efficiency can be determined thereafter. Development and implementation of robust and efficient algorithms for multiphase equilibrium calculations, and a straightforward but more fundamental approach to quantification of displacement efficiency will significantly improve our fundamental knowledge for solvent injection in which complex multiphase behavior is involved.

In this dissertation, a robust algorithm is presented for isobaric-isothermal (PT) phase equilibrium calculations with the unified formulation for phase-stability/-split calculations. It is also applied to the isobaric-isenthalpic (PH) specification, or isenthalpic flash. The new algorithm is implemented in an in-house compositional

reservoir simulator to demonstrate improved efficiency and robustness. Quantification of displacement efficiency in three-phase flow is examined by use of the distance parameters in volume space with the composition path obtained from the in-house compositional reservoir simulator.

The objectives of this research are as following:

- Develop a robust and efficient multiphase PT flash algorithm to simultaneously perform phase-stability/-split calculations, capable of handling an arbitrary number of phases;

- Implement the new simultaneous PT flash algorithm in a compositional simulator and further test the robustness and the efficiency of the flash algorithm;

- Validate the utility of the volume-based distance parameter to quantify displacement efficiency in three-phase oil displacements.

To achieve the first objective, a unified formulation is developed for simultaneous phase-stability/split calculation on the basis of the classical criterion of phase equilibrium (Baker et al. 1982). The main novelty lies in the unified usage of the tangent-plane-distance (TPD) function (Baker et al. 1982, Michelsen 1982a) for multiphase PT flash for an arbitrary number of iterative compositions. Flexibility of the new PT flash algorithm is enhanced in terms of the information regarding the GFE used during the iterative solutions by controlling the number of iterative compositions initialized. The new formulation is applied to isenthalpic flash by introducing an additional energy equation. The robustness of the developed algorithms will be extensively tested.

To achieve the second objective, a 1D convective-only flow simulator with no volume change of mixing is developed. The new multiphase PT flash algorithm is implemented in this flow simulator. This implementation is also important for further confirmation of the robustness and efficiency of the new PT flash algorithm.

5

To achieve the third objective, volumetric-based distance parameters are used to study oil displacement efficiency in three-phase flow with seven field cases. Displacement efficiency is quantified by defining two minimum distance conditions for three-phase flow.

1.3 OUTLINE OF THIS DISSERTATION

This dissertation consists of six chapters. This chapter (Chapter 1) provides a brief statement of the problems, an introduction to the objectives of this dissertation, and an outline of this dissertation.

Chapter 2 discusses the required basics for understanding of multiphase reservoir flow.   The first section introduces the low reservoir temperature oil displacements by CO_2.   The second part reviews the existing approaches to quantifying displacement efficiency in the literature.   The third part reviews the fundamental mass conservation equations for reservoir flow.   The fourth part gives a review on compositional simulations of oil displacements by CO_2.   The fifth section reviews the prior phase-stability/-split algorithms relevant to compositional reservoir simulation.

In chapter 3, a new algorithm is presented for multiphase PT flash for an arbitrary number of phases on the basis of the unified formulation developed for simultaneous phase-stability/split calculations.   The correct set of equations is solved with successive substitution for stationary points of the tangent plane distance defined at a reference phase composition.   Case studies are used to show that the new simultaneous PT flash algorithm finds more stable solutions with a lower Gibbs free energy for the complex cases tested, for which the conventional method only finds local minima.   The algorithm developed in this chapter is implemented in an in-house multiphase compositional

simulator to study the displacement efficiency in three-phase flow and further demonstration of its robustness and efficiency.

In Chapter 4, the formulation developed in chapter 3 is applied to multiphase isenthalpic flash. A new analysis is presented regarding a well-known computational difficulties (narrow-boiling behavior) by coupling energy and phase behavior equations through the temperature dependency of K values. Various cases are shown to demonstrate the robustness of the proposed algorithm.

In Chapter 5, the utility of distance parameters is presented for quantification of displacement efficiency for low temperature oil displacements by CO_2 where three hydrocarbon phases are present. An in-house 1D compositional simulator with the new simultaneous multiphase PT flash algorithm is used. Simulations are performed for seven reservoir oils.

Chapter 6 summarizes and concludes the major work conducted for this dissertation. Recommendations for future work related to this research are also presented.

CHAPTER 2: Background

This chapter describes the required basics for understanding multiphase reservoir flow. The first section introduces the low reservoir temperature oil displacements by CO_2. The second part reviews the existing approaches to quantify displacement efficiency. The third part reviews the conservation equations for reservoir flow. The fourth part gives a review on compositional simulations of oil displacements by CO_2. The fifth section reviews the prior phase-stability/-split algorithms.

2.1 LOW RESERVOIR TEMPERATURE OIL DISPLACEMENT BY CO_2

Mixtures of reservoir oil and injection gas, such as CO_2 and enriched gas, can exhibit complex phase behavior, when reservoir temperature is typically below 120ºF. This section provides a review of prior studies on complex phase behavior of mixtures of injection gas and reservoir oil and oil displacement by CO_2 involving such complex phase behavior.

Solvent injection has been widely used to improve oil recovery (Orr 2007, Lake et al. 2014). Mixtures of reservoir oil and injection gas have been studied in the literature by use of numerical simulations and experimental approaches, including slim-tube displacements and multiple-contact measurements (Shelton and Yarborough 1977, Metcalfe and Yarborough 1979, Gardner et al. 1981, Orr and Jessen 1984, Shu and Hartman 1988, Sharma et al. 1989, Turek et al. 1988, Hornbrook et al. 1991, Okuyiga 1992, Khan et al. 1992, Creek and Sheffield 1993, DeRuiter et al. 1994, Mohanty et al. 1995, Okuno 2009, Okuno and Xu 2014ab). Three-hydrocarbon-phase flow has also been observed for various reservoir oils at low reservoir temperature conditions (Varotsis et al. 1986, Tanner et al. 1992, McGuire et al. 2001, Malik and Islam 2000). This three-

hydrocarbon-phase flow includes the solvent-rich liquid (L_2) phase that coexists with the gaseous (V) phase and the oleic (L_1) phase. Such phase behavior has also been reported for simple binary mixtures (e.g., Rodrigues and Kohn 1967, Hottovy et al. 1981, Enick et al. 1985, Peters et al. 1993, Galindo and Blas 2002) and ternary mixtures (e.g., Horn and Kobayashi 1967, Llave et al. 1987).

A conventional way to study the multiphase behavior of reservoir oil and solvent is to use a pressure-composition (P-x) diagram. Three hydrocarbon phases are typically present within a small pressure range at high solvent concentrations in a P-x diagram at reservoir temperatures below 120ºF. Two liquid phases often occur at a higher pressure above the three-phase region. However, a P-x diagram is not sufficient to represent the entire pressure-temperature-composition (P-T-x) space. This is because a P-x diagram for reservoir oil/injection solvent only represents the phase behavior along the mixing line between the oil and solvent at a fixed temperature, which is only a small portion of the phase behavior that actually spans the entire P-T-x space (Okuno 2009).

In composition space, a three-phase region is bounded by a lower critical endpoint (LCEP) and an upper critical endpoint (UCEP) (Rowlinson and Freeman 1961, Davenport et al. 1966, Wagner et al. 1968, Enick et al. 1985, Peters 1994, Galindo and Blas 2002, Polishuk et al. 2004). Uzunov (1993) defined a CEP as a critical state where two of the three equilibrium phases merge in the presence of a third phase. **Figure 2.1** shows a schematic of a three-phase region bounded by CEP tie lines for a quaternary system at a fixed temperature and pressure. Four is the minimum number of components required to model three-phase behavior involving CEPs at a given temperature and pressure. The LCEP is the CEP where L_1 and L_2 phases merge in the presence of the V phase ($L_1 = L_2 + V$), and the UCEP is the CEP where V and L_2 phases merge in the presence of the L_1 phase ($V = L_2 + L_1$).

Okuno et al. (2011) explained the mechanism for high displacement efficiency as the result of the composition path approaching CEPs. As explained by Okuno et al. (2011), high displacement efficiency is possible because the L_2 phase serves as a buffer between the L_1 and V phases. Okuno and Xu (2014b) examined further the development of multi-contact miscibility in compositional simulation by introducing new distance parameters based on interphase mass transfer near CEPs.

Various cubic equation-of-state (EOS) were studied in the literature to see if a cubic EOS can be used to quantitatively predict three-phase behavior. For example, van Konynenburg (1968) and Scott and van Konynenburg (1970) studied the three-phase curves and critical loci of binary mixtures using the van der Waals EOS with the van der Waals mixing rule. Their results show that most types of fluid phase behavior can be qualitatively predicted by use of the van der Waals EOS. Various binary and ternary mixtures have also been studied by applying the Soave-Redlich-Kwong (SRK) EOS (Deiters and Schneider 1976, Deiter and Pegg 1989, Gregorowicz and de Loos 1996) and Peng-Robinson (PR) EOS (Gauter 1999, Gauter et al. 1999, Mushrif 2004, Yang 2006). However, only qualitatively accurate predictions of the three-phase behavior were given by use of these methods mentioned.

Adjustments of fluid properties (e.g., critical temperature T_C, critical pressure P_C, and acentric factor ω) and/or binary interaction parameters (BIPs) were then introduced to improve the accuracy of three-phase behavior prediction. For example, Larson et al. (1989), Khan (1992), and Creek and Sheffield (1993) showed that PR EOS is capable of modeling three-phase behavior for mixtures of reservoir oil and injection solvent after careful characterization of reservoir fluids. Kumar and Okuno (2016) proposed a reservoir fluid characterization method for the purpose of multiphase behavior prediction

for 90 reservoir fluids (48 gas condensates, 7 volatile oils, 29 other oils, 4 heavy oils, and 2 bitumens) with PR EOS.

2.2 DISPLACEMENT EFFICIENCY

Minimum miscibility pressure (MMP) is one of the important design parameters in gas injection. In thermodynamics, MMP is defined as the minimum displacement pressure at which complete miscibility along a composition path from the injection gas to the reservoir oil is developed in absence of dispersion. There are both experimental and computational approaches for MMP estimation.

2.2.1 Experimental Measurements

In laboratory, MMP can be estimated through slim-tube experiments, mixing-cell experiments, rising bubble/failing drop experiments, and vanishing interfacial tension experiments. These experiments are designed to represent the complex interplay between reservoir oil and injection gas.

2.2.1.1 Slim-Tube Experiments

Slim-tube experiments are widely used to estimate MMP in laboratory. Typically, the tube used has a large ratio of its length to its diameter. The length of the slim-tube is between 5 and 120 ft (Orr et al. 1982, Elsharkawy et al. 1992), and the diameter varies between 0.12 and 0.63 in, with 0.25 in as a typical diameter (Danesh 1998, Elsharkawy et al. 1992). Due to the large ratio of length to diameter of the tube, slim-tube experiments are considered as 1D oil displacement.

Multiple slim-tube experiments are to be performed before estimating MMP. One commonly used criterion to determine MMP is to plot oil recovery with respect to pressure when recovery is recorded after typically 1.2 pore volume of gas are injected (Yellig and Metcalfe 1980, Danesh 1998). Then, the break-over pressure in such a plot

is the estimated MMP. Other criteria are also used by different researchers. For example, Holm and Josendal (1974) defined MMP when 80% oil recovery is achieved at gas breakthrough; Jacobson (1972), Glaso (1990), and Hudgins et al. (1990) considered the MMP is achieved when the ultimate oil recovery is approximately 90% to 95%.

2.2.1.2 Mixing-Cell Experiments

Mixing-cell experiments, relying on the contacts between oil and injected gas, can accurately estimate MMP, if properly conducted. During each contact, oil and gas are mixed at a certain ratio in a pressure-volume-temperature (PVT) cell and brought to equilibrium. A PVT cell is used to conduct repeated contacts between oil and gas in a forward or a backward manner.

In a forward manner, after each contact, the equilibrium gas is retained while the equilibrium oil is replaced by fresh reservoir oil. That is, at each stage, the equilibrium gas from the previous stage contacts fresh oil. In a backward manner, equilibrium oil is retained and the gas is replaced with fresh injected gas. Multiple contacts are repeated until there is no further change in the composition of the phases. A series of experiments are performed at several pressures before MMP is visually determined (i.e., repeated contacts result in a single phase that can be seen from the window on PVT cell).

2.2.1.3 Rising Bubble/Falling Drop Experiments

Rising bubble experiments were firstly introduced by Christiansen and Haines (1987) to perform as an alternative to slim-tube experiments. The experiment set-up consists of an eight-inch-long high pressure transparent tube that is filled with oil and is kept at the experimental conditions. Then, gas is injected from the bottom of the tube with a needle, resulting in the formation of a bubble rising in the tube. The shape of the rising bubble is used to estimate if MMP is achieved (Christiansen and Haines 1987).

Falling drop experiments are modified rising bubble experiments (Zhou and Orr 1998). The principle of falling drop experiments is the same as the rising bubble experiments, except that a bubble of oil is introduced into a chamber filled with gas.

2.2.1.4 Vanishing Interfacial Tension Experiments

Vanishing interfacial tension experiments were proposed by Rao (1997). The experiment apparatus consists of a high pressure and high temperature cell filled with injection gas. A globule of oil is then dropped into the cell through a capillary tube. The interfacial tension between the oil droplet and the gas is determined through the analysis of the shape of the hanging oil droplet and the densities of the oil and gas.

Same procedure is repeated using different pressures by changing the amount of gas injected. A plot of interfacial tensions versus pressures is used to estimate MMP. Specifically, MMP is determined when the extrapolation of the plot reaches zero. Thus, this method works based on the measurements of the interfacial tension between the oil and injection gas at various pressures at a fixed temperature.

2.2.1.5 Summary of Experiments Methods

Experimental methods for MMP estimate are typically expensive, time-consuming, or depend significantly on the qualities of the experiments (Ahmadi and Johns 2011). Results of slim-tube experiments can be highly uncertain because of the insufficient data points (Walsh and Orr 1990, Johns et al. 2002) and dispersion. For three-phase displacement, the recovery curve can bend abruptly with pressure or gas enrichment (Okuno et al. 2011). Also, each experiment involves extensive procedures to restore the slim-tube before next experiment is performed. Elsharkawy et al. (1992) raised the concern that the asphaltene precipitation could block the slim-tube and/or increase required displacement pressure. Sometimes, deposited asphaltene can

completely plugs the tube and cause the failure of the test. In addition, the measured MMP by experiments is usually not unique because of the multiple criteria to determine MMP by different researchers (Yellig and Metcalfe 1987, Holm and Josendal 1974).

Mixing-cell methods were designed to measure MMP only if the displacement type is purely a vaporizing drive or a condensing drive. The methods cannot be used to estimate MMP for a combined vaporizing/condensing drive (Menzie and Nielsen 1963, Bryant and Monger 1988, Turek et al. 1988). Besides, the formation of a single phase is difficult to decide by observing through the PVT cell; different people may obtain different results when repeating the same procedure.

Rising bubble method is not reliable in MMP estimatation for a purely condensing drive and a combined vaporizing/condensing drive (Zhou and Orr 1998). This limitation primarily comes from the principle used. In a rising bubble experiment, gas contacts with oil when gas rises from the bottom of the tube. The resulting gas becomes richer as it approaches to the top of the tube, which mimics the forward contact of gas and oil in the reservoir. Therefore, rising bubble experiments is more likely to predict MMP for a vaporizing drive, if performed properly. Similarly, it is uncertain that if falling drop experiments can be applied to estimate MMP for a purely vaporizing drive or a combined vaporing/condensing drive (Zhou and Orr 1998).

The limitation of vanishing interfacial tension experiment is that the experiment can be only performed along the mixing line between the oil and gas. Orr and Jessen (2008) analyzed the estimated MMP for multi-component mixtures and concluded that the measured MMP through vanishing interfacial tension experiments can deviate from the analytical MMP significantly, depending on the location of the overall composition.

Experimental methods used to predict MMP are expensive in cost and in time. However, they provide useful data that can be used to verify the reliability of MMP obtained from computational methods as will be discussed below.

2.2.2 Computational Methods

There are currently three computational methods for MMP estimate; 1D simulation of slim-tube displacements, analytical methods by the method of characteristics (MOC), and multiple mixing-cell methods. Although computational methods are faster and more convenient than experimental measurements, the former ones significantly rely on the accuracy of fluid characterizations using an equation-of-state (EOS), especially for near critical region.

2.2.2.1 1D Simulation of Slim-Tube Displacements

1D slim-tube simulation mimics the flow in porous media that occurs in slim-tube experiments in a compositional simulator (Yellig and Metcalfe 1980). 1D flow equations are solved with tuned EOS parameters for the reservoir flow of oil and injection gas. Flow equations can be simplified by assuming incompressible flow, no volume change on mixing, and no effect of pressure on phase behavior (Dindoruk 1992).

As is used in slim tube measurements, oil recoveries at 1.2 pore volume of gas injected are recorded with various pressures. MMP is defined as the pressure at which 90% recovery is achieved. To obtain a reliable result, it is crucial that accurate representation of complex phase behaviors between reservoir oil and injection gas are utilized.

Stalkup (1987) and Johns et al. (2002) studied the effect of numerical dispersion on the accuracy of MMP prediction using fine-grid compositional simulations. Stalkup (1987) plotted oil recovery with respect to the reciprocal of the square root of grid block

number and extrapolated the oil recovery to zero dispersion. Johns et al. (2002) studied the effect of dispersion on minimum miscibility enrichment at various dispersion levels for different displacement mechanisms. Use of higher-order methods in 1D slim-tube simulations can reduce the effect of dispersion, rather than completely eliminating its effect (Mallison et al. 2005). One way to minimize the effect of dispersion on the accuracy of MMP prediction is to run the simulations for varying grid block numbers and then extrapolate to the oil recovery when the block size is infinitely large.

2.2.2.2 Analytical Method by MOC

Analytical solution of dispersion-free 1D convective flow equations are solved by MOC for obtaining the composition path in order to estimate MMP (Helfferich 1981, Dindoruk 1992, Johns 1992, Dumore et al. 1984, Orr 2007, Lake et al. 2014). Analytical solutions of 1D oil displacement by use of MOC are well studied for conventional two-phase (i.e., L_1 and V phases) to estimate the MMP (Orr 2007).

Helfferich (1981) generalized the theory of multiphase multicomponent displacements in porous media. Helfferich (1981) derived coherence condition that states all dependent variables at any given point in space and time have the same characteristic velocity, i.e., the oil and gas compositional mixture will break into several coherent waves that travel at different speeds in porous media.

Monroe et al. (1990) firstly extended the MOC solution to quaternary displacements. Their results showed that there exists a third key tie line in the displacement route, the crossover tie line. Later, Orr et al. (1993) and Johns et al. (1993) confirmed the existence of the crossover tie line for condensing/vaporizing drives. They also proposed a method to construct and find the key tie lines (the gas tie line, the oil tie line, and the crossover tie line) geometrically, assuming that consecutive key tie

16

lines were connected by a shock along non tie-line paths.   MMP is then defined as the pressure at which any of the three key tie lines' lengths become zero.

Johns et al. (1993) further demonstrated that it is the crossover tie line that controls the development of miscibility in condensing/vaporizing drives.   Johns and Orr (1996) extended the theory of Orr et al. (1993) and Johns et al. (1993) to multicomponent systems.

Analytical solutions for three-phase displacements in a water-alternating-gas process were proposed by LaForce and Johns (2005ab), and have been demonstrated by their coworkers (e.g., LaForce et al. 2008ab, LaForce and Orr 2008, 2009, LaForce 2012).   LaForce and Johns (2005) developed MOC solution for three-phase partial miscible flow in water/alcohol/oil systems.   LaForce et al. (2008ab) extended their previous work to four-component systems and confirmed that their MOC solutions match with experimental results.

They studied the analytical composition paths and development of miscibilities for three-phase systems with four components consisting of CO_2, water, and two hydrocarbons.   They showed that MCM can be developed not only at two-phase critical point, at which L_1 and V phases are critical, but also along the critical tie line, at which L_1 and V phases are critical in the presence of an aqueous (W) phase.   The latter case represents the CEP of type $L_1 = V + W$.   Results showed that the reservoir oil in the $L_1 + W$ region was displaced completely by CO_2 in the $V + W$ region through the CEP tie line. However, to the best of our knowledge, MOC solution for three-phase displacements with more than four components is not available (Li et al. 2015).

2.2.2.3 Mixing-Cell Methods

Mixing-cell method consists of a series of virtual PVT cells, in which phase equilibrium calculations are performed. The basic idea is to mix (numerically) gas and oil in recursive contacts, resulting in new equilibrium compositions.

The multiple mixing-cell method used to estimate MMP for two phases with any number of components was developed by Ahmadi and Johns (2011). The methods track tie lines that form in the cell contacts. MMP is determined when the first tie line in any cell becomes a critical tie line. However, MMP estimated from a mixing cell method is reliable only for good fluid characterizations because of the use of a cubic EOS.

Li et al. (2015) extended the method of Ahmadi and Johns (2011) to three phases. Their method relies on repeated contacts of neighboring cells and finds the pressure at which one of the tie lines in any cell becomes zero length. Li et al. (2015) assume that fluid movement from cell to cell is independent of phase labeling and three-phase relative permeabilities. Phases are ordered based on compositional distance between their compositions and the initial oil and injection gas compositions, and named as fast phase, slow phase, and intermediate phase if present. Zero tie line length is used to determine if miscibility is achieved.

2.2.2.4 Summary of Computational Methods

Calculation of MMP with an algorithm on the basis of MOC is fast and precise; however, it can be very inaccurate because MOC only solves for a selected number of tie lines in composition space (Ahmadi et al. 2011). Yuan and Johns (2005) showed that there exist multiple sets of intersecting tie lines. Orr and Jensen (1984) reported that two-phase regions can bifurcate into separate two-phase regions so that multiple critical points exist between the intersecting key tie lines. For such a case, the bifurcation causes the MOC method to fail in MMP estimation because the key tie lines no longer

control miscibility. In addition, no analytical solution is available for three- phase displacement with more than four components (Li et al. 2015).

Slim-tube simulation results can be affected by numerical dispersion (Stalkup 1987, Johns et al. 2002), which results in the loss of miscibility, and also the robustness of the phase behavior calculation algorithm used. Due to dispersion, the composition path solved from flow equations can pass the two-phase region. Use of higher-order methods can reduce, but not eliminate, the effect of dispersion (Mallison et al. 2005).

The main drawback of multiple mixing-cell method of Li et al. (2015) for MMP estimate for three phases lies in the assumption that the movement of fluids does not depend on three-phase relative peameabilities. Unlike conventional two phases, a third phase exists in the presence of two miscible phases when miscibility occurs for three phases. Hence, the effect of three-phase mobility on fluid flow should not be neglected when estimating miscibility conditions for three phases.

Despite the mixing-cell method of Li et al. (2015) for three-phase flow, Okuno and Xu (2014ab) investigated mass transfer on multiphase transition between two and three phases for three-hydrocarbon-phase flow on the basis of fundamental mass conservation. Two conditions for the multiphase transitions that yield high local displacement efficiency by three hydrocarbon phases were derived by Okuno and Xu (2014ab). In the next section, we will show the working equations and the derivations of their method.

2.3 FLOW EQUATIONS AND DISTANCE PARAMETERS

In this section, we firstly derive the 1D convective-only flow equations from general mass conservations equations given some assumptions. Then, we will derive

the two conditions developed by Okuno and Xu (2014ab) that were used to evaluate high local displacement efficiency for three hydrocarbon phases.

2.3.1 Conservation of Mass

The transport of a component i through a permeable medium is governed by mass conservation,

$$\frac{\partial}{\partial t} \sum_{j=1}^{N_P} \left(\phi x_{ij} \underline{\rho_j} S_j \right) + \nabla \cdot \sum_{j=1}^{N_P} x_{ij} \underline{\rho_j} \vec{u}_j - \nabla \cdot \sum_{j=1}^{N_P} \left(\phi \vec{\overline{K}}_{ij} \cdot \nabla \underline{\rho_j} x_{ij} \right) = 0, \qquad (2.1)$$

where i is component index, j is phase index, $i = 1, 2, ..., N_C$, ϕ is porosity, x_{ij} is the mole fraction of component i in phase j, $\underline{\rho_j}$ is the molar density of phase j, S_j is saturation of phase j, $\vec{u}_j$ is flux of phase j, $\vec{\overline{K}}_{ij}$ is the dispersion tensor for component i in phase j, N_C is number of components, and N_P is number of phases.

In equation 2.1, the first terms gives the rate of change of moles of component i, the second terms is the net rate of inflow of component i by convection, and the third terms describes the net rate of inflow of component i due to dispersion, in which diffusion and hydrodynamic dispersion are both included due to the same mathematical representations of the two mechanisms.

With the following assumptions:

- 1D convective flow with no gravity,
- constant temperature, negligible pressure change across the displacement length, and negligible capillary pressure,
- porosity is independent of time,
- no volume change of mixing,
- local equilibrium,
- no chemical reaction/absorption on the solid phase,

equation 2.1 is simplified to

$$\frac{\partial C_i}{\partial t_D} + \frac{\partial F_i}{\partial x_D} = 0 \ \text{ for i} = 1, 2, \ldots, (N_C - 1),$$ (2.2)

where t_D is the dimensionless time measured in pore volumes, x_D is the dimensionless distance from the injector, C_i is the overall volume fraction of component i, and F_i is the overall fractional flow of component i. In equation 2.2, C_i and F_i are given as

$$C_i = \sum_{j=1}^{N_P} S_j c_{ij} \ \text{ and}$$ (2.3)

$$F_i = \sum_{j=1}^{N_P} f_j c_{ij},$$ (2.4)

where f_j is the fractional flow of phase j, and c_{ij} is the volume fraction of component i in phase j. Equation 2.2 is a simplified continuity equation in the form of first-order hyperbolic partial differential equation (PDE).

2.3.2 Distance Parameters

Okuno and Xu (2014a) presented an analysis of mass conservation for multiphase transition in three-hydrocarbon-phase displacement. Ideal displacement occurs when L_1 phase is completely displaced by non-L_1 phase in the presence of another phase. The ideal condition can be applied to CO_2 water-alternating-gas (WAG) injection in which L_1 phase is completely displaced by V phase in the presence of W phase (LaForce and Orr 2008, 2009, LaForce and Jessen 2010, LaForce et al. 2008ab, LaForce 2012). It can also be applied to three-hydrocarbon-phase oil displacements as presented in Okuno and Xu (2014ab). They studied several oil displacements in which L_1 phase is completely displaced by L_2 phase in the presence of V phase. It is important to note that Okuno and Xu (2014ab) did not use MMP to represent the ideal condition in their papers, because there exists two phases even at the ideal displacement conditions.

Mass balance equations in weak form for 1D convection-only compositional flow equations (equation 2.2) are discretized for a multiphase transition between $N_P{}^U$ and $N_P{}^D$

21

phases, where N_P^U and N_P^D represent the number of phases at the upstream side and the downstream side, respectively. The discretized form is

$$\sum_{j=1}^{N_P^U} \gamma_j^U \underline{c}_j^U = \sum_{j=1}^{N_P^D} \gamma_j^D \underline{c}_j^D, \tag{2.5}$$

subject to $\sum_{j=1}^{N_P^U} \gamma_j^U = 1.0$ and $\sum_{j=1}^{N_P^D} \gamma_j^D = 1.0$.

In equation 2.5, $\gamma_j = (v_D S_j - f_j)/(v_D - 1)$ (2.6)

holds for both upstream and downstream sides, $v_D = \Delta x_D/\Delta t_D = (F_i^U - F_i^D)/(C_i^U - C_i^D)$ by use of one-point upstream weighting for the flux term, and $\underline{c}_j$ is a vector consisting of c_{ij} for $i = 1, 2, \ldots, N_C$ and $j = 1, 2, \ldots, N_P$.

They concluded that a multiphase transition between N_P^U and N_P^D phases occurs through an intersection between the extension of the two tie simplexes defined by $\underline{x}_j^U$ ($j = 1, 2, \ldots, N_P^U$) and $\underline{x}_j^D$ ($j = 1, 2, \ldots, N_P^D$), where $\underline{x}_j$ is a vector consisting of the compositions of equilibrium phase j. That is, the redistribution of components on a phase transition between N_P^U and N_P^D phases must occur through an intersection of the N_P^U-phase tie-simplex extension and the N_P^D-phase tie-simplex extension.

Two conditions were derived by Okuno and Xu (2014a) for the redistribution of components on multiphase transition corresponding to the constraints to be satisfied for the leading edge and the trailing edge of the three-hydrocarbon-phase region, respectively, as follows:

$$\delta^L = \left\| \gamma_{N_1}^U \underline{c}_{N_1}^U - \gamma_{N_1}^D \underline{c}_{N_1}^D \right\|_2 < \varepsilon, \tag{2.7}$$

$$\delta^T = \left\| \gamma_{L_1}^U \underline{c}_{L_1}^U - \gamma_{L_1}^D \underline{c}_{L_1}^D \right\|_2 < \varepsilon. \tag{2.8}$$

The two conditions can also be re-written by use of phase compositions as following:

$$\delta^L = \left\| \Gamma_{N_1}^U \underline{x}_{N_1}^U - \Gamma_{N_1}^D \underline{x}_{N_1}^D \right\|_2 < \varepsilon, \tag{2.9}$$

$$\delta^T = \left\| \Gamma_{L_1}^U \underline{x}_{L_1}^U - \Gamma_{L_1}^D \underline{x}_{L_1}^D \right\|_2 < \varepsilon. \tag{2.10}$$

In equations 2.7 to 2.10, the subscript L_1 represents the oleic phase, N_1 represents a non-oleic phase, the parameter Γ_j ($j = 1, 2, \ldots, N_P$) determines the relative location of the N_P-phase tie simplex and an intersection involved in the phase transition.

Okuno and Xu (2014a) showed that δ^L and δ^T defined in equations 2.9 and 2.10 can correctly identify the local displacement efficiency by three hydrocarbon phases. When the two conditions are satisfied on phase transition between two and three phases, two non-oleic phases can collectively achieve high displacement efficiency. Also, their results showed that δ^L and δ^T (equations 2.9 and 2.10) can be successfully used to explain the non-monotonic trend in oil recovery by three hydrocarbon phases for quaternary displacements and the West Sak oil displacements.

In Okuno and Xu (2014ab), calculations of δ^L and δ^T were on the basis of equations 2.9 and 2.10. The mapping of δ^L and δ^T from volume space to composition space was essential in their calculations due to the use of UTCOMP, an EOS compositional multiphase reservoir simulator on the basis of implicit-pressure/explicit-concentration formulation developed at the University of Texas at Austin, to obtain the composition path. Use of UTCOMP resulted in varying v_D used in the term γ of equations 2.6, because volume change of mixing is considered in UTCOMP formulation. However, in Okuno and Xu (2014ab), the transform of δ^L and δ^T from volume space to composition space was not given. In the following section, we will firstly derive the mapping from volume space to composition space and then explain the advantages of using volumetric-based distance parameters.

Definition of c_{ij}, volume fraction of component i in phase j, can be expressed as follows:

$$\frac{\text{volume of component i in phase j}}{\text{volume of phase j}}$$
$$= \frac{\text{mole of phase j}}{\text{volume of phase j}} \cdot \frac{\text{volume of component i in phase j}}{\text{mole of component i in phase j}} \cdot \frac{\text{mole of component i in phase j}}{\text{mole of phase j}}.$$

This gives
$$c_{ij} = \underline{\rho}_j \cdot \frac{1}{\underline{\rho}_i} \cdot x_{ij}, \tag{2.11}$$

where $\underline{\rho}_j$ is the molar density of phase j, $\underline{\rho}_i$ is the molar density of component i, x_{ij} is the mole fraction of component i in phase j,

We then define $\overline{\overline{D}} = \text{diag}(1/\underline{\rho}_1, 1/\underline{\rho}_2, \ldots, 1/\underline{\rho}_{N_C}) \in \mathbb{R}^{N_C \times N_C}, \tag{2.12}$

where $\overline{\overline{D}}$ is a diagonal matrix whose diagonal elements are $(1/\underline{\rho}_1, 1/\underline{\rho}_2, \ldots, 1/\underline{\rho}_{N_C})$.

Combination of equations 2.11 and 2.12, we have
$$\underline{c}_j = \underline{\rho}_j \cdot \overline{\overline{D}} \cdot \underline{x}_j, \tag{2.13}$$

where $\underline{c}_j$ is a vector consisting of c_{ij} for i = 1, 2, …, N_C and j = 1, 2, …, N_P, and $\underline{x}_j$ is a vector consisting of x_{ij} for i = 1, 2, …, N_C and j = 1, 2, …, N_P.

We define an intersection as follows:
$$\underline{c}_{int} = \sum_{j=1}^{N_P} \gamma_j \underline{c}_j. \tag{2.14}$$

Combination of equations 2.13 and 2.14 gives
$$\underline{c}_{int} = \underline{\rho}_{int} \cdot \overline{\overline{D}} \cdot \underline{x}_{int} = \sum_{j=1}^{N_P} \gamma_j \underline{\rho}_j \cdot \overline{\overline{D}} \cdot \underline{x}_j. \tag{2.15}$$

Re-arrangement of equation 2.15 yields
$$\overline{\overline{D}} \left(\underline{\rho}_{int} \underline{x}_{int} - \sum_{j=1}^{N_P} \gamma_j \underline{\rho}_j \underline{x}_j \right) = 0. \tag{2.16}$$

Since $\overline{\overline{D}} \neq 0$, equations 2.16 is equivalent to
$$\underline{\rho}_{int} \underline{x}_{int} - \sum_{j=1}^{N_P} \gamma_j \underline{\rho}_j \underline{x}_j = 0. \tag{2.17}$$

Similarly, from molar balance, we define
$$\underline{x}_{int} = \sum_{j=1}^{N_P} \Gamma_j \underline{x}_j, \tag{2.18}$$

where Γ_j for j = 1, 2, …, N_P is a parameter to determine the relative location of the tie simplex and an intersection involved in the phase transition, and $\sum_{j=1}^{N_P} \Gamma_j = 1.0$.

Combination of equations 2.17 and 2.18 yields
$$\left(\sum_{j=1}^{N_P} \gamma_j \underline{\rho}_j \underline{x}_j \right) / \underline{\rho}_{int} = \underline{x}_{int} = \sum_{j=1}^{N_P} \Gamma_j \underline{x}_j, \tag{2.19}$$

resulting in $\Gamma_j = \left(\gamma_j \underline{\rho}_j \right) / \left(\sum_{j=1}^{N_P} \gamma_j \underline{\rho}_j \right). \tag{2.20}$

24

Hence, the volume based distance parameters defined in equations 2.7 and 2.8 can be transformed into composition based distance parameters defined in equations 2.9 and 2.10.

Direct use of volumetric information from the solutions of equations 2.2 to calculate δ^L and δ^T defined in equations 2.7 and 2.8 avoids the mapping from volume space to composition space as discussed above. Hence, the construction of an intersection between the downstream two-phase tie line and upstream three-phase tie triangle is not necessary. When compositions change drastically at the phase transition, the intersection constructed by use of compositional information can be significantly affected due to the small angle between the tie line and tie triangle. This is especially true when calculation conditions are near miscibility. Hence, in this dissertation, we only calculate distance parameters by use of equations 2.7 and 2.8 on the basis of volumetric information. This is a more direct validation of the utility of the distance parameters to quantify displacement efficiency in three-phase flow, although accuracy of the resulting composition path is lost due to the ideal mixing assumption used in the formulation.

2.4 EOS COMPOSITIONAL SIMULATIONS

Various researchers have performed numerical simulations on the studies of sweep efficiency for gas injection (e.g., Mohanty et al. 1995, Guler et al. 2001, Li et al. 2003, Wang et al. 2003). Chang (1990) developed a four-phase flow ($L_1 + V + L_2 + W$) simulator, UTCOMP, with three-hydrocarbon-phase flash. Chang (1990) used UTCOMP to study various reservoir flow patterns in CO_2 flooding, including viscous fingering, channeling, gravity override, and dispersive flow, with a wide range of endpoint mobility ratio, gravity number, effective aspect ratio, Péclet number, and

Dykstra-Parsons coefficients.   UTCOMP was later applied to study 1D and two-dimensional (2D) simulations of CO_2 injection for four oil samples from West Texas (Khan et al. 1992).

Tchelepi and Orr (1994) studied the effect of channeling and gravity override on the displacement efficiency.   They concluded that gravity segregation is much more effective in three dimensional (3D) than in 2D simulations in both homogeneous and heterogeneous porous media.   Whether flow is 2D or 3D, the presence of heterogeneity lowers the range of viscous/gravity ratio over which the transition from gravity- to fingering-dominated flow occurs.

Guler et al. (2001) studied the presence of multiple liquid phases in multi-dimensional simulations with Alaskan heavy oil.   Their results showed that gravity and dispersion affect the compositional propagation in multi-dimensional multiphase flow, causing the less obvious coexistence of multiple liquid phases.

Nghiem and Li (1986) presented a three-phase ($L_1 + V + L_2$) flow simulator to study 1D slim tube displacements by CO_2 with a 15-component EOS fluid model.   They concluded that the high displacement efficiency results from the near miscibility between the L_1 phase and L_2 phase in the two-liquid-phase region, not in the three-phase region. It is likely because of the low number of grid blocks used in the simulations.

Godbole et al. (1995) used an in-house simulator to model three hydrocarbon phases for the Kuparuk miscible flood.   Wang et al. (2003) used a compositional table-look-up approach to model three hydrocarbon phases and applied four-phase-flow simulations to a sector model.   Mohanty et al. (1995) confirmed the existence of three-hydrocarbon phases in a 1D compositional simulator using UTCOMP.

Okuno et al. (2011) studied the displacement efficiency for low temperature CO_2 flooding using UTCOMP.   They concluded that high displacement efficiency occurs

when the composition path traverses near the upper critical endpoint (UCEP, $L_1 + L_2 = V$), and the lower critical endpoint (LCEP, $L_1 = L_2 + V$). At the leading edge of three-phase region, L_2 phase extracts the reservoir oil due to the near-LCEP behavior. Then, at the trailing edge, L_2 phase efficiently merge into V phase due to the near-UCEP behavior.

Okuno and Xu (2014a) investigated the local displacement efficiency of the three-hydrocarbon-phase oil displacement and concluded that high displacement efficiency occurs as the consequence of the balance between the local displacement efficiency and the propagation rate of the three hydrocarbon phases. Local displacement efficiency depends significantly on how components are redistributed through multiphase transitions between two and three phases.

In three-hydrocarbon-phase simulations, it is common to use approximate three-phase relative permeability models that usually do not fit the experimental data well (Delshad et al. 1989). One challenge in three hydrocarbon-phase modelling is to define the threshold phase mass density to distinguish the solvent-rich liquid phase and vapor phase (Perschke et al. 1989, Xu and Okuno 2015). It is crucial since the relative permeability models depend on the phase identifies. When phases are mislabeled, discontinuities in the simulation results can occur, resulting failures in subsequent calculations (Okuno 2009). Xu and Okuno (2015) studied the effect of relative permeability on oil displacements by three hydrocarbon phases. A new method for robust phase identification was developed and implemented in a 1D convective flow simulator with no volume change on mixing. Their new method used tie triangles and their normal unit vectors tabulated as part of the simulation input information. The extensions of the limiting tie triangles at the upper and lower critical endpoints (UCEP and LCEP) define three different regions in composition space; the super-UCEP, super-

27

LCEP, and sub-CEP regions. Results showed that the new method can properly recognize five different two-phase regions surrounding the three-phase region, and the new method can quantify the relative location of the current overall composition to the three-phase region in composition space.

2.5 PHASE BEHAVIOR CALCULATIONS

This section firstly summarizes the conventional formulations and current algorithms for PT flash, in which computational difficulties associated with current PT flash are explained. Then, existing formulations and algorithms for PH flash are reviewed and computational difficulties with unknown temperature conditions are explained. At last, one of the most common used cubic EOS, the Peng-Robinson EOS (Peng and Robinson 1978) is reviewed. The Peng-Robinson EOS is used throughout this dissertation, although any cubic EOS can be used for the purpose of generalization.

2.5.1 Isobaric-isothermal Flash

This section firstly presents the conventional formulations of phase-stability/-split calculations at constant pressure and temperature for an overall composition of interest. Then, a review of various algorithms for multiphase PT phase-stability/-split calculations is given.

2.5.1.1 Phase Stability Tests

Conventional Formulations

Phase stability is to determine whether a phase is stable at a fixed temperature, pressure, and composition. If that phase is unstable, a phase-split calculation is then performed to obtain the equilibrium compositions. Baker et al. (1982) demonstrated that a stable equilibrium state must be the global minimum of the Gibbs free energy. Hence, the tangent plane to the Gibbs free energy surface at a stable equilibrium state at a

fixed temperature and pressure must lie below the Gibbs free energy surface at any composition.   This is the necessary and sufficient condition for phase stability.

Michelsen (1982a) developed an algorithm for phase stability analysis on the basis of Baker et al. (1982).   A TPD function is defined as the difference between the Gibbs free energy and the tangent plane to the Gibbs free energy at a phase composition of interest.   A phase is stable when the TPD is non-negative.

The TPD function is derived using the first-order Taylor expansion of the Gibbs free energy at a phase composition of interest.   A tangent plane $T(\underline{x})$ to the Gibbs free energy surface at a phase composition $\underline{z}$ is

$$T(\underline{x}) = \underline{G}(\underline{z}) + \sum_{i=1}^{N_C}(x_i - z_i)\left(\partial\underline{G}(\underline{x})/\partial x_i\right)\big|_{\underline{x}=\underline{z}}$$

$$= \underline{G}(\underline{z}) + \sum_{i=1}^{N_C}(x_i - z_i)\left[\overline{G}_i(\underline{z}) - \overline{G}_{N_C}(\underline{z}) + \sum_{k=1}^{N_C} x_k(\partial\overline{G}_k/\partial x_k)\right]$$

$$= \underline{G}(\underline{z}) + \sum_{i=1}^{N_C} x_i\overline{G}_i(\underline{z}) - \sum_{i=1}^{N_C} z_i\overline{G}_i(\underline{z})$$

$$= \sum_{i=1}^{N_C} x_i\overline{G}_i(\underline{z}). \tag{2.21}$$

In equation 2.21, $\underline{G}$ is the molar Gibbs free energy of a mixture, i and k are component index, N_C is the number of components, $\overline{G}$ is the partial molar Gibbs free energy.

Then, the TPD function is expresses as

$$D(\underline{x}) = \underline{G}(\underline{x}) - T(\underline{x}) = \sum_{i=1}^{N_C} x_i[\overline{G}_i(\underline{x}) - \overline{G}_i(\underline{z})], \tag{2.22}$$

or in dimensionless form as

$$D_R(\underline{x}) = D(\underline{x})/RT = \sum_{i=1}^{N_C} x_i[\ln x_i\varphi_i(\underline{x}) - \ln z_i\varphi_i(\underline{z})], \tag{2.23}$$

where φ_i is the fugacity coefficient of component i.

One of the widely used methods to test if a phase is stable was proposed by Michelsen (1982a).   The idea is to locate stationary points of the TPD function and check the sign of TPD to identify phase stability.   At a stationary point, the first-order derivatives of $D(\underline{x})$ given in equation 2.22 are all zero, i.e.,

$$\partial D(\underline{x})/\partial x_i = \frac{\partial}{\partial x_i}\left[\sum_{i=1}^{N_C} x_i[\overline{G}_i(\underline{x}) - \overline{G}_i(\underline{z})]\right]$$

$$= \left[\overline{G}_i(\underline{x}) - \overline{G}_i(\underline{z})\right] - \left[\overline{G}_{N_C}(\underline{x}) - \overline{G}_{N_C}(\underline{z})\right] = 0. \tag{2.24}$$

Equation 2.24 can be re-arranged as

$$\overline{G}_i(\underline{x}) - \overline{G}_i(\underline{z}) = \overline{G}_{N_C}(\underline{x}) - \overline{G}_{N_C}(\underline{z}). \tag{2.25}$$

Substitution of equation 2.25 into equation 2.22 gives

$$D(\underline{x}) = \sum_{i=1}^{N_C} x_i\left[\overline{G}_i(\underline{x}) - \overline{G}_i(\underline{z})\right] = \sum_{i=1}^{N_C} x_i\left[\overline{G}_{N_C}(\underline{x}) - \overline{G}_{N_C}(\underline{z})\right]$$

$$= \overline{G}_{N_C}(\underline{x}) - \overline{G}_{N_C}(\underline{z}) = \overline{G}_i(\underline{x}) - \overline{G}_i(\underline{z}). \tag{2.26}$$

Re-arrangement of equation 2.26 yields the well-known stationarity equations as

$$\ln X_i \varphi(\underline{x}) - \ln z_i \varphi(\underline{z}) = 0, \tag{2.27}$$

where R is the universal gas constant and $X_i = x_i \exp\left(-\frac{D}{RT}\right) = x_i \exp(-D_R)$ for i = 1, 2, ..., N_C.

Stationary point method tries to find stationary points from equation 2.27 and checks whether $\sum_{i=1}^{N_C} X_i > 1.0$ for i = 1, 2, ..., N_C. If a stationary point at which $\sum_{i=1}^{N_C} X_i > 1.0$ is identified, the tested phase with a composition of $\underline{z}$ is unstable. Otherwise, it is a stable phase.

Another method is to minimize the TPD function in composition space subject to the following constraint

$$\sum_{i=1}^{N_C} x_i = 1.0 \text{ and } x_i \geq 0 \text{ for } i = 1, 2, ..., N_C. \tag{2.28}$$

Phase stability test searches for a composition at which the TPD function is negative. If such a composition is identified, the current phase is unstable (Michelsen 1982a).

Although phase stability test is simpler than phase split due to the fact that material balance equations that consider the equilibrium phase amounts and their compositions are not needed, it is still difficult to locate all stationary points of the TPD function.

Conventional Algorithms

The possibility of finding all stationary points of the TPD function increases with the use of more initial estimates. For single-phase stability test, Wilson's correlation (1969),

$$K_i = P_{Ri}\exp[5.373(1 + \omega_i)(1 - T_{Ri})], \tag{2.29}$$

is used. In equation 2.29, K_i is the K-value of component i, $P_{Ri} = P/P_{Ci}$, $T_{Ri} = T/T_{Ci}$, P_{Ci} and T_{Ci} are the critical pressure and temperature for component i, respectively, P and T are pressure and temperature of interest, respectively, ω_i is the acentric factor of component i.

For two phases, Michelsen (1982a) suggested using a V-like and a L-like guess defined as following:

$$X_i = z_i K_i, \tag{2.30}$$

$$X_i = z_i/K_i, \tag{2.31}$$

where z_i is the overall composition of component i in a mixture.

For multiple phases, Michelsen (1982a) suggested four initial guesses. The first and second guesses are to use the lightest component and the heaviest component as near-pure phases. The third guess used the arithmetic mean of present phase compositions as follows:

$$X_i = \sum_{j=1}^{N_P} x_{ij}/N_P, \tag{2.32}$$

where N_P is the number of present phases and x_{ij} is the mole fraction of component i in phase j. The fourth guess assumed an ideal gas mixture as follows:

$$X_i = z_i \varphi(\underline{z}). \tag{2.33}$$

In addition to the four initial guesses, Li and Firoozabadi (2012) also proposed to other sets of initial guesses to improve the reliability of phase stability test.

Global minimization algorithms (e.g., Trangenstein 1987, McDonald and Floudass 1997, Pan and Firoozabadi 1998) were proposed in the literature to find the global minimum of the TPD function. However, the method of Trangenstein (1987) and Pan and Firoozabadi (1998) cannot guarantee to converge to the global minimum. The method of McDonald and Floudas (1997) is only applicable to the cases when liquid phases are modeled by use of NRTL, UNIQUAC, UNIFAC models.

Successive substitution (SS) is widely used to find a stationary point due to its simplicity and robustness. SS is linearly convergence. However, it becomes significantly slow in a near critical region, which frequently occurs in gas injection simulations. The independent variables used are X_i.

Newton's method can be used to achieve faster convergence rate. However, reliable initial guesses should be provided to Newton's method by a first-order method, e.g., SS. In the UTCOMP simulator, Perschke (1988) implemented the use of Newton's method after switching from SS when a certain switching criterion is achieved.

Local minimization of TPD function can also be used. The algorithm of Trangenstein (1987) was implemented by Perschke (1988) in the UTCOMP simulator. Michelsen (1982a) proposed the use of BFGS quasi-Newton method to find the local minima of the TPD function. The use of BFGS is slower than Newton's method, since less curvature information is used in the search of descent direction.

Trivial solutions can occur in the results of phase stability tests (Michelsen 1982a). Trivial solution is obtained when the independent variable, X_i, is equal to the test phase composition or existing equilibrium phase composition at the convergence (Okuno 2009). When a trivial solution is found by use of an initial guess, subsequent initial guesses are tested until phase instability is detected.

2.5.1.2 Phase Split

Conventional Formulations

A multiphase equilibrium calculation for a fixed P and T requires the global minimization of the Gibbs free energy subject to material balance. The molar Gibbs free energy of a multiphase multicomponent system is

$$\underline{G} = \sum_{j=1}^{N_P} \sum_{i=1}^{N_C} \beta_j x_{ij} \overline{G}_{ij}, \tag{2.34}$$

where N_P is the number of equilibrium phases, x_{ij} is the mole fraction of component i in phase j, β_j is the mole fraction of phase j, and $\overline{G}_{ij}$ is the molar Gibbs free energy of component i in phase j. Material balance equations are given by

$$z_i = \sum_{j=1}^{N_P} \beta_j x_{ij} \ \text{ for } i = 1, 2, \ldots, N_C, \tag{2.35}$$

$$\sum_{i=1}^{N_C} z_i = 1.0, \tag{2.36}$$

$$\sum_{j=1}^{N_P} \beta_j = 1.0 \ \text{ and } \ \beta_j \geq 0 \ \text{ for } j = 1, 2, \ldots, N_P, \tag{2.37}$$

$$\sum_{i=1}^{N_C} x_{ij} = 1.0 \ \text{ and } \ x_{ij} \geq 0 \ \text{ for } i = 1, 2, \ldots, N_C \text{ and } j = 1, 2, \ldots, N_P. \tag{2.38}$$

Substitution of the definition of fugacity coefficient into equation 2.34 yields

$$\underline{G} = RT \sum_{j=1}^{N_P} \sum_{i=1}^{N_C} \beta_j x_{ij} \ln(x_{ij}\varphi_{ij}) + \underline{G}^{IG} \sum_{j=1}^{N_P} \sum_{i=1}^{N_C} \beta_j x_{ij}, \tag{2.39}$$

where φ_{ij} is the fugacity coefficient of component i in phase j, and $\underline{G}^{IG}$ is the molar Gibbs free energy for idea gas. Since $\underline{G}^{IG}$ is dependent on temperature and pressure, it becomes a constant for flash calculations at a fixed temperature and pressure. Combining equations 2.35 and 2.36, minimization of equation 2.39 is equivalent to minimizing the following dimensionless molar Gibbs free energy

$$\underline{G}_R = (\underline{G} - \underline{G}^{IG})/RT = \sum_{j=1}^{N_P} \sum_{i=1}^{N_C} \beta_j x_{ij} \ln(x_{ij}\varphi_{ij}). \tag{2.40}$$

Equality of fugacity is another formulation derived from the first-order necessary optimality condition for minimizing the Gibbs free energy

$$\overline{G}_{ij} - \overline{G}_{iN_P} = 0 \ \text{ for } i = 1, 2, \ldots, N_C \text{ and } j = 1, 2, \ldots, (N_P-1). \tag{2.41}$$

Equation 2.41 is equivalent to the fugacity equations as follows:

$$\ln f_{ij} - \ln f_{iN_P} = 0 \quad \text{for } i = 1, 2, \ldots, N_C \text{ and } j = 1, 2, \ldots, (N_P-1), \qquad (2.42)$$

where f_{ij} is the fugacity of component i in phase j. Equations 2.35 to 2.38 must be satisfied in solutions of equation 2.42. The $N_P{}^{th}$-phase is the reference phase in equations 2.41 and 2.42. Hence, the solution of fugacity equality can be a minimum, a maximum, or a saddle point of the Gibbs free energy.

Conventional Algorithms

Phase split algorithm gives the amounts of equilibrium phases and their compositions at a fixed temperature and pressure for an overall composition of interest. Conventional algorithms subsequent to Michelsen (1982ab) are based on the sequential use of phase-stability/-split. That is, phase stability is tested for the overall composition or one of the phases from a multiphase solution, at which the tangent plane to the Gibbs free energy surface is defined. If phase instability is detected, a phase-split calculation is performed under the assumption that one more equilibrium phase is present.

In flash calculations based on solving the fugacity equations (equation 2.42), the independent variables are K values or the logarithm of K values (Nghiem and Li 1984, Abhvani and Beaumont 1987). K values are defined as the tendency of the components to prefer one phase over another and are given by

$$K_{ij} = x_{ij}/x_{iN_P} \quad \text{for } i = 1, 2, \ldots, N_C \text{ and } j = 1, 2, \ldots, (N_P-1), \qquad (2.43)$$

where K_{ij} is the K-value of component i in phase j and the $N_P{}^{th}$-phase is the reference phase

SS is one of the conventional methods to solve fugacity equations. In SS, the equality of fugacity equations can be written in terms of K values and fugacity coefficients as follows:

$$\ln K_{ij}^{(k+1)} = \ln \varphi_{iN_P}^{(k)} - \ln \varphi_{ij}^{(k)} \qquad (2.44)$$

for i = 1, 2, …, N_C and j = 1, 2, …, (N_P−1), where the superscript in the parentheses is the iteration step number. K values are updated at each iteration by solving the fugacity equations subject to material balance constraints. The material balance equations are solved for phase compositions for a given set of K values; i.e., Rachford Rice (RR) equations (1952).

SS is considered a robust algorithm as it is a gradient-based method for Gibbs free energy minimization (Okuno 2009). However, the SS method significantly slow in near-critical regions (Michelsen 1982b) due to its linear-convergence rate for optimization. A large number of iterations are required to get convergence using SS near critical regions (Mehra et al. 1983, Ammar and Renon 1987). Several acceleration approaches are proposed to improve the convergence rate; e.g., Michelsen (1982b), Mehra et al. (1982, 1983), Nghiem and Heidemann (1982). Perschke (1988) implemented the algorithm proposed by Mehra et al. (1983) in UTCOMP for two- and three-phase split calculations.

SS is linearly convergent but accepts a larger range of initial guesses to get convergence compared to Newton's method (Okuno 2009). On the other hand, Newton's method is a fast and quadratically convergent only if a reasonable initial guess is provided (Okuno 2009). Therefore, SS can also be used to provide reliable initial guesses for second-order Newton's method due to the robustness of SS (Ammar and Renon 1987, Michelsen 1982b, Mehra et al. 1982, Nghiem et al. 1983).

Algorithms based on solving the fugacity equations are root-finding procedures, which are not reliable for systems with more than two phases (Michelsen 1982b). This is because the global minimum of the Gibbs free energy is not guaranteed for such a case. As the number of components and phases increase, the number of local minima, saddle points, and local maxima also increase. Also, the solution can converge to a

composition where the phases have the same density and composition, i.e., a trivial solution (Okuno 2009). Use of a minimization algorithm can avoid the trivial solution, since trivial solutions have higher Gibbs free energy than the correct solution (Trangenstein 1987).

Many algorithms were proposed in the literature for the minimization of the Gibbs free energy for phase split calculations (Gautam and Seider 1979, Lucia et al. 1985, Trangenstein 1985, 1987, Ammar and Renon 1987). Michelsen (1982b) proposed an algorithm for minimization of Gibbs free energy based on Newton's method. Perschke (1988) used Newton's algorithm combined with a line-search technique and implemented the algorithm in the UTCOMP simulator.

Newton's method can fail to converge to the correct solution when the Hessian matrix is not positive definite, a nearly singular Hessian matrix, or due to the existence of multiple minima. For the cases where multiple minima exist, the modified Cholesky decomposition is used to tune the Hessian matrix to be positive definite (Gill and Murray 1974, Perschke 1988, Okuno 2009).

Second-order Newton method for minimization of Gibbs free energy quadratically converges to final solution, but requires reliable initial guesses. Conventionally, robust first-order method, e.g., SS, is used to generate good starting guesses for Newton's method of minimization. For cases with near critical condition and/or near phase boundary, the convergence radius of second-order Newton's method can be very small, and a large number of SS iterations are required before switching to second-order Newton's method (Okuno 2009). Although the trust-region methods (e.g., Nghiem et al. 1983, Michelsen and Mollerup 2007, Alsaifi and Englezos 2011) were proposed to reduce the iterations by combining SS and Newton's method, the use of trust-region methods only yield a good approximation of the minimum Gibbs free energy,

rather than giving the exact minimum of the Gibbs free energy.   Furthermore, solving trust-region sub-problems can further increase the computational cost.

Conventionally, the independent variables used in second-order Newton's method are $w_{ij} = x_{ij}\beta_j$ for i = 1, 2, …, N_C and j = 1, 2, …, N_P.   In the second-order Newton's method, exact Hessian matrices are required to be calculated at each iteration.   The requirement restrains the application of the method for complex thermodynamic models due to high computational complexity and cost.   Use of quasi-Newton method avoids the computation of exact Hessian matrices.   Instead, the Hessian matrix for current iteration is approximated by use of the information from the previous iteration step.   Quasi-Newton method with an approximation of Hessian matrix provides a super-linear convergence rate for minimizing Gibbs free energy, which is quite close to the performance of second-order Newton's method.   In quasi-Newton method, only the objective function and its gradient vectors are calculated, which saves extra calculations in phase-split calculations as required by Newton's method.   Although novel, the performance of quasi-Newton method is very sensitive to scaling of design parameters (Dennis and Schnabel 1996).

In the literature, many researchers have proposed to use quasi-Newton method in phase-stability/-split calculations.   Michelsen (1982ab) used quasi-Newton method for phase equilibrium calculations.   Nghiem (1983) developed a compositional simulator with the use of quasi-Newton SS method for phase behavior modelling.   Lucia and Macchietto (1983) and Venkataraman and Lucia (1986, 1987) proposed thermodynamically consistent quasi-Newton formula with hybrid method developed by Lucia and Macchietto (1983).   The hybrid method is to split the approximated Hessian matrix into two parts, one of which is calculated analytically and the other is approximated via a quasi-Newton update.

The BFGS quasi-Newton method is a widely used method in phase equilibrium calculations. The convergence rate of BFGS quasi-Newton method is super-linear, and the Hessian matrix required at each iteration is guaranteed to be positive definite by use of a rank two update (Dennis and Schnabel 1996). Ammar and Renon (1987) developed a BFGS quasi-Newton method with line search to update the natural log of equilibrium ratios. This method was further tested by Garcia-Sanchez et al. (1996) in multicomponent multiple liquid-phase equilibria systems, modeling of micro-emulsion from excess Gibbs energy models, and vapor-liquid equilibria of nitrogen-hydrocarbon systems using the PC-SAFT EOS.

Lucia et al. (2000) proposed a modified BFGS quasi-Newton method for solving constrained multiphase flash problems. Hoteit and Firoozabadi (2006) solved the phase stability test problems using BFGS update. Nichita et al. (2002 and 2009) applied BFGS method in the local minimization algorithm in the frame of the Tunneling global optimization method. Haugen and Beckner (2013) proposed an analytical Quasi-Newton method adaptive to cubic EOS on the basis of the reduction principles.

For the cases in which Hessian matrix is not positive definite, trust-region method can be used instead of line search. It is superior to Newton's method with line search because Newton's method requires a positive-definite Hessian matrix to guarantee descend searching direction. Trust-region method can be used to correct the non-positive definite Hessian matrix by adding a diagonal matrix so that the Hessian matrix becomes positive definite. For each iteration, trust-region method searches for an optimal solution within a confined region defined by a trust radius, which is updated on an iteration by iteration basis depending on the quality of the quadratic approximation to the objective function. The trust radius is obtained by calculating the ratio of actual

reduction of objective function to that of the predicted reduction. Larger trust radius is obtained when the quadratic approximation is accurate; otherwise, restricted step is used.

Nghiem et al. (1983) firstly used trust-region method in phase equilibrium calculations for two phases. Lucia and Liu (1998) modified the method of Nghiem et al. (1983) to accelerate the calculations of phase equilibrium. Lucia and Liu (1998) used the Dogleg method, a linear combination of Cauchy point and Newton search direction for optimization. Cauchy point provides an optimal stepsize that minimizes a quadratic model within the trust region along the steepest descent direction. Dogleg method provides an enhanced search direction which is superior to Cauchy point by using the curvature information of the Hessian matrix. However, these methods will exhibit convergence problem when the Hessian matrix is not positive definite.

Lucia and Yang (2003) used trust-region method to calculate the descend direction with the terrain global method. The terrain global method is an algorithm that is capable of finding all physically meaningful solutions and singular points. The method consists of a series of downhill, equation-solving computations, uphill and predictor-corrector calculation. Lucia et al. (2012) tested the terrain global method in the multi-scale framework for multiphase flash. Alsaifi and Englezos (2011) applied a trust-region Gauss-Newton method for simultaneous phase-stability/-split with PC-SAFT equation of state. A comment issue remains in all trust-region method is that use of Dogleg method, a linear combination of Cauchy point calculation and Newton method, only results in good approximation of the minimum Gibbs free energy, rather than giving the exact minimum of the Gibbs free energy.

Michelsen and Mollerup (2007) also proposed a modification on the issue associated with the non-positive definite Hessian matrix. If the Hessian matrix is not

positive definite, a diagonal matrix is added to the Hessian and makes the Hessian positive definite.

Other algorithms were also proposed in the literature for phase split. For example, interval analysis, firstly proposed by Moore in 1966, is used to find all root of the given set of nonlinear equations with mathematical certainty. This method has been applied to various problems associated with phase behavior calculations. For example, it has been used to perform phase equilibrium calculations (Xu et al. 2000, Burgos et al. 2004), phase stability determination (Hua et al. 1996, 1998ab, Tessier et al. 2000; Xu et al. 2005), computation of critical points (Stradi et al. 2001), and isothermal flash calculations using SAFT equation of state (Xu et al, 2002).

Several authors have reported that although interval method is very robust, it has its own limitations. Firstly, computational cost increases significantly when a large system of equations is to be solved. This frequently occurs in multi-component multiphase system (Hua et al. 1996, 1998ab). Secondly, it is difficult to implement in existing process simulators. As is reported by Gecegormez and Demirel (2005), the phase stability test in context of generation of global phase diagram implemented using interval Newton/generalized bisection approach in MATLAB programming platform is not advantageous with respect to computational cost, even for binary system.

In Hua et al. (1996, 1998ab), they performed interval Newton/generalized bisection approach to determine the phase stability by locating all stationary points of the TPD equations. The stationary points are then used as initial estimates for flash calculation. Successive quadratic programming algorithm is then used to perform local minimization of Gibbs free energy to locate the prospective global minima of the Gibbs free energy surface. The interval Newton/generalized bisection approach is then used to determine whether the global minimum is identified. As is reported by the authors, the

efficiency and reliability of their algorithm are significantly enhanced. However, the comparison between their method and the conventional sequential phase-stability/-split algorithms is not given. Also, one of the tested cases shows that their method is able to find correct equilibrium phase compositions, where the method of Michelsen incorrectly predicts that the mixture is stable. Furthermore, the cases tested by their method are up to four components. Hence, the capability of their method on real reservoir fluids is uncertain.

Xu et al. (2000, 2002) also applied the interval based method to reliably compute phase stability and phase equilibrium using SAFT EOS. However, the computation cost required in their method is high even for binary system and can increase further as the number of components increases. Also, their method requires special computing environment and difficult to implement in existing process simulation packages, as they stated.

Except for the conventional way of performing phase-stability/-split in a sequential manner as explained above, Gupta et al. (1990) presented a novel methodology to perform phase-stability and -split calculations simultaneously. In their algorithm, the RR and stability equations were solved simultaneously for phase amounts and "stability variables" by use of Newton's method for root finding. The stability equations of Gupta et al. (1990) indicate that either the stability variable or the phase amount of an individual phase is zero at the global minimum of the Gibbs free energy. The stability variables of Gupta et al. (1990) were derived from the first-order condition for unconstrained minimization of the Gibbs free energy as formulated by them. K values were then updated in the outer loop by successive substitution. Unlike the conventional successive substitution, however, the flash algorithm of Gupta et al. (1990) involves the

41

simultaneous root-finding of the RR and stability equations, which can cause convergence issues as discussed below.

Various issues with Gupta et al.'s algorithm were reported in previous papers, and have been also identified in the current research. Firstly, a few researchers (Abdel-Ghani 1995, Alsaifi and Englezos 2011) reported numerical issues associated with the degeneracy of equations (called "stability equations" in their papers) near phase boundaries on the basis of Gupta et al.'s formulation. Secondly, the initialization scheme that they proposed often results in K values that give an unbounded feasible region for RR solution. As proved in Okuno et al. (2010), such a RR problem has no solution, which stops the flash calculation from proceeding. Even if it is successfully initialized, the original algorithm of Gupta et al. may not be robust since it does not check the feasibility of each RR solution during the iteration. Thirdly, it is not clear how their algorithm selects the reference composition that is required to set the system of equations to be solved. It is likely that negative phase amounts are used as the indicator for improper selection of the reference composition, as mentioned in Alsaifi and Englezos (2011).

Alsaifi and Englezos (2011) used the trust-region-Gauss-Newton method with the original formulation of Gupta et al. It was reported that, unlike the algorithm of Gupta et al., their algorithm did not encounter convergence issues near phase boundaries. However, no comparison was given between the two algorithms. It is not entirely clear how the reported improvement was achieved. The algorithm developed by us in this research does not require the equations [called "stability equations" in Gupta et al. (1990)] that caused the convergence issues near phase boundaries.

Chaikunchuensakun et al. (2002) also proposed a simultaneous solution of phase-stability and -split calculations on the basis of minimization of the Gibbs free energy.

42

They used a quasi-Newton method with an approximate Hessian matrix, rather than an analytical one. Use of pseudocritical properties of the fluid of interest was proposed for identification of the states of the reference and potential equilibrium phases. If the ratio of the system pressure to the pseudocritical pressure of the fluid is greater than a value that is heuristically determined (e.g., 1.0 as used in their paper), the fluid is identified as a liquid; otherwise, the mixture is a vapor. However, they stated that their algorithm is only for local minimization, and does not attempt to search for a global solution for multiphase PT flash (2002). Also, it is not clear why the phase identification is required in their algorithm.

2.5.2 Isenthalpic Flash

Steam injection is a widely used method for heavy-oil recovery (Lake et al. 2014). Flow of fluid and energy is coupled with multiphase behavior of water-hydrocarbons mixtures in steam injection. Therefore, compositional effects are important in understanding and designing steam injection.

A common selection of independent variables in EOS thermal simulation is the component mole numbers, pressure, and enthalpy for each grid block (Brantferger 1991, Liu et al. 2009). Use of enthalpy as an independent variable associated with the energy conservation equation is more general than use of temperature since the former can naturally accommodate the cases of one degree of freedom (e.g., two-component, three-phase systems) (Brantferger 1991). In this simulation formulation, phase behavior at each grid block at each time step is calculated at a given P, enthalpy (H), and overall composition; i.e., isenthalpic or PH flash.

This section firstly presents the conventional formulations of phase-stability/-split calculations at constant pressure and enthalpy for an overall composition of interest.

43

Then, a review of various algorithms for multiphase PH phase-stability/-split calculations is given.

2.5.2.1 Conventional Formulations

The most fundamental formulation for PH flash is maximization of entropy (equivalently, minimization of negative entropy) subject to the enthalpy constraint with the variables of temperature and component mole numbers in equilibrium phases (Brantferger 1991, Brantferger et al. 1991). That is, for a given pressure (P), specific molar enthalpy ($\underline{H}_{spec}$) and overall composition (z_i for i = 1, 2, …, N_C), it is to find temperature (T) and x_{ij} (i = 1, 2, …, N_C, and j = 1, 2, …, N_P) that maximize

$$\underline{S}^t = \Sigma_{j=1}^{N_P} \beta_j \underline{S}_j, \qquad (2.45)$$

where $\underline{H}_{spec}$ is the specified molar enthalpy, z_i is the overall mole fraction of component i, x_{ij} is the mole fraction of component i in phase j, $\underline{S}^t$ is the total molar entropy, β_j is the mole fraction of phase j, $\underline{S}_j$ is the molar entropy of phase j, N_C is the number of components, and N_P is the number of equilibrium phases. The following constraints are to be satisfied:

$$z_i = \Sigma_{j=1}^{N_P} \beta_j x_{ij}, \qquad (2.46)$$

$$\Sigma_{j=1}^{N_P} \beta_j = 1.0 , \qquad (2.47)$$

$$\underline{H}^t = \Sigma_{j=1}^{N_P} \beta_j \underline{H}_j = \underline{H}_{spec}, \qquad (2.48)$$

for i = 1, 2, …, N_C, and j = 1, 2, …, N_P, where $\underline{H}^t$ is the total molar enthalpy and $\underline{H}_j$ is the molar enthalpy of phase j.

2.5.2.2 Conventional Algorithms

Brantferger et al. (1991) developed a second-order algorithm for the constrained entropy maximization using Newton's method. The Hessian matrix was modified through the Cholesky decomposition when it was ill-conditioned. However, the non-linearity of the enthalpy constraint made it difficult to ensure robust maximization of the

44

entropy (Brantferger et al. 1991, Michelsen 1987, 1993, 1999, Van Odyck et al. 2009). Michelsen (1999) then proposed another objective function, for which the solution existed at a saddle point of the function. However, it was mentioned that the proposed method could be problematic when narrow-boiling phases were involved (Michelsen 1987, 1999).

Another type of PH-flash formulation uses PT flash that is nested in the outer temperature iteration loop (Agarwal et al. 1991). This method fundamentally fails for one degree of freedom, where pressure and temperature are interdependent (Brantferger et al. 1991, Chien 1989, Agarwal et al. 1991).

The term "narrow-boiling" has been used in the literature to refer to the enthalpy behavior that is very sensitive to temperature (Michelsen 1987, Agarwal et al. 1991). Details of the convergence behavior and computational efficiency were not discussed for these function-maximization methods. These methods are quadratically convergent near the solution. It is likely that their robustness depends significantly on initialization of the iteration variables as is the case with minimization of the Gibbs free energy at a given T and P; i.e., PT flash (Mehra et al. 1982, Nghiem et al. 1983, Michelsen 1982b, Ammar and Renon 1987, Pan and Firoozabadi 2003).

The limiting narrow-boiling behavior occurs for one degree of freedom, where the enthalpy exhibits a discontinuity in temperature space. In such a case, the interdependency of pressure and temperature excludes one of the PH flash algorithms proposed in the literature, which has PT flash nested in the outer temperature iteration loop (Agarwal et al. 1991, Brantferger et al. 1991, Michelsen 1993, Néron et al. 2012).

Algorithms using Newton's method can be initialized by more robust, but linearly convergent algorithms. In PT flash, for instance, the traditional SS algorithm and its accelerated variants are commonly used to provide initial estimates for Newton's method

45

(Chang 1990, Chang et al. 1990, Perschke 1988, Perschke et al. 1989, Michelsen 1998, Michelsen and Mollerup 2004). A PH-flash algorithm developed by Michelsen (1987) had some algorithmic features in common with the SS algorithm for PT flash, and was referred to as the direct substitution (DS) algorithm. In the DS algorithm, the fugacity equations and enthalpy constraint were solved with K values and temperature as independent variables. For each iteration, one Newton's iteration step was performed using the Rachford-Rice equations (Rachford and Rice 1952) and the enthalpy constraint as functions of independent phase mole fractions and temperature. Then, K values were updated based on the temperature change that was just obtained by the Newton's iteration step. Unlike the PH flash algorithm using nested PT flash mentioned before, the DS algorithms do not have the issue associated with one degree of freedom since temperature and K values are updated within a single iteration loop (Michelsen 1987, Agarwal et al. 1991).

The DS algorithm of Michelsen (1987) was modified later by Agarwal et al. (1991). The main difference between the DS algorithms of Michelsen and Agarwal et al. was that the latter performed a quasi-Newton update of K values (Nghiem 1983, Nghiem and Li 1984) prior to the Newton's iteration step for the Rachford-Rice equations and the enthalpy constraint. In general, this preliminary K-value update reduces the number of iterations required for convergence. Siu et al. (1991) used the DS algorithm of Agarwal et al. (1991) in their fully implicit thermal wellbore model.

Michelsen (1987) and Agarwal et al. (1991) reported that their DS algorithms could exhibit non-convergence when narrow-boiling phases were involved. The convergence issue was indicated by temperature oscillations in their algorithms, but the reason for the oscillations was not detailed. The suggested remedy was to select the phase compressibility factors in such a way that K values did not to converge to unity

46

during the iteration.   Although its details were not entirely clear in their papers, it is unlikely that this approach always resolve the convergence issues.   For example, there are cases where only a single root exists in solution of a cubic EOS for an oscillating single-phase fluid.   More importantly, the direct reason for the convergence issue caused by the presence of narrow-boiling behavior is not the root selection in solution of a cubic EOS.

Zhu and Okuno (2014a) demonstrated in their two-phase case studies that the DS algorithms of Michelsen (1987) and Agarwal et al. (1991) can exhibit non-convergence with Michelsen's remedy.   They concluded that temperature oscillation is a consequence of, not the reason for, narrow-boiling behavior.   Zhu and Okuno (2014a) showed for two phases that the system of equations solved in the DS algorithm becomes nearly degenerate for narrow-boiling fluids.   Then, they developed a modified two-phase DS algorithm that can adaptively switch between a bisection and Newton's step depending on the condition number of the Jacobian matrix.   The bisection algorithm solves for temperature based solely on the enthalpy constraint when narrow-boiling behavior is detected by a large condition number of the Jacobian matrix.   The modified DS algorithm successfully solved the two-phase PH flash calculations for which the prior DS algorithms (Michelsen 1987, Agarwal et al. 1991) showed non-convergence.

To sum up, DS algorithm for PH flash is a root-finding approach, instead of direct maximization of the total entropy.   It searches for K values and T that satisfy equations 2.46 to 2.48 and the fugacity equations (equation 2.42).   As in the traditional SS algorithm for PT flash, K values, K_{ij}, are related to β_j and x_{ij} through the Rachford-Rice equations; that is, β_j can be obtained from solution of the Rachford-Rice equations.   The Rachford-Rice equations are

$$g_j = \sum_{i=1}^{N_C} \left(x_{iN_P} - x_{ij} \right) = \sum_{i=1}^{N_C} \left(1 - K_{ij} \right) z_i / t_i = 0, \qquad (2.49)$$

for j = 1, 2, …, (N_P − 1), where $t_i = 1 + \sum_{j=1}^{N_P-1}(K_{ij} - 1)\beta_j$ for i = 1, 2, …, N_C. Then, the corresponding x_{ij} can be obtained from $x_{iN_P} = z_i/t_i$ and $K_{ij} = x_{ij}/x_{iN_P}$ for j ≠ N_P.

The DS algorithms developed by Michelsen (1987) and Agarwal et al. (1991) involve solution of the system of N_P equations consisting of equation 2.49 and the enthalpy constraint

$$g_{N_P} = \underline{H}^t - \underline{H}_{spec} = 0 \tag{2.50}$$

for T and β_j (j = 1, 2, …, N_P − 1) based on Newton's method for root-finding. The calculations of enthalpy and associated derivatives, and the Jacobian matrix required is presented in **Appendix A** for a general N_C-component N_P-phase system. **Appendix B** presents the step-wise descriptions and flow charts for the DS algorithm of Michelsen (1987) and Agarwal et al. (1991).

The PH-flash algorithms mentioned above assume a certain number of equilibrium phases. With the PH specification, the number of equilibrium phases is unknown not only in composition space, but also in temperature space. It can be determined at the solution temperature upon convergence. As presented in Brantferger (1991) phase stability with PH specification can be analyzed only at a given temperature, which is not the equilibrium temperature until convergence.

Although phase stability analysis was not clearly described in most of the prior publications on thermal compositional simulation (e.g., Heidari et al. 2014, Siu et al. 1991, Varavei and Sepehrnoori 2009, Zaydullin et al. 2014), it may be performed alternately with flash calculation for a fixed number of phases (Brantferger 1991, Brantferger et al. 1991). As in conventional PT flash, however, sequential use of phase-stability and flash calculations is a series of local solutions, which requires obtaining false solutions and correcting them until the correct solution is obtained. Such PH flash becomes more difficult as the number of equilibrium phases increases because it tends to

be attracted to a larger number of false solutions. It also becomes more difficult for a narrow-boiling fluid because false solutions at false temperatures may deviate substantially from the correct solution at the solution temperature for such a case.

Gupta et al. (1990) proposed a novel formulation for PH flash that combines phase-stability and flash calculations. In their algorithm, the enthalpy, Rachford-Rice (RR), and stability equations were solved simultaneously for temperature, phase amounts, and stability variables. The stability variables of Gupta et al. (1990) were derived from the first-order condition for unconstrained minimization of the Gibbs free energy as formulated by them. K values were updated in the outer loop based on the temperature change that was obtained from the internal iteration loop. It was reported that their algorithm could handle fluids with one degree of freedom. This is conceivable because the number of equilibrium phases is part of the solution in their PH flash (Zhu and Okuno 2014ab, 2015ab, 2016). To the best of our knowledge, the formulation and algorithm of Gupta et al.'s for PH flash have not been used in the literature since their original publication (Gupta et al. 1990). Various issues of their PH flash will be resolved in this paper, but briefly introduced here.

Firstly, non-convergence can occur when it attempts to solve the degenerate system of equations for a narrow-boiling fluid without using the method of Zhu and Okuno (2014ab, 2015ab, 2016). When narrow-boiling behavior occurs, it occurs within a phase region in which the number of phases is fixed. This is true even for the limiting case of one degree of freedom, for which the entire phase region of one freedom is narrow-boiling [e.g., a three-phase region (or point) for a binary system at a given pressure]. Thus, the coupling of phase-stability and flash calculations in itself does not necessarily improve the degeneracy issue associated with narrow-boiling behavior. Zhu

49

and Okuno (2015ab) presented non-convergence cases with the conventional PH flash algorithms even if the correct number of phases was used.

Secondly, it does not even start the iteration when the initial K values proposed by them yield ill-posed RR problems that have no solution. Their initial K values often form an unbounded feasible region for the RR solution. No solution exists for such a case, as proved by Okuno et al. (2010).

Thirdly, their algorithm is initialized with an assumed maximum number of phases. During the iteration, if some of the phases (or iterative compositions) become close to one another, they are added together to decrease the number of iterative compositions. Subsequent computations are performed only for the distinct iterative compositions. That is, the number of iterative compositions only decreases, but does not increase, in their PH-flash algorithm. No scheme was proposed to handle the situation in which new phases appear in subsequent iterations as temperature changes in PH flash. This is problematic when the number and identities of phases change within the temperature domain of interest, as in steam injection simulation.

Fourthly, how to select a reference composition that was required to set the system of equations is unclear (Gupta et al. 1990, Alsaifi and Englezos 2011). Alsaifi and Englezos (2011) only stated in their paper on PT flash that a negative phase amount occurred when a reference composition was improperly selected.

2.5.3 Peng-Robinson Equation-of-State

As is explained in section 2.1.1, three-hydrocarbon-phase behavior was characterized by use of a cubic EOS (e.g., PR EOS and SRK EOS) for various solvent injection cases (e.g., Sharma et al. 1989, Okuyiga 1992, Khan et al. 1992, Creek and Sheffield 1993, Mohanty et al. 1995, Godbole et al. 1995, Guler et al. 2001, Kumar and

Okuno 2016).　Their results indicate that these EOSs are capable of correlating three-hydrocarbon-phase behavior quantitatively.　In this dissertation, PR EOS will be used in all phase behavior calculations.　The PR EOS is given as following:

$$P = RT/(\underline{V} - b) - a/[\underline{V}(\underline{V} + b) + b(\underline{V} - b)], \tag{2.51}$$

where $a = 0.45724(R^2 T_C^2/P_C)\alpha$,

$b = 0.07780 RT_C/P_C$,

$\alpha^{0.5} = 1 + \kappa[1 - (T/T_C)0.5]$,

$\kappa = 0.37464 + 1.54226\omega - 0.26992\omega^2$　for $\omega < 0.49$,

$\kappa = 0.379642 + 1.48503\omega - 0.164423\omega^2 + 0.016666\omega^3$　for $\omega \geq 0.49$.

The attraction (a) and covolume (b) parameters in a dimensionless form are $A = aP/(RT)^2$ and $B = bP/RT$.

The van der Waals mixing rules are used for the A and B parameters for a mixture.　That is,

$$A_m = \sum_{i=1}^{N_C} \sum_{k=1}^{N_C} x_i x_k A_{ik} \tag{2.52}$$

$$B_m = \sum_{i=1}^{N_C} x_i B_i, \tag{2.53}$$

where $A_{ik} = (A_i A_k)^{0.5}(1 - k_{ik})$.　k_{ik} is the binary interaction parameter between components i and k.

The fugacity coefficient of component i in phase j is

$$\ln\varphi_{ij} = \frac{B_i}{B_{mj}}(Z_j - 1) - \ln(Z_j - B_{mj})$$

$$- \frac{A_{mj}}{2\sqrt{2}B_{mj}}\left(\frac{2\sum_{k=1}^{N_C} x_k A_{ik}}{A_{mj}} - \frac{B_i}{B_{mj}}\right)\ln\left[\frac{Z_j + (1+\sqrt{2})B_{mj}}{Z_j + (1-\sqrt{2})B_{mj}}\right]. \tag{2.54}$$

The compressibility factor for phase j, Z_j, is calculated from the cubic EOS;

$$Z_j^3 + (B - 1) Z_j^2 + (A - 3B^2 - 2B) Z_j + (B^3 + B^2 - AB) = 0. \tag{2.55}$$
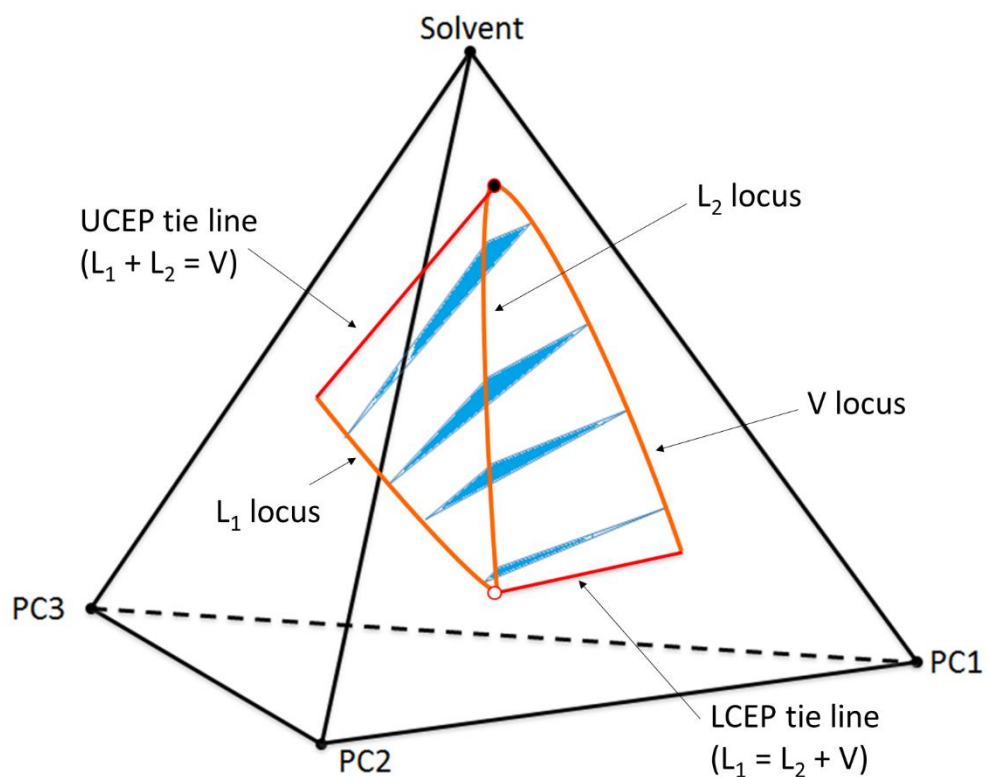
Figure 2.1.   Schematic of a three-phase region bounded by CEP tie lines for a quaternary system at a fixed temperature and pressure.   Four is the minimum number of components required to model three-phase behavior involving CEPs at a given temperature and pressure. The LCEP is the CEP where L_1 and L_2 phases merge in the presence of the V phase ($L_1 = L_2 + V$), and the UCEP is the CEP where V and L_2 phases merge in the presence of the L_1 phase ($V = L_2 + L_1$).

CHAPTER 3: A Unified Algorithm for Phase-Stability/Split Calculation for Multiphase PT Flash[1]

Conventional method for multiphase flash is the sequential usage of phase-stability and -split calculations. Multiphase flash requires the conventional method to obtain multiple false solutions in phase-split calculations and correct them in phase-stability analysis. Improvement of the robustness and efficiency of multiphase flash is important for compositional flow simulation with complex phase behavior.

This chapter presents a new algorithm that solves for stationary points of the tangent plane distance (TPD) function defined at an equilibrium-phase composition for isothermal-isobaric flash. A solution from the new algorithm consists of two groups of stationary points; tangent and non-tangent stationary points of the TPD function. Hence, equilibrium phases, at which the Gibbs free energy is tangent to the TPD function, are found as a subset of the solution.

Unlike the conventional method, the new algorithm does not require to find false solutions for robust multiphase flash. The advantage of the new algorithm in terms of robustness is more pronounced for more complex phase behavior, for which multiple local minima of the Gibbs free energy are present. It is straightforward to implement the algorithm because of the simple formulation, which also allows for an arbitrary number of iterative compositions. It can be robustly initialized even when no reliable information is available for the fluid of interest. Although the main focus of this chapter is on robust solution of multiphase flash, the new algorithm can be used to initialize a 2nd-order convergent method in the vicinity of a solution.

3.1 INTRODUCTION

A multiphase equilibrium calculation for a fixed pressure and temperature requires global minimization of the Gibbs free energy subject to material balance. The conventional algorithms after Michelsen (1982ab) are based on the sequential usage of phase-stability and -split calculations. That is, a phase-stability calculation is performed for the overall composition specified or one of the phases from a multiphase solution, at which the tangent plane to the Gibbs free energy surface is defined. If it detects phase instability, a phase-split calculation is performed under the assumption that one more equilibrium phase is present.

For instance, calculation for three equilibrium phases starts with testing the stability for the overall composition specified. Once phase instability is detected, a two-phase-split calculation is conducted for the overall composition. Then, phase stability is tested for one of the two phases obtained from the two-phase flash. After detecting the instability of the two-phase solution, a three-phase-split calculation is performed. Finally, one of the three phases is used to test the stability of the three-phase solution.

There are many algorithms presented in the literature for each of phase-split and -stability calculations for an assumed number of phases. Successive substitution is the classical algorithm used for each of phase-split and -stability calculations. It is linearly convergent for non-ideal mixtures, but known to be reliable (Mehra et al. 1983, Ammar and Renon 1987, Kaul 1992, Pan and Firoozabadi 2003, Michelsen and Mollerup 2004). Therefore, it is commonly used to provide an initial estimate for higher-order methods to achieve the final convergence (Mehra et al. 1982, Michelsen 1982b, Nghiem et al. 1983, Ammar and Renon 1987, Pan and Firoozabadi 2003).

Various algorithms were developed and compared for phase-split calculations for an assumed number of phases and phase-stability testing (Gautam and Seider 1979,

Ohanomah and Thompson 1984, Lucia et al. 1985, Trangenstein 1985, Trangenstein 1987, Ammar and Renon 1987, Litvak 1994, and Teh and Rangaiah 2002), such as interval methods (e.g., Hua et al. 1996, 1998ab, Xu et al. 2000, 2002, 2005, Tessier et al. 2000, Burgos et al. 2004), and trust region methods (Nghiem et al. 1983, Lucia and Liu 1998, Lucia and Yang 2003, and Lucia et al. 2012). A widely-used algorithm is minimization of the Gibbs free energy by use of Newton's method with a line-search technique, in which the modified Cholesky decomposition of Gill and Murray (1974) is used to provide a search direction when the Hessian matrix is not positive definite (Michelsen 1982ab, Perschke et al. 1989). A popular quasi-Newton method is the BFGS method for an inverse of the Hessian matrix approximation. Lucia and Macchietto (1983) and Venkatraman and Lucia (1986, 1987) developed a thermodynamically consistent quasi-Newton method on the basis of Lucia and Macchietto (1983).

The sequential use of phase-split and -stability calculations has been successfully applied for various compositional flow problems in the literature (e.g., Mehra et al. 1983, Nghiem and Li 1984, Perschke 1988, Han and Rangaiah 1998), and is called the conventional approach in this chapter. However, it is a series of local solutions for assumed numbers of phases, which requires obtaining and correcting false solutions for multiphase problems. Correction of false solutions in phase-stability analysis is highly sensitive to the initial guess used for the search for potential equilibrium phases. Also, it is not always possible to obtain a reasonable set of initial K values for multiphase reservoir fluids.

For example, three different types of two equilibrium phases ($L_1 + V$, $L_1 + L_2$, and $L_2 + V$) exist in composition space that contains three equilibrium phases ($L_1 + L_2 + V$), where L_1, L_2, and V stand for the oleic, solvent-rich liquid, and gaseous phases,

respectively. When $L_1 + L_2$ or $L_2 + V$ is of the global minimum in the Gibbs free energy at the specified flash conditions, conventional algorithms initiated with Wilson's correlation often fail to converge to the correct solution, or tend to be attracted by local minima before reaching to the correct solution through negative flash. However, no method has been established to estimate K values for a hydrocarbon mixture involving the L_2 phase.

One way to improve the robustness of multiphase flash is to use multiple initial guesses in a series of phase-stability analysis as suggested in Michelsen (1982b), Perschke (1988), and Li and Firoozabadi (2012). However, it still requires obtaining and correcting false solutions, which are often near local minima of the Gibbs free energy subject to material balance. As will be shown in this chapter, many stability calculations with different initial K values may be required to obtain merely a false solution in multiphase flash.

Gupta et al. (1990) presented a novel methodology to perform simultaneous phase-stability and -split calculations. Various issues with the algorithm of Gupta et al. (1990) and it variants (Abdel-Ghani 1995, Chaikunchuensakun et al. 2002, Alsaifi and Englezos 2011) are discussed in details in chapter 2.

This chapter presents the correct set of equations and constraints that can be easily solved for simultaneous phase-stability and -split calculation for PT multiphase flash. The formulation does not require the stability equations that the algorithm of Gupta et al. (1990) and its variants (Abdel-Ghani 1995, Chaikunchuensakun et al. 2002, Alsaifi and Englezos 2011) used. The main novelty lies in the unified usage of TPD function (Baker et al. 1982, Michelsen 1982a) for PT multiphase flash for an arbitrary number of iterative compositions. It allows for the flexibility in terms of the amount of information regarding the Gibbs free energy used during the iterative solution, by

controlling the number of iterative compositions initialized. A new algorithm is developed on the basis of successive substitution augmented with some important steps for global convergence for the formulated PT multiphase flash. Case studies are given to demonstrate the robustness and efficiency of the developed algorithm.

3.2 FORMULATION AND ALGORITHM

Global minimization of the Gibbs free energy in composition space for PT flash is formulated in such a way that all stationary points of the TPD function defined at the overall composition specified or one of the equilibrium phases must be non-negative. This is a direct representation of the classical criterion for phase equilibrium as explained in Baker et al. (1982). Section 2.5.1.1 gives the derivation of TPD equations. Equation 2.27 has been widely used to search for a stationary point of D_R in the stationary-point method of phase-stability analysis (Michelsen 1982a), as part of the conventional sequential phase-stability/-split calculation. In the stationary-point method, $\underline{z}$ is used to test the stability of the overall composition $\underline{z}$. For testing the stability of a multiphase system, $\underline{z}$ is set to one of the equilibrium phases under consideration. It is important to emphasize that equations 2.24 through 2.27 hold only when $\underline{x}$ corresponds to a stationary point of D_R.

Equation 2.27 reduces to the fugacity equations for N_P stationary points that are on the tangent plane T (i.e., N_P equilibrium phase compositions, at which $D_R = 0$). At all other stationary points, D_R should be positive since the T plane cannot lie above the G surface at any composition at an equilibrium state (Baker et al. 1982). Hence,

$$D_{Rj} = D_j/RT = \sum_{i=1}^{N_C} x_{ij}\left(\ln x_{ij}\varphi_{ij} - \ln x_{ir}\varphi_{ir}\right) \geq 0 \tag{3.1}$$

for j = 1, 2, …, N_S at a specified T and P. N_S is the number of stationary points of the dimensionless tangent plane distance function, D_R, defined with a reference equilibrium-

phase composition (x_{ir}, where i = 1, 2,..., N_C).   The fugacity coefficient of component i

at sampling composition j is denoted as φ_{ij}.   Note that $N_S = N_P + N_U$, where N_U is the

number of stationary points that are not equilibrium phases (i.e., N_U stationary points at

which $D_R > 0$).   Equation 3.1 can be also written as

$$D_{Rj} = \ln x_{ij}\varphi_{ij} - \ln x_{ir}\varphi_{ir} \geq 0 \tag{3.2}$$

when $\underline{x}_j$ (j = 1,2 ...,N_S) are all stationary points.

The unified formulation for phase-stability/-split calculation in the current chapter

is to find a set of x_{ij} (i = 1, 2, ..., N_C, and j =1, 2, ..., N_S) such that D_{Rj} = 0 subject to

equations 2.35 to 2.38 for equilibrium phases j = 1, 2, ..., N_P, and D_{Rj} > 0 subject to

equation 2.38 for the other stationary points that are not equilibrium phases j = (N_P + 1),

(N_P + 2)..., N_S.   The algorithm presented in this chapter uses the D_R function with

adaptive selection of the reference composition, $\underline{x}_r$, for an arbitrary number of iterative

compositions, which converge to stationary points with tangent plane distances D_{Rj}.

The TPD function is used in a unified manner for all stationary points of the TPD

at an equilibrium state, which consist of tangent stationary points (i.e., equilibrium-phase

compositions with zero TPD) and the other stationary points (i.e., compositions with

positive TPD values).   That is, equilibrium phases are considered as a subset of TPD

stationary points in the new formulation.   Then, multiphase PT flash is to find a tangent

plane to the Gibbs free energy such that it does not lie above the Gibbs free energy at all

stationary points identified.   In what follows, we first show working equations and then

a step-wise description of the algorithm.   The corresponding flow chart is given in

Appendix C.

The algorithm developed to solve the formulated problem does not require the

number of equilibrium phases to be set prior to the iteration.   It aims to find stationary

points of the TPD function defined at one of equilibrium phases upon convergence.

58

Iterative compositions are distributed in composition space in the initialization step, and they search for stationary points along the search directions determined by the traditional successive substitution. That is, the algorithm uses the TPD equations

$$f_{ij} = \ln[x_{ij}\varphi_{ij}] - \ln[x_{ir}\varphi_{ir}] - \theta_j = 0 \qquad (3.3)$$

to update all iterative compositions x_{ij} ($i = 1, 2, \ldots, N_C$ and $j = 1, 2, \ldots, N_S$) through K values on the basis of successive substitution. In equation 3.3, N_C is the number of components, and N_S is the number of iterative "sampling" compositions that capture thermodynamic information in composition space during the iteration.

It is important to note that the equations and variables used in the algorithm given in this section correspond to those in the formulation only upon convergence, because the formulation is based on an equilibrium state. For example, θ_j (equation 3.3) = D_{Rj} (equation 3.2) at an equilibrium state upon convergence. The number of iterative sampling compositions becomes the number of stationary points upon convergence, but both are denoted as N_S in this section. The reference composition x_{ir} ($i = 1, 2, \ldots, N_C$) is one of the sampling compositions during the iteration, and becomes one of tangent stationary points upon convergence.

As stated early in section, N_P equilibrium phases satisfy $D_{Rj} = 0$ along with equations 2.35 to 2.38 for $j = 1, 2, \ldots, N_P$. The other N_U stationary points satisfy $D_{Rj} > 0$ and equation 2.38 for $j = (N_P + 1), (N_P + 2)\ldots, N_S$, where $N_S = N_P + N_U$. During the iteration, N_S sampling compositions belong to either set P or U. In set P, $\theta_j = 0$ and $\beta_j > 0$ for $j = 1, 2,\ldots, N_P$. In set U, $\theta_j > 0$ and $\beta_j = 0$ for $j = (N_P + 1), (N_P + 2)\ldots, N_S$. Upon convergence, the sampling compositions in set P correspond to equilibrium phases, and sampling compositions in set U correspond to stationary points of the converged TPD function, at which D_R values are positive. In other words, the converged sampling

compositions in set P are tangent stationary points, and those in set U are non-tangent stationary points.

Successive substitution is performed to solve equation 3.3 together with equations 2.35 to 2.38 for K values, which are defined as

$$K_{ij} = x_{ij}/\left(e^{\theta_j}x_{ir}\right) \qquad (3.4)$$

for $i = 1, 2, \ldots, N_C$, and $j = 1, 2, \ldots, N_S$ except for the reference, r. The reference composition $\underline{x}_r$ is selected from set P adaptively, as will be described later.

For set P, equation 3.4 becomes $K_{ij} = x_{ij}/x_{ir}$. The conventional RR equations give the relationship between K values and mole fractions of apparent phases (β_j's) as follows:

$$g_j = \sum_{i=1}^{N_C}\left(x_{ir} - x_{ij}\right) = \sum_{i=1}^{N_C}\left(1 - K_{ij}\right)z_i/t_i = 0 \qquad (3.5)$$

for sampling point $j \neq r$ within set P, where $t_i = 1 - \sum_{k=1,k\neq r}^{Np}(1 - K_{ik})\beta_k$ for $i = 1, 2, \ldots, N_C$. Compositions are given as $x_{ir} = z_i/t_i$ and $x_{ij} = K_{ij}x_{ir}$ for sampling point $j \neq r$.

For set U, the summation constraint $\Sigma_i x_{ij} = 1.0$ gives

$$\theta_j = -\ln\left[\sum_{i=1}^{N_C} K_{ij}x_{ir}\right] \qquad (3.6)$$

for sampling composition j within set U. Compositions for set U are given as $x_{ij} = e^{\theta_j}K_{ij}x_{ir}$ for $i = 1, 2, \ldots, N_C$.

The fundamental structure of the current algorithm broadly follows the traditional successive substitution algorithm, but phase-stability and -split calculations are performed in an integrated manner. That is, each iteration first solves equations 3.5 for compositions for set P for a given set of K values and overall composition. Then, equation 3.6 is used to obtain compositions for set U for a given set of K values and reference composition. After that, K values are updated for sets P and U by use of equations 3.3 and 3.4; i.e.,

$$\ln K_{ij} = \ln\varphi_{ir} - \ln\varphi_{ij}. \qquad (3.7)$$

One of the most important factors that affect global convergence of the algorithm is how iterative sampling compositions are distributed in composition space (e.g., the number of initial sampling compositions and their locations). Sampling compositions can be initialized by use of a correlation suitable for the fluid of interest, such as Wilson's correlation, Li and Firoozabadi (2012), and Zhu and Okuno (2015b, 2016); or use of certain information from the previous time-step in flow simulation; or use of tie-simplex information in composition space (Iranshahr et al. 2010); or a systematic distribution in composition space if no reliable information is available regarding equilibrium phase compositions. Ideally, they are supposed to converge to all stationary points of TPD so that the global minimum of the Gibbs free energy is assured upon convergence. Such a possibility is generally expected to increase as more sampling compositions are used, unless they are placed close to each other. As an example for the fourth type of initialization, **Appendix C** describes the initialization method used in the case studies in this chapter, which systematically distribute sampling compositions in composition space. Obviously, there are many other distributions that are equally applicable for engineering applications.

In general, flash calculation is more efficient when it is initialized with certain reliable information available for expected equilibrium phases. In case studies in this chapter, the fourth type of initialization is used since they are all stand-alone multiphase flash. In one of the case studies, however, the new algorithm is tested with Wilson's correlation, and is shown to efficiently find a lower Gibbs free energy than the conventional sequential method.

Other important steps for enhanced robustness include the feasibility check for each RR solution by use of the method of Okuno et al. (2010). The constraint, $a_i^T \beta \leq b_i$, where $a_i = \{1 - K_{ij}\}$, $\beta = \{\beta_j\}$, $b_i = \min\{1 - z_i, \min_j\{1 - K_{ij}z_i\}\}$ for i = 1, 2, …, N_C, is to

be satisfied for compositions in set P if there exists a bounded feasible region for each RR solution as described in Okuno et al. (2010). Also, the constraints regarding β_j and θ_j described previously are used for classification of sampling compositions for sets P and U during the iteration.

The PR EOS (Peng and Robinson 1976, 1978) with the van der Waals mixing rules is used to calculate thermodynamic properties in this research. A stepwise description of the algorithm used in this chapter is given below.

Step 1. Set N_S sampling compositions $\underline{x}_j^{(k)}$ for $j = 1, 2,\ldots, N_S$. The number in the bracket represents the iteration-step number; $k = 1$ for the initial step.

Step 2. Calculate D_{Rj} for $j = 1, 2,\ldots, N_S$ with $\underline{z}$ as the reference composition by use of equation 3.1. Select the sampling composition with the minimum D_R value as the reference composition, $\underline{x}_r^{(1)}$. Calculate K values, $\underline{K}_j^{(1)}$, by use of $\ln K_{ij} = \ln\varphi_{ir} - \ln\varphi_{ij}$ for $i = 1, 2, \ldots, N_C$ and $j = 1, 2,\ldots, N_S$ except for r. Recalculate D_{Rj} with $\underline{x}_r^{(1)}$, and set N_U as the number of sampling compositions with positive D values. $N_P = N_S - N_U$. If $N_P > 1$, continue to step 3.

If $N_P = 1$, select $\underline{z}$ as $\underline{x}_r^{(1)}$. This increases N_S by one because $\underline{z}$ becomes part of the sampling compositions. Calculate $\underline{K}_j^{(1)}$, D_{Rj}, N_U, and N_P as described previously. If $N_P = 1$, go to step 6; otherwise, go to step 3.

Step 3. Check the feasibility of the RR solution for set P by use of the method of Okuno et al. (2010). If feasible, go to step 5. Otherwise, continue to step 4.

Step 4. Exclude from set P as many sampling compositions as required until the feasibility is satisfied for the given RR problem. Update N_P. $N_U = N_S - N_P$. If $N_P = 1$, go to step 6. Otherwise, continue to step 5.

62

Step 5. Perform the convex minimization to obtain $\underline{x}_j^{(k)}$ and $\beta_j^{(k)}$ for set P that satisfy equation 3.5, as presented in Okuno et al. (2010). The convergence criterion is that $\left\|g_j\right\|_\infty < \varepsilon_g$. $\varepsilon_g = 10^{-10}$ is used in this research, but it can be a larger number for practical applications.

Step 6. Obtain $\underline{x}_j^{(k)}$ and $\theta_j^{(k)}$ for set U by use of equation 3.6.

Step 7. Check to see if there is any $\theta_j^{(k)}$ that is negative in set U. If so, select the sampling composition that has minimum θ_j value as $\underline{x}_r$, and update N_U. $N_P = N_S - N_U$. Go to step 10. Otherwise, continue to step 8.

Step 8. Check to see if there is any $\beta_j^{(k)}$ that is negative in set P. If so, select the sampling composition with $0 < \beta_j < 1$ as $\underline{x}_r$ and update N_U. $N_P = N_S - N_U$. Go to step 10. Otherwise, continue to step 9.

Step 9. Check for convergence. Stop if $\left\|f_{ij}\right\|_\infty < \varepsilon_f$ (In this chapter, $\varepsilon_f = 10^{-10}$ is used, but it can be a larger number for practical applications). Otherwise, continue to step 10.

Step 10. Check to see if there are any compositions to be merged on the basis of the criterion that the max norm for two compositions is less than ε_x (e.g., $\varepsilon_x = 10^{-3}$). If so, perform necessary updates for N_S and N_U. $N_P = N_S - N_U$.

Step 11. Update K values by use of equations 3.3 and 3.4; i.e., $\ln K_{ij}^{(k+1)} = \ln\varphi_{ir}^{(k)} - \ln\varphi_{ij}^{(k)}$ for $i = 1, 2, \ldots, N_C$ and $j \neq r$. Increase the iteration-step index by one; $k = k + 1$. Go to step 6 if $N_P = 1$. Otherwise, go to step 3.

Steps 1, 5, 9, and 10 require user-specified values. The procedure presented in Appendix C is used for step 1 in this chapter. However, it can be replaced by other procedures, such as correlations for the fluid under consideration, the flash solution from

the previous time step in flow simulation, and use of a random number generator. Steps 5 and 9 require convergence criteria, and step 10 requires a merging criterion.

Step 2 sets the reference composition that is required to define equation 3.3 in the initialization. First, TPD is calculated by function D_R (equation 3.1) at N_S sampling compositions with the overall composition $\underline{z}$ as the reference composition, $\underline{x}_r$. Then, the initial reference composition is re-defined that gives the minimum D_R among the N_S sampling compositions. Note that equation 3.2 cannot be used for this initialization step as the N_S initial sampling compositions are not stationary points of TPD defined at $\underline{z}$. Steps 7 and 8 describe how to update a reference composition when the constraints regarding β_j and θ_j are not satisfied during the iteration.

In step 4, the exclusion of sampling compositions from set P is performed on the basis of their D_{Rj} values from equation 3.1. That is, the sampling composition with the largest D_{Rj} value among set P is first excluded. The subsequent exclusions, if necessary, are in the order of decreasing D_R. If step 4 is taken in the first iteration (k = 1), the D_{Rj} values calculated in step 2 are directly used.

In step 5, it is crucial to precisely implement the multiphase RR algorithm as described in Okuno et al. (2010). In particular, it is recommended to confirm the following for each RR solution:

- The feasible region for β_j (j = 1, 2, …, N_P) should be based on non-negativity of components' mole fractions, $0 \leq x_{ij} \leq 1$ (i = 1, 2, …, N_C, and j = 1, 2, …, N_P). Note that the function to be minimized in the RR solution is non-monotonic and convex within its feasible region (Michelsen 1994, Michelsen and Mollerup 2004, Okuno et al. 2010).

- The initial values for β_j (j = 1, 2, …, N_P) should be placed inside the feasible region.

- Under-relaxation should be performed if a Newton step is found to bring the iterate to the infeasible domain, in order to keep β_j ($j = 1, 2, \ldots, N_P$) feasible. It is straightforward to calculate the maximum step size to be taken to reach a feasibility limit along a given search direction (Newton's direction) because the feasibility limits are all linear (Equation 10 in Okuno et al. 2010).

The new algorithm is to locate stationary points of TPD that gives the global minimum of the Gibbs free energy at the specified T and P with the well-known convergence behavior of successive substitution (Mehra et al. 1983, Ammar and Renon 1987, Kaul 1992). Michelsen (1982a) showed that successive substitution for the stationary-point method of phase stability analysis converges to a minimum, instead of a maximum or saddle point, of the TPD function. It has been observed in this research that the developed algorithm also converges to minima of the TPD function.

In the new algorithm, equilibrium phases are found as a subset of the converged stationary points; that is, the number of phases is part of the solution. One of the main differences from the conventional flash is that the unified TPD equations (equation 3.3) can be solved with an arbitrary number of sampling compositions. This gives the flexibility in terms of robustness and efficiency that the algorithm offers; e.g., use of more sampling compositions increases the level of robustness at the expense of the increased number of equations, at least for the initial stage of iteration. As will be discussed later, extra sampling compositions naturally merge for a case in which N_S is greater than the number of stationary points present upon convergence.

The algorithm presented above is substantially different from that of Gupta et al. (1990). An important difference comes from the difference in formulation; that is, they introduced an additional set of equations, $\beta_j \theta_j = 0$, called "stability equations" in their papers. A similar set of equations, $\beta_j \theta_j / (\beta_j + \theta_j) = 0$, were then solved simultaneously

65

with the RR equations in their algorithm. However, our formulation clearly shows that the complete formulation does not require Gupta et al.'s stability equations. The correct set of equations in this chapter does not have the degeneracy issues that Gupta et al.'s algorithm exhibits near phase boundaries due to their stability equations, as reported by Alsaifi and Englezos (2011).

The robustness of the current algorithm also comes from careful initialization (step 1) and adaptive selection of the reference composition (steps 2, 7 and 8). The initialization scheme of Gupta (1990) eliminates the sampling compositions that have positive D values from equation 3.1 with $\underline{z}$ as the reference composition. However, this often leads to a complete failure of the calculation.

The simplicity of the formulation has led to the straightforward iteration steps, which are essentially the widely used successive substitution. Unlike in other related publications after Gupta et al. (1990), such as Abdel-Ghani (1995), Chaikunchuensakun et al. (2002), and Alsaifi and Englezos (2011), the robust solution of multiphase RR equations (Okuno et al. 2010) further enhances the robustness of the current algorithm.

3.3 CASE STUDIES

The new algorithm can make multiphase flash problems straightforward by not having to solve for false solutions and correct them. This section presents case studies to demonstrate the robustness and simplicity of the new algorithm with the initialization method presented in Appendix C. The convergence criteria used for the new algorithm are stated in the previous section (e.g., $\varepsilon_f = \varepsilon_g = 10^{-10}$ and $\varepsilon_x = 10^{-3}$).

The new algorithm is compared with the conventional method of sequential phase-stability/split calculations and the method of Gupta et al. (1990). In the sequential method used for this section, single-phase stability analysis is performed with

two initial guesses, searching for a V-like phase first and a L-like phase next, on the basis of Wilson's K values (Michelsen 1982a). For stability analysis for multiple phases, initial guesses recommended by Firoozabadi (1999) and Li and Firoozabadi (2012) are used in addition to the V-like and L-like guesses, in the following order: a V-like phase, a L-like phase, compositions near vertices in composition space, the midpoint of phase compositions, and $\varphi_i x_i$ for $i = 1, 2,\ldots, N_C$.

Calculations in this section use only successive substitution for a fair comparison in terms of robustness. However, the new algorithm based on successive substitution can be switched to any 2nd-order convergent method in the vicinity of a solution, when the residual of equation 3.3 becomes less than a certain criterion as will be shown for case 4. Direct application of Newton's method for the formulated problem requires further investigated. The iteration scheme used for the new algorithm is essentially the traditional successive substitution. As presented in Heidemann and Michelsen (1995), successive substitution may not converge if negative binary interaction parameters are used for attraction terms in a cubic-EOS fluid model.

The convergence criterion used for stability analysis in the conventional method is that the max norm of stationarity equations is less than 10^{-10}. The convergence criterion used for phase-split calculations in the conventional method is that the max norm of fugacity equations is less than 10^{-10}. Use of 10^{-10} for these convergence criteria are equivalent to the use of $\varepsilon_f = 10^{-10}$ for the new algorithm. The criterion used for a trivial solution in the conventional stability analysis is 10^{-3}, which is equivalent to the merging criterion $\varepsilon_x = 10^{-3}$ in the new algorithm.

The number of fugacity-coefficient calculations is reported as a measurement of computational cost, in addition to the number of iterations required for convergence, for each case. Both metrics depend on the initial N_S and their locations with the new

algorithm; i.e., results regarding the computational cost will be different if other initialization methods are used.   A calculation for a vector consisting of $\ln\varphi_i$ for i = 1, 2,…, N_C is counted as one.

The new PT flash algorithm finds all stationary points of the TPD function defined at one of equilibrium phases upon convergence.   We studied the number of stationary points of 24 simple mixtures available in the literature.   Results were given in Appendix C.

3.3.1   Case 3.1

Case 3.1 uses mixtures of H_2O, C_3, and n-C_{16} to graphically show a few important features of the new algorithm.   The properties used for the components are given in **Table 3.1.**   Appendix C also gives a sample input file for case 3.1.   **Figure 3.1** shows the two- and three-phase regions in composition space at 430 K and 35 bars for the ternary system.   In this figure, L, V, and W represent the oleic, gaseous, and aqueous phases, respectively.

The new algorithm is applied with the initial N_S of six along the mixing line between (0.0, 0.9, 0.1) and (0.9, 0.0, 0.1).   Out of the six sampling compositions, three compositions are placed near the compositional vertices, and the others are the central points in the three regions surrounding a given overall composition (R_i for i = 1, 2, and 3 as given in Appendix C).   The six sampling compositions initially distributed merge into three stationary points that correspond to the L, V, and W phases on the Gibbs free energy surface.   **Figure 3.2** shows the Gibbs free energy surface at 430 K and 35 bars, and the tangent planes converged for three overall compositions with the H_2O concentrations of 0.10, 0.75, and 0.84 along the mixing line.   It has been visually

68

confirmed that the algorithm has successfully converged to the global minimum of the Gibbs free energy subject to material balance for each overall composition.

Figure 3.3 shows the behavior of the converged β_j and θ_j along the mixing line. One non-tangent stationary point in set U is observed in the two-phase regions (L + V and L + W) along the mixing line. The D_R values at such non-tangent stationary points in Figure 3.2 can be confirmed with Figure 3.3b; e.g., θ_W of 0.2478 for $z_{H2O} = 0.1$. They qualitatively indicate how close the current equilibrium state is to a phase transition as can be seen in Figure 3.3b. Hence, the new algorithm provides more global information about the Gibbs free energy than the conventional sequential method, when it converges to non-tangent stationary points with positive D_R values.

Figures 3.1, 3.2, and 3.3 present that different sets of equilibrium phases can be easily calculated as thermodynamically stable stationary points by use of the unified algorithm that directly converges to the correct solution. Unlike the current algorithm, the negative flash approach (Whitson and Michelsen 1989) may indicate phase instability by negative β values, when obtaining a false solution.

The new algorithm is compared with the method of Gupta et al. (1990) by using the overall composition of 75% H_2O, 15% C_3, and 10% n-C_{16} at 560 K and 65 bars. The critical endpoint of type $L_1 = V + W$ is calculated for this mixture at 569.35 K and 130.07 bars on the basis of the PR EOS. The correct solution of $L_1 + V$ is given in **Table 3.2.** The method of Gupta et al. (1990) cannot converge to this solution for several reasons. Firstly, the initialization scheme proposed by Gupta (1990) yields a RR problem with an unbounded feasible domain, resulting in a failure in initialization. Secondly, even when initialized successfully with the method given in Appendix C (e.g., $N_S = 6$), their algorithm stops from proceeding at the 10th iteration step due to an open feasible domain

69

encountered for RR solution. This type of failures occurs for the next cases with the algorithm of Gupta et al. (1990), although they are not presented in this section.

As an example for the new algorithm, **Figure 3.4** shows the convergence behavior in terms of N_P and N_U, and the residual of equation 3.3, when it is initialized with $N_S = 6$ (i.e., three compositions near the compositional vertices and the other three at the centers of R_i for $i = 1$, 2, and 3 by use of $N_{Smax} = 6$ and $n = 1.0$). The new algorithm converges to the correct solution given in Table 3.2 in 21 iterations. Merging of sampling compositions (in set P and/or set U) occurs at the 4th, 5th, and 7th iterations, as indicated by decreasing N_S ($= N_U + N_P$) in Figure 3.4a. Hence, the algorithm takes 7 iteration steps to identify the correct number of stationary points in this case, when started with the 6 sampling compositions. A stable linear convergence rate is observed until the convergence is achieved, as with the normal successive substitution (Figure 3.4b). The reference composition, $\underline{x}_r$, remains the same after the 8th iteration in this case. The total number of fugacity coefficient computations is 84, in which 25 computations were performed for initialization to determine a reference composition; hence, on average, each iteration took approximately 3 computations of fugacity coefficient vectors. **Appendix D** shows a series of ternary diagrams to explain the motion of sampling compositions for selected iterations.

It has been confirmed that the new algorithm still converges to the correct solution in 22 iteration steps when initialized with only three sampling compositions near the composition vertices for this relatively simple case. The total number of fugacity coefficient computations is 66, in which 13 computations were performed in initialization; hence, the average number of fugacity coefficient computations is 3 per iteration.

70

The conventional method of sequential phase-stability/-split calculation is also tested for this case. In the single-phase stability test, a trivial solution is detected in 53 iteration steps with a V-like composition for the first trial. Then, instability is detected in 14 iteration steps with a L-like composition for the second trial. Then, the subsequent two-phase-split calculation converges to the solution (Table 3.2) in 24 iterations. Phase instability cannot be detected with all 9 guesses for this two-phase solution. The total number of iterations required in this two-phase stability test is 175. Hence, the total number of iterations required for the conventional sequential method is 266, in comparison with 21 for the new algorithm with N_S of 6. The total number of fugacity coefficient computations is 301 with the conventional algorithm, in comparison with 84 with the new algorithm with N_S of 6. For this case, the new algorithm with N_S of 6 requires much fewer iterations and fugacity calculations than the conventional sequential algorithm.

Unlike in Gupta et al. (1990), the RR routine embedded in the new algorithm is guaranteed to converge to the correct solution as shown in Okuno et al. (2010). It is important to confirm the existence of the unique solution for a given multiphase RR problem prior to the iteration (Okuno et al. 2010).

3.3.2 Case 3.2

The simplicity of the formulation and algorithm developed in this research yields the robustness in multiphase flash by not having to obtain false solutions. The advantage over the conventional sequential methods is pronounced when the correct solution in a multiphase calculation does not include either the L_1 or V phase, which can frequently occur in many gas and steam injection processes with multiple partially miscible phases.

This case uses the binary system of C_1 and H_2S at 190 K and 40.53 bars to show several issues of the sequential method and the robustness of the new algorithm. **Table 3.3** gives the components' properties. The Gibbs free energy surface in composition space exhibits three lobes corresponding to the L_1, L_2, and V phases in the order of increasing C_1 concentration (z_{C1}) **(Figure 3.5).** The sequential method fails to find the correct solutions with $L_2 + V$ for z_{C1} from 0.968 to 0.982, as explained below.

For $0.968 \leq z_{C1} < 0.980$, the sequential algorithm finds a L phase in the single-phase stability analysis, and the subsequent two-phase flash results in a local minimum with $L_1 + V$. Then, the stability analysis for one of the two phases finds the L_2 phase. However, three-phase PT flash is not possible for a binary mixture, for which P and T are interdependent (i.e., the degree of freedom is one). Hence, the final result from the sequential algorithm is the $L_1 + V$ phases that have been obtained. **Table 3.4** shows the correct solution from the new algorithm and the incorrect solution from the sequential method at z_{C1} of 0.970 at 190 K and 40.53 bars.

The new algorithm converges to the correct two-phase solution ($L_2 + V$) directly without having to find any false solution. Here, the convergence of the new algorithm is explained for the case with the initial N_S of eight ($N_{Smax} = 16$ and $n = 1.0$). Two of them are distributed near the vertices of composition space, and three sampling compositions are evenly distributed for each side of the overall composition. **Figure 3.6** shows the variation of N_P and N_U, and the residual of equation 3.3 with respect to the number of iterations for this case. The new algorithm successfully converges to the correct solution (Table 3.4) in 92 iterations. The converged Gibbs free energy ($\underline{G}_R$) from the new algorithm, -0.53949050, is confirmed to be lower than the value, -0.53769775, from the sequential method.

72

In the initialization, N_P of one occurs in the initialization, which increases N_S by one as the overall composition becomes part of the sampling compositions in such a case (step 2 in the algorithm). Reselection of reference composition (steps 7 and 8 of the new algorithm) occurs frequently from iterations one to six, in which step 8 is only used at the 4th iteration and step 7 at the other five iterations. Merging of sampling compositions occurs at the 1st, 10th, and 31st iterations, as shown by decreasing N_S ($= N_P + N_U$) in Figure 3.6a. From the 31st iteration, N_S becomes the total number of stationary points, three, on the D_R function. At the convergence, two of the three stationary points correspond to the two equilibrium phases (i.e., set P), and the other is a non-tangent stationary point (i.e., set U) with a positive D_R (Table 3.4). The residual of equation 3.3 shown in Figure 3.6b indicates a linear convergence rate for a fixed reference composition, $\underline{x}_r$. The total number of fugacity-coefficient computations is 348, out of which 33 computations are performed in the initialization to determine a reference composition. The average number of fugacity-coefficient computations per iteration is approximately 3. **Appendix D** also demonstrates the motion of all sampling compositions for selected iteration steps, in which merging and convergence of sampling compositions are clearly shown.

To see the number of iterations required for robust convergence with respect to the initial N_S used, the initial N_S was controlled by changing N_{Smax} by two with $n = 1.0$ with the procedure given in Appendix C. The initial N_S required for robust convergence is 8 in this case. The numbers of iterations required for convergence are 92, 86, and 76 for the initial N_S of 8, 10, and 12. The number of stationary points detected upon convergence is 3 for $N_S \geq 8$. The numbers of fugacity-coefficient calculations are 348, 341, and 327 for the initial N_S of 8, 10, and 12.

73

When initialized with N_S of 4 (two near the edges of composition space and the other two at the centers of both sides of the overall composition), the algorithm does not converge to the global minimum of the Gibbs free energy. To explain this, **Figure 3.7** shows the TPD in composition space at 190 K and 40.53 bars. The correct two-phase solution of $L_2 + V$ is represented by the black dots on the D_R function. The hollow square dot is a local minimum located on D_R. Only two stationary points are located when the algorithm is initialized with only four sampling compositions. These two stationary points correspond to the L_1 and V lobes on the Gibbs free energy surface (see Figure 3.5), which do not yield the global minimum of the Gibbs free energy.

For $0.980 \leq z_{C1} \leq 0.982$, the sequential algorithm fails to find any phase instability in single-phase stability analysis. However, the new algorithm properly converges to the L_2 and V phases. **Table 3.5** shows the solution for z_{C1} of 0.980. The Gibbs free energy ($\underline{G}_R$) at the solution, -0.49203424, is confirmed to be lower than the single-phase Gibbs free energy -0.49183831.

Even if the degree of freedom is more than one for the sequential method, it has been observed in various flow-simulation cases that the sequential method initiated with Wilson's K values tends to fail to find the correct solution that does not involve the L_1 or V phase. An example is the ternary mixture of 60% CO_2, 12% C_1, and 28% n-C_{20} at 250 K and 38 bars. Three phases of L_1, L_2, and V are present in composition space, and the overall composition in the L_1-L_2 region is located in the vicinity of the tie triangle. The sequential method cannot find phase instability in the two-sided stability analysis with the V and L estimates from Wilson's correlation. Case 4 will provide another example of this kind.

3.3.3 Case 3.3

This case uses a mixture of North Ward Estes (NWE) oil (Khan et al. 1992), H_2O, CO_2, n-C_4, and n-C_{10}. The NWE oil has been characterized with six components; therefore, there are ten components altogether. Components' properties and the overall composition are given in **Table 3.6.** The CEP of type $V = L_2 + L_1$ is calculated by use of the PR EOS at 452.80 K and 86.04 bars for this mixture. Three equilibrium phases, $V + L_1 + L_2$, coexist at 459 K and 87 bars (i.e., close to the CEP).

The new algorithm is tested with different initial numbers of sampling compositions (N_S). For this purpose, N_S is controlled by changing N_{Smax} from 20 to 95 by adding 15 with n = 1.0. The number of stationary points (minima) detected upon convergence is four for all initial N_S tested; three tangent-stationary points (i.e., set P) and one non-tangent-stationary point (i.e., set U).

To explain this case specifically, the new algorithm is initialized with $N_S = 20$ ($N_C = 10$, $N_{Smax} = 20$, and n = 1.0). In addition to ten sampling compositions placed near the ten composition vertices, ten sampling compositions are distributed at the central points of regions R_i for i = 1, 2,…, 10 in composition space around the overall composition (Appendix C).

Figure 3.8 shows the convergence behavior in terms of N_P, N_U, N_S, and the residual of equation 3.3 with the new algorithm. The new algorithm converges to the correct solution in 823 iterations, as shown in **Table 3.7,** in which the compositions of V and L_2 are close to each other. Upon convergence, three equilibrium compositions are in set P, and one non-tangent stationary compositions is in set U. The non-tangent stationary point is converged near 100% water with $\theta = 0.79$. The Gibbs free energy ($\underline{G}_R$) converged with the new algorithm is -2.67985726.

In the initialization, two sampling compositions are in set P, and the other 18 compositions are in set U. Merging of sampling compositions in set P and/or set U reduces N_S during the iteration (Figure 3.8c). Reselection of the reference composition occurs frequently between iterations one and eleven, iterations 21 and 62, and iterations 148 and 206, resulting in the oscillation of N_P and N_U during these iterations (Figures 3.8a and 3.8b). Accordingly, the residuals of equation 3.3 for sets P and U also exhibit oscillations, as can be seen in Figures 3.8d and 3.8e. At the 206th iteration, the correct N_P of three is identified, from which the residual of equation 3.3 for set P starts decreasing steadily (Figures 3.8a and 3.8d). At the 243rd iteration, N_U decreases from two to one, which makes the residual of equation 3.3 for set U decrease discontinuously, as presented in Figures 3.8b and 3.8e. From the 243rd iteration on, a stable linear convergence rate is observed with the final number of stationary points ($N_P = 3$ and $N_U = 1$). Between the 700th and the 823rd iterations, the residual of equation 3.3 for set U exhibits oscillations around 10^{-14}, which is much lower than the convergence criteria (10^{-10} as used in this section). This is likely because, in this particular case, the residual for set U is sensitive to the TPD function which is varying with varying compositions in set P before the final convergence (i.e., the TPD is defined with a reference composition in set P).

The numbers of iterations required for convergence are 823 and 737 for the initial N_S of 20 ($N_{Smax} = 20$ with n = 1.0) and 40 ($N_{Smax} = 96$ with n = 1.0), respectively. For N_S of 20, the total number of fugacity-coefficient computations is 3861, out of which 81 computations are for the initialization. Therefore, the number of fugacity calculations per iteration is approximately 5 for this case.

The conventional sequential phase-stability/-split calculation is also tested for this case. **Figure 3.9** shows the number of iterations required for each step of the

conventional sequential method.   The initialization procedure for the conventional method was explained earlier in this section.   Single-phase stability analysis detects an instability with a V-like phase composition at the 96th iteration.   Then, the subsequent two-phase split calculation converges to a false two-phase solution in 456 iterations. After that, two-phase stability analysis detects an instability of the two-phase solution using the 2nd initial guess.   The first guess takes 128 iterations, but they are unable to identify any phase instability.   The 2nd guess then takes 166 iterations until phase instability is detected.   A three-phase split calculation is performed with the initial K-value estimates obtained from two-phase-stability test, and converges to a solution in 708 iterations.   Phase instability cannot be detected for this three-phase solution using all of the 23 sets of initial guesses.   The number of iterations taken by this three-phase stability analysis is 9782.   That is, the conventional sequential method requires 11336 iterations for its final solution of three phases.   The total number of fugacity-coefficient calculations is 13234 with the sequential method.   Computations in the three-phase stability are counted for a fair comparison with the new algorithm because the new algorithm has found a non-tangent stationary point as shown in Table 3.7.   However, the new algorithm is shown to require fewer iterations and fugacity computations even without considering the three-phase stability for the sequential method.   These results show that the convergence of the new algorithm is more rapid than that of the sequential algorithm in terms of iteration and fugacity calculation for this case.

3.3.4   Case 3.4

Case 3.4 uses a four-component EOS fluid model based on the Bob Slaughter Block (BSB) oil that was originally characterized by Khan et al. (1992) with seven components.   This quaternary model for the BSB oil (BSB-Q) was used previously in

Okuno et al. (2011). Parameters for the BSB-Q oil are given in **Table 3.8**. The new and conventional algorithms are compared for flash calculation of the BSB-Q oil at 313.706 K and 82.737 bars.

The new algorithm converges to two tangent stationary points (L_1 and L_2) in set P and one non-tangent stationary point (V) in set U, when 12 or more sampling compositions are initially distributed based on the method given in Appendix C. **Table 3.9** summarizes the converged solution.

For the initial N_S of 12, the convergence is achieved in 161 iterations. The converged $\underline{G}_R$ value is −3.45251125. The total number of fugacity-coefficient vector computations is 720, of which 49 computations are for the initialization. The number of fugacity-coefficient vector computations is approximately 4 per iteration. **Figure 3.10** shows the convergence behavior of the new algorithm. It requires 42 iterations to identify the correct number of stationary points; i.e., $N_P = 2$ and $N_U = 1$ (Figures 3.10a and 3.10b). Merging of sampling compositions occurs at iteration steps 8, 11, 16, 19, 20, 21, 23, 37, and 42, resulting in reduction of N_S as shown in Figure 3.10c. Reselection of the reference composition, $\underline{x}_r$, by use of steps 7 and 8 of the new algorithm occurs frequently until the 26th iteration. At the 42nd iteration, N_U becomes the final number of non-tangent stationary points through merging, resulting a significant decrease in the residual for set U (Figure 3.10e).

The conventional sequential method is shown to converge to an incorrect solution for this case. **Figure 3.11** shows the number of iterations required for each step of the sequential phase-stability/-split calculations. The single-phase stability finds an instability with a V-like initial composition (i.e., the first guess) in 18 iterations. Then, the subsequent two-phase flash converges in 47 iterations. After that, two-phase stability analysis with six different estimates finds no instability after the total of 688

iterations. With the 7th initial guess (i.e., the midpoint), an instability is detected in 128 iterations. Three-phase flash is performed with the initial K values obtained from two-phase stability analysis and converges in 141 iterations. This three-phase flash results in negative phase amounts, i.e., negative flash. Hence, another two-phase flash is performed, and it converges in 49 iterations. Then, phase stability analysis for the new two-phase solution with 11 different initial guesses finds no instability, taking 855 iterations. Finally, two phases are assumed to be stable, after the total of 1926 iterations. The number of fugacity-coefficient vector calculations is 2323. However, the converged $\underline{G}_R$ value is -3.45110691, which is higher than the $\underline{G}_R$ obtained from the new algorithm (-3.45251125). This indicates that the two-phase solution obtained from the conventional sequential method is a local minimum of Gibbs free energy. The new algorithm converged to a lower Gibbs free energy with much fewer iterations and fugacity computations.

The new algorithm based on successive substitution can be used to initialize a 2nd-order convergent method with set P, as mentioned previously. Here, the current case is used to show the convergence behavior of the new algorithm and an in-house 2nd-order algorithm (Okuno et al. 2010b) with different switching criteria. The final convergence criterion used for the 2nd-order algorithm is 10^{-10}, as in all case studies in this section. The switching criterion used with equation 1 for sets P and U range from 10^{-2} to 10^{-6}. **Table 3.10** summarizes the number of iterations for the new algorithm before switching and the 2nd-order algorithm after switching for each of the switching criteria used. After switching to the 2nd-order algorithm, the correct convergence is achieved rapidly in three or fewer iterations for all the cases tested. As an example, the convergence behavior before and after switching is shown in Figure 3.10d with the switching criterion of 10^{-2}. The new algorithm is used until the 38th iteration, and is switched to the 2nd-order

algorithm when the residual of equation 3.3 is below 10^{-2} for both sets P and U. Then, the rapid convergence is achieved in three iterations, as shown by the star markers in Figure 3.10d. The total number of iterations required for convergence is 41. Use of the 2nd-order algorithm after switching at 10^{-2} results in four times more rapid convergence in terms of number of iterations in comparison with the use of the new algorithm alone.

Another test is conducted by using Wilson's correlation to initialize the new algorithm with only two sampling compositions, one V-like and one L-like compositions. The new algorithm converges in 190 iterations to the same solution presented in Table 3.9; i.e., two tangent stationary points (L_1 and L_2) in set P and one non-tangent stationary point (V-like) in set U. The total number of fugacity-coefficient vector computations is 582, of which 9 computations are for the initialization. Hence, the number of fugacity-coefficient vector computations is approximately 3 per iteration.

Figure 3.12 shows the convergence behavior of the new algorithm. The correct number of stationary points [i.e., $N_P = 2$ and $N_U = 1$ (Figures 3.12a and 3.12b)] is identified at the 55th iteration. In the initialization, N_P of one occurs, which increases N_S by one when the overall composition becomes an additional sampling composition (step 2). Merging of sampling compositions does not occur for this case. Hence, N_S remains three until the final convergence is achieved. Reselection of reference composition, x_r, by use of steps 7 and 8 of the new algorithm occurs at iteration steps 1, 2, 20, and 55. In Figure 3.12c, a significant increase in the residual of the TPD equations occurs for set P at the 20th iteration when N_P is increased from two to three. N_U is zero between iteration steps 20 and 54, for which the residual of the TPD equations for set U does not exist in Figure 3.12d. From the 55th iteration until the convergence, N_P and N_U are the final numbers of tangent stationary points and non-tangent stationary points; i.e., two and three, respectively.

It was observed that the current algorithm could exhibit non-convergence when the binary interaction parameters of PC2 with C_1 and PC1 were set to -0.5. Hence, the current algorithm is considered to possess the inherent limitation of successive substitution (Heidemann and Michelsen 1995) as mentioned at the beginning of this section.

3.4 SUMMARY

This chapter presented a new algorithm for isothermal-isobaric flash for an arbitrary number of phases. The unified formulation developed for simultaneous phase-stability/split calculation is based on the classical criterion of phase equilibrium, as explained in Baker et al. (1982). The correct set of equations is solved with successive substitution for stationary points of the tangent plane distance defined at a reference phase composition. Although the main focus of this chapter was on robust solution of multiphase flash, the new algorithm can be used also to initialize a 2nd-order convergent method in the vicinity of a solution. Conclusions are as follows:

1.   The number of equilibrium phases is part of the solution in the new algorithm, in contrast to the sequential stability/flash approach. It is not necessary to find false solutions and correct them for robust multiphase flash with the new algorithm. The advantage of the new algorithm in terms of robustness is more pronounced for more complex phase behavior, in which multiple local minima of the Gibbs free energy are present.

2.   The new algorithm can be initialized even when no reliable information is available about the equilibrium phases of the fluid of interest. In the method used for initializing the algorithm, N_C sampling compositions are distributed near compositional vertices, and the others are systematically distributed around the overall composition

specified. No K-value correlation is necessary to initialize the new algorithm. This also yields the flexibility that the new algorithm offers in terms of robustness and efficiency. For example, one can initialize the algorithm with more sampling compositions for enhanced robustness by capturing more information regarding the Gibbs free energy during the iteration. If reasonable estimates are available for equilibrium phases (e.g., correlations, the solution from the previous time step in flow simulation, and tie-simplex tabulation), one can use them to reduce the number of equations to be solved.

3. The new algorithm does not use the stability equations of Gupta et al. (1990) because they are not necessary with the formulation presented in this research. Consequently, there is no need to solve the augmented Jacobian matrix that must be solved at each iteration in the algorithm of Gupta et al. (1990). Also, the new algorithm does not exhibit the convergence problems that are associated with the stability equations of Gupta et al. (1991).

4. Case studies showed that the new algorithm finds more stable solutions (lower Gibbs free energy) for the complex cases tested, for which the conventional method only finds local minima. It was shown that the new algorithm can find non-tangent stationary points of the tangent-plane-distance function, if present, in addition to equilibrium phases.

5. The iteration scheme of the new algorithm is the traditional successive substitution, of which convergence behavior has been studied in the literature (e.g., Michelsen 1982a, Mehra et al. 1983, Ammar and Renon 1987, Kaul 1992). The new algorithm can be used to initialize a 2nd-order convergent method as demonstrated in case 4. It is expected to be more difficult for the algorithm to converge for mixtures that exhibit a large negative deviation from an ideal solution, according to the analysis of Heidemann and Michelsen (1995).

Table 3.1: Properties of the components for case 3.1

Component	T_C, K	P_C, bars	Acentric factor
H_2O	647.3000	220.8900	0.3440
C_3	369.8000	42.4600	0.1520
$n-C_{16}$	717.0000	14.1900	0.7420
Binary interaction parameters:			
	H_2O	C_3	$n-C_{16}$
H_2O	0.0000	0.6841	0.3583
C_3		0.0000	0.0000
$n-C_{16}$			0.0000

Table 3.2: Solution for case 3.1 with the new algorithm

Component	L	V
H_2O	0.32452700	0.79574966
C_3	0.09549610	0.15586062
$n-C_{16}$	0.57997690	0.04838973
β	0.09708713	0.90291287
θ	0.00000000	0.00000000
$\underline{G}_R/RT$	-0.96787252	

Properties of the components are given in Table 3.1. The overall composition is 75% H_2O, 15% C_3, and 10% $n-C_{16}$. The specified temperature and pressure are 560 K and 65 bars, respectively. The algorithm of Gupta et al. (1990) fails for this case, due to an open feasible domain in the RR problem based on their initialization scheme.

Table 3.3: Properties of the components for case 3.2

Component	P_C, bars	T_C, K	Acentric factor
C_1	46.0016	190.6000	0.0080
H_2S	89.3686	373.2000	0.1000
The binary interaction parameter between C_1 and H_2S is 0.0800.			

Table 3.4: Results for case 3.2 with the new and conventional algorithms

	New algorithm			Conventional algorithm	
	L_1	V	L_2	L_1	V
C_1	0.18666898	0.98270136	0.93610375	0.12587785	0.97953529
H_2S	0.81333102	0.01729864	0.06389625	0.87412215	0.02046471
β	0.00000000	0.72742456	0.27257544	0.01116888	0.98883111
θ	0.13266274	0. 00000000	0. 00000000	-	-
$\underline{G}_R/RT$	-0.53949050			-0.53769775	
Properties of the components are given in Table 3.3. The overall composition is 97% C_1 and 3% H_2S for this table. The specified temperature and pressure are 190 K and 40.53 bars, respectively.					

Table 3.5: Solution for case 3.2 with the new algorithm.

Component	L_1	V	L_2
β	0.00000000	0.94202784	0.05797216
θ	0.13266274	0.00000000	0.00000000
$\underline{G}_R/RT$	-0.49203424		
Properties of the components are given in Table 3.3. The overall composition is 98% C_1 and 2% H_2S. The specified temperature and pressure are 190 K and 40.53 bars, respectively. The correct set of three phase compositions is identical to the one presented in Table 3.4. The conventional algorithm fails to find phase instability in single-phase stability analysis for this flash calculation.			

Table 3.6: Properties of the components for case 3.3

Component	Overall composition	MW, g/mol	P_C, bars	T_C, K	Acentric factor
CO_2	0.1200	44.0100	73.7600	304.2000	0.2250
C_1	0.0489	16.0430	46.0000	190.6000	0.0080
$n-C_4$	0.4400	58.1240	38.0000	425.2000	0.1930
$n-C_{10}$	0.1000	142.2850	21.0800	617.6000	0.4900
C_{2-3}	0.1121	38.4000	45.0500	343.6400	0.1300
C_{4-6}	0.1000	72.8200	33.5100	466.4100	0.2440
C_{7-14}	0.0300	135.8200	24.2400	603.0700	0.6000
C_{15-24}	0.0100	257.7500	18.0300	733.7900	0.9030
C_{25+}	0.0090	479.9500	17.2600	923.2000	1.2290
H_2O	0.0300	18.0150	220.8900	647.3000	0.3440

Binary interaction parameters:

	CO_2	C_1	$n-C_4$	$n-C_{10}$	C_{2-3}	C_{4-6}	C_{7-14}	C_{15-24}	C_{25+}	H_2O
CO_2	0.000	0.120	0.120	0.114	0.120	0.120	0.090	0.090	0.090	0.667
C_1		0.000	0.000	0.042	0.000	0.000	0.000	0.000	0.000	0.732
$n-C_4$			0.000	0.008	0.000	0.000	0.000	0.000	0.000	0.684
$n-C_{10}$				0.000	0.000	0.000	0.000	0.000	0.000	0.357
C_{2-3}					0.000	0.000	0.000	0.000	0.000	0.679
C_{4-6}						0.000	0.000	0.000	0.000	0.605
C_{7-14}							0.000	0.000	0.000	0.491
C_{15-24}								0.000	0.000	0.327
C_{25+}									0.000	0.242
H_2O										0.000

Table 3.7: Results for case 3.3 with the new algorithm

Component	L_2	L_1	V	Non-tangent stationary point
CO_2	0.11738916	0.07803457	0.15787879	0.00010037
C_1	0.04753232	0.02844412	0.06839099	0.00002118
$n\text{-}C_4$	0.44144075	0.38822000	0.43634612	0.00000002
$n\text{-}C_{10}$	0.10303175	0.13284012	0.05967230	0.00000000
$C_{2\text{-}3}$	0.11120735	0.08458583	0.12808134	0.00000070
$C_{4\text{-}6}$	0.10094542	0.09554283	0.09080736	0.00000000
$C_{7\text{-}14}$	0.03083866	0.04300449	0.01794197	0.00000000
$C_{15\text{-}24}$	0.01029303	0.02618153	0.00310814	0.00000000
C_{25+}	0.00795880	0.09401603	0.00068515	0.00000000
H_2O	0.02936275	0.02913048	0.03708783	0.99987773
β	0.89781487	0.01911965	0.08306548	0.00000000
θ	0.00000000	0.00000000	0.00000000	0.79007647
$\underline{G}_R/RT$	-2.67985726			

Table 3.8: Properties of the components for case 3.4

Component	Overall composition	T_C, K	P_C, bars	Acentric factor
CO_2	0.7218	304.200	73.765	0.225
C_1	0.0214	160.000	46.002	0.008
PC1	0.1870	529.028	27.318	0.481
PC2	0.0698	795.328	17.309	1.042

Binary interaction parameters:

	CO_2	C_1	PC1	PC2
CO_2	0.0000	0.0550	0.0810	0.1050
C_1		0.0000	0.0000	0.0000
PC1			0.0000	0.0000
PC2				0.0000

Table 3.9: Results for case 3.4 with the new algorithm

Component	V	L_1	L_2
CO_2	0.92939195	0.62612349	0.86182262
C_1	0.05933155	0.01782033	0.02660759
PC1	0.01127539	0.24083442	0.10820073
PC2	0.00000111	0.11522177	0.00336906
β	0.00000000	0.59418965	0.40581035
θ	0.00154683	0. 00000000	0. 00000000

Table 3.10: Number of iterations when the new algorithm is used to initialize a 2nd-order convergent method for case 3.4

Switching criterion	10^{-2}	10^{-3}	10^{-4}	10^{-5}	10^{-6}
Number of iterations required for the new algorithm	38	50	66	82	98
Number of iterations required for the 2nd-order method	3	2	2	2	1
Total number of iterations required for final convergence	41	52	68	84	99
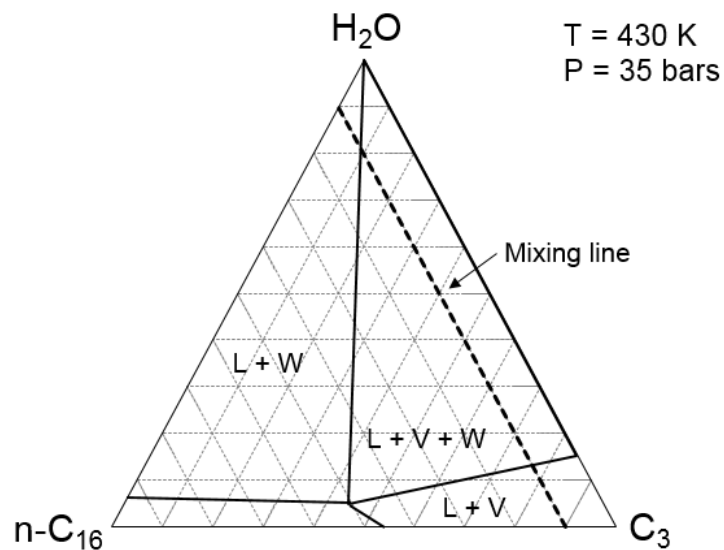
Figure 3.1. Phase boundaries for the ternary system of H_2O, C_3, and n-C_{16} at 430 K and 35 bars.   L, V, and W stand for the oleic, gaseous, and aqueous phases, respectively. Properties of the components are given in Table 3.1.   The mixing line between (0.0, 0.9, 0.1) and (0.9, 0.0, 0.1) is used to show the variation of parameters in Figures 3.2 and 3.3.

(a)

(b)

89
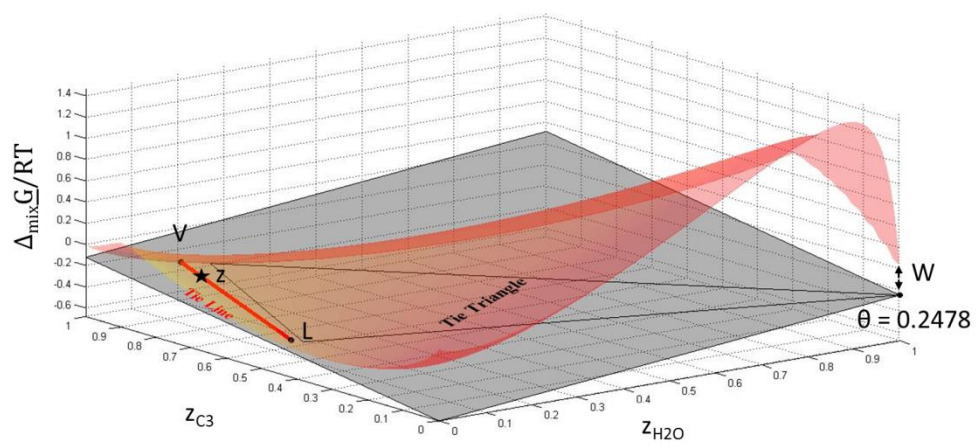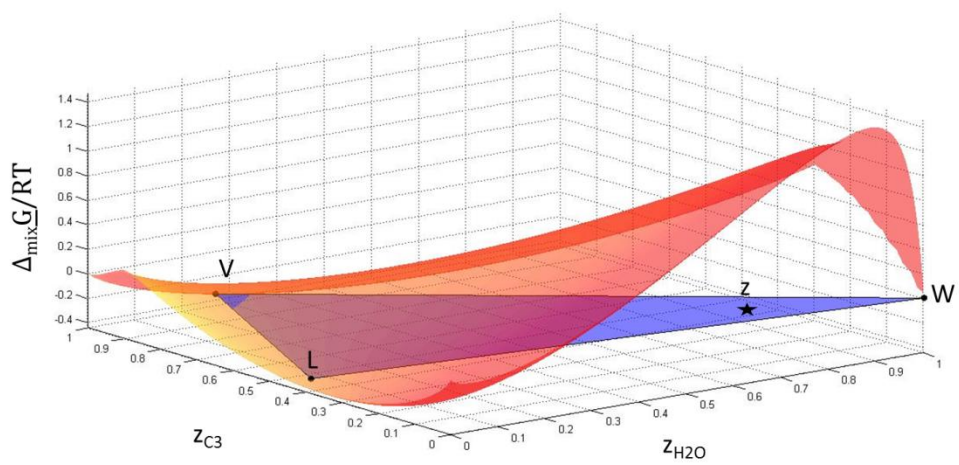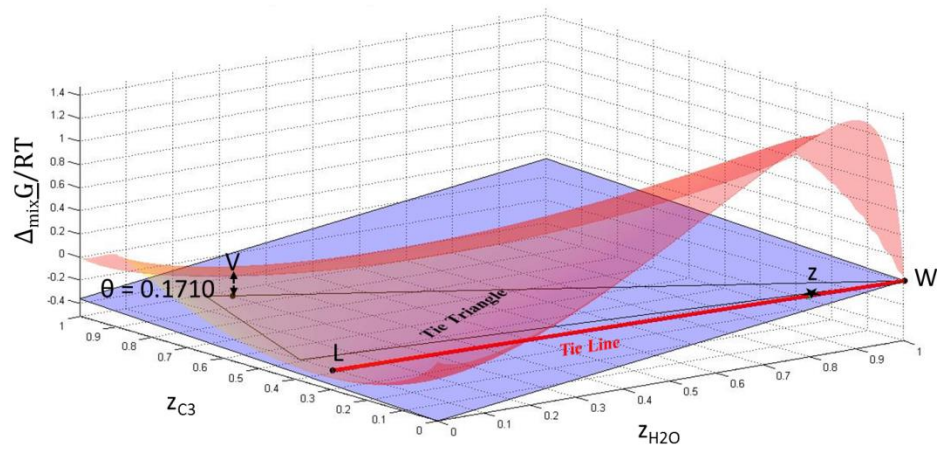
(c)

Figure 3.2. Gibbs free energy surface at 430 K and 35 bars, and the tangent planes converged for three compositions on the mixing line given in Figure 3.1. (a) $z_{H2O} = 0.1$. (b) $z_{H2O} = 0.75$. (c) $z_{H2O} = 0.84$.
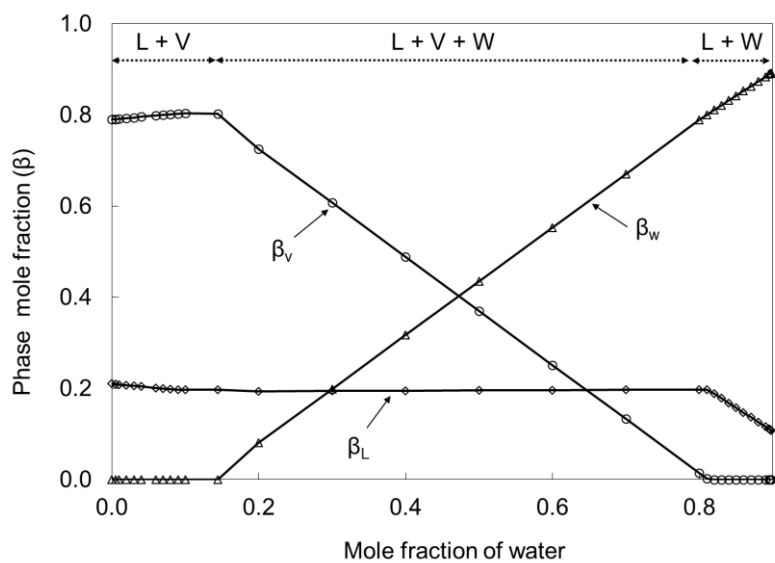
(a)
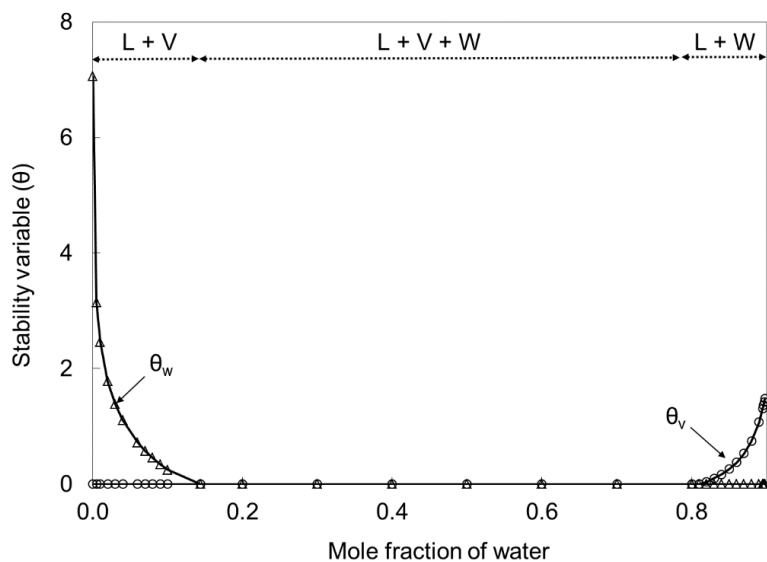
(b)

Figure 3.3. Variation of parameters with the new algorithm applied along the mixing line given in Figure 3.1 at 430K and 35 bars. (a) Phase mole fraction. (b) Stability variable. $\theta_L = 0$ in b as the L phase is always present along the mixing line.
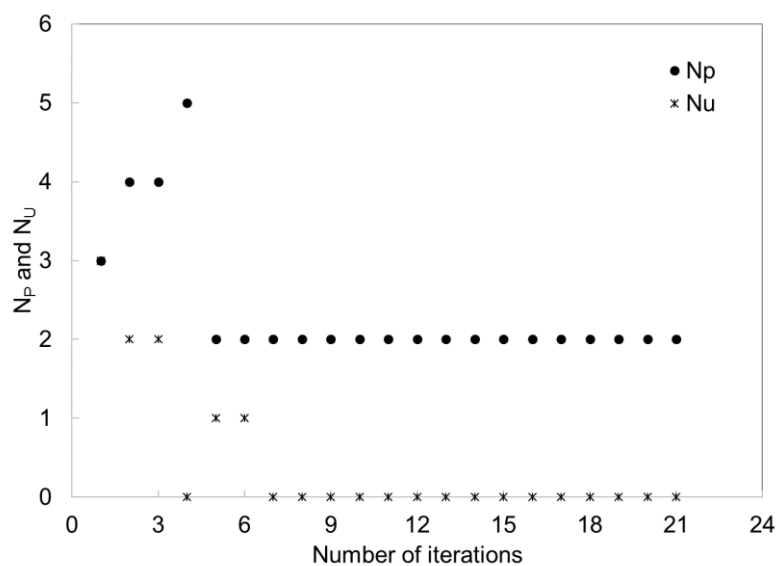
(a)
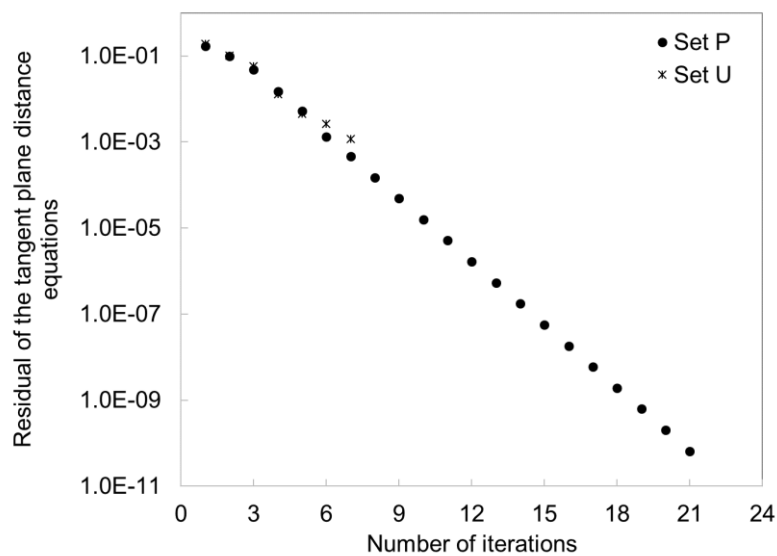
(b)

Figure 3.4. Convergence behavior of the new algorithm for case 3.1 with the overall composition of 75% H_2O, 15% C_3, and 10% $n-C_{16}$ at 560 K and 65 bars. Properties of the components are given in Table 3.1. (a) N_P and N_U. (b) Residual of equation 3.3 for sets P and U.

92
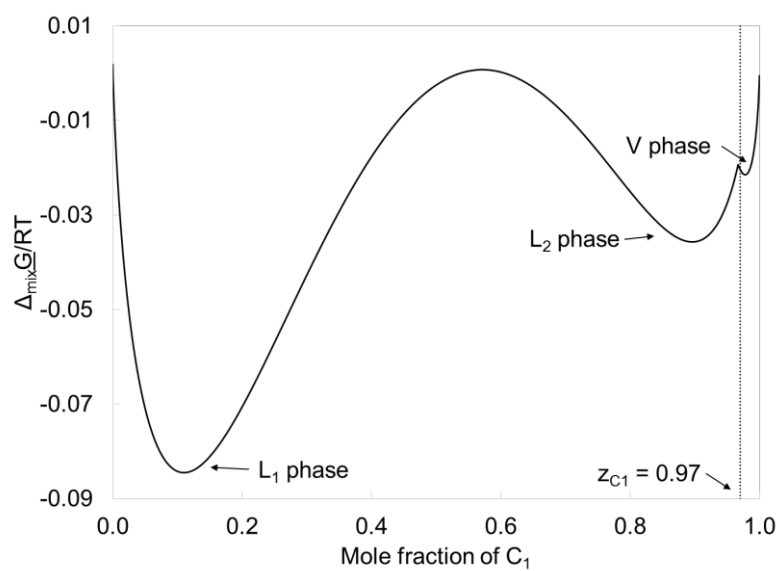
Figure 3.5. Gibbs free energy surface in composition space for the binary system of C_1 and H_2S at 190 K and 40.53 bars. Properties of the components are given in Table 3.3. The three lobes indicated correspond to the L_1, L_2, and V phases in the order of increasing C_1 mole fraction in composition space.
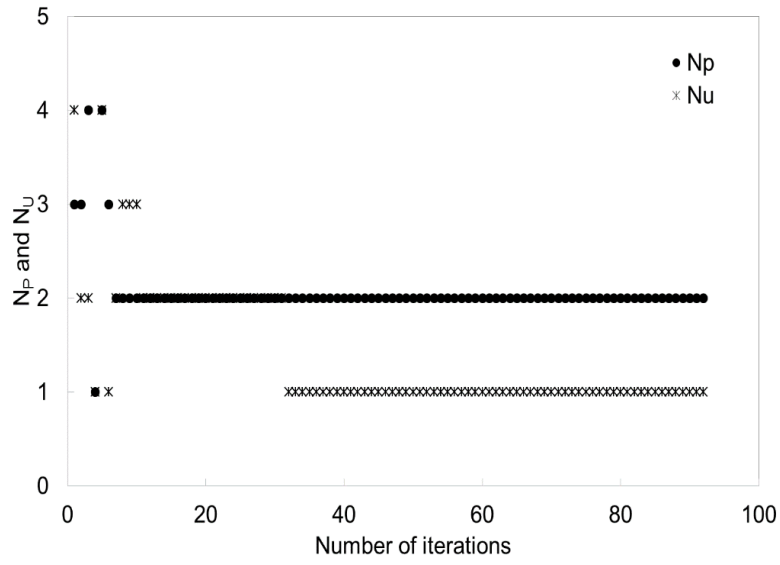
(a)
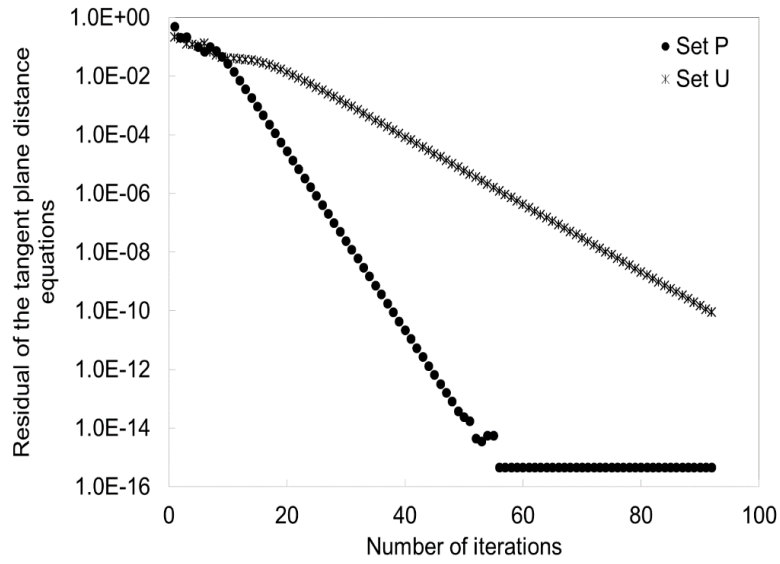
(b)

Figure 3.6. Convergence behavior of the new algorithm for case 3.2 at 190 K and 40.53 bars. Properties of the components are given in Table 3.3. (a) N_P and N_U. (b) Residual of equation 3.3 for sets P and U.
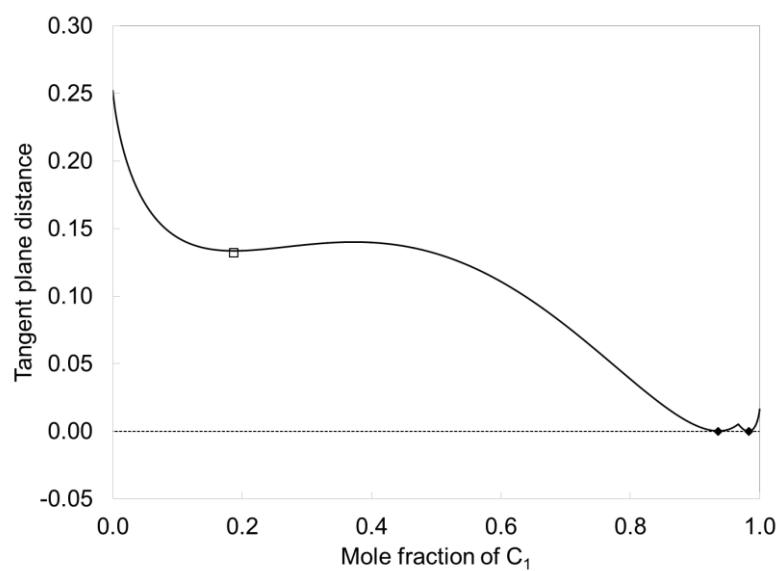
Figure 3.7. Tangent plane distance in composition space for the binary system of C_1 and H_2S. Properties of the components are given in Table 3.3. The temperature and pressure are 190 K and 40.53 bars, respectively.
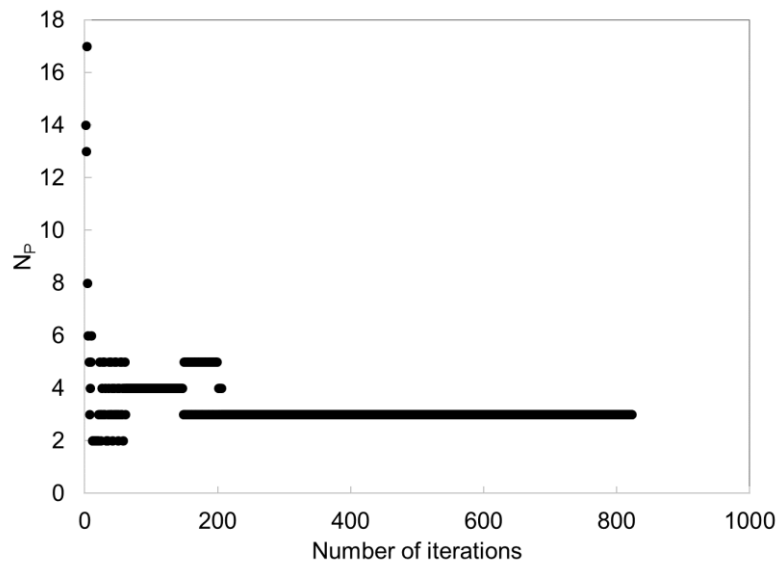
(a)
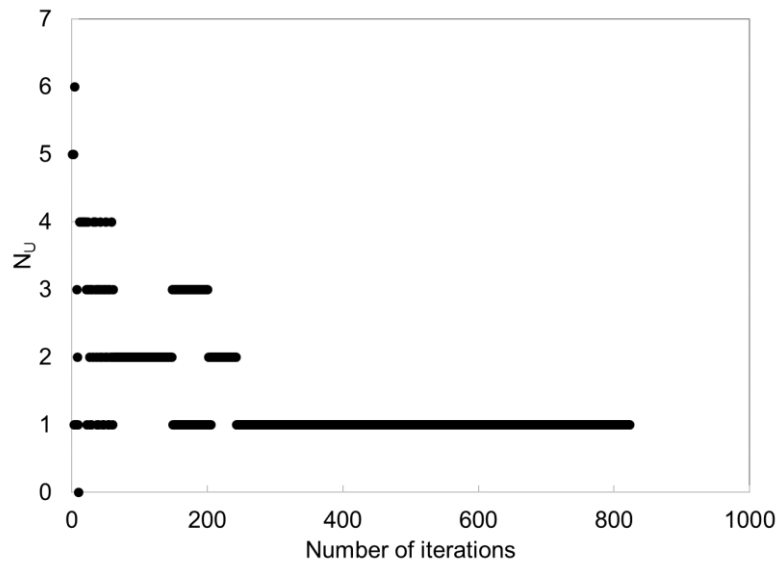
(b)

Figure 3.8. (Continued below)
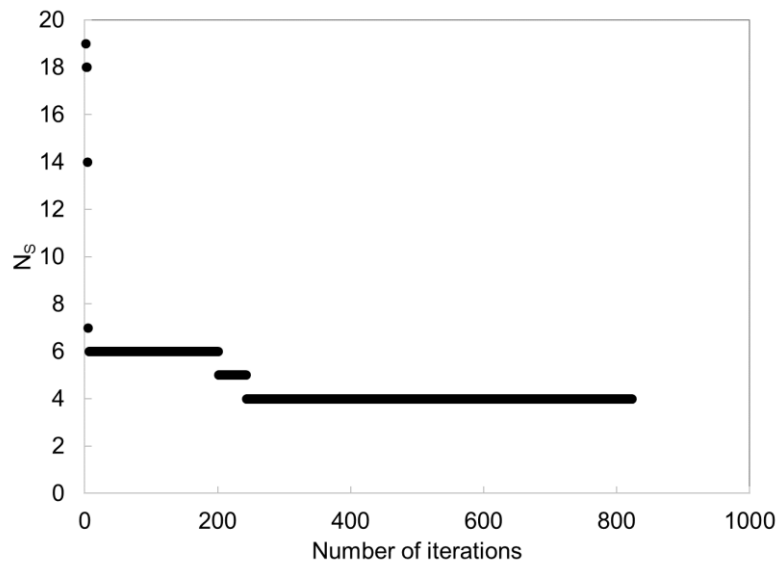
(c)
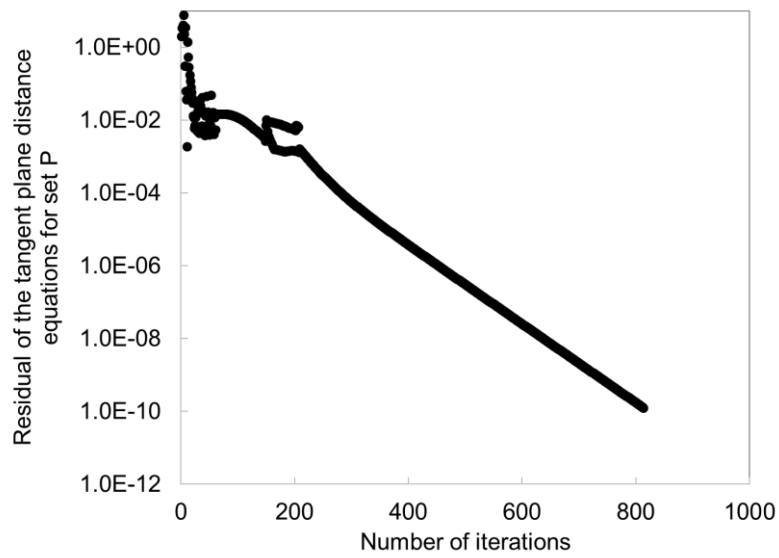
(d)

Figure 3.8. (Continued below)
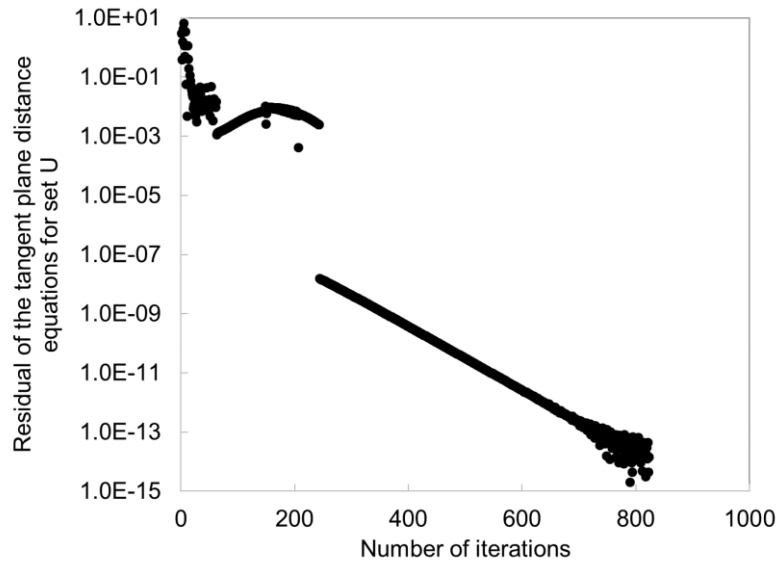
(e)

Figure 3.8. Convergence behavior of the new algorithm for case 3.3 (Table 3.6). The temperature and pressure are 459 K and 87 bars, respectively. (a) N_P, (b) N_U, (c) N_S, (d) Residual of equation 3.3 for set P, (e) Residual of equation 3.3 for set U.
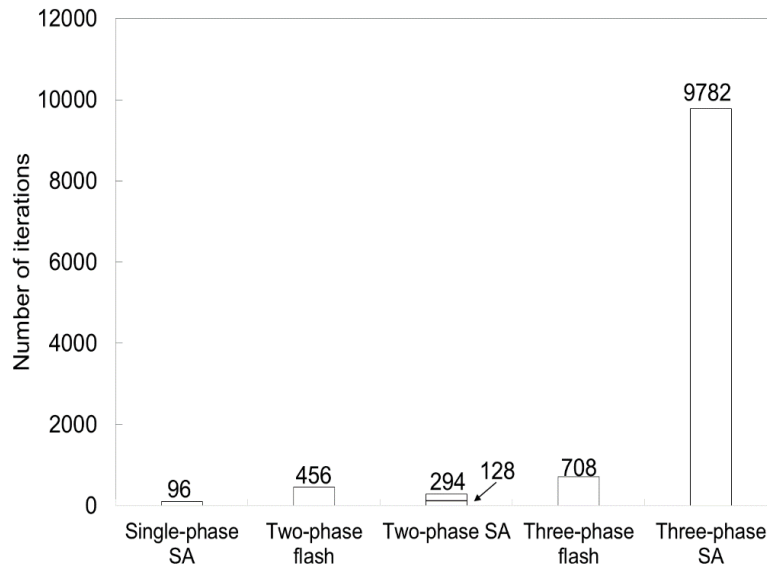
Figure 3.9. Number of iterations required for each step in the conventional sequential method of PT flash for case 3.3. The total number of iterations required for convergence with the conventional sequential algorithm is 11336, if the number of iterations for initial guesses that cannot identify phase-instability for two and three phases is counted.
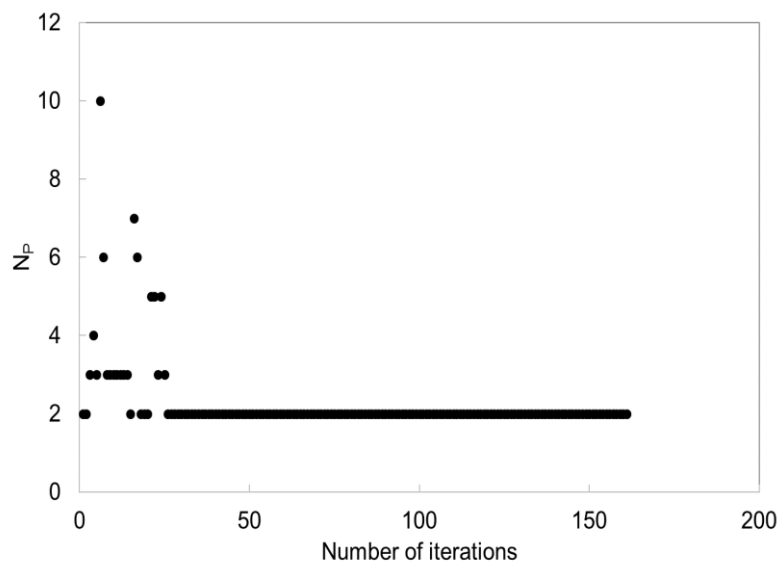
(a)
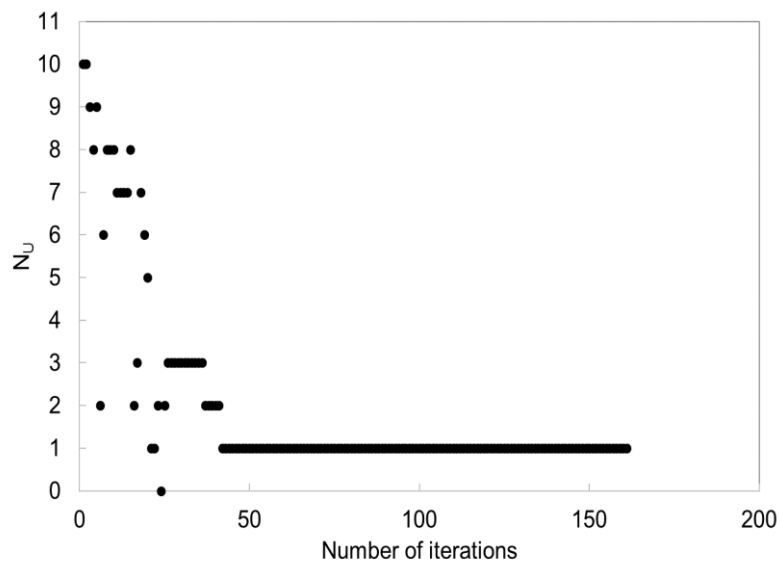
(b)

Figure 3.10. (Continued below)
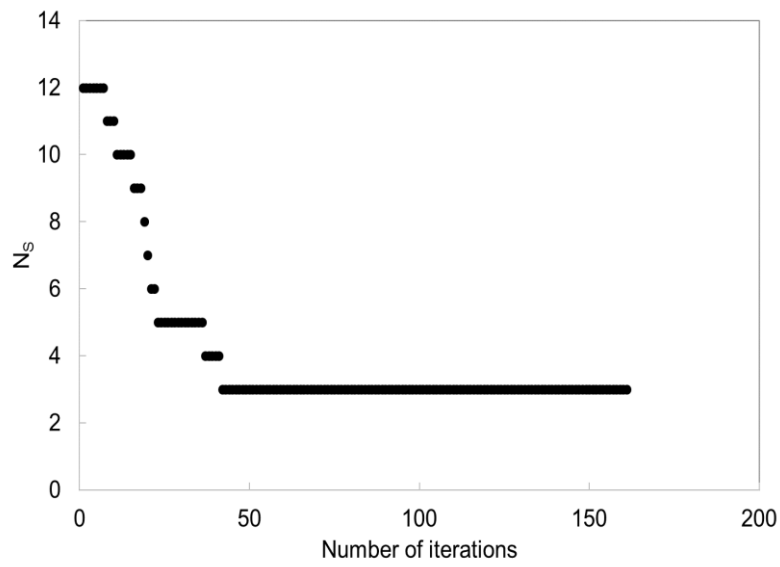
(c)
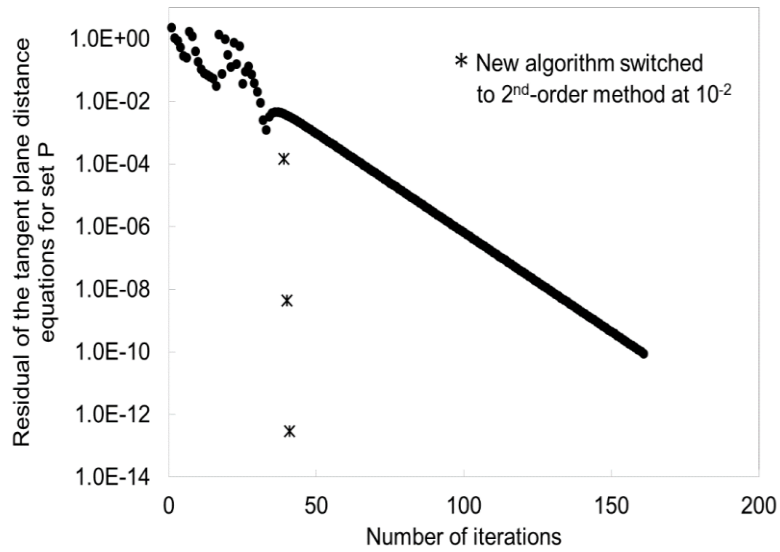
(d)

Figure 3.10. (Continued below)
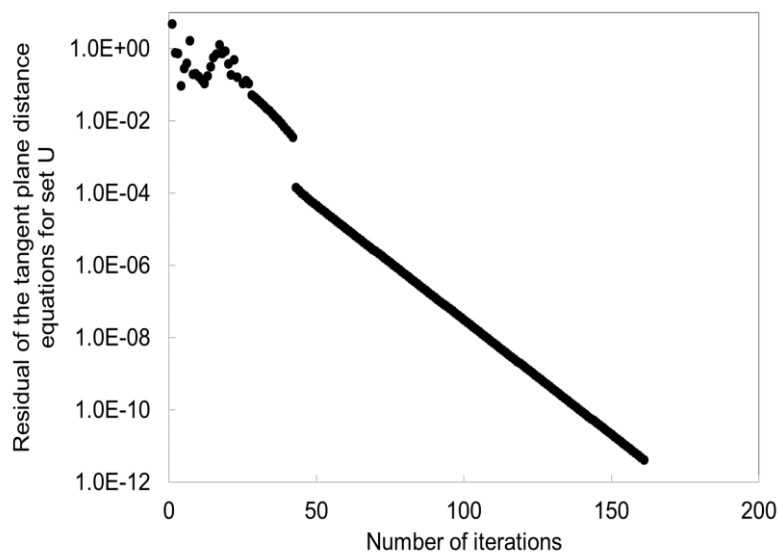
(e)

Figure 3.10. Convergence behavior of the new algorithm for case 3.4. Properties of the components are given in Table 3.8. The temperature and pressure are 313.706 K and 82.737 bars, respectively. (a) N_P, (b) N_U, (c) N_S, (d) Residual of equation 3.3 for set P, (e) Residual of equation 3.3 for set U. Figure 3.10d also shows the convergence behavior of a 2nd-order convergent method that has been initialized by the new algorithm with the switching criterion of 10^{-2} for equation 3.3 for sets P and U.
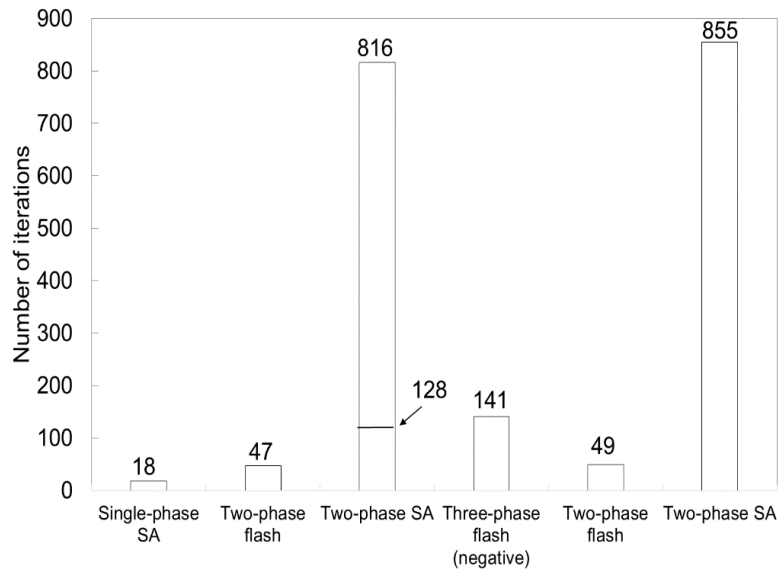
Figure 3.11. Number of iterations required for each step in the conventional sequential method of PT flash for case 3.4. The total number of iterations required for convergence by use of the conventional sequential algorithm is 1926, if the number of iterations for the initial guesses that cannot identify phase-instability for two and three phases is counted.
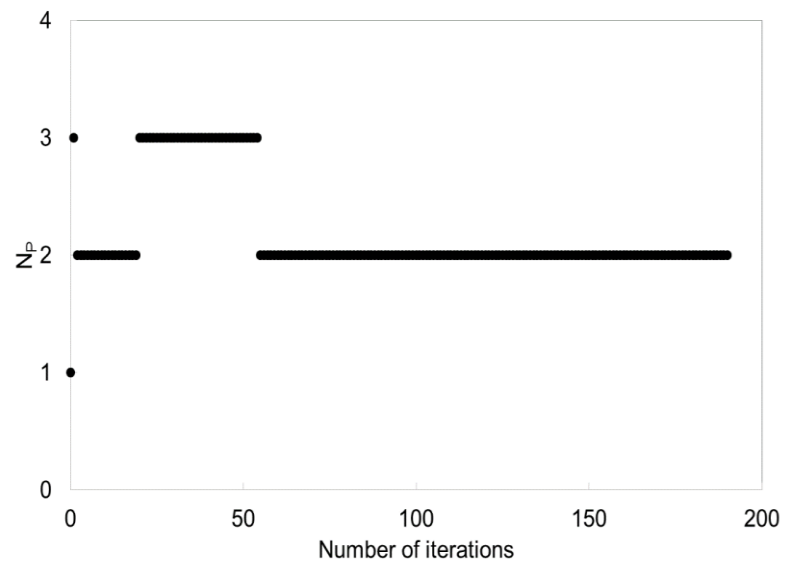
(a)
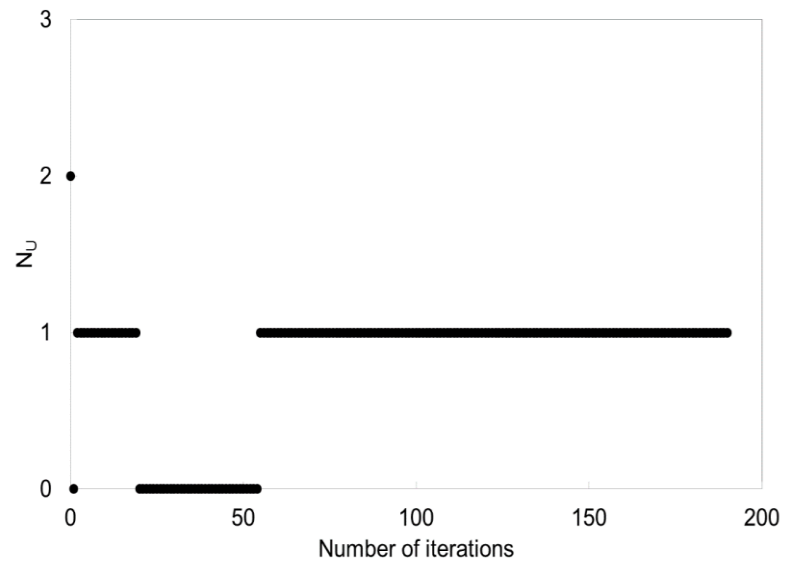
(b)

Figure 3.12. (Continued below)
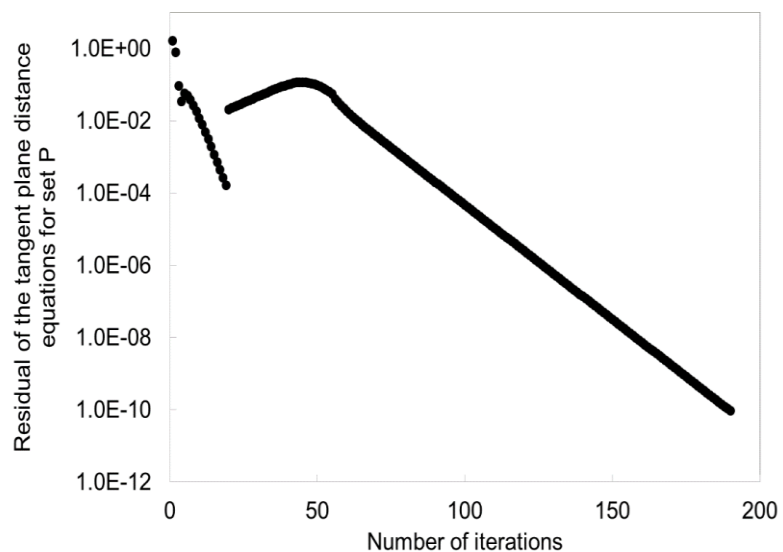
(c)
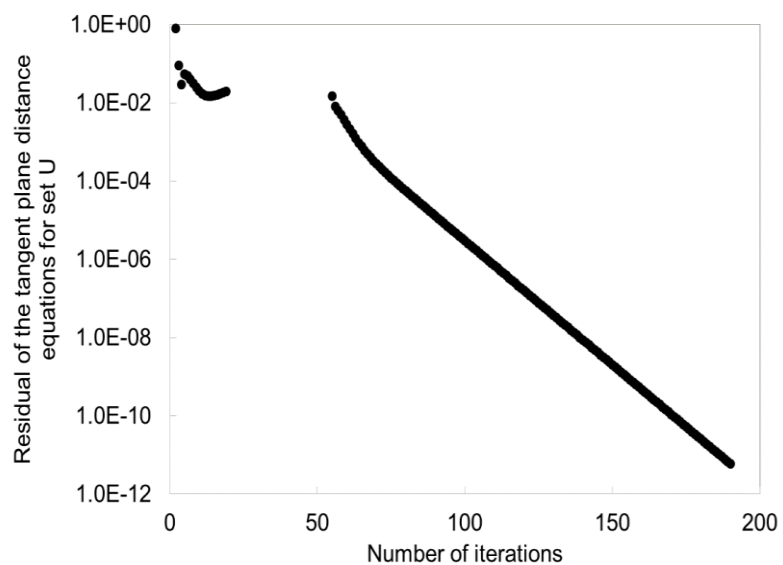
(d)

Figure 3.12. Convergence behavior of the new algorithm for case 3.4 with Wilson's correlation in initialization. Properties of components are given in Table 3.8. The temperature and pressure are 313.706 K and 82.737 bars, respectively. (a) N_P, (b) N_U, (c) Residual of equation 3.3 for set P, (d) Residual of equation 3.3 for set U.

CHAPTER 4: Multiphase Isenthalpic Flash Integrated with Stability Analysis[2]

Robust isenthalpic (PH) flash is important in compositional simulation of steam injection, which involves at least three phases consisting of the oleic, gaseous, and aqueous phases. However, multiphase PH flash is challenging for multiphase non-isothermal flow simulation using an EOS, because the number of equilibrium phases is unknown in temperature and composition space, and the system of equations in PH flash becomes nearly degenerate for narrow-boiling fluids. The term "narrow-boiling" is used in the literature to refer to enthalpy that is sensitive to temperature.

The first objective of this chapter is to present a new analysis of narrow-boiling behavior by coupling energy and phase behavior equations through the temperature dependency of K values. The second objective is to develop two algorithms for PH flash that resolves the two technical challenges mentioned above. The first algorithm proposed is based on the direct substitution (DS) algorithm. A detailed analysis is given for narrow-boiling behavior and its effects on the DS algorithm. The second algorithm is formulated by use of the tangent plane distance function, in which phase-split computation is integrated with phase-stability analysis. The formulated PH flash is solved by the DS algorithm with an arbitrary number of sampling compositions, at which phase stability is measured during the iteration. The number of equilibrium phases is not required to be fixed in the new simultaneous PH flash algorithm.

---

[2] Parts of this chapter have been published in the following papers which were supervised by R. Okuno:
- Zhu, D. and Okuno, R. 2014a. A Robust Algorithm for Isenthalpic Flash of Narrow-Boiling Fluids, *Fluid Phase Equilibria* **379**: 26-51.
- Zhu, D. and Okuno, R. 2015b. Robust Isenthalpic Flash for Multiphase Water/Hydrocarbon Mixtures. *SPE Journal* **20**(6): 1350-1365.
- Zhu, D. and Okuno, R. 2016. Multiphase Isenthalpic Flash Integrated with Stability Analysis, *Fluid Phase Equilibria* **423**: 203-219.

4.1 INTRODUCTION

Numerical solution of isothermal compositional reservoir flow has been extensively studied (Belkadi et al. 2013, Chang 1990, Chang et al. 1990, Iranshahr et al. 2013, Khan 1992, Mehra et al. 1982, Mohebbinia 2013, Okuno et al. 2010, Pan and Tchelepi 2011, Perschke 1988, Perschke et al. 1989, Rezaveisi et al. 2014, Trangenstein 1987, Trangenstein and Bell 1989, Wang and Stenby 1994, Wang and Baker 1995, Zaydullin et al. 2012). For thermal compositional reservoir flow, however, the literature is relatively scarce (Brantferger 1991, Chien et al. 1989, Grabowski et al. 1979, Heidari et al. 2014, Iranshahr et al. 2010, Ishimoto et al. 1987, Liu et al. 2009, Rubin and Buchanan 1985, Siu et al. 1991, Varavei and Sepehrnoori 2009, Zaydullin et al. 2014). Reliable solution of the coupled equations of mass balance, energy balance, and phase behavior requires a detailed understanding of numerical difficulties that may occur in thermal compositional simulation. This paper is concerned with two major issues in isenthalpic flash for thermal compositional simulation with a cubic EOS; one is narrow-boiling behavior and the other is phase stability analysis.

Narrow-boiling behavior refers to the total enthalpy that is sensitive to temperature (Agarwal et al. 1991, Gupta et al. 1990, Michelsen 1987, 1999, Zhu and Okuno 2014ab, 2015ab, 2016). It is related to how the energy balance affects phase behavior in thermal compositional simulation. The limiting narrow-boiling behavior occurs for fluid systems with one degree of freedom, for which the enthalpy exhibits a discontinuity in temperature space (Agarwal et al. 1991, Gupta et al. 1990, Brantferger et al 1991, Gernert et al. 2014, Michelsen 1993, Van Odyck et al. 2009).

Various researchers reported convergence difficulties associated with narrow-boiling behavior in their steam injection simulations (Brantferger 1991, Heidari et al.

2014, Btantferger et al. 1991, Van Odyck et al. 2009). The difficulties may be better handled in flow simulation with PH flash than with PT flash, because in the former type of thermal simulation formulation (e.g., Brantferger 1991, Btantferger et al. 1991) narrow-boiling behavior is handled in local flash calculations that are decoupled from the global mass and energy flow equations. Even in stand-alone flash calculations, however, robust PH flash for narrow-boiling fluids has been a technical challenge (Brantferger 1991, Heidari et al. 2014, Agarwal et al. 1991, Gupta et al. 1990, Michelsen 1987, 1999, Zhu and Okuno 2014ab, Btantferger et al. 1991). Various algorithms have been proposed for PH flash and discussed in details in chapter 2. Also, it is not well understood under what thermodynamic conditions narrow-boiling behavior occurs; this question is addressed as one of the two main objectives in this chapter.

Due to the various issues ranging from fundamental to implementation problems, no algorithm has been established for multiphase PH flash integrated with phase-stability analysis. In this chapter, a detailed analysis of the enthalpy sensitivity to temperature is given, which explains the reason for the convergence issues that the prior DS algorithms can pose for narrow-boiling fluids. Also, we will address the unanswered question regarding thermodynamic conditions for narrow-boiling behavior.

Two algorithms are proposed; one is the modified DS algorithm, and the other one is a coupling of phase-stability and flash calculations that is reformulated on the basis of Brantferger's research on phase stability with PH specification (Brantferger 1991, Brantferger et al. 1991). Case studies will be given to demonstrate that the developed algorithms can robustly perform multiphase PH flash even for narrow-boiling fluids, which none of the prior PH-flash algorithms (Brantferger 1991, Heidari et al. 2014, Agarwal et al. 1991, Gupta et al. 1990, Michelsen 1987, 1999, Zhu and Okuno 2014ab, Brantferger et al. 1991) addressed in detail.

4.2 ANALYSIS OF NARROW-BOILING BEHAVIORS

As explained in chapter 2, Michelsen (1987) and Agarwal et al. (1991) reported that their DS algorithms have convergence difficulties when narrow-boiling behavior is involved. A fluid with the narrow-boiling behavior exhibits a significant sensitivity of enthalpy to temperature (Agarwal et al. 1991, Michelsen 1987). This section investigates fundamental reasons for the narrow-boiling behavior and its effects on PH flash using the DS equations.

4.2.1 Gibbs Free Energy Analysis

Appendix A presents the analytical expression of the sensitivity of dimensionless total molar enthalpy ($\underline{H}_D{}^t$) to dimensionless temperature (T_D) in terms of $\partial\beta_V/\partial T_D$. β_V is the phase mole fraction of V phase. By definition, however, $\partial\beta_V/\partial T_D$ is zero in the Jacobian matrix in the DS algorithms (see Appendix A for the expressions for the Jacobian matrix). This section gives another analysis of the narrow-boiling behavior through the Gibbs free energy in composition-temperature space.

Phase equilibrium predictions at temperature and pressure are determined by the geometric properties of the single-phase Gibbs free energy (i.e., the Gibbs free energy assuming a single phase even in multiphase regions) in composition space. PT flash calculation, or minimization of the Gibbs free energy, is to correct the non-convex portion of the single-phase Gibbs free energy that contains the specified overall composition. The single-phase Gibbs free energy change on mixing in a dimensionless form ($\Delta_m\underline{G}/RT$) is calculated as

$$\Delta_m\underline{G}/RT = \sum_{i=1}^{Nc} x_i\left[\ln\varphi_i(T, P, \underline{x}) - \ln\varphi_i(T, P)\right], \tag{4.1}$$

where $\varphi_i(T, P, \underline{x})$ is the fugacity coefficient of component i in a mixture, and $\varphi_i(T, P)$ is the fugacity coefficient of component i as a pure component.

If β_V is sensitive to T_D for a fixed overall composition and pressure, the Gibbs free energy should behave in such a way that at least one of the equilibrium phase compositions drastically changes with a small change in temperature. This is illustrated in a simple example (case 4.1) given below.

Case 4.1 uses a binary mixture of 99.00% methane (C_1) and 1.00% n-butane (C_4), for which properties are given in **Table 4.1**. **Figure 4.1** shows the phase envelope in P-T space, where the critical point is calculated to be 197.57 K and 53.05 bars. The contour lines for β_V in Figure 4.1a indicate that the sensitivity of β_V to T varies in the two-phase region. The contour lines are significantly dense near the bubble-point curve. PH flash is challenging near the bubble-point at 50 bars since it presents narrow-boiling behavior and is close to the critical point. Figure 4.1b shows the magnified P-T diagram near the critical point. At 50 bars, two phases exist from 194.98 K to 228.20 K, and β_V increases from 0.00 to more than 0.90 with a temperature increase of 2.00 K from the bubble-point temperature 194.98 K. **Figure 4.2** shows that $\underline{H}^t$ and β_V at 50 bars are sensitive to temperature near the bubble point. The $\partial\beta_V/\partial T_D$ can be higher than 70, where T_D is calculated using equation A-1.1 with $T_{ref} = 300$ K.

Figure 4.3 presents the Gibbs free energy surfaces (equation 4.1) in composition space at two different temperatures, $T_1 = 195.00$ K and $T_2 = 201.00$ K, at 50.00 bars. V and L represent the vapor and oleic phases, respectively. As can be seen from Figure 4.1, T_1 and T_2 are in the two-phase region, but T_1 is close to the bubble-point temperature. In Figure 4.3, equilibrium phases are indicated as follows: the filled circle for the V phase at T_1, the hollow circle for the V phase at T_2, the filled square for the L phase at T_1, and the hollow square for the L phase at T_2. At T_1, the two phases are present near the C_1 edge in composition space. Details of the Gibbs free energy surfaces near the C_1 edge are shown in Figure 4.3b.

As temperature increases from T_1 to T_2 ($T_2 - T_1 = 6.00$ K), the composition and the Gibbs free energy of the L phase drastically change. However, this does not occur for the V phase. At T_1, the total $\Delta_m\underline{G}/RT$ is -2.065×10^{-2}, where the C_1 concentration is 98.96% for the L phase and 99.61% for the V phase. The Gibbs free energy values are -2.141×10^{-2} for the L phase and -9.549×10^{-3} for the V phase. At T_2, the total $\Delta_m\underline{G}/RT$ is -1.435×10^{-2}, where the C_1 concentration is 80.26% for the L phase and 99.64% for the V phase. The Gibbs free energy values are -2.209×10^{-1} for the L phase and -7.280×10^{-3} for the V phase. The L phase composition moves away from the fixed overall composition while the V phase composition changes only slightly. As a result, β_V exhibits a drastic change from 0.0644 at T_1 to 0.9669 at T_2.

Figure 4.4 shows the significant non-linearity of the phase compositions with respect to temperature. The derivatives of $\ln x_{C4}$ and $\ln y_{C4}$ with respect to T_D are close to zero for temperatures above 205 K in the two-phase region. However, they rapidly increase as the bubble-point temperature is approached. A similar level of non-linearity is observed for the fugacity coefficients since they are thermodynamic properties dependent on the phase composition.

Case 4.1 has graphically demonstrated that the sensitivity of a phase composition causes the sensitivity of thermodynamic quantities and their associated parameters (e.g., β_V) to temperature for a fixed pressure and overall composition in a two-phase region. Then, the sensitivity of β_V to temperature causes $\underline{H}_D^t$ to be sensitive to temperature as discussed above with Figure 4.2. This can be also confirmed using equation A-1.14. **Figure 4.5** shows the values for α_1, α_2, and α_3 in equation A-1.14 for case 4.1 between 194.98 K and 228.20 K. The α_1 values are positive near zero. Therefore, the first term of equation A-1.14, which is also positive as shown in **Figure 4.6,** does not adversely affect the sensitivity of $\underline{H}_D^t$. Figure 4.5 indicates that the second and third terms cause

$\underline{H}_D^t$ to rapidly increase with temperature near the bubble point. Figure 4.6 shows that the three terms exhibit significant non-linearity with respect to temperature. The large positive values of $\partial\beta_V/\partial T_D$ are multiplied by negative α_2 values for the second term of equation A-1.14. The α_3 values are sensitive near the bubble-point temperature, but $\partial\beta_V/\partial T_D$ is not multiplied by α_3 for the third term. The $\partial\beta_V/\partial T_D$ value influences the sensitivity of $\underline{H}_D^t$ to temperature mainly through the second term of equation A-1.14 in this case.

4.2.2 Narrow-Boiling Behavior with Three Phases

A characteristic of narrow-boiling behavior is that the amounts of phases (i.e., β's) change rapidly with a small change in temperature, as indicated by its phenomenological name. The amounts of phases depend on the relative location of the overall composition to the equilibrium phases in composition space. This is illustrated below using a simple ternary example (case 4.2).

Case 4.2 uses a ternary mixture of 75% water (w), 15% propane (C_3) and 10% n-C_{16} (C_{16}), for which properties are given in **Table 4.2.** **Figure 4.7** shows phase boundaries in P-T space, where the critical endpoint of type L = V + W is calculated at 569.35 K and 131.07 bars. W, V and L represent the aqueous, vapor and oleic phases, respectively. At 80 bars, three phases exist from 491.17 K to 549.25 K. Three-phase PH flash for this mixture is challenging near the boundary between L + V + W and L + V since it presents narrow-boiling behavior. **Figure 4.8** shows that $\underline{H}^t$ at 80 bars is sensitive to temperature near the phase boundary.

Figure 4.9 presents the tie triangles in composition space at 80 bars at two different temperatures, T_1 = 530 K and T_2 = 548 K. The three equilibrium phases at T_1 and T_2 are shown as solid and dashed tie triangles, respectively. As temperature

increases from T_1 to T_2 ($T_2 - T_1 = 18$ K), the compositions of the L and V phases drastically change, while the W phase stays in the vicinity of the water vertex of composition space. Consequently, the overall composition becomes close to the L-V edge of the tie triangle at T_2. This can be confirmed in Figure 4.7, where T_2 is close to the phase boundary between L + V + W and L + V at 80 bars.

At T_1, the C_3 concentration is 37.03% for the V phase and 26.22% for the L phase, and the C_{16} concentration is 3.51% for the V phase and 44.67% for the L phase. The phase mole fractions are 0.203, 0.261 and 0.536 for the L, V and W phases, respectively. At T_2, the C_3 concentration is 17.17% for the V phase and 12.76% for the L phase, and the C_{16} concentration is 4.16% for the V phase and 49.21% for the L phase. The phase mole fractions are 0.138, 0.771, and 0.091 for the L, V and W phases, respectively.

The concentrations of C_3 in the V and L phases decrease rapidly during the temperature increase from T_1 to T_2 ($T_2 - T_1 = 18$ K). This results from the variation of the Gibbs free energy in composition-temperature space. Since graphical illustration of the Gibbs free energy in composition-temperature space is difficult for more than two components, it is implied by presenting $\ln(x_{ij})$ (associated with the ideal term of the Gibbs free energy). **Figure 4.10** shows that the gradients of $\ln(x_{C16})$ and $\ln(x_w)$ with respect to T_D do not change very much in the three-phase region. The derivatives of $\ln(x_{C3})$ decrease with increasing temperature within the three-phase region, especially for the L and V phases. A similar level of non-linearity is observed for the fugacity coefficients (associated with the excess term of the Gibbs free energy) within the three-phase region since they are thermodynamic properties dependent on the phase compositions.

112

The variation of phase compositions (Figure 4.9) that is determined by the Gibbs free energy in composition-temperature space results in significant changes in phase mole fractions, β's. **Figure 4.11** shows that β_V and β_W become progressively larger and smaller, respectively, as the phase boundary between $L + V + W$ and $L + V$ is approached. Within the three-phase region, β_V increases from 0% to 86%, and β_W decreases from 71% to 0% with increasing temperature. This ternary example showed that narrow-boiling behavior involves rapid changes in the properties and amounts of equilibrium phases with temperature, but the sensitivities depend on how the equilibrium phase compositions vary relative to the overall composition in temperature space.

4.2.3 Near Degeneracy of the DS Equations

The DS equations consist of two types of equations, the enthalpy and material-balance equations, which are solved for T_D and β's. Previous two sections showed that the narrow-boiling behavior occurs when at least one of the two or three phase compositions is sensitive to temperature, resulting in β's to be sensitive to temperature. This section discusses the effects of narrow-boiling behavior on the DS Jacobian matrix, which significantly affects the computational robustness.

4.2.3.1 Two-Phase Case

The two-phase case was used in section 4.2.1 to explain the narrow-boiling behavior through the Gibbs free energy in composition-temperature space. As presented in Appendix A, the Jacobian matrix for the DS algorithm contains $\partial \ln K_i / \partial T_D$; thus, the behavior of phase compositions affects the condition number of the Jacobian matrix. This is depicted in **Figure 4.12** for case 4.1.

Figure 4.12 shows that $\partial \ln K_{C4} / \partial T_D$ substantially increases with increasing temperature near the bubble-point temperature. This sensitive K_{C4} directly affects the

condition number of the Jacobian matrix as shown in **Figure 4.13**.   All calculations in this chapter use the double-precision floating-point numbers, and the Jacobian matrix with a condition number higher than 10^6 is considered to be ill-conditioned.   The condition number of the Jacobian matrix is calculated using the one-norm approximation in this research. lnK_{C4} is significantly sensitive to temperature between 194.98 K and 204.40 K, where the Jacobian matrix is ill-conditioned.   That is, narrow-boiling behavior adversely affects the robustness of the DS algorithm through the Jacobian matrix.   K values during the DS solution are calculated as the fugacity-coefficient ratio, not from the definition (i.e., $K_i = y_i/x_i$ for two phases), until its convergence.   However, the fugacity coefficients are directly related to phase compositions since they are thermodynamic properties dependent on the phase composition.   Therefore, the ill-conditioned Jacobian can occur due to sensitive phase compositions during the DS iteration.

The Jacobian matrix becomes even more ill-conditioned if the scaling of the total enthalpy and temperature (i.e., equations A-1.1 and A-1.2) are not conducted.   Figure 4.13 shows the condition numbers with and without scaling of the variables for case 4.1. It is observed that the condition number of the Jacobian matrix with the dimensionless variables is systematically lower than that with the dimensional variables.   Higham (2002) described the importance of scaling Jacobian elements in solution of a system of equations.   Castier (2009) used scaled independent variables in his isochoric-isoenergetic flash algorithm.

Although Michelsen (1987, 1993, 1999) did not fully explain how the narrow-boiling behavior affected the robustness of the DS algorithm, he stated that the non-linearity of the enthalpy constraint in his PH flash algorithm led to a more complex solution procedure.   In the DS algorithms of Michelsen (1987) and Agarwal et al.

114

(1991), strong temperature oscillations during the iteration were used as an indicator for the narrow-boiling behavior. After detecting the temperature oscillations in a certain way, the remedy proposed was to split the oscillating single phase into two phases of initially equal amounts and compositions. As explained in section 2.5.2, solutions of a cubic EOS in this and the subsequent iteration steps selected the lower compressibility factor for the L phase and the higher for the V phase. They found, however, that this approach did not always improve the non-convergence issues associated with the narrow-boiling behavior (Michelsen 1987, Agarwal et al. 1991). For example, it is not unusual that there exists only one root in solution of a cubic EOS for an oscillating single-phase system. For such a case, K values calculated as the fugacity-coefficient ratio become unity in the next iteration step, yielding a singular Jacobian matrix.

The convergence behavior of the prior DS algorithms (Michelsen 1987, Agarwal et al. 1991) is shown for case 4.1 at 50 bars and $\underline{H}_{spec}$ of -6500 J/mol. The solution temperature is 195.65 K, which is close to the bubble-point temperature in the two-phase region (see Figure 4.1). That is, the solution exists in the region of the narrow-boiling behavior. The initial temperature value is set to 190.00 K. The oscillation testing procedure presented in section 2.5.2 is used with the C constant of 10^2.

Figure 4.14 shows the temperature variations during the iterations for the two DS algorithms with Michelsen (1987) and Agarwal et al. (1991). The temperature oscillation is identified at the 6th iteration step for the DS algorithm of Agarwal et al. (1991). A similar oscillation is observed for the DS algorithm of Michelsen (1987) in Figure 4.14, but the oscillation testing procedure with the C value used does not identify it until the 22nd iteration step. Although Michelsen (1987) and Agarwal et al. (1991) did not explain how to detect temperature oscillation in their papers, this case indicates that efficient and robust identification of a temperature oscillation in their DS algorithms is

115

not an easy task and would require some heuristic approach. The DS algorithm of Agarwal et al. (1991) results in a lower level of temperature oscillation than that of Michelsen (1987) in this case. This is likely because of the preliminary update of K values in the DS algorithm of Agarwal et al. (1991), which is essentially the only difference between the two DS algorithms.

Once a temperature oscillation is identified, the prior DS algorithms take the remedy proposed by Michelsen (1987), which was discussed in section 2.5.2 and Appendix B. **Figure 4.15** shows the compressibility factor in composition space at the 22nd iteration step for Michelsen's DS algorithm (218.42 K), and at the 6th iteration step for Agarwal et al.'s DS algorithm (202.67 K).   It is shown that only one root exists in the cubic equation solution when the temperature oscillations are identified. This results in a singular Jacobian matrix; thus a complete failure of the calculation. **Figure 4.16** clearly presents the non-convergence of the DS iterations in terms of the enthalpy constraint (i.e., $g_2 = 0$, equation 2.50 with N_P of two) for case 4.1.

4.2.3.2 Three-Phase Case

The three-phase case was used in section 4.2.2 to explain narrow-boiling behavior through rapid changes of the amounts of phases (i.e., β's) with a small change in temperature.   Gaussian elimination of the column with $\partial g_{N_P}/\partial T_D$ in the DS Jacobian matrix clearly shows that the matrix tends to be ill-conditioned for narrow-boiling fluids (see Appendix A for the DS Jacobian matrix).   Then, the limiting singularity of the Jacobian matrix can be easily understood when $\partial g_{N_P}/\partial T_D$ tends to infinity.

Figure 4.17 shows the derivatives of g_1, g_2, and g_3 (equations 2.49 and 2.50 with N_P of three) in the three-phase region for case 4.2 (see Figure 4.8 for phase boundaries in temperature).   Temperature and enthalpies are scaled with $T_{ref} = 300$ K and $\underline{H}_{sepc} =$

116

15000 J/mol, respectively, in case 4.2. The derivatives of g_3 (equation 2.50 with N_P of three) are greater than those of g_1 and g_2 (equation 2.49 with N_P of three) by a few orders of magnitude. Also, the derivatives of g_1 and g_2 with respect to T_D exhibit significant sensitivity in the region of narrow-boiling behavior presented in Figure 4.8 (at temperatures approximately higher than 534 K).

Figure 4.18 presents the condition number of the Jacobian matrix in the three-phase region for case 4.2. It increases as temperature increases up to 549.25 K, where the W phase disappears. All calculations in this research use the double-precision floating-point numbers, and the Jacobian matrix with a condition number higher than 10^6 is considered to be ill-conditioned. On this basis, the Jacobian matrix is ill-conditioned at temperatures higher than approximately 534 K in Figure 4.18. Figure 4.18 also presents that the condition number based on one-norms is close to that based on singular value decomposition (SVD) in this case.

To further illustrate the degenerate equations, the Jacobian matrices for case 4.2 at two different temperatures, 491.83 K and 549.25 K, are factorized using SVD. The higher temperature is in the narrow-boiling region. The condition number can be calculated as the ratio of the maximum singular value to the minimum singular value given in the diagonal matrix. Hence, the condition number is 1.36×10^5 at 491.83 K and 2.50×10^7 at 549.25 K. The corresponding one-norm approximation is 1.52×10^5 at 491.83 K and 2.50×10^7 at 549.25 K.

This example shows that it is no longer appropriate to solve the DS equations simultaneously, when they are nearly degenerate. The DS algorithm presented later in this chapter decouples temperature from the other variables when solving degenerate DS equations. A question as to under what conditions the narrow-boiling behavior occurs in thermal oil recovery will be present in the following section.

4.2.4 Conditions for Narrow-Boiling Behavior

In this section, the thermodynamic conditions for narrow-boiling behavior are investigated on the basis of the PR EOS. The term "narrow-boiling" has been used in the literature to indicate the enthalpy behavior that is substantially sensitive to temperature. Narrow-boiling behavior occurs as a result of the significant interplay between the energy balance and phase behavior equations, as explained below.

Zhu and Okuno (2014ab) concluded that narrow-boiling behavior occurs when at least one of the phase compositions (x_{ij} for $i = 1, 2, …, N_C$ and $j = 1, 2, …, N_P$) drastically changes with a small change in temperature so that phase mole fractions (β_j for $j = 1, 2, …, N_P$) significantly change. That is, it is related directly to the sensitivity of K values to temperature. Therefore, narrow-boiling behavior can be effectively analyzed on the basis of the equation 2.49 and the dimensionless form of equation 2.50 that are coupled through the temperature dependency of K values as presented in Zhu and Okuno (2014a). The dimensionless form of equation 2.50 is formed by dividing $\underline{H}_{spec}$. Note that the analysis presented in this section only includes equilibrium phases; i.e., $\underline{x}_j$ for $j = 1, 2, …, N_P$.

Appendix A gives the analytical expressions of each element in the $N_P \times N_P$ Jacobian matrix for a N_C-component N_P-phase system. The Jacobian matrix is formed by dimensionless equations 2.49 and 2.50 with respect to independent β_j and T_D. The major block of $(N_P - 1) \times (N_P - 1)$ in the Jacobian matrix comes from the RR equations with respect to independent β's. This part corresponds to the Hessian matrix of the convex function that was used by Okuno et al. (2010) to solve RR as a convex minimization problem in multiphase compositional reservoir simulation.

Appendix A also shows that if the total enthalpy becomes sensitive to temperature (i.e., narrow-boiling behavior, or $\partial g_{NP}/\partial T_D$ becomes large), the Jacobian tends to be ill-

conditioned regardless of the curvature of the RR convex function. This is consistent with the cases shown in Zhu and Okuno (2014a), and also can be understood from the following equation;

$$\underline{H}_D^t = \Sigma_{j=1}^{N_P} \beta_j \underline{H}_{Dj}, \tag{4.2}$$

where $\underline{H}_{Dj}$ is the dimensionless molar phase enthalpy. Equation 4.2 shows that the total enthalpy becomes sensitive to temperature if a small temperature change causes K values to drastically change so that the RR solution gives substantially different β's between the two temperatures.

More specific conditions for narrow-boiling behavior can be derived on the basis of the analysis of a convex function whose gradient vectors consist of the RR equations as follows. Okuno et al. (2010) presented a non-monotonic convex function whose gradient vectors consist of the RR equations as

$$F(\boldsymbol{\beta}) = \Sigma_{i=1}^{N_C}(-z_i \ln|t_i|), \tag{4.3}$$

where $\boldsymbol{\beta}$ is the vector of independent mole fractions [i.e., β_j for $j = 1, 2,..., (N_P - 1)$]. A derivation of the function can be found in Okuno et al. (2010). The convex function in Okuno et al. is similar to the ones presented in Michelsen (1994) and Leibovici and Nichita (2008). Multiphase RR equations can be correctly solved by the following formulation:

$$\text{Minimize } F(\boldsymbol{\beta}) = \Sigma_{i=1}^{N_C}(-z_i \ln|t_i|) \text{ subject to } a_i^T \boldsymbol{\beta} \leq b_i, \tag{4.4}$$

where $a_i = \{1 - K_{ij}\}$, and $b_i = \min\{1 - z_i, \min_j\{1 - K_{ij}z_i\}\}$ for $i = 1, 2, ..., N_C$, and $j = 1, 2, ..., (N_P - 1)$. The feasible region was derived on the basis of the non-negativity of phase component mole fractions, $0 \leq x_{ij} \leq 1$ for $i = 1, 2, ..., N_C$, and $j = 1, 2, ..., N_P$, as presented in Okuno et al. (2010).

The Hessian matrix of $(N_P - 1) \times (N_P - 1)$ for the minimization is

$$\nabla^2 F = \{H_{kj}\} = \{Y^T DY\}, \tag{4.5}$$

119

where $H_{kj} = \sum_{i=1}^{N_C}\left[(1 - K_{ij})(1 - K_{ik})z_i\right]/t_i^2$, $D = \text{diag}(z_1, \dots, z_{N_C}) \in \mathbb{R}^{N_C \times N_C}$, and $Y = \{Y_{ij}\} = \{(1 - K_{ij})/t_i\} \in \mathbb{R}^{N_C \times (N_P - 1)}$. The D matrix is positive definite because z_i (i = 1, 2,…, N_C) are all positive (i.e., positive composition space). The Hessian matrix is only positive semi-definite if Y is not of full rank; i.e., at critical points, including critical endpoints where two of three equilibrium phases merge in the presence of the other non-critical phase. In such cases, there exists a direction along which F is constant as proved by Okuno et al. (2010). No solution exists in the minimization for such cases.

If the D matrix is not positive definite (in negative composition space), the positive definiteness of the Hessian matrix is not guaranteed even if Y is of full rank. Negative z_i values do not occur in practical simulations, but were considered here to indicate the limiting behavior of the Hessian matrix in composition space.

In summary, the degree of positive definiteness of the Hessian matrix tends to become lower as the overall composition becomes closer to an edge of positive composition space (e.g., at least one component is of nearly-zero concentration) and/or the solution conditions (temperature, pressure, overall composition) become closer to a critical point. The solution of the minimization for such cases tends to be sensitive to the K values used, because of small gradients of the convex function. This leads to narrow-boiling behavior. This can be easily confirmed by plotting the RR convex function for two phases near a critical point or near the vertex of a component with a K value close to unity in positive composition space, for example.

Appendix A shows that the system of equations are degenerate if the Hessian matrix is semi-positive definite. Therefore, the following are conditions that can cause narrow-boiling behavior: (i) the overall composition is near an edge of positive composition space, and (ii) the solution conditions (temperature, pressure, and overall composition) are near a critical point, including a critical endpoint.

These conditions are qualitative unless a quantitative definition is given for narrow-boiling behavior. Therefore, the degeneracy level of the system of equations is quantified on the basis of the condition number of the Jacobian matrix in this research, as in Zhu and Okuno (2014a) (see Appendix A for the Jacobian matrix). The condition number of 10^6 is used to detect narrow-boiling behavior in computations with the double-precision floating-point numbers.

The two conditions mentioned above are contained by the general condition for narrow-boiling behavior that K values are sensitive to temperature. Although the two specific conditions are qualitative, the analysis of the RR convex function gives the clear limiting conditions towards which the tendency of narrow-boiling behavior increases. For instance, the RR problem is uniquely defined only for $N_C \geq N_P$ (i.e., more than one degree of freedom). For one degree of freedom (e.g., three phases for a binary system), K values discontinuously changes at the temperature of interest, which causes the limiting narrow-boiling behavior as an exact discontinuity of enthalpy with respect to temperature. This is a special case of the first condition mentioned previously in this section.

4.3 MULTIPHASE DIRECT SUBSTITUTION WITH ADAPTIVE NEWTON-BISECTION

This section first describes the working equations in the modified DS algorithm for PH flash for a general N_C-component N_P-phase system, where N_C and N_P are the numbers of components and equilibrium phases, respectively. Case studies will be given to demonstrate the robustness of the modified DS algorithm.

4.3.1 Modified DS Algorithm

The isenthalpic-flash formulation is presented in section 2.5.2. The PH flash calculations in this section consider mutual solubilities of water and hydrocarbons.

Particularly, water solubilities in the oleic phase may not be ignored at elevated temperatures as observed by a number of authors (e.g., Griswold and Kasch 1942, Tsonopoulos and Wilson 1983, Heidman et al. 1985, Glandt and Chapman 1995, Economou et al. 1997, Tsonopoulos 1999, Amani et al. 2013ab). The BIPs for water with n-alkanes are taken from the correlation of Venkatramani and Okuno (2014). Their BIP correlation was developed based on BIP values that were optimized in terms of three-phase predictions for water/n-alkane binaries by use of the PR EOS with the van der Waals mixing rules. PH flash in this research solves for three and more equilibrium phases as predicted by the PR EOS, instead of assuming the complete immiscibility between the L and W phases. Some equations were repeated below for complete readability in this chapter.

The DS algorithm searches for K values and T that satisfy equations 2.46 through 2.48 and the fugacity equations

$$f_{ij} = \ln(x_{ij}\varphi_{ij}) - \ln(x_{iN_P}\varphi_{iN_P}) = 0 \qquad (4.6)$$

for $i = 1, 2, \ldots, N_C$, and $j = 1, 2, \ldots, N_P - 1$, where φ_{ij} is the fugacity coefficient of component i in phase j, and x_{ij} is the mole fraction of component i in phase j. The K value of component i in phase j is defined as

$$K_{ij} = x_{ij}/x_{iN_P}, \qquad (4.7)$$

where $i = 1, 2, \ldots, N_C$, and $j = 1, 2, \ldots, (N_P - 1)$. The $N_P{}^{th}$ phase is the reference phase in equations 4.6 and 4.7.

K values are related to mole fraction of phase j (β_j) and x_{ij} through the RR equations; that is, β_j can be obtained from solution of the RR equations. The RR equations are

$$g_j = \sum_{i=1}^{N_C}(x_{ij} - x_{iN_P}) = \sum_{i=1}^{N_C}(K_{ij} - 1)z_i/t_i = 0 \qquad (4.8)$$

122

for j = 1, 2, ..., (N_P − 1), where $t_i = 1 + \sum_{j=1}^{N_P-1}(K_{ij} - 1)\beta_j$ for i = 1, 2, ..., N_C (Okuno 2009, Okuno et al. 2010), and z_i is the overall mole fraction of component i.   Then, the corresponding x_{ij} can be obtained from $x_{iN_P} = z_i/t_i$ and equation 4.7 for j ≠ N_P.

The DS algorithm in this research uses the enthalpy constraint in a dimensionless form;

$$g_{N_P} = (\underline{H}^t - \underline{H}_{spec})/\underline{H}_{spec} = \underline{H}_D^t - 1.0 = 0, \tag{4.9}$$

where $\underline{H}^t$ is the total molar enthalpy, $\underline{H}_{spec}$ is the specified molar enthalpy, and $\underline{H}_D^t = \underline{H}^t/\underline{H}_{spec}$.   The system of N_P dimensionless equations (equations 4.8 and 4.9) is solved for dimensionless variables T_D and β_j (j = 1, 2, ..., N_P − 1) based on Newton's method for root-finding, where $T_D = T/T_{ref}$. T_{ref} is some reference value to make temperature better scaled in PH flash.   For example, T_{ref} can be a temperature near the original reservoir temperature in thermal oil recovery processes (e.g., 300 K as used in this chapter).   The Jacobian matrix required is presented in **Appendix A** for a general N_C-component N_P-phase system.   The W phase is considered as the reference phase throughout this section.

The multiphase DS algorithm in this chapter is an extension of the two-phase DS algorithm presented in Zhu and Okuno (2014a).   The main advantage over other multiphase DS algorithms (Michelsen 1987, Agarwal et al. 1991) lies in how it handles narrow-boiling behavior.   The DS algorithm in this chapter checks for the narrow-boiling behavior on the fly on the basis of the condition number of the Jacobian matrix. When near degeneracy of the system of equations is detected by a large condition number (e.g., greater than 10^6), a robust bisection algorithm solves for T_D based solely on the enthalpy constraint (equation 4.9).   This decoupling of T_D from the other variables, β's, is performed only if the system of equations is nearly degenerate.   Otherwise, the normal Newton's iteration step is used.   That is, the algorithm adaptively switches between Newton's iteration step and the bisection method.   Also, the upper and lower

temperature limits (T_D^U and T_D^L) are used not to have unrealistic temperature values during the iterations. A step-wise description of the three-phase modified DS algorithm is given below.

Step 1. Specify $\underline{H}_{spec}$, P, and z_i, along with model parameters such as critical temperature T_C, critical pressure P_C, acentric factor ω, and $N_C \times N_C$ BIPs.

Step 2. Input an initial guess for dimensionless temperature, $T_D^{(1)}$, where the number in the bracket represents the iteration-step number $k = 1$. Calculate initial estimates for K values ($K_{iL}^{(k)}$ and $K_{iV}^{(k)}$).

Step 3. Solve equation 4.8 with N_P of three ($g_1^{(k)}$ and $g_2^{(k)}$) for the liquid and vapor phase mole fractions ($\beta_L^{(k)}$ and $\beta_V^{(k)}$) for the kth iteration step so that $|g_1^{(k)}| < \varepsilon_m$ and $|g_2^{(k)}| < \varepsilon_m$ (e.g., $\varepsilon_m = 10^{-10}$. It can be a larger value for practical applications.). Calculate the corresponding $x_{ij}^{(k)}$.

Step 4. Calculate the residual of the enthalpy constraint (equation 4.9 with N_P of three, i.e., $g_3^{(k)}$). If $|g_3^{(k)}|$ is less than the tolerance ε_h, stop (e.g., $\varepsilon_h = 10^{-10}$. It can be a larger value for practical applications.). Otherwise, continue to step 5.

Step 5. Calculate $\ln\varphi_{ij}^{(1)}$ and phase heat capacities ($C_{Pj}^{(1)}$) for $j = L$, V and W.

Step 6. Calculate the residuals of the fugacity equations (equation 4.6 with N_P of three, i.e., $f_{iL}^{(k)}$ and $f_{iV}^{(k)}$).

Step 7. Calculate $T_D^{(2)} = T_D^{(1)} - (\underline{H}_{spec}g_3^{(1)})/(T_{ref}\sum_j\beta_jC_{Pj})^{(1)}$, and initial estimates for K values (equation 4.7 with N_P of three, i.e., $K_{iL}^{(2)}$ and $K_{iV}^{(2)}$).

Step 8. Solve equation 4.8 with N_P of three ($g_1^{(k)}$ and $g_2^{(k)}$) for $\beta_L^{(k)}$ and $\beta_V^{(k)}$ for the kth iteration step so that $|g_1^{(k)}| < \varepsilon_m$ and $|g_2^{(k)}| < \varepsilon_m$. Calculate the corresponding $x_{ij}^{(k)}$.

Step 9. Calculate $g_3^{(k)}$, $f_{iL}^{(k)}$, and $f_{iV}^{(k)}$. If $|g_3^{(k)}| < \varepsilon_h$, $|f_{iL}^{(k)}| < \varepsilon_f$, and $|f_{iV}^{(k)}| < \varepsilon_f$ (e.g., $\varepsilon_f = 10^{-10}$) for $i = 1, 2, \ldots, N_C$, stop. Otherwise, continue to step 10.

124

Step 10. Perform a QNSS step for intermediate K values, $K_{ij}^{(k+0.5)}$ for $j = L$ and V;

$$\ln\vec{K}_j^{(k+0.5)} = \ln\vec{K}_j^{(k)} + \frac{\left(\ln\vec{K}_j^{(k)} - \ln\vec{K}_j^{(k-1)}\right)^T \vec{f}_j^{(k-1)}}{\left(\ln\vec{K}_j^{(k)} - \ln\vec{K}_j^{(k-1)}\right)^T \left(\vec{f}_j^{(k)} - \vec{f}_j^{(k-1)}\right)} \vec{f}_j^{(k)}, \qquad (4.10)$$

where $\vec{K}_j$ and $\vec{f}_j$ are vectors consisting of N_C K values and N_C fugacity equations for phase j, respectively.

Step 11. Calculate $x_{ij}^{(k+0.5)}$ based on $\beta_L^{(k)}$, $\beta_V^{(k)}$, $K_{iL}^{(k+0.5)}$ and $K_{iV}^{(k+0.5)}$.

Step 12. Construct the 3×3 Jacobian matrix based on $x_{ij}^{(k+0.5)}$.

Step 13. Perform one Newton's iteration step to obtain $\beta_L^{(k+1)}$, $\beta_V^{(k+1)}$, and $T_D^{(k+1)}$.

Step 14. Check to see if $T_D^L < T_D^{(k+1)} < T_D^U$. If so, continue to step 15. Otherwise, calculate $T_D^{(k+1)}$ using the Regula Falsi method. Then, solve equations 4.8 with N_P of three ($g_1^{(k)}$ and $g_2^{(k)}$) for $\beta_L^{(k+1)}$ and $\beta_V^{(k+1)}$ for the $(k+1)^{th}$ iteration step so that $|g_1^{(k+1)}| < \varepsilon_m$ and $|g_2^{(k+1)}| < \varepsilon_m$. Calculate the corresponding $x_{ij}^{(k+1)}$.

Step 15. Calculate $g_3^{(k+1)}$, $f_{iL}^{(k+1)}$, and $f_{iV}^{(k+1)}$. If $|g_3^{(k+1)}| < \varepsilon_m$, $|f_{iL}^{(k+1)}| < \varepsilon_f$, and $|f_{iV}^{(k+1)}| < \varepsilon_f$ for $i = 1, 2, \ldots, N_C$, stop. Otherwise, continue to step 16.

Step 16. Calculate the condition number of the Jacobian matrix. If it is greater than 10^6, go to step 18. Otherwise, continue to step 17.

Step 17. Update K values; $\ln K_{ij}^{(k+1)} = \ln K_{ij}^{(k)} + (\partial\ln K_{ij}/\partial T_D)^{(k)}(T_D^{(k+1)} - T_D^{(k)})$. Go to step 8 after increasing the iteration step number by one; $k = k + 1$.

Step 18-1. Set t_L to the highest temperature among T_D^L, $T_D^{(k)}$, and $T_D^{(k+1)}$ that gives a negative g_3. Set t_U to the lowest temperature among $T_D^{(k)}$, $T_D^{(k+1)}$, and T_D^U that gives a positive g_3.

Step 18-2. $T_D^{(k+2)} = 0.5(t_L + t_U)$.

Step 18-3. Perform PT flash at $T_D^{(k+2)}$ to calculate $\beta_L^{(k+2)}$, $\beta_V^{(k+2)}$ and $x_{ij}^{(k+2)}$ such that $|f_{ij}^{(k+2)}| < \varepsilon_f$ for $i = 1, 2, \ldots, N_C$ and $|g_1^{(k+2)}| < \varepsilon_m$ and $|g_2^{(k+2)}| < \varepsilon_m$.

Step 18-4. Calculate the condition number of the Jacobian matrix. If it is greater than 10^6, continue to step 18-5. Otherwise, go to step 9.

Step 18-5. Calculate $g_3^{(k+2)}$. If $|g_3^{(k+2)}|$ is less than the tolerance ε_h, stop. Otherwise, $t_L = T_D^{(k+2)}$ for $g_3^{(k+2)} < 0$, and $t_U = T_D^{(k+2)}$ for $g_3^{(k+2)} > 0$. Then, go to step 18-2 after increasing the iteration step number by one; $k = k + 1$.

Steps 16 and 18-4 require the condition number of the Jacobian matrix. The condition numbers in these steps are calculated as $\|J\|_1 \cdot \|J^{-1}\|_1$, where $\|J\|_1$ is the one-norm of the Jacobian matrix J. Later in this section, condition numbers by use of the one-norm will be compared with more rigorous condition numbers by use of the SVD.

Steps 2, 7, 14, and 18-3 require K-value estimates at a given temperature. In this research, a simple but general method is developed for such K-value estimates for the L, V, and W phases on the basis of the following three assumptions: (i) Raoult's law for the W-V equilibrium relation for water, and for the L-V equilibrium relation for hydrocarbons, (ii) the water concentration in the W phase (x_{wW}) is nearly 100%, and (iii) $K_{iL} = x_{iL}/x_{iW}$ is large for hydrocarbons. That is,

$$K_{wL} \approx x_{wL}, \tag{4.11}$$

$$K_{wV} = x_{wV}/x_{wW} \approx P_w^{vap}/P, \tag{4.12}$$

$$K_{iL} = x_{iL}/x_{iW} \quad \text{for hydrocarbon component i,} \tag{4.13}$$

$$K_{iV} = x_{iV}/x_{iW} \approx (P_i^{vap}/P)K_{iL} \quad \text{for hydrocarbon component i.} \tag{4.14}$$

The correlation of Eubank et al. (1994) can provide x_{wL} for equation 4.11 as

$$\ln(x_{wL}) = -21.2632 + 5.9473 \times 10^{-2}T - 4.0785 \times 10^{-5}T^2 \tag{4.15}$$

for T < 550 K. For simplicity, K_{iL} is assumed to be 10^8 for all hydrocarbon components in this paper, although further improvement is possible by considering the effects of temperature and carbon number (CN) on K_{iL}. The vapor pressures of well-defined

126

components can be estimated by use of Wagner's correlation (Wagner 1973, McGarry 1983). Vapor pressures of pseudocomponents are directly calculated from the PR EOS. This method can be also used for the V, L, and W phases in multiphase flash for four and more phases. In a four-phase system consisting of the oleic (L_1), solvent-rich liquid (L_2), V, and W phases, for example, a complete set of K-value estimates is given by the above method and a certain K-value set for L_1 and L_2.

In step 14, if $T_D^{(k+1)}$ does not lie between T_D^L and T_D^U, a Regula Falsi iteration step is used to update $T_D^{(k+1)}$ as follows:

$$T_D^{(k+1)} = T_D^L - g_3^{(k)}(T_D^L - T_D^U)/(g_3^L - g_3^U),$$ (4.16)

where g_3^L and g_3^U are the dimensionless enthalpy constraints (equation 4.9 with N_P of three) calculated at T_D^L and T_D^U, respectively.

4.3.2   Case Study

Case 4.3 uses five components used in Luo and Barrufet (2005) as follows: 50% water (w), 15% pseudocomponent 1 (PC1), 10% pseudocomponent 2 (PC2), 10% pseudocomponent 3 (PC3), and 15% pseudocomponent 4 (PC4). The properties of this mixture are given in **Table 4.3.** Since the BIPs used by Luo and Barrufet (2005) are unknown, the correlation of Venkatramani and Okuno (2014) is used to assign BIPs for water with the pseudocomponents in this paper. Although this will result in underestimation of x_{wL}, as explained in Venkatramani and Okuno (2014), these BIP values are sufficient for demonstration of the robustness of the DS algorithm for narrow-boiling fluids.

Figure 4.19 presents the phase envelope in P-T space. The critical point is calculated at 741.86 K and 70.50 bars. **Figure 4.20** shows $\underline{H}^t$ from 350 K to 500 K at 30

bars. $\underline{H}^t$ is sensitive to temperature near the phase transition from L + V + W to L + V. Three phases are present between 402.01 K and 490.20 K at this pressure.

Figure 4.21 shows that β_V and β_W are sensitive to temperature in the narrow-boiling region. β_V increases from 0% to 54%, and β_W decreases from 48% to 0% as temperature increases within the three-phase region. The sensitivities of β_V and β_W to temperature are attributed to changes of phase compositions with temperature. **Figure 4.22** presents components' concentrations in the L and V phases. The W phase always consists of more than 99.99% water within the three-phase region, and its composition is not shown. The L and V phases become richer in water with increasing temperature. The PC1 concentration substantially decreases in the L and V phases with increasing temperature. The other three components in the L and V phases change only slightly with temperature. The L-V edge of the tie triangle moves predominantly in the direction parallel to the water-PC1 edge in composition space.

Figure 4.23 presents the condition number within the three-phase region at 30 bars. T_{ref} of 300 K and $\underline{H}_{spec}$ of −30,000 J/mol are used to make temperature and enthalpies dimensionless. The condition number significantly increases near the boundary between L + V + W and L + V. A PH flash calculation at 30 bars and −30,000 J/mol is considered for this five-component mixture. The solution temperature is 483.63 K. The initial temperature is set to 450 K. **Figure 4.24** shows the convergence behavior of the DS algorithm for this PH flash in terms of T and g_3 (equation 4.9 with N_P of three). The convergence is achieved at the 26th iteration. The Jacobian condition number is 1.04×10^6 at the 3rd iteration step, and the bisection algorithm robustly solves for T_D based solely on the enthalpy constraint after that.

The critical point for the five-component mixture in P-H space is calculated at 70.50 bars and −3633.99 J/mol. The DS algorithm is tested for 350 discrete P-H

conditions in the three-phase region, where the initial temperature is fixed at 450 K.   All the calculations successfully converge to the correct solutions.   **Figure 4.25** shows that the number of iterations required tends to increase with the condition number of the Jacobian matrix at the convergence.   Figure 4.25 also shows the sensitivity of the iteration number to $\Delta T = |T_{sol} - T_{ini}|$, where T_{sol} is the solution temperature and T_{ini} is the initial temperature, 450 K.   The results show that the convergence behavior of the DS algorithm is insensitive to the initial temperature in these calculations.

4.4 MULTIPHASE PH FLASH INTEGRATED WITH STABILITY ANALYSIS

The new simultaneous PH flash integrated with stability analysis is formulated by combining the conventional PH-flash formulation with the PT stability criterion that the tangent plane to the Gibbs free energy surface at a stable equilibrium state cannot lie above the Gibbs free energy surface at any composition.   Then, a robust algorithm is developed for the formulated PH flash.

4.4.1   New Simultaneous PH Flash Algorithm

The new formulation is a simple integration of the PH-flash formulation (section 2.5.2) with Brantferger's analysis (1990, 1991).   As is explained in Brantferger (1991) and Brantferger et al. (1991), phase stability with PH specification can be analyzed at a given T, which defines the Gibbs free energy in composition space along with the specified P.   That is, the tangent plane to the Gibbs free energy surface at a stable equilibrium state at the solution T and specified P cannot lie above the Gibbs free energy surface at any composition (Baker et al. 1982, Michelsen 1982a).   This is the same as the stability criteria that must be satisfied in PT flash as given in chapter 3.

In other words, the formulation of simultaneous PH flash is the extension of that of with PT flash as discussed in chapter 3.   Temperature is an additional variable to be

solved for from enthalpy constraint. That is, the unified formulation for phase-stability and flash calculations in PH flash is to find a set of T and x_{ij} ($i = 1, 2, \ldots, N_C$, and $j = 1, 2, \ldots, N_S$) such that $D_j = 0$ subject to equations 2.35 to 2.38 for equilibrium phases $j = 1, 2, \ldots, N_P$, and $D_j > 0$ subject to equation 2.38 for unstable stationary points $j = (N_P + 1)$, $(N_P + 2)\ldots, N_S$. In what follows, we will present the solution scheme to the formulated PH flash. The main feature is the unified usage of the tangent plane distance function, D, for PH flash with adaptive selection of the reference composition for an arbitrary number of iterative compositions. A step-wise description is presented along with key equations. We duplicate some key equations that were given previously below to enhance readability.

The developed algorithm uses the tangent plane distance equations

$$f_{ij} = \ln x_{ij}\varphi_{ij} - \ln x_{ir}\varphi_{ir} - \theta_j = 0, \tag{4.17}$$

to update all iterative compositions x_{ij} ($i = 1, 2, \ldots, N_C$ and $j = 1, 2, \ldots, N_S$) through K values on the basis of direct substitution. Note that $\theta_j = D_j$ at an equilibrium state upon convergence. The N_S sampling compositions converge to stationary points; i.e., N_S becomes equal to the number of stationary points upon convergence. A reference composition is expressed as x_{ir} ($i = 1, 2, \ldots, N_C$). K values are defined as

$$K_{ij} = x_{ij}/\left(e^{\theta_j}x_{ir}\right), \tag{4.18}$$

for $i = 1, 2, \ldots, N_C$, $j = 1, 2, \ldots, N_S$, and $j \neq r$.

At an equilibrium state upon convergence, equation 4.17 becomes equation 3.2 (i.e., $\theta_j = D_j$), and the reference composition ($\underline{x}_r$) corresponds to one of equilibrium phases, which was denoted as x_{ir} in equation 3.1. Furthermore, $D_j = 0$ for N_P equilibrium phases (i.e., $j = 1, 2, \ldots, N_P$) and $D_j > 0$ for N_U unstable stationary points [i.e., $j = (N_P + 1)$, $(N_P + 2)\ldots, N_S$] upon convergence, where $N_S = N_P + N_U$.

130

During the iteration, a correct equilibrium state is searched for by updating temperature and N_S sampling compositions. The sampling compositions belong to either set P or set U. In set P, $\theta_j = 0$ and $0 < \beta_j < 1$ for j = 1, 2,…, N_P. In set U, $\theta_j > 0$ and $\beta_j = 0$ for j = (N_P + 1), (N_P + 2)…, N_S. Equation 4.17 is solved together with the material balance (equations 2.46 and 2.47) and the enthalpy constraint, $g_{N_P} = \underline{H}_D^t - 1.0 = 0$ (equation 4.9), for K values and T_D, where $T_D = T/T_{Ref}$, and T_{Ref} is some reference value that makes temperature better scaled (Zhu and Okuno 2014ab). The reference composition ($\underline{x}_r$) is selected from set P adaptively, as described later. To update the compositions in set P and U, the approach used in chapter 3 (equations 3.4 to 3.6) is used here.

The algorithm presented in this section is applicable for an arbitrary number of sampling compositions, which converge to stationary points of the tangent plane distance function at an equilibrium state upon convergence. As will be presented later, sampling compositions naturally merge for a case in which N_S is greater than the number of stationary points present upon convergence. This is the same as what occurs in the simultaneous PT flash algorithm given in chapter 3.

N_S sampling compositions can be initialized by various approaches as discussed in chapter 3. A random distribution and a distribution near vertices in composition space are useful when no reliable information is available for equilibrium phases of the fluid of interest.

The algorithm requires more sampling compositions than the number of equilibrium phases, which, in general, is unknown prior to the calculation. N_C sampling compositions may be sufficient in most petroleum applications, in which a few pseudo components are used in addition to well-defined light components, such as methane, ethane, and propane. However, at least (N_C + 1) sampling compositions are required for

one degree of freedom for multicomponent mixtures. In general, the iterative solution with this algorithm becomes more robust as N_S increases, because more information about the Gibbs free energy is carried by more sampling compositions, unless all sampling compositions are distributed concentratedly. However, use of more sampling compositions lowers the computational efficiency, as will be shown in the case studies. With N_S less than N_C, the algorithm may fail to find the correct number of equilibrium phases, unless specific information about equilibrium phases is available prior to the calculation.

The fundamental structure of the current algorithm broadly follows the direct substitution algorithm developed by Michelsen (1987), but is newly designed for integrated flash-stability calculations on the basis of the PH-flash algorithm developed by Zhu and Okuno (2014b). Each iteration first solves equations 3.5 and 3.6 for sets P and U, respectively, in sequence for a given set of K values and overall composition. Then, the traditional direct substitution with equation 4.17 is used to update K values for sets P and U in composition space. After that, one Newton's iteration step is performed for $(N_P - 1)$ β's and T_D by use of the system of N_P equations (equations 4.9 and 3.5), as in Michelsen (1987). Finally, K values for sets P and U are updated in temperature space for the subsequent iteration.

This fundamental structure is augmented by various important steps for robustness. Firstly, it is crucial to check the feasibility for each RR solution by use of the method of Okuno et al. (2010). This has been discussed in details in chapter 3. Also, the decoupling of T_D from β's is necessary to solve degenerate systems of equations (equations 4.9 and 3.5) for narrow-boiling fluids, as presented in Zhu and Okuno (2014ab). A new analysis of narrow-boiling behavior will be presented in the next section. Furthermore, the upper and lower temperature limits (T_D^U and T_D^L) are

used not to have unrealistic temperature values during the iterations. In this research, the upper and lower temperature limits are selected at 288.15 K and 675 K, respectively. The limits are set to cover a sufficiently wide range of temperatures for the application of interest. The initial guess for temperature should be within the limits.

The PR EOS (Peng and Robinson 1976) with the van der Waals mixing rules is used to calculate thermodynamic properties in this research. Pertinent derivatives can be found in Appendix A. A stepwise description of the multiphase isenthalpic flash algorithm integrated with stability analysis and the flow chart of the algorithm presented in this section is given in **Appendix E**.

The algorithm presented in this paper is substantially different from that of Gupta et al. (1990). As is the case in their simultaneous PT flash, stability equations were solved simultaneously with equation 3.5 and 4.9 in their algorithm. However, the unified formulation presented earlier in this section clearly shows that the complete formulation does not require Gupta et al.'s stability equations. Consequently, the Jacobian matrix used in our algorithm is always smaller than that of Gupta et al. which is of $(2N_P - 1) \times (2N_P - 1)$.

A second difference is that the algorithm of Gupta et al. (1990) uses Newton's iteration step even for a narrow-boiling fluid, for which the system of equations is nearly degenerate (Zhu and Okuno 2014ab). This leads to non-convergence as studied in detail by Zhu and Okuno (2014ab). The algorithm in this research adaptively switches between Newton's iteration and bisection depending on the condition number of the Jacobian matrix. A third difference lies in the stopping criteria. In this chapter, the fugacity and enthalpy equations are properly satisfied upon convergence. This is in contrast to the algorithm of Gupta et al. (1990), which tests only the difference between two consecutive iteration steps in terms of temperature and phase compositions. Other

133

differences associated with the initialization step and the selection of a reference composition, $\underline{x}_r$, have been discussed in chapter 3.

4.4.2   Case Study

In this section, the algorithm developed in this research is applied to a ternary mixture consisting of a single component bitumen.   Sampling compositions are initialized by use of a random distribution and a distribution near vertices in composition space, unless otherwise stated.   That is, when $N_S = N_C$, the N_S compositions are placed near the NC vertices in composition space.   When $N_S > N_C$, N_C sampling compositions are placed near the compositional vertices, and the other $(N_S - N_C)$ sampling compositions are distributed by use of a random-number generator.   A sampling composition selected near a compositional vertex consists of 99.9% that component and 0.1% the equimolar mixture of the other components in this section.

Case 4.4 uses three components consisting of 2.2% water (w), 92.8% n-butane (C_4), and 5.0% bitumen (C_B).   The components' properties are given in **Table 4.4**.   The critical properties for water were taken from (Venkatramani 2014).   They are not physical values, but were optimized in terms of vapor pressure and density using the PR EOS.   This mixture is used because it gives very complicated phase behavior and serves as a challenging case for the algorithm developed in this research.   Whether this phase behavior occurs in reality is uncertain and beyond the scope of this research.

Figure 4.26 shows $\underline{H}^t$ from 375 K to 475 K at 35 bars.   At 35 bars, C_B-rich phase (L_1) + C_4-rich phase (L_2) + aqueous phase (W) exists from 375 K to 400.89 K, $L_1 + L_2$ from 400.89 K to 416.24 K, $L_1 + L_2$ + vapor phase (V) from 416.24 K to 418.55 K, and $L_1 + V$ from 418.55 K to 475 K. $\underline{H}^t$ is highly non-linear with respect to temperature near the phase transition between $L_1 + L_2$ and $L_1 + L_2 + V$.

Figure 4.27 shows the Jacobian condition number in the $L_1 + L_2 + V$ region at 35 bars. The scaling of temperature and enthalpy is conducted with T_{ref} of 300 K and $\underline{H}_{spec}$ of 5,000 J/mol. The Jacobian condition number exceeds 10^6 between 416.24 K and 417.55 K, indicating narrow-boiling behavior. Figure 4.27 also shows that the Hessian matrix of the RR convex function is reasonably well-conditioned; hence, the RR portion of the system of equations is not problematic in the three-phase region. However, Figure 4.26 clearly shows that the total enthalpy is sensitive to temperature near the phase boundary between $L_1 + L_2$ and $L_1 + L_2 + V$. In this case, therefore, the narrow-boiling behavior occurs because K values are sensitive to temperature.

A PH flash calculation at 35 bars and 5,000 J/mol is considered for this ternary fluid. The initial T is set to 375 K, at which $L_1 + L_2 + W$ coexist. In this calculation, N_S is set to six, of which three sampling compositions are placed near the compositional vertices. The other three sampling compositions are randomly distributed (see **Table 4.5a**). The solution temperature is 416.89 K in the narrow-boiling region (see Figure 4.26).

Figure 4.28 shows the iterative solution in terms of T, residual of equation 4.9 (g_{NP}), and N_P. At the 30th iteration when T is 417.10 K, narrow-boiling behavior is detected by a large condition number of the Jacobian matrix. From this iteration on, T_D is decoupled from β's until it linearly converges to the correct solution at the 63rd iteration. The iterative temperature fluctuates between different phase regions, indicating the complex solution (Figure 4.28a). As shown in Figure 4.28c, N_P also fluctuates until the correct number of phases is detected at the 33th iteration. Two sampling compositions merge at the 2nd iteration in this case. However, N_S remains six during the iteration, because a new sampling point is added once the merging occurs as described in the algorithm section.

Figures 4.29 shows the six sampling compositions at different iteration steps.   In these ternary diagrams, solid dots represent the sampling compositions in set P, which are considered for material balance.   Hollow dots represent the sampling compositions in set U, which are excluded from material balance.   The 1st iteration starts with all sampling compositions included in material balance in this case.   Therefore, the initial β's are calculated through the conventional RR equations, and the θ's are zero.

At the 2nd iteration, two sampling compositions merge.   Table 4.5b shows the compositions of sampling points at the 2nd iteration before the merging.   Sampling compositions 2 and 4 are merged.   Sampling composition 4 is deleted.   Then, a new sampling composition is added in order to maintain N_S of six.   The new sampling composition is selected from the previous iteration step, which is the one that has a greater difference from the deleted sampling composition.   Then, sampling composition 4 is replaced by (0.2025, 0.6906, 0.1069).   After that, only sampling compositions 4 and 6 are included in material balance, as shown by the two solid dots in figure 4.29b. Figures 4.29c and 4.29d show the sampling compositions at the 23rd and 28th iterations, in which the iterative temperatures lie in different phase regions as shown in Figure 4.28a. Figure 4.29e shows the sampling compositions at the 63rd iteration, in which three equilibrium compositions are obtained.   The final set of sampling compositions is presented in Table 4.5c.   The three equilibrium phases are compositions 2, 4, and 6. The θ values at the other three compositions are positive, indicating that they are unstable.

Different initialization schemes proposed in the literature are tested for case 1. Use of the scheme proposed by Gupta et al. (1990) results in an unbounded feasible region for the RR solution, which prevents the algorithm from proceeding at the 1st

iteration. With the K-value correlation developed by Zhu and Okuno (2014b), the algorithm successfully converges in 64 iterations.

The algorithm of Gupta et al. (1990) is also tested for this case. It can be initialized if the K-value correlation of Zhu and Okuno (2014b) is used. However, it stops from proceeding at the 9th iteration due to an unbounded feasible region for the RR solution. Even if the RR issue is resolved by a proper modification, it still stops from proceeding at the 32nd iteration due to narrow-boiling behavior. This is because narrow-boiling behavior causes the system of equations to be nearly degenerate; thus, the decoupling of the variables should be performed as in this research. Their algorithm may also fail to converge to the correct solution because the number of phases can only decrease during the iteration with their algorithm.

One of the advantages of the new algorithm is that N_S gives the flexibility in terms of robustness and efficiency. It becomes more robust with increasing N_S at the expense of computational efficiency. As N_S increases, the algorithm becomes more robust because the possibility of finding all stationary points of the tangent-plane distance function increases. In case 4.4, the number of stationary points detected upon convergence is 3 with N_S of 3, 4 with N_S of 4 and 5, and 5 with N_S of 6 and higher. **Figure 4.30** shows the number of iterations required when starting with different N_S. All calculations start at the same initial T at 375 K. The three sampling points that are always used are near the compositional vertices. The other sampling compositions are randomly distributed for $N_S > 3$. The proposed algorithm successfully converges to the correct solution as long as N_S is greater than two. The number of iterations required tends to increase with increasing N_S because the algorithm with more sampling compositions may take more iterations when merging and adding some of the sampling compositions. This is a common observation for all the cases tested in this research.

The required number of iterations is 41 with the three sampling compositions placed near the compositional vertices. Interestingly, this is much lower than the number of iterations, 64, required when the K-value correlation by Zhu and Okuno (2014b) is used, although the number of sampling points is the same for the two cases. This indicates that a physically-derived correlation for K values does not necessarily result in fewer iterations than a random distribution and a distribution near vertices in composition space with the algorithm developed.

4.5 SUMMARY

This chapter presented a detailed analysis for narrow-boiling behavior and its effects on the DS isenthalpic flash for two and three phases. A modified DS algorithm was then developed based on the analysis. This chapter also presented a new algorithm for multiphase PH flash integrated with stability analysis. The correct set of equations is solved for stationary points on the tangent-plane-distance function that is defined at an adaptively selected reference composition. We also analyzed narrow-boiling behavior on the basis of the multiphase PH-flash equations, where energy and phase behavior equations are coupled through the temperature dependency of K values. Cases were presented to demonstrate the robustness of the developed algorithms and the narrow-boiling conditions derived. Conclusions are as following:

1. Narrow-boiling behavior is characterized by the enthalpy behavior that is substantially sensitive to temperature. The total enthalpy for a fixed overall composition and pressure becomes sensitive to temperature when at least one of the phase compositions drastically changes with a small change in temperature so that the phase mole fractions significantly change. The mechanistic understanding of the

narrow-boiling behavior was presented using the Gibbs free energy surfaces in binary composition space at different temperatures.

2. The prior DS algorithms (e.g., Michelsen 1987, Agarwal et al. 1991) have convergence issues when narrow-boiling behavior is involved. The fundamental reason is that the system of equations solved in the algorithms becomes degenerate for narrow-boiling fluids. The prior DS algorithms use temperature oscillation as an indicator for narrow-boiling fluids. However, temperature oscillation in these algorithms is a consequence of, not the reason for, the narrow-boiling behavior. That is, it is not a good indicator that improves the robustness.

3. The modified DS algorithm developed in this chapter adaptively switches between Newton's iteration step and the bisection algorithm depending on the DS Jacobian condition number that offers an unambiguous criterion regarding the computational accuracy and robustness in the DS algorithm. The bisection algorithm solves for temperature based solely on the enthalpy constraint when narrow-boiling behavior is identified by a large condition number of the Jacobian matrix. This decoupling of temperature from the other variables is plausible when the system of equations is degenerate.

4. The new simultaneous PH flash algorithm can robustly solve PH flash for narrow-boiling fluids. It does not require a special treatment for one degree of freedom, for which the total enthalpy is discontinuous in temperature. This is because the algorithm does not require to fix the number of equilibrium phases in the iteration. The advantage of the proposed algorithm is pronounced when the fluid of interest exhibits complex phase appearance/disappearance, and/or when narrow-boiling behavior is involved, as in thermal compositional flow simulation.

5.   The initialization of new simultaneous PH flash algorithm is possible even when no reliable information is available about the equilibrium phases of the fluid of interest.   No K-value correlation is necessary to initialize the new algorithm.

6.   The new simultaneous PH flash algorithm offers the flexibility in terms of robustness and efficiency depending on the number of sampling compositions (N_S) used. It becomes more robust with increasing N_S at the expense of computational efficiency. As N_S increases, the algorithm becomes more robust because the possibility of finding all stationary points of the tangent-plane distance function increases.   However, the number of iterations required tends to increase with increasing N_S because the algorithm with more sampling compositions may take more iterations when merging and adding some of the sampling compositions.

7.   The general condition for narrow-boiling behavior is that the interplay between the energy and phase behavior equations is significant.   Two subsets of the narrow-boiling condition were derived by analyzing the convex function whose gradient vectors consist of the RR equations; (i) the overall composition is near an edge of composition space, and (ii) the solution conditions (temperature, pressure, and overall composition) are near a critical point, including a critical endpoint.   A special case of the first specific condition is the fluids with one degree of freedom, for which enthalpy is discontinuous in temperature space.

8.   The analysis of the RR convex function gave the clear limiting conditions toward which the tendency of narrow-boiling behavior increases.   Narrow-boiling behavior tends to occur in thermal compositional simulation likely because water is by far the most dominant component in the fluid systems formed in the simulation.

Table 4.1. Properties for the components for case 4.1

Component	Mole fraction	T_C, K	P_C, bar	ω	$C_{P1}{}^0$	$C_{P2}{}^0$	$C_{P3}{}^0$	$C_{P4}{}^0$
C_1	0.99	190.6	46.0	0.008	19.250	5.212×10^{-2}	1.197×10^{-5}	-1.132×10^{-8}
C_4	0.01	425.2	38.0	0.193	9.487	3.313×10^{-1}	-1.108×10^{-4}	-2.822×10^{-9}
Binary interaction parameters are all zero.								
Critical temperature: 197.57 K								
Critical pressure: 53.05 bars								
Two-phase temperature region at P = 50.00 bars: [194.98, 228.20] K								
Units for $C_{P1}{}^0$, $C_{P2}{}^0$, $C_{P3}{}^0$, $C_{P4}{}^0$ are J/(mol K), J/(mol K^2), J/(mol K^3), J/(mol K^4), respectively.								

Table 4.2. Properties for the components for case 4.2

Component	Mole fraction	T_C, K	P_C, bar	ω	$C_{P1}{}^0$	$C_{P2}{}^0$	$C_{P3}{}^0$	$C_{P4}{}^0$
Water	0.75	647.3	220.89	0.344	32.200	1.907×10^{-3}	1.055×10^{-5}	-3.596×10^{-9}
C_3	0.15	369.8	42.46	0.152	-4.220	3.063×10^{-1}	-1.586×10^{-4}	3.215×10^{-8}
C_{16}	0.10	717.0	14.19	0.742	-13.000	1.529	-8.537×10^{-4}	1.850×10^{-7}

Binary interaction parameters:

	Water	C_3	C_{16}
Water	0.0000	0.6841	0.3583
C_3	0.6841	0.0000	0.0000
C_{16}	0.3583	0.0000	0.0000

Units for $C_{P1}{}^0$, $C_{P2}{}^0$, $C_{P3}{}^0$, $C_{P4}{}^0$ are J/(mol·K), J/(mol·K^2), J/(mol·K^3), J/(mol·K^4), respectively.

Table 4.3. Properties for the components for case 4.3

Component	Mole fraction	T_C , K	P_C, bar	ω	C_{P1}^0	C_{P2}^0	C_{P3}^0	C_{P4}^0
Water	0.50	647.3	220.9	0.344	32.20	1.907×10^{-3}	1.055×10^{-5}	-3.596×10^{-9}
PC1	0.15	305.6	48.8	0.098	-3.50	5.764×10^{-3}	5.090×10^{-7}	0.000
PC2	0.10	638.9	19.6	0.535	-0.404	6.572×10^{-4}	5.410×10^{-8}	0.000
PC3	0.10	788.9	10.2	0.891	-6.10	1.093×10^{-2}	1.410×10^{-6}	0.000
PC4	0.15	838.9	7.7	1.085	-4.50	8.049×10^{-3}	1.040×10^{-6}	0.000

Binary interaction parameters:

	Water	PC1	PC2	PC3	PC4
Water	0.00000	0.71918	0.45996	0.26773	0.24166
PC1	0.71918	0.00000	0.00000	0.00000	0.00000
PC2	0.45996	0.00000	0.00000	0.00000	0.00000
PC3	0.26773	0.00000	0.00000	0.00000	0.00000
PC4	0.24166	0.00000	0.00000	0.00000	0.00000

Units for C_{P1}^0, C_{P2}^0, C_{P3}^0, C_{P4}^0 are J/(mol·K), J/(mol·K^2), J/(mol·K^3), J/(mol·K^4), respectively.

Table 4.4. Properties for the components for case 4.4. The critical properties of water were taken from Venkatramani (2014).

Component	Mole fraction	T_C, K	P_C, bar	ω	C_{P1}^0	C_{P2}^0	C_{P3}^0	C_{P4}^0
Water	0.022	672.48	277.15	0.2699	32.200	1.907×10^{-3}	1.055×10^{-5}	-3.596×10^{-9}
C_4	0.928	421.56	36.01	0.2127	9.490	3.313×10^{-1}	-1.108×10^{-4}	-2.822×10^{-9}
C_B	0.050	847.17	10.64	1.0406	-31.900	3.612	-2.044×10^{-3}	4.486×10^{-7}

Binary interaction parameters:

	Water	C_4	C_B
Water	0.0000	0.5602	0.1100
C_4	0.5602	0.0000	0.0750
C_B	0.1100	0.0750	0.0000

Units for C_{P1}^0, C_{P2}^0, C_{P3}^0, C_{P4}^0 are J/(mol·K), J/(mol·K^2), J/(mol·K^3), J/(mol·K^4), respectively.

Table 4.5a. Six sampling compositions at the 1st iteration (case 4.4)

	Composition 1	Composition 2	Composition 3	Composition 4	Composition 5	Composition 6
x_{ij}	$5.011728395 \times 10^{-2}$	$5.00000000 \times 10^{-4}$	$5.00000000 \times 10^{-4}$	$2.024691358 \times 10^{-1}$	$2.026337137 \times 10^{-1}$	$9.99000000 \times 10^{-1}$
	$8.484938271 \times 10^{-1}$	$9.99000000 \times 10^{-1}$	$5.00000000 \times 10^{-4}$	$6.906419752 \times 10^{-1}$	$4.016934042 \times 10^{-1}$	$5.00000000 \times 10^{-4}$
	$1.013883334 \times 10^{-1}$	$5.00000000 \times 10^{-4}$	$9.99000000 \times 10^{-1}$	$1.068888890 \times 10^{-1}$	$3.956728821 \times 10^{-1}$	$5.00000000 \times 10^{-4}$

Table 4.5b. Six sampling compositions at the 2nd iteration before the merging of compositions 2 and 4 (case 4.4)

	Composition 1	Composition 2	Composition 3	Composition 4	Composition 5	Composition 6
x_{ij}	$9.999996463 \times 10^{-1}$	$1.048995656 \times 10^{-2}$	$1.033333973 \times 10^{-2}$	$1.051640199 \times 10^{-2}$	$9.013291891 \times 10^{-3}$	$8.932510699 \times 10^{-3}$
	$3.536746148 \times 10^{-7}$	$9.767356013 \times 10^{-1}$	$9.753538516 \times 10^{-1}$	$9.767748394 \times 10^{-1}$	$9.444418053 \times 10^{-1}$	$9.413768141 \times 10^{-1}$
	$2.538515500 \times 10^{-11}$	$1.277444214 \times 10^{-2}$	$1.431284427 \times 10^{-2}$	$1.270875861 \times 10^{-2}$	$4.654490280 \times 10^{-2}$	$4.969067520 \times 10^{-2}$

Table 4.5c. Six sampling compositions at the 63rd iteration (case 4.4)

	Composition 1	Composition 2	Composition 3	Composition 4	Composition 5	Composition 6
x_{ij}	$9.963029187 \times 10^{-1}$	$3.987093567 \times 10^{-2}$	$4.042558722 \times 10^{-2}$	$2.821421577 \times 10^{-2}$	$2.844511013 \times 10^{-2}$	$1.762505600 \times 10^{-2}$
	$1.753511927 \times 10^{-11}$	$9.599949394 \times 10^{-1}$	$9.517664807 \times 10^{-1}$	$7.764909338 \times 10^{-1}$	$8.109556208 \times 10^{-1}$	$9.629795682 \times 10^{-1}$
	$3.697081246 \times 10^{-3}$	$1.341248777 \times 10^{-4}$	$7.807932011 \times 10^{-3}$	$1.952948503 \times 10^{-1}$	$1.605992690 \times 10^{-1}$	$1.939537572 \times 10^{-2}$
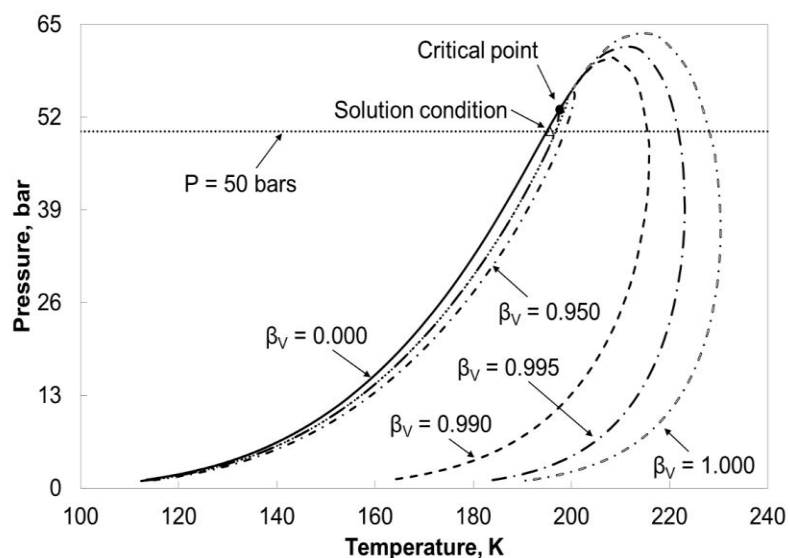
(a)
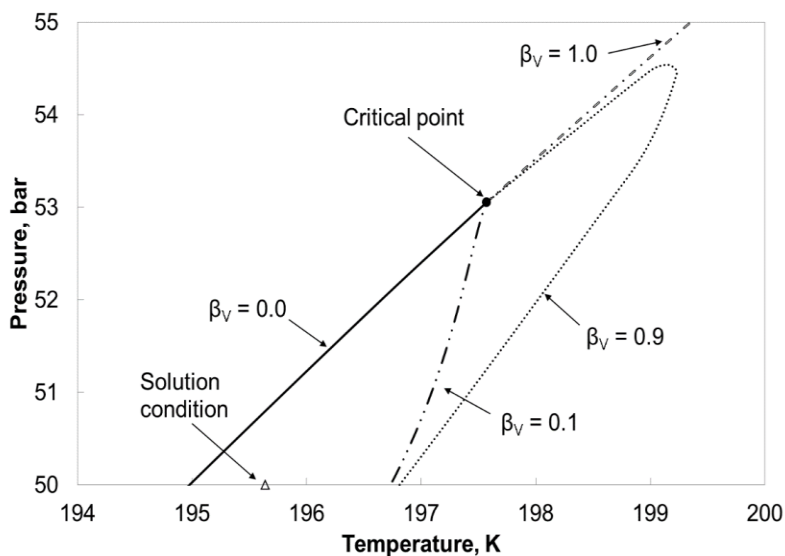
(b)

Figure 4.1. Two-phase envelope in P-T space for a mixture of 99% C_1 and 1% C_4. The properties used for the components are given in Table 4.1. The critical point is calculated at 197.57 K and 53.05 bars with PR EOS. (a) β_V contour lines are significantly dense near bubble-point curve. The solution temperature (195.65 K) for an example PH calculation at P = 50 bars and $\underline{H}_{spec}$ = −6500 J/mol exists in the vicinity of the bubble-point curve. (b) Magnified PT diagram near the critical point.

144
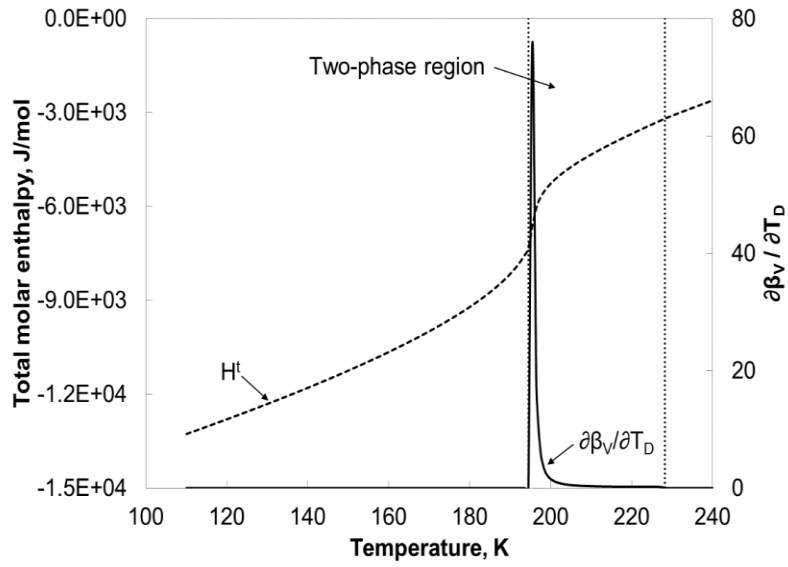
Figure 4.2. The total molar enthalpy and the sensitivity of β_V to temperature at 50 bars for a mixture of 99% C_1 and 1% C_4. The properties used for the components are given in Table 4.1. Two phases are present from 194.98 K to 228.20 K. The total molar enthalpy and β_V at 50 bars are sensitive to temperature near the bubble point. The $\partial\beta_V/\partial T_D$ can be higher than 70, where T_D is calculated using equation A-1.1 with T_{ref} of 300 K.
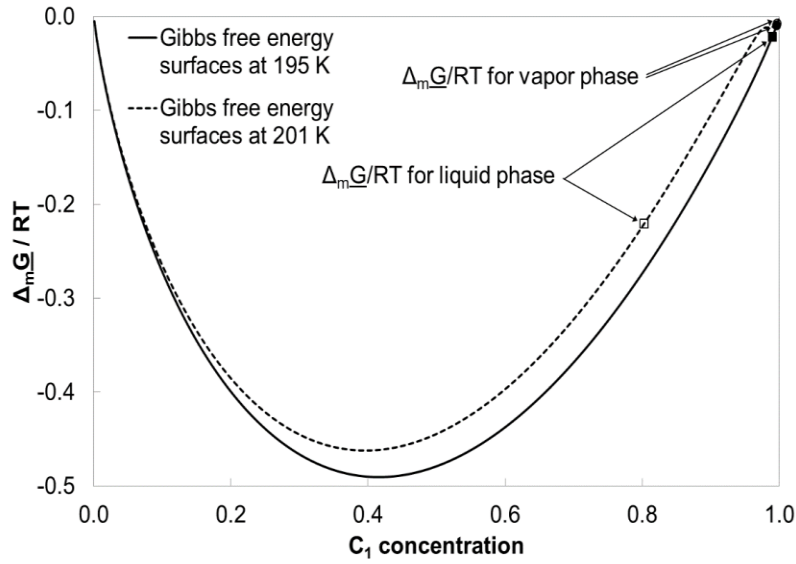
(a)
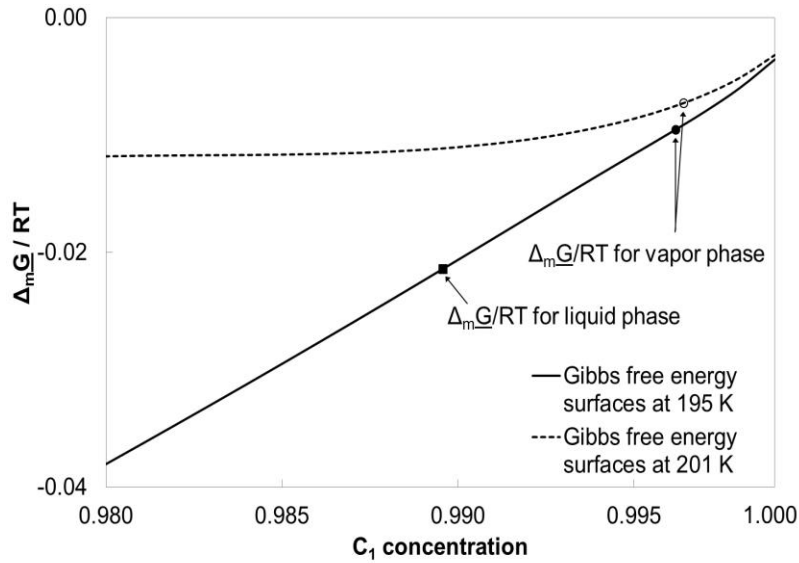
(b)

Figure 4.3. (a) Gibbs free energy surfaces in binary composition space at 50 bars at two different temperatures $T_1 = 195$ K and $T_2 = 201$ K. The properties used for the components are given in Table 4.1. (b) Magnified Gibbs free energy surfaces near the C_1 edge of composition space. As temperature increases from T_1 to T_2, the L phase composition drastically changes. β_V changes from 0.0644 at T_1 to 0.9669 at T_2.

146
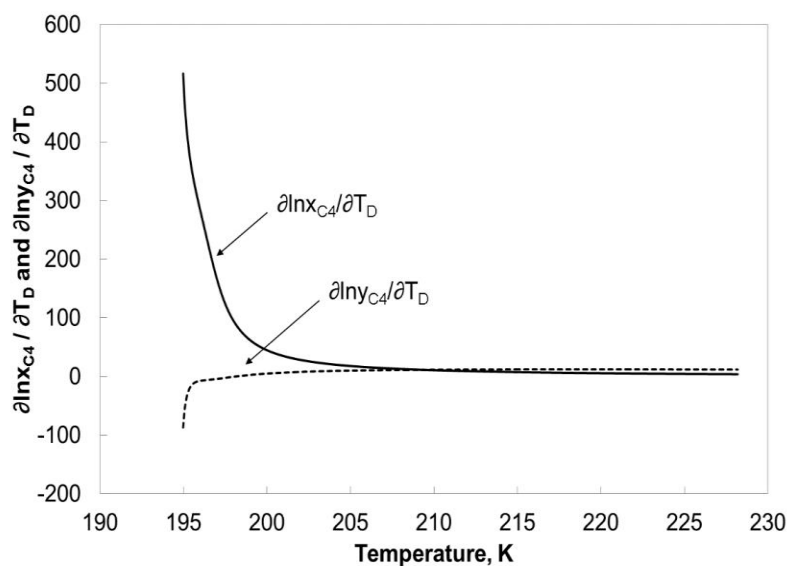
Figure 4.4. Sensitivities of the C_4 concentrations in the V and L phases to temperature at 50 bars for a mixture of 99% C_1 and 1% C_4.   The properties used for the components are given in Table 4.1.
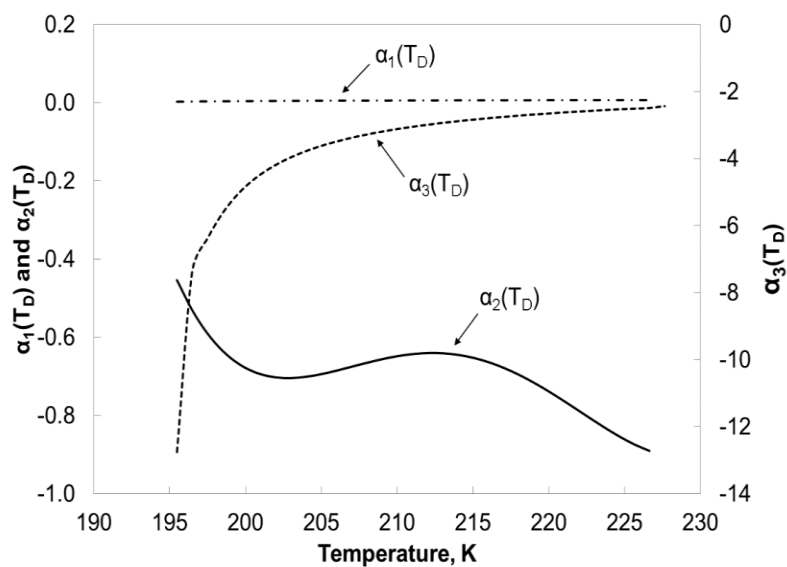
Figure 4.5. Three parameters α_1, α_2, and α_3 of equation A-1.14 at 50 bars for a mixture of 99% C_1 and 1% C_4.   The properties used for the components are given in Table 4.1.

147
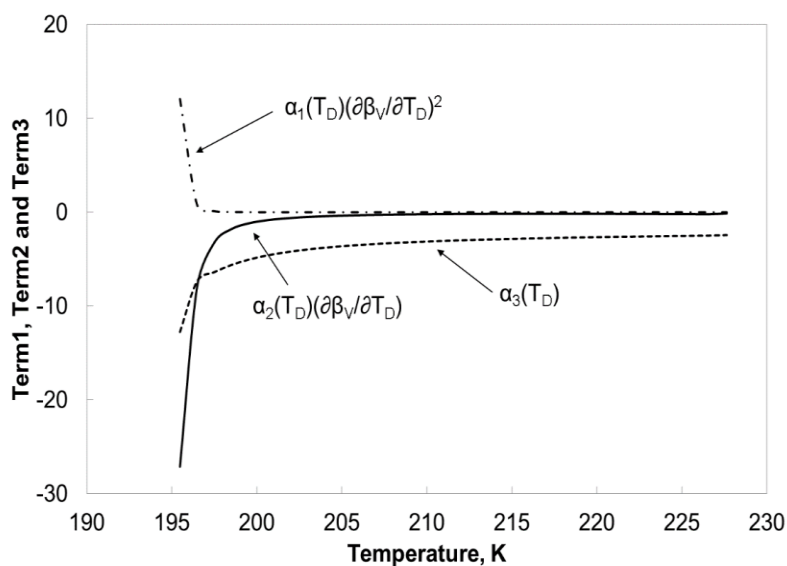
Figure 4.6. Three terms of equation A-1.14 at 50 bars for a mixture of 99% C_1 and 1% C_4. The properties used for the components are given in Table 4.1.
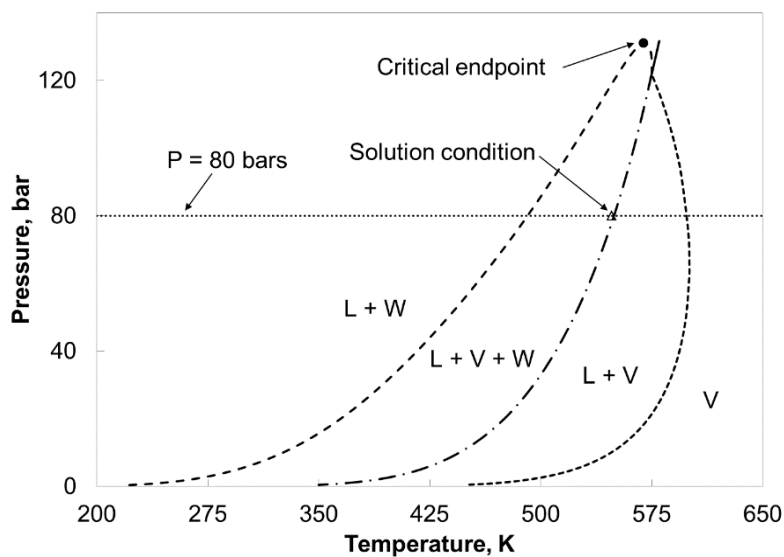
Figure 4.7. Phase boundaries in P-T space for a mixture of 75% water, 15% C_3, and 10% C_{16}. The properties used for the components are given in Table 4.2. The critical endpoint of type $L = V + W$ is calculated at 569.35 K and 131.07 bars with the PR EOS.

148
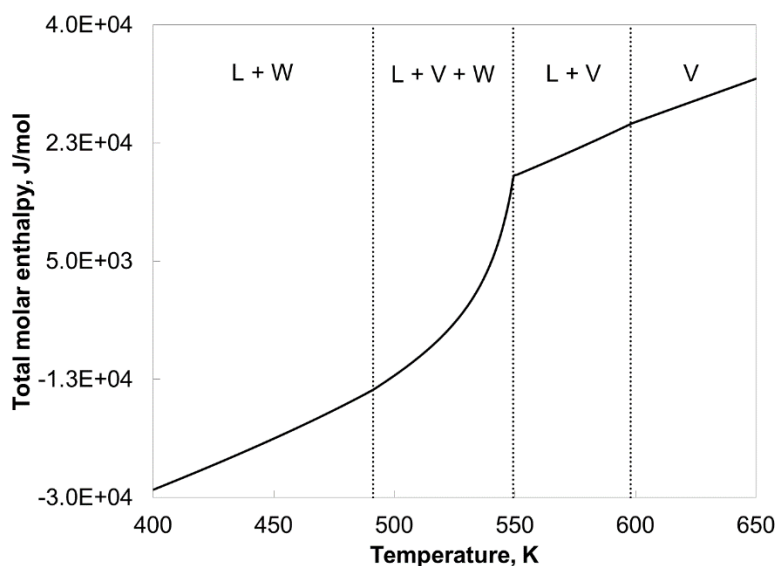
Figure 4.8. Total molar enthalpy at 80 bars for a mixture of 75% water, 15% C_3, and 10% C_{16}. The properties used for the components are given in Table 4.2. Three phases are present from 491.17 K to 549.25 K. The total molar enthalpy at 80 bars is sensitive to temperature near the phase boundary between L + V + W and L + V.
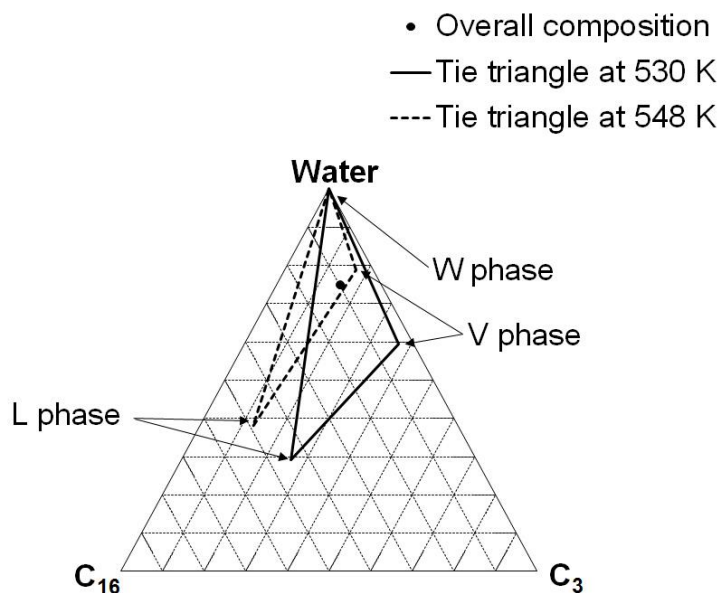
Figure 4.9. Tie triangles in composition space at 80 bars at two different temperatures T_1 = 530 K and T_2 = 548 K. The overall composition is 75% water, 15% C_3, and 10% C_{16}. The properties used for the components are given in Table 4.2.

149
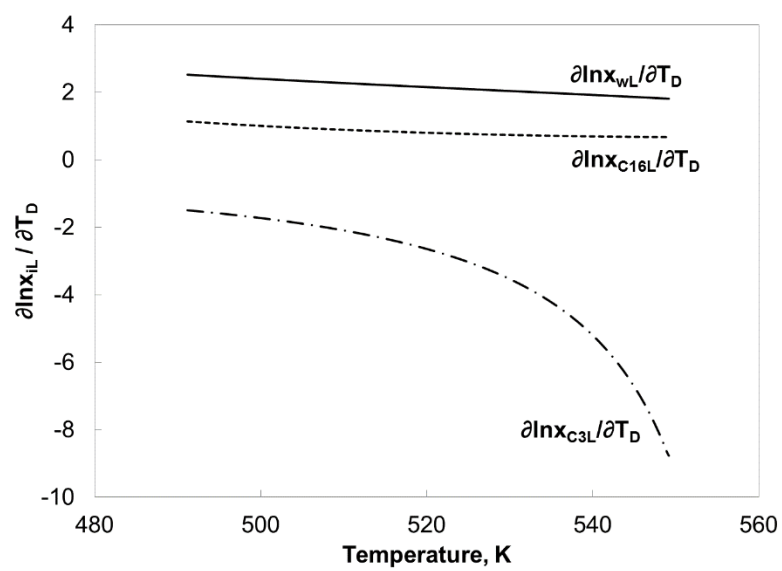
(a)
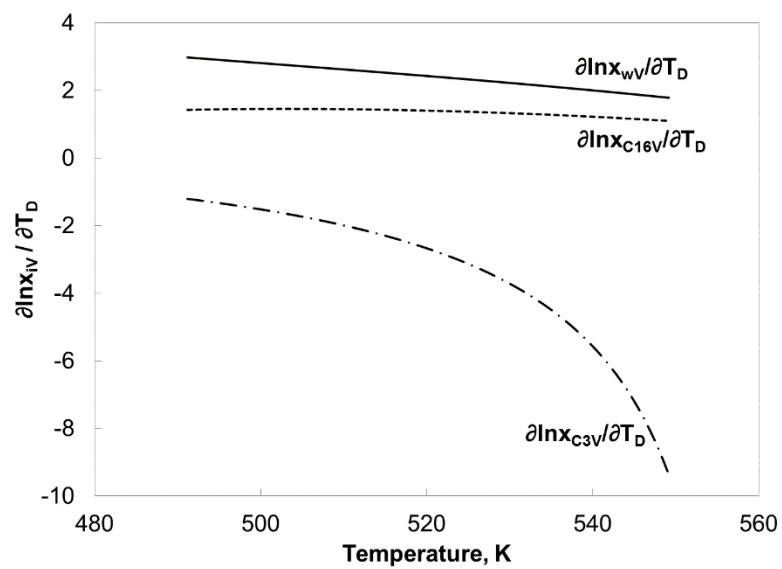
(b)

Figure 4.10. (Continued below)
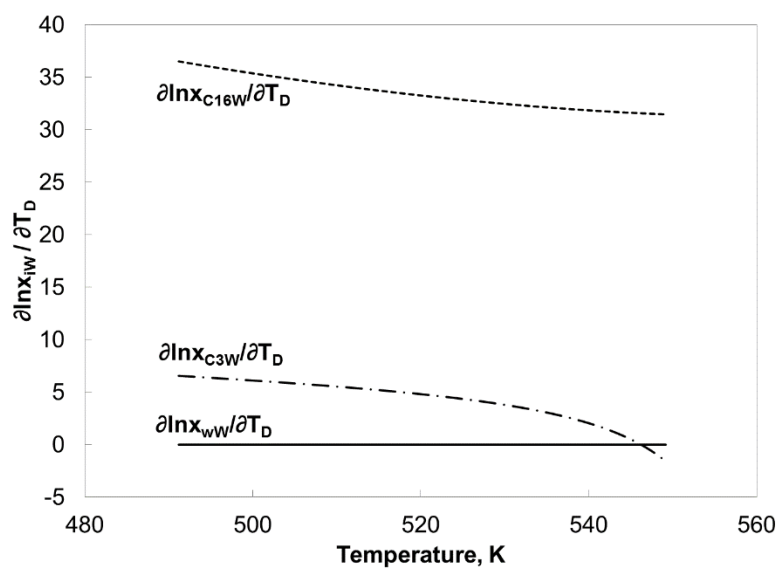
(c)

Figure 4.10. Sensitivities of the phase compositions to temperature at 80 bars for a mixture of 75% water, 15% C_3, and 10% C_{16}. (a) L phase, (b) V phase, and (c) W phase. The properties used for the components are given in Table 4.2.
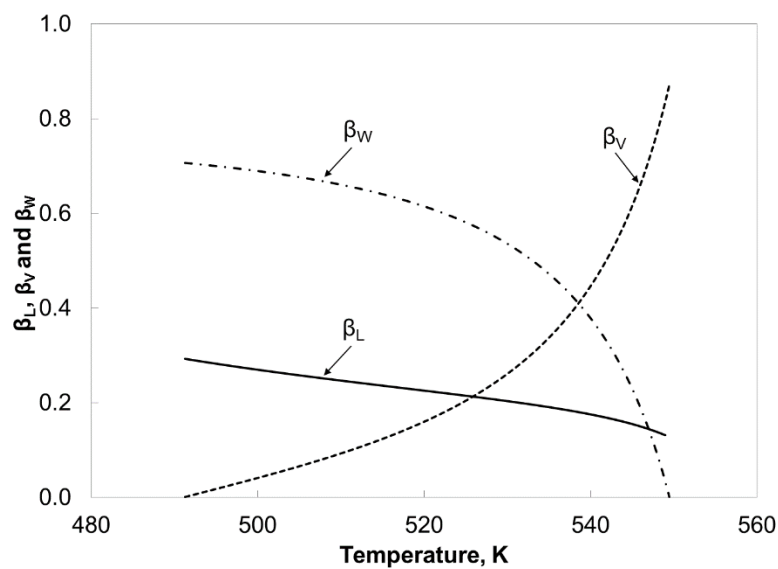
Figure 4.11. Mole fractions of the L, V, and W phases in temperature space at 80 bars for a mixture of 75% water, 15% C_3, and 10% C_{16}. The properties used for the components are given in Table 4.2.
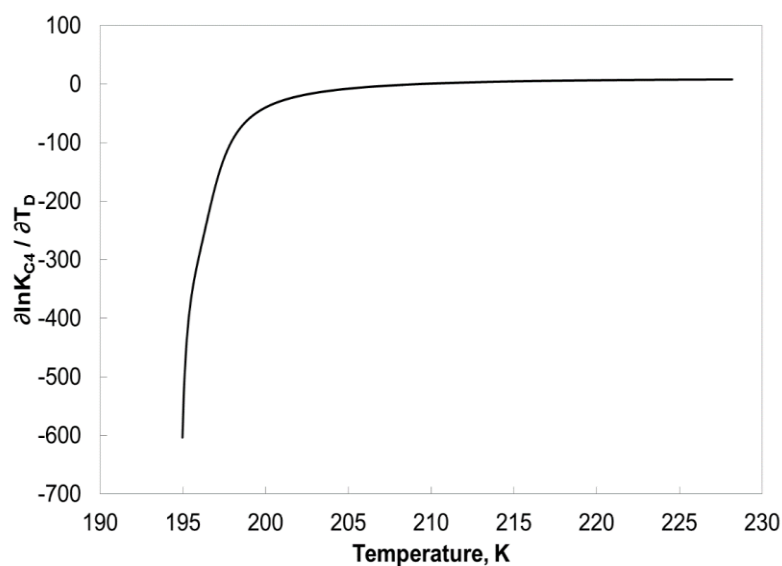
Figure 4.12. The first-order derivative of lnK_{C4} with respect to T_D, showing the sensitivity of K_{C4} to temperature at 50 bars for a mixture of 99% C_1 and 1% C_4. The properties used for the components are given in Table 4.1.
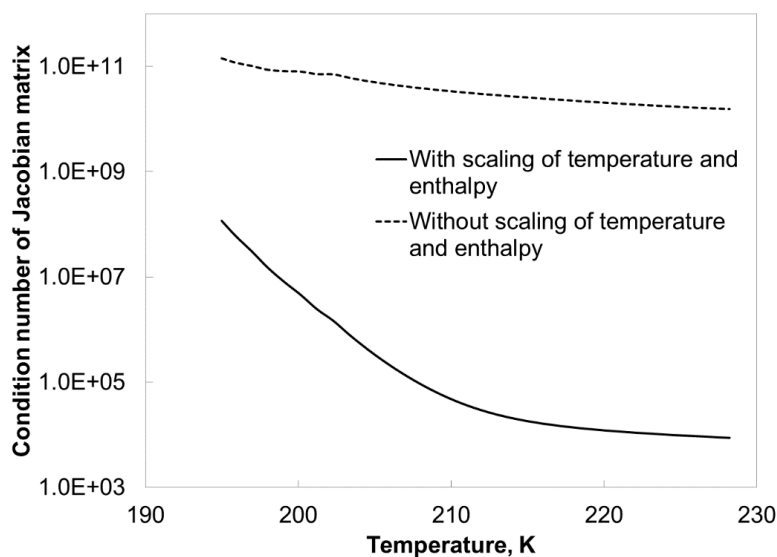
Figure 4.13. The condition numbers of the Jacobian matrices with and without scaling of temperature and enthalpy at 50 bars for a mixture of 99% C_1 and 1% C_4. The scaling is conducted using equations A-1.1 and A-1.2 with $\underline{H}_{spec}$ of -6500 J/mol and T_{ref} of 300K. The properties used for the components are given in Table 4.1.
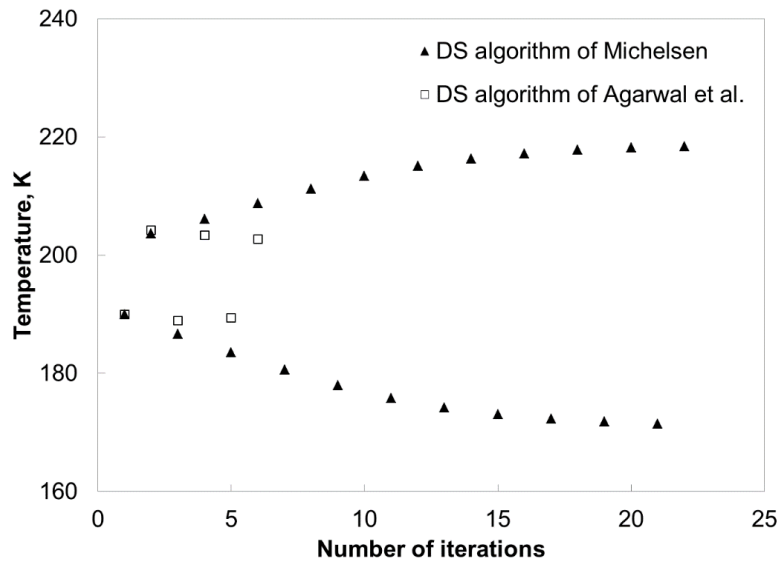
Figure 4.14. Convergence behavior of the DS algorithms of Michelsen and Agarwal et al. in terms of temperature at P = 50 bars and $\underline{H}_{spec}$ = −6500 J/mol for a mixture of 99% C_1 and 1% C_4 (Table 4.1). The solution temperature is 195.65 K. The temperature oscillation is identified at the 6th iteration step for the DS algorithm of Agarwal et al. A similar oscillation is observed for the DS algorithm of Michelsen, but the oscillation testing procedure with the C value used does not identify it until the 22nd iteration step (see section 2.5.2 and Appendix B for details of their DS algorithms).
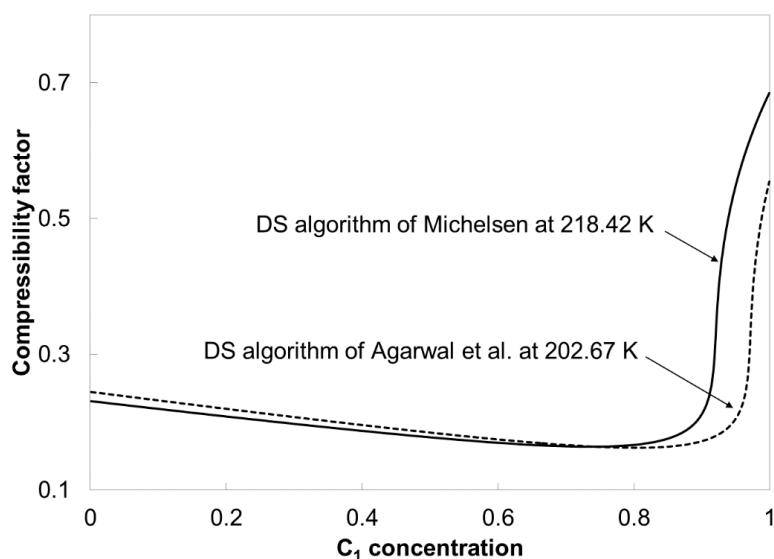
Figure 4.15. Compressibility factors in composition space when temperature oscillations are detected at P = 50 bars and $\underline{H}_{spec}$ = -6500 J/mol for a mixture of 99% C_1 and 1% C_4. Temperature oscillation occurs at the 22nd iteration step (218.42 K) for Michelsen's DS algorithm, and at the 6th iteration step (202.67 K) for Agarwal et al.'s DS algorithm.   In either case, only one compressibility factor exists in the cubic equation solution.
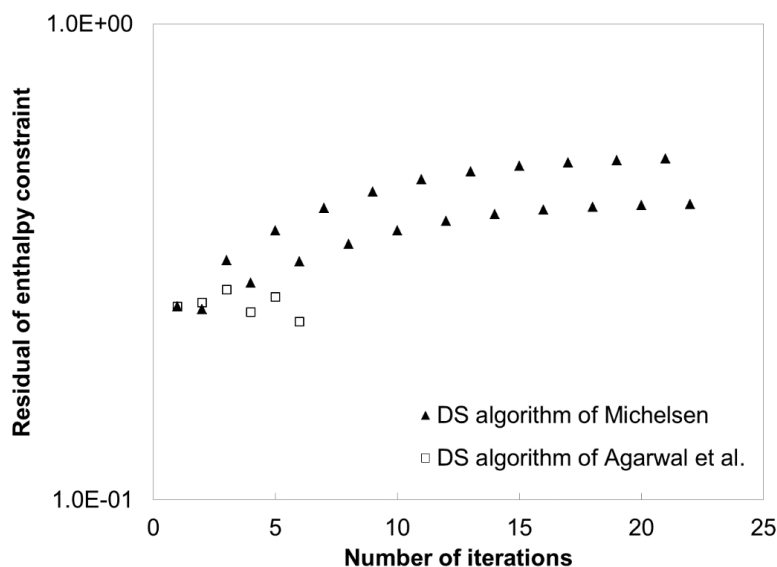
Figure 4.16. Convergence behavior of the DS algorithms of Michelsen and Agarwal et al. in terms of the enthalpy constraint in PH flash at 50 bars and $\underline{H}_{spec}$ = −6500 J/mol for a mixture of 99% C_1 and 1% C_4 given in Table 4.1.

154
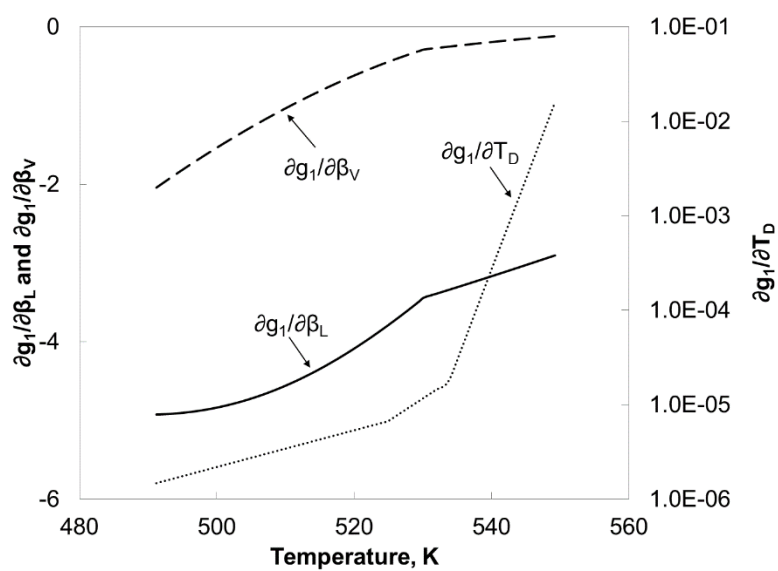
(a)
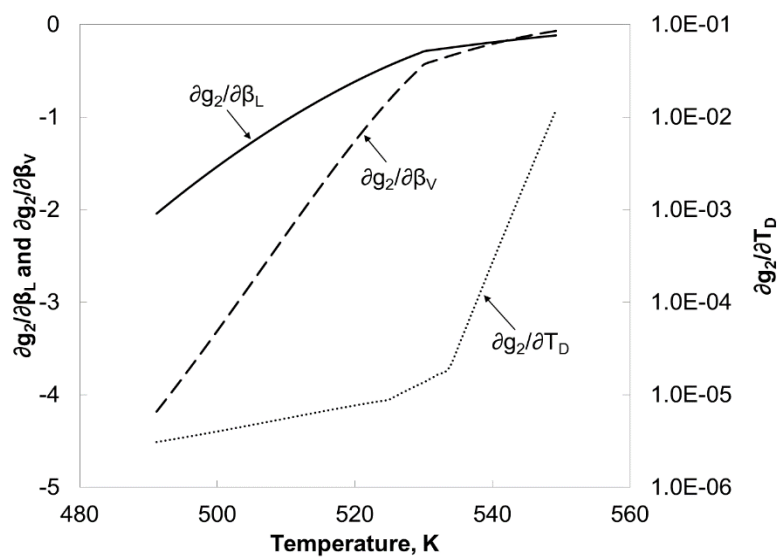
(b)

Figure 4.17. (Continued below)

155
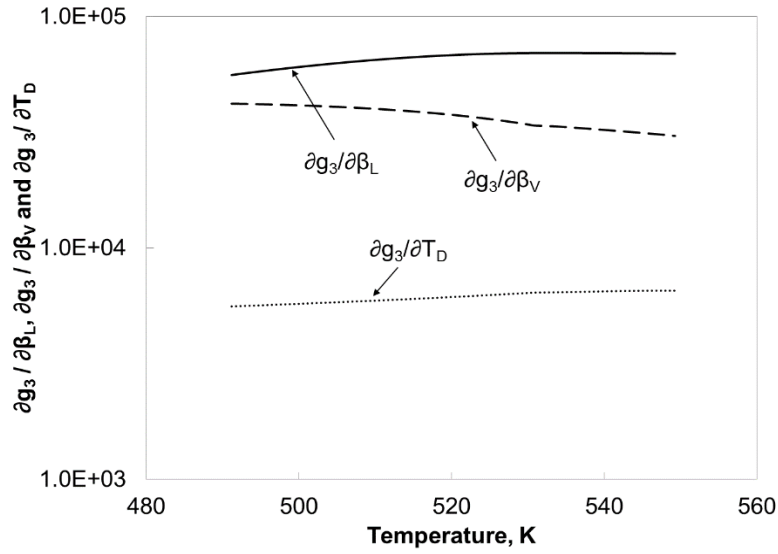
(c)

Figure 4.17. Elements of the 3×3 Jacobian matrix, at 80 bars for a mixture of 75% water, 15% C_3, and 10% C_{16} given in Table 4.2. (a) Derivatives of g_1, $\partial g_1/\partial \beta_L$, $\partial g_1/\partial \beta_V$, and $\partial g_1/\partial T_D$. (b) Derivatives of g_2, $\partial g_2/\partial \beta_L$, $\partial g_2/\partial \beta_V$, and $\partial g_2/\partial T_D$. (c) Derivatives of g_3, $\partial g_3/\partial \beta_L$, $\partial g_3/\partial \beta_V$ and $\partial g_3/\partial T_D$. The equations of g_1 and g_2 are defined in equation 2.49 with N_P of three. The g_3 equation is defined in equation 2.50 with N_P of three.
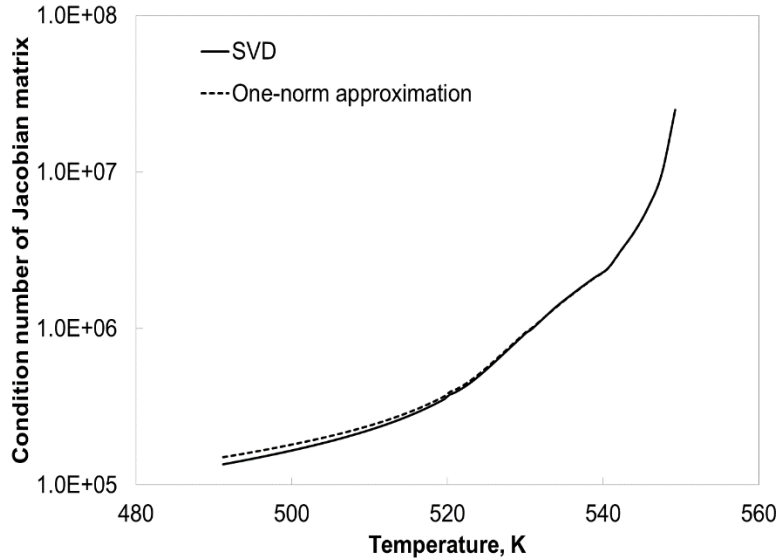
Figure 4.18. Condition number of the Jacobian matrix within the three-phase region at 80 bars for a mixture of 75% water, 15% C_3, and 10% C_{16} given in Table 4.2.

156
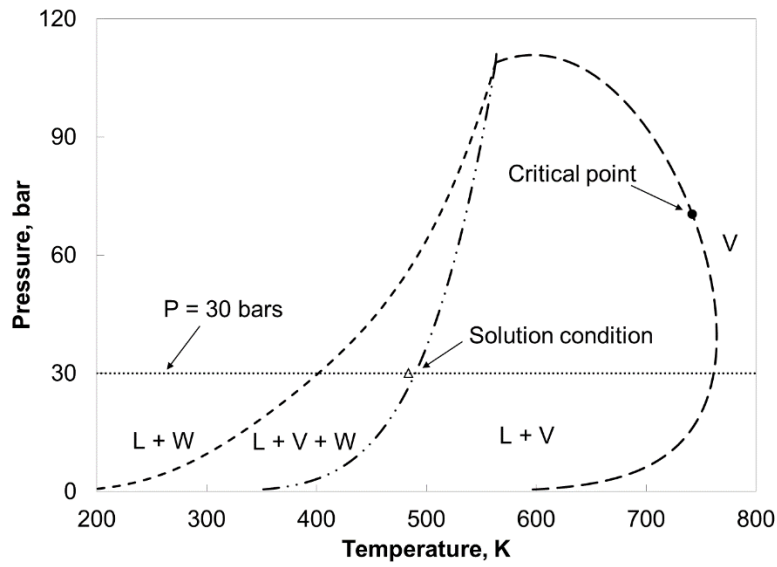
Figure 4.19. Phase boundaries in P-T space for the five-component mixture given in Table 4.3. The critical point is calculated at 741.86 K and 70.50 bars using the PR EOS.
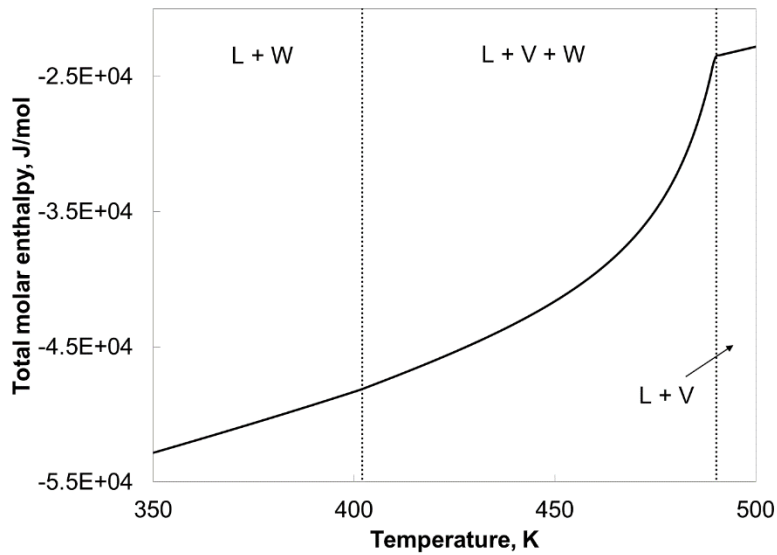
Figure 4.20. Total molar enthalpy at 30 bars for the five-component mixture given in Table 4.3. Three phases are present from 402.01 K to 490.20 K. The total molar enthalpy at 30 bars is sensitive to temperature near the phase boundary between L + V + W and L + V.

157
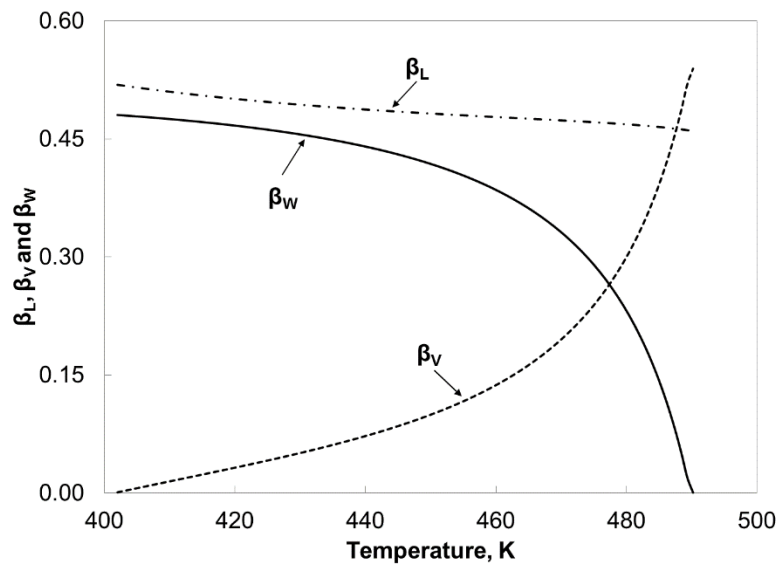
Figure 4.21. Mole fractions of the L, V, and W phases at 30 bars for the five-component mixture given in Table 4.3.

158
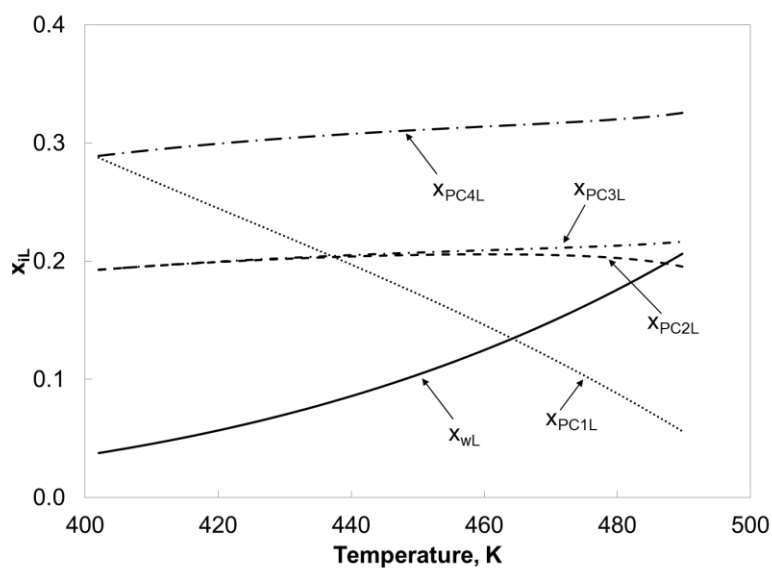
(a)
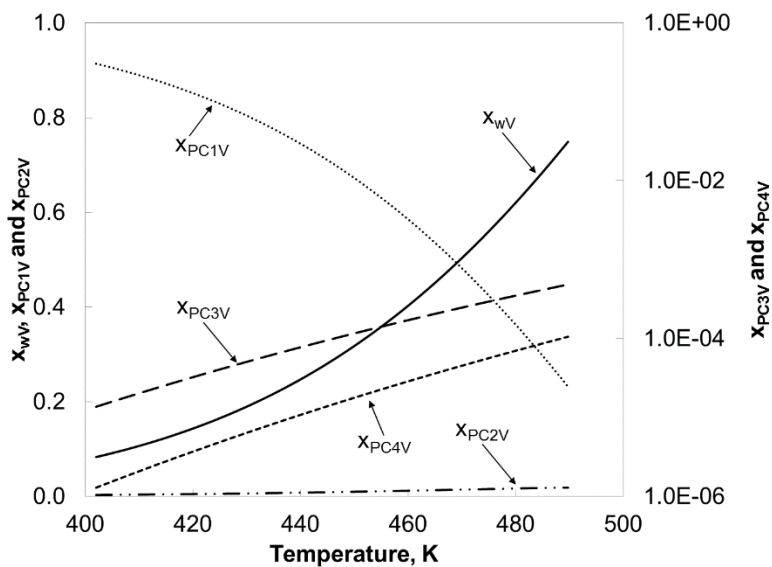
(b)

Figure 4.22. Concentrations of the components at 30 bars for the five-component mixture given in Table 4.3. (a) L phase, (b) V phase. The W phase consists of more than 99.99% water within the three-phase region, and its composition is not shown.
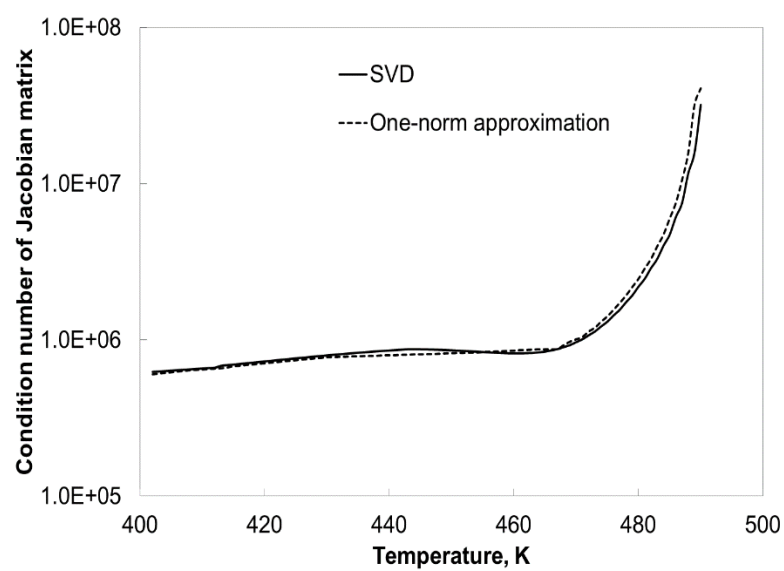
Figure 4.23. Condition number of the Jacobian matrix within the three-phase region at 30 bars for the five-component mixture given in Table 4.3.
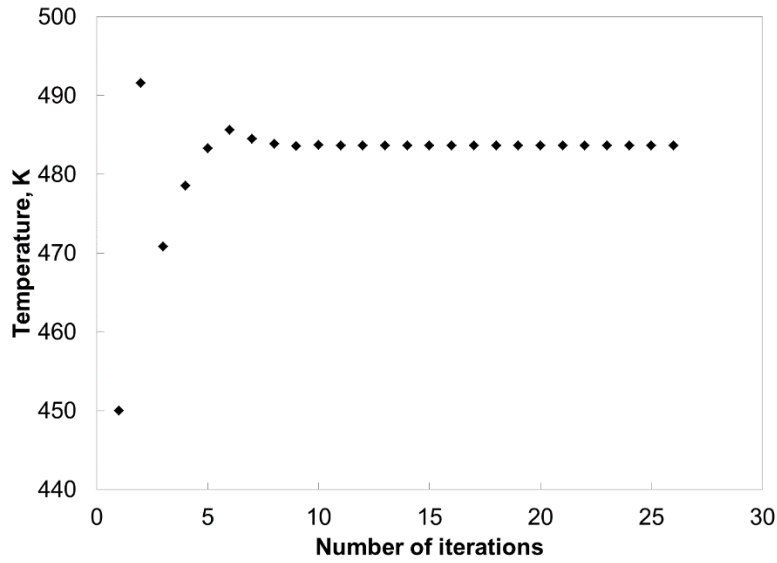
(a)
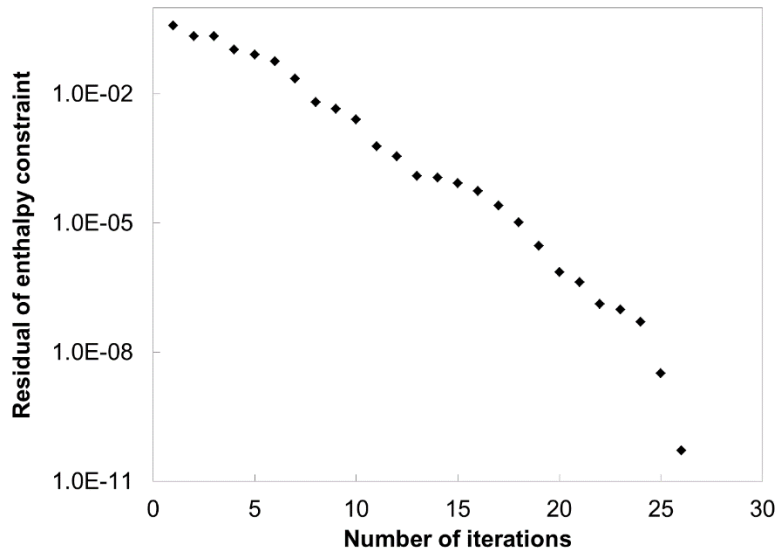
(b)

Figure 4.24. Convergence behavior of the DS algorithm in PH flash at P = 30 bars and $\underline{H}_{spec}$ = −30,000 J/mol for the five-component mixture given in Table 4.3. The solution temperature is 483.63 K. (a) Convergence behavior of the DS algorithm in terms of temperature. A high sensitivity of enthalpy to temperature is detected at the 3rd iteration (470.80 K) when the condition number of the Jacobian matrix is 1.04×10^{6}. (b) Convergence behavior of the DS algorithm in terms of the enthalpy constraint.

161
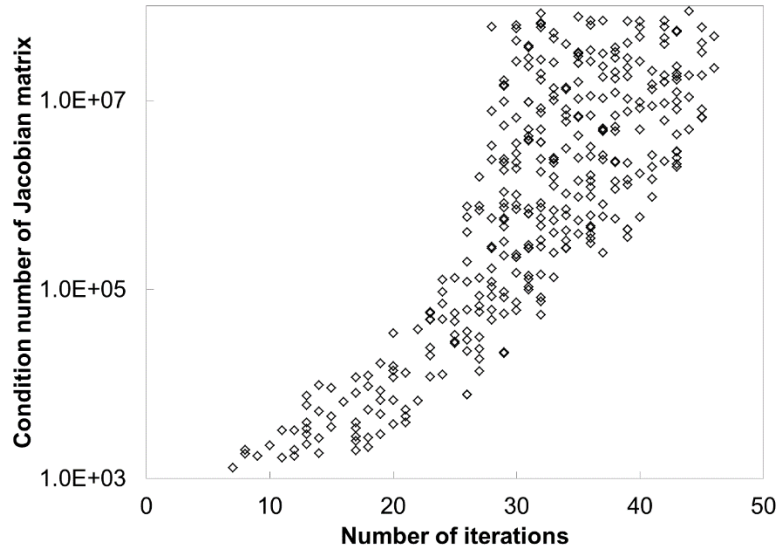
(a)
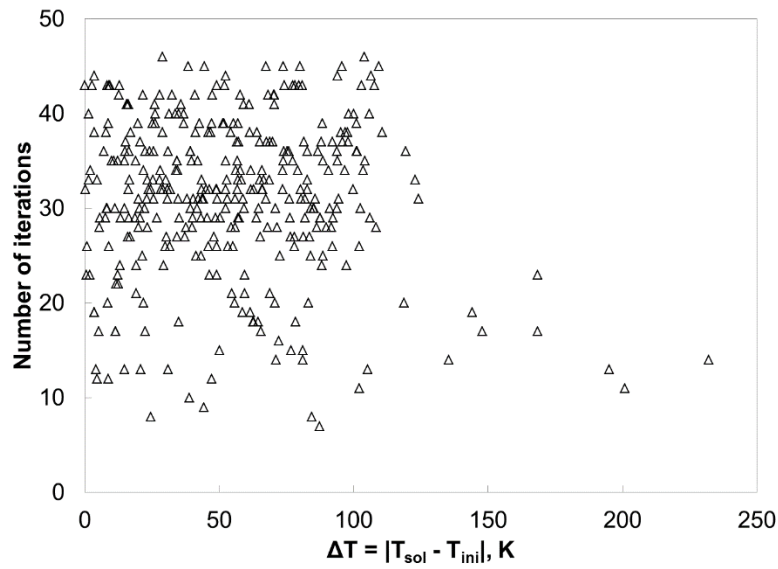
(b)

Figure 4.25. (a) Number of iterations required for 350 different PH flash calculations in the three-phase region is correlated to the condition number of the Jacobian matrix at the converged solution.   All the calculations converged to the correct solutions with the DS algorithm presented in this paper.   (b) The highest deviation of T_{ini} from T_{sol} is 230 K; however, the convergence behavior of the DS algorithm is insensitive to the initial temperature in these calculations.

162
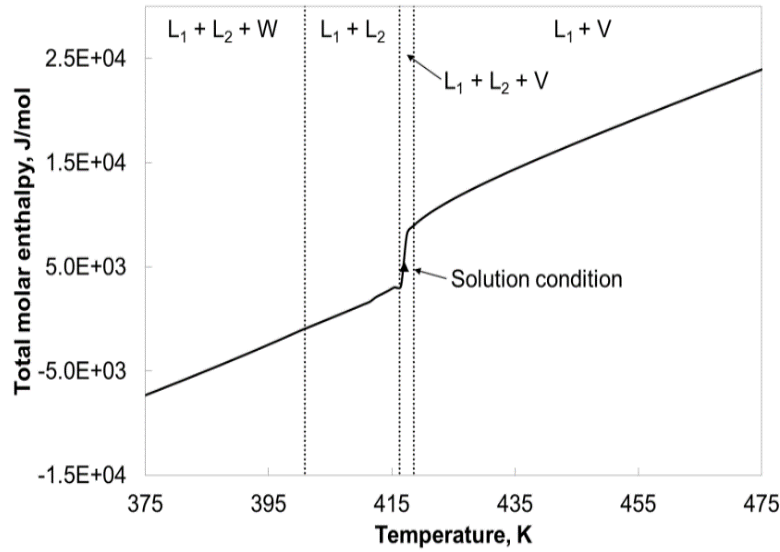
Figure 4.26. Total molar enthalpy at 35 bars for the ternary mixture given in Table 4.4. At 35 bars, C_B-rich phase (L_1) + C_4-rich phase (L_2) exists from 400.89 K to 416.24 K, $L_1+ L_2$ + vapor phase (V) from 416.24 K to 418.55 K. $\underline{H}^t$ is highly non-linear with respect to temperature near phase transition from $L_1+ L_2$ to $L_1+ L_2$ + V.
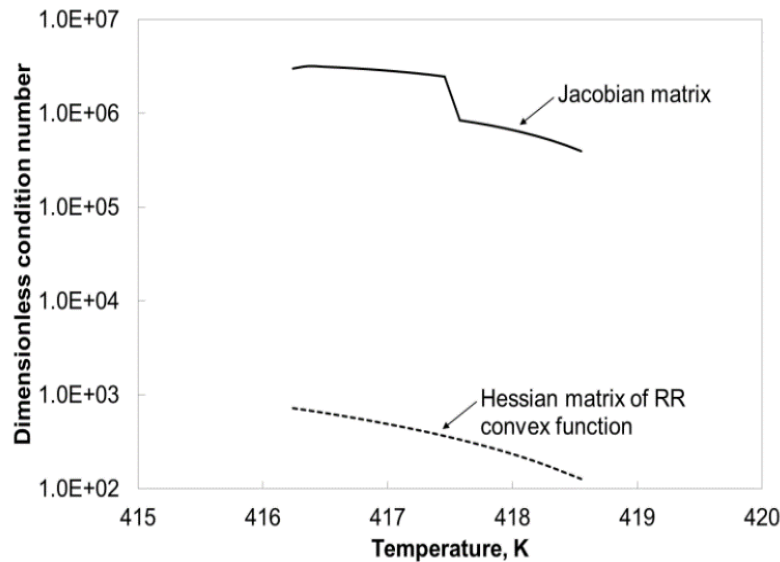
Figure 4.27. Dimensionless condition number of Jacobian matrix and the Hessian matrix of the RR convex function in $L_1 + L_2$ + V region at 35 bars for the ternary mixture given in Table 4.4. The scaling of temperature and enthalpy is conducted with T_{ref} of 300 K and $\underline{H}_{spec}$ of 5,000 J/mol. The Hessian matrix is reasonably well-conditioned; hence, the RR portion of the system of equations is not problematic in the three-phase region.

163
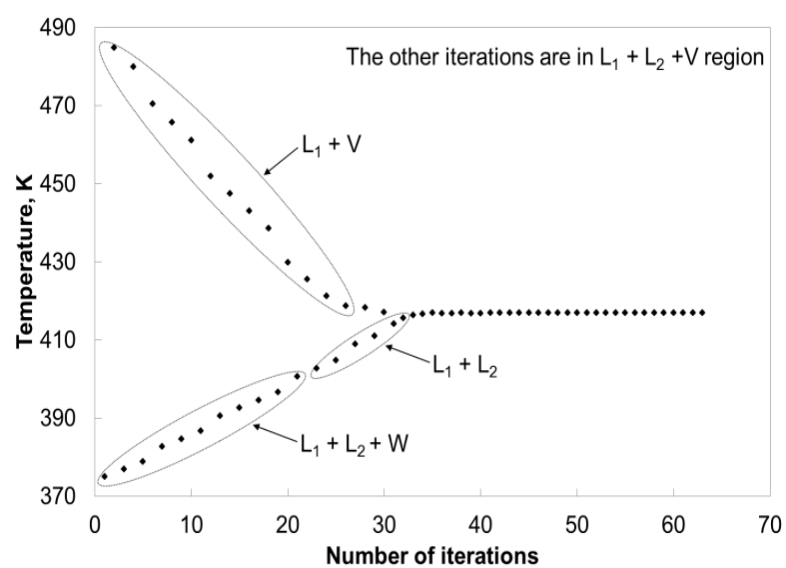
(a)
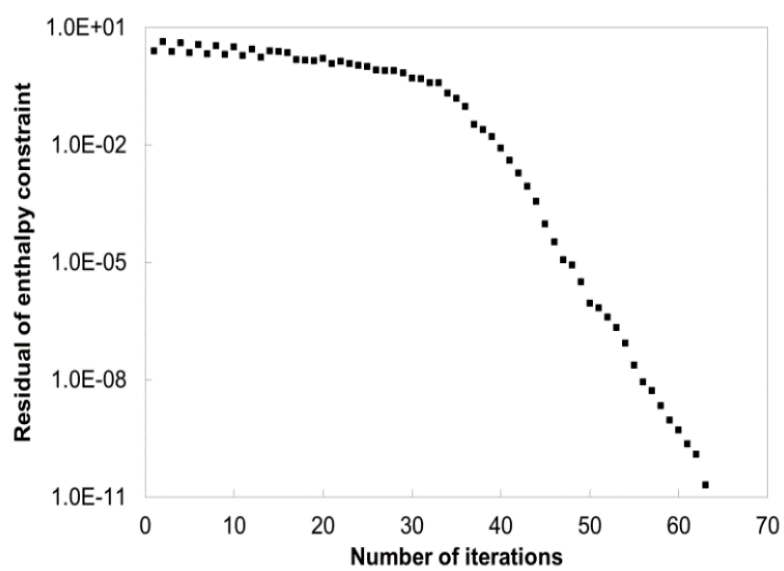
(b)

Figure 4.28. (Continued below)
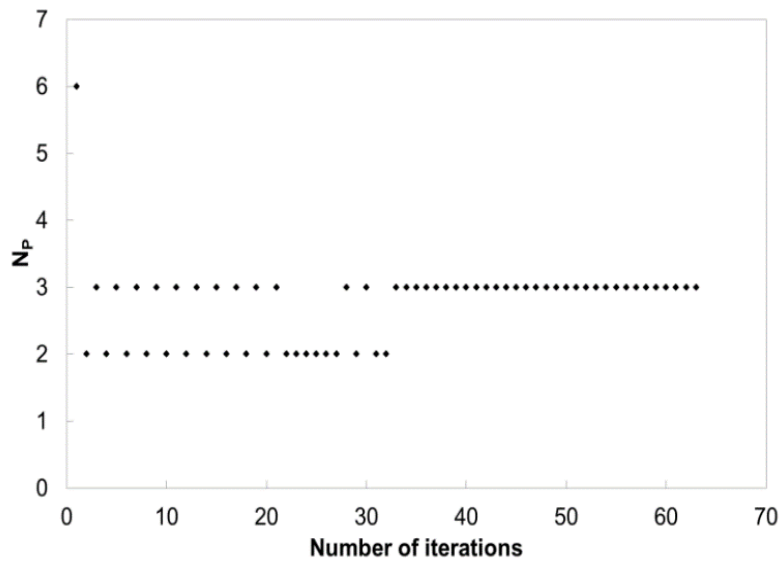
(c)

Figure 4.28. Convergence behavior of the current algorithm for the ternary mixture given in Table 4.4 at 35 bars and 5,000 J/mol: (a) T, (b) residual of equation 4.9, and (c) N_P. The initial T is set to 375 K, where $L_1 + L_2 + W$ coexist.   In this calculation, N_S is set to six, of which three sampling points are placed near compositional vertices.   The other three sampling compositions are randomly distributed (see Table 4.5a).   The solution temperature is 416.89 K, where narrow-boiling behavior occurs (see Figure 4.26).
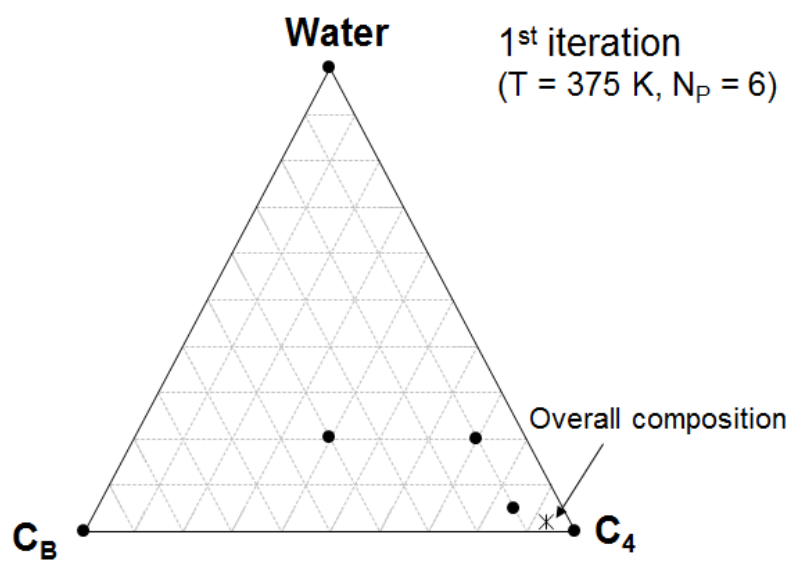
(a)
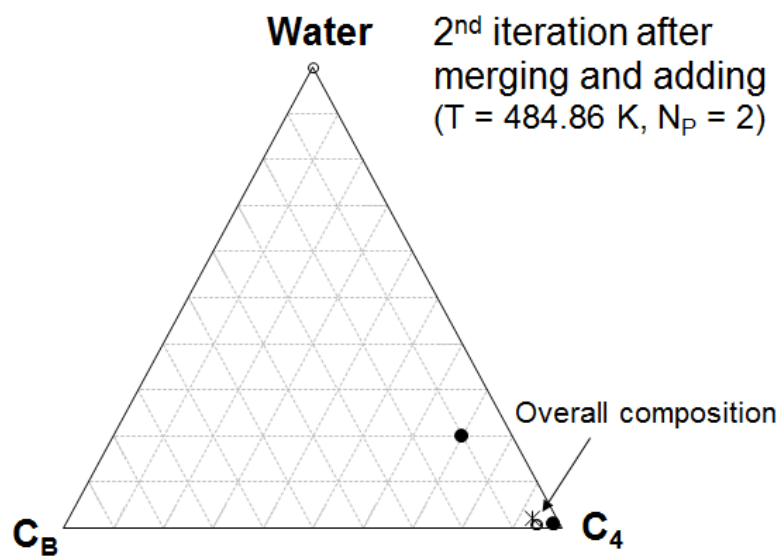
(b)

Figure 4.29. (Continued below)
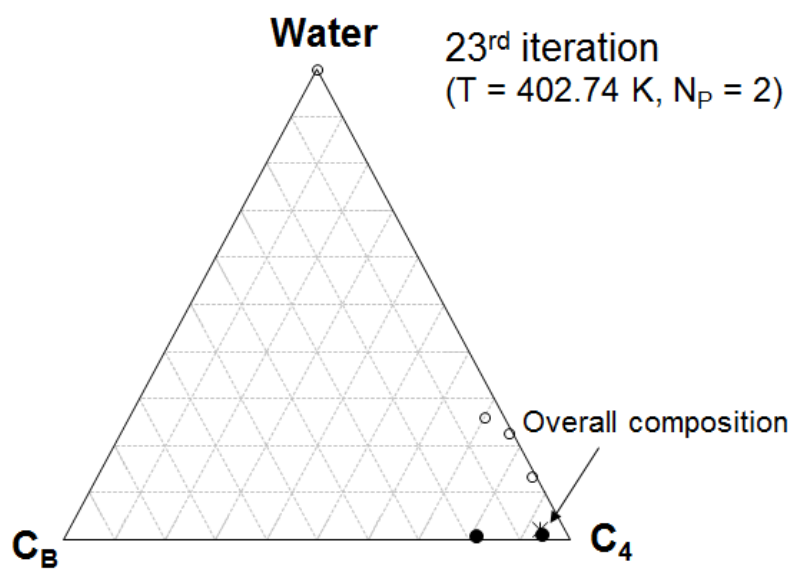
(c)
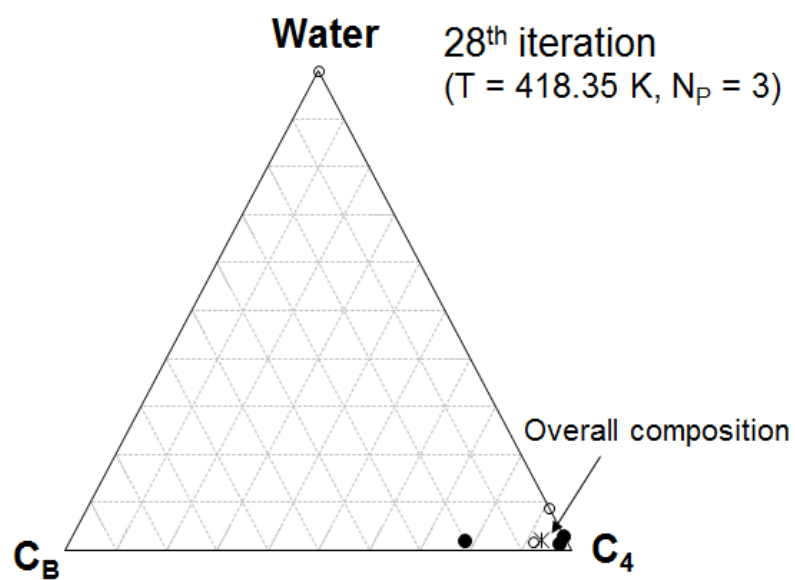
(d)

Figure 4.29. (Continued below)

(e)
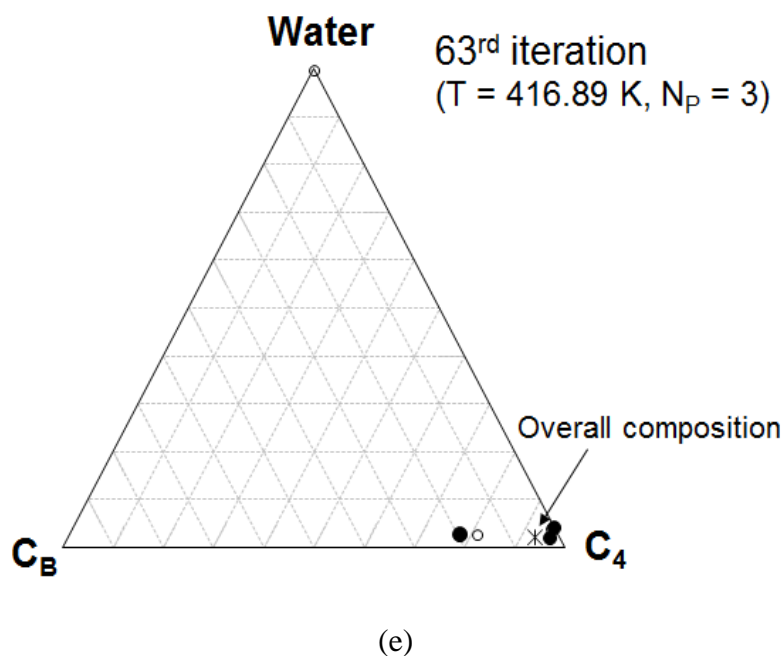
Figure 4.29. Ternary diagrams at 35 bars for the ternary mixture given in Table 4.4 at different iteration steps. Solid dots represent the sampling compositions in set P, which are considered for material balance. Hollow dots represent the sampling compositions in set U, which are excluded from material balance. (a) Ternary diagram at the 1st iteration where L_1, L_2, and W coexist (T = 375 K). (b) Ternary diagram point at the 2nd iteration where L_1 and V coexist (T = 484.86 K) after merging, adding and re-selecting reference. (c) Ternary diagram at the 23rd iteration where L_1 and L_2 coexist (T = 402.74 K). (d) Ternary diagram at the 28th iteration where L_1, L_2, and V coexist (T = 418.35 K). (e) Ternary diagram at the 63rd iteration where L_1, L_2, and V coexist (T = 416.89 K).
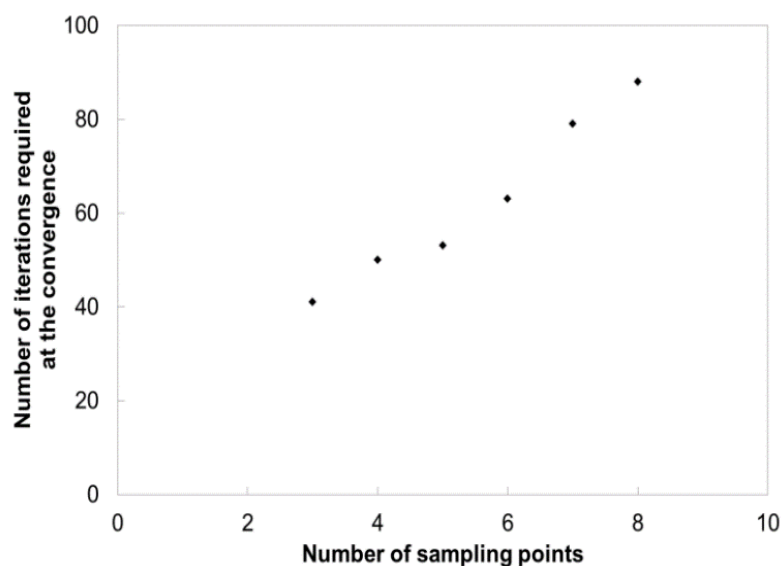
Figure 4.30. Number of iterations required for convergence increases with the number of sampling points used. Properties of the ternary mixture given in Table 4.4. Flash conditions are 35 bars and 5,000 J/mol. All calculations start at the same initial T (375 K). The three sampling points that are always used are near the compositional vertices. The other sampling compositions are randomly distributed for $N_S > 3$. The proposed algorithm successfully converges to the correct solution as long as N_S is greater than two.

CHAPTER 5: Quantification of Displacement Efficiency in Multiphase Oil Displacement

Solvent injection at reservoir temperatures typically below 120°F often exhibits complex phase behavior, in which a solvent-rich liquid (L_2) phase coexists with the oleic (L_1) phase and gaseous (V) phase. Oil displacement in the presence of such multiphase behavior is complicated by the interaction of multiphase flow and multiple partially miscible phases. Understanding of interphase mass transfer upon phase transitions is fundamentally important to explain and utilize the solvent-rich liquid phase for efficient oil displacement by solvent.

A method was proposed to estimate a minimum miscibility pressure (MMP) for three-hydrocarbon-phase flow by Li et al. (2015). One of the main assumptions in their mixing-cell method is that phase flow does not depend on its relative permeability. This is a reasonable assumption for the conventional thermodynamic MMP defined for two-hydrocarbon-phase flow of oil and gas, above which there is only single-phase flow at a given point in space and time. In low-temperature solvent injection, however, it is known experimentally and numerically that complete miscibility of three phases is unlikely even when nearly 100% efficiency of oil displacement is achieved.

Okuno and Xu (2014ab) presented a detailed study of the mass conservation on multiphase transitions between two and three phases in three-hydrocarbon-phase flow. Their description of how components must be redistributed among phases upon phase transition (i.e., interphase mass transfer) yielded a new parameter, called the distance parameter. The distance parameter becomes zero when multicontact miscibility between the displaced (e.g., L_1) and displacing (e.g., L_2) phases is developed in the presence of another immiscible phase (e.g., V). The distance parameter was used successfully to

quantify the efficiency of local displacement of the L_1 phase by a non-L_1 phase (e.g., L_2) (Okuno and Xu 2014ab). In their research, however, a rigorous EOS-based compositional simulator, UTCOMP, was used to obtain composition path, requiring the mapping of the distance parameter from volume to composition. Although UTCOMP properly accounted for volume change on mixing in its phase behavior calculation, the mapping often made the calculated distance parameters less accurate near a displacement front where the solvent concentration rapidly increased.

The central hypothesis that motivated this research is that distance parameters can be calculated more accurately in volume space for a given composition path. This is expected to be a more direct and accurate way to validate the utility of distance parameters to quantify displacement efficiency in three-phase flow for a given composition path.

A composition path in multiphase oil displacement is obtained by numerically solving 1D convective compositional flow equations with no volume change on mixing in this chapter. To this end, an in-house simulator has been developed by using the simultaneous multiphase PT phase-stability/-split algorithm presented in chapter 3. Case studies use seven reservoir oils, for which fluid models are available in the literature. The numbers of iterations and fugacity coefficient calculations are used to quantify the computational efficiency of the PT flash algorithm during the simulation.

5.1 INTRODUCTION

Enhanced oil recovery (EOR) techniques involve injection of fluids which are not usually present in the reservoir and are used to increase oil recovery and efficiency (Lake et al. 2014). Gas injection is one of the most widely used and prolific EOR techniques

(Oil and Gas Journal 2014), and CO_2 injection is increasingly being considered also for the purpose of CO_2 sequestration (Li et al. 2015). The number of gas injection projects is expected to increase because of the applications for oil shale (Sheng 2015) or heavy oil (Okuno and Xu 2014a) reservoirs. CO_2 injection has been widely applied to a number of oil reservoirs in West Texas (Mizenko 1992, Stein et al. 1992, Tanner et al. 1992, Fulco 1999, McGuire et al. 2001), in Canada (Malik and Islam 2000), in Alaska (McGuire et al. 2001), and in the North Sea (Varotsis et al. 1986). The incremental oil recovery from CO_2 flooding is estimated to be $7 - 23\%$ of the original oil-in-place (Jarrell et al. 2002). Field pilot tests were also reported for coinjection of solvent (e.g., propane, butane, and diluents) with steam for bitumen recovery in Canada (Gupta et al. 2005, Gupta and Gittins 2006, Dickson et al. 2011).

Mixtures of reservoir oil and injection gas has been studied in the literature by use of numerical simulations and experimental measures, including slim-tube displacements and multiple-contact measurements for the complex multiphase behaviors (Shelton and Yarborough 1977, Metcalfe and Yarborough 1979, Gardner et al. 1981, Orr and Jessen 1984, Shu and Hartman 1988, Sharma et al. 1989, Turek et al. 1988, Roper 1989, Hornbrook et al. 1991, Okuyiga 1992, Khan et al. 1992, Creek and Sheffield 1993, DeRuiter et al. 1994, Reid 1994, Godbole et al. 1995, Mohanty et al. 1995, Okuno 2009, Okuno and Xu 2014ab). At low reservoir temperatures typically below 120°F, solvent injection can involve complex phase behavior, which consists of three hydrocarbon phases, the L_1, V, and L_2 phases.

Such phase behavior has also been studied for simple binary mixtures (e.g., Rodrigues and Kohn 1967, Hottovy et al. 1981, Enick et al. 1985, Peters et al. 1993, Galindo and Blas 2002) and ternary mixtures (e.g., Horn and Kobayashi 1967, Llave et

172

al. 1987). For example, Peters et al. (1993) studied the phase behavior of binary mixtures of propane with hexacontane (n-$C_{60}H_{122}$). Their measurements cover a temperature range from 310 K up to 430 K with pressures up to 15 MPa. Three-phase equilibrium of type $L_1 + L_2 + V$ occurs in the near-critical region of propane. Llave et al. (1987) examined the phase equilibrium behavior of mixtures of nitrogen, methane, and propane, for temperatures between approximately 116 K and 160 K. Their results show that the presence of methane results in the three-phase region extending upward in temperature from the binary $L_1 + L_2 + V$ locus. The three-phase region is bounded from above by an upper critical endpoint (CEP) locus and from below by a lower critical endpoint locus, and these two critical endpoint loci intersect at a tri-critical point at 160 K and 62 bars. This finding of Llave et al. (1987) is summarized by Peters (1994). As given by Peters (1994), three-phase behavior bounded by two CEPs has been observed for various n-alkane binaries; C_1 and n-C_6/n-C_7, C_2 and n-C_{18} through n-C_{25}, and C_3 and n-alkanes heavier than n-C_{30}.

Mixtures of CO_2 and reservoir oils have also been studied by many researchers for EOR. Creek and Sheffield (1993) examined several mixtures consisting of Permian Basin reservoir oils with CO_2, and presented experimental measurements of fluid properties in three-phase ($L_1 + L_2 + V$) region. Turek et al. (1988) studied mixtures of CO_2 and several West Texas reservoir oils from the San Andres, Grayburg, and Devonian Chert formations. Their stated that a three-phase region exists within a narrow pressure range, in which the L_2 phase vaporizes with decreasing pressure, because they observe that the L_2-phase composition is similar to the V-phase composition in the three-phase region. This indicates that the fluid they examined has a composition close to CEP.

Slim-tube experiments in the literature show high displacement efficiency of more than 90% can be achieved in oil displacement by CO_2 (e.g., Yellig and Metcalfe 1980, Gardner et al. 1981, Orr et al. 1983, Henry and Metcalfe 1983, Khan 1992, Creek and Sheffield 1993) or enriched gas (e.g., Shelton and Yarborough 1977, DeRuiter et al. 1994, Mohanty et al. 1995) involving three hydrocarbon-phases at low temperatures. For example, Mohanty et al. (1995) studied the significance of three-hydrocarbon-phase flow in the displacement of West Sak oil by light-hydrocarbon-gas mixtures (methane through n-butane). They also conducted slim-tube displacements with these hydrocarbon-gas mixtures. Their results show that oil recovery at 1.2 PV injective (PVI) first decreased, then increased, and finally decreased again with decreasing gas enrichment. Oil recoveries at 1.2 PVI were 89%, 93%, and 65% at 51-, 62-, and 70%-C_1 dilution, respectively. They explained that oil recovery at 1.2 PVI was higher at 62% -C_1 dilution than at 51%-C_1 dilution because the L_2 phase was nearly miscible with the L_1 phase at the three-phase displacement front; oil became less viscous at the front; and the front moved fast enough to exit the slim tube by 1.2 PVI.

Various numerical simulation studies were also reported in the literature to study the impact of multiphase behavior on sweep efficiency in gas floods (e.g., Mohanty et al. 1995, Guler et al. 2001). Guler et al. (2001) evaluated the mixtures of CO_2 with natural gas liquid (NGL) as a method to enhance viscous oil recovery from Schrader Bluff and other oil reservoirs at Milne Point, Alaska. Mixtures of CO_2 and NGL with the crude oil showed a large three-phase ($L_1 + L_2 + V$) region at the reservoir temperature. Therefore, four-phase flow may occur in the reservoir when water injection is alternated with miscible gas injection. They also studied how important it is to simulate four-phase flow rather than use a three-phase flow approximation.

174

Nghiem and Li (1986) performed one-dimensional simulations for low-temperature oil displacements by CO_2 using a 15-component EOS fluid model. A recovery factor of 87% was achieved at 1.2 PVI in their simulation involving three-hydrocarbon-phase flow. However, the number of grid blocks used in their simulations was only 40.

Chang (1990) used UTCOMP to study various reservoir flow patterns in CO_2 flooding, including viscous fingering, channeling, gravity override, and dispersive flow, with a wide range of endpoint mobility ratio, gravity number, effective aspect ratio, Péclet number, and Dykstra-Parsons coefficients. The UTCOMP simulator is an EOS compositional multiphase reservoir simulator on the basis of the implicit pressure explicit concentration formulation developed at the University of Texas at Austin.

Tchelepi and Orr (1994) studied the effect of channeling and gravity override on the displacement efficiency and concluded that they were the dominant factors, especially for a highly heterogeneous reservoir. Mohanty et al. (1995) simulated the existence of three-hydrocarbon phases in 1D compositional simulation of West Sak oil displaced by enriched gas using UTCOMP. Guler et al. (2001) studied the presence of multiple liquid phases in multi-dimensional simulations with Alaskan heavy oil. Their results showed that gravity and dispersion affect the compositional propagation in multi-dimensional multiphase flow, resulting in the less obvious coexistence of multiple liquid phases.

Okuno et al. (2011) studied the displacement efficiency for low temperature CO_2 flooding using UTCOMP. Four-component mixtures were used in their study to perform systematic investigation of oil displacement involving three hydrocarbon phases. They concluded that high displacement efficiency occurs when the composition path traverses near the UCEP ($L_1 + L_2 = V$), and the LCEP ($L_1 = L_2 + V$). At the leading edge of three-

phase region, the L_2 phase extracts the reservoir oil due to the near-LCEP behavior. Then, at the trailing edge, the L_2 phase efficiently merge into V phase due to the near-UCEP behavior. Hence, the L_2 phase serves as a buffer between the immiscible L_1 and V phases with the three-phase region. Their conclusion was also confirmed in simulations of CO_2 flooding for multicomponent West Texas oils (Okuno 2009).

An important parameter to design a solvent injection process is the minimum miscibility pressure (MMP). Thermodynamic MMP is theoretically defined as the minimum displacement pressure at which complete miscibility along a composition path from the injection gas to the reservoir oil is developed in absence of dispersion (i.e., 1D 100% convective flow). For this traditional miscibility development between oil and gas through two-phase flow, a thermodynamic MMP is calculated as the pressure at which any of the key tie lines becomes zero length. At the MMP so defined, there is only a single-hydrocarbon-phase flow at a given point and time, making the "thermodynamic" MMP independent of fractional flow.

Slim tube experiments are the standard laboratory technique to estimate a MMP. Slim tube experiments are time-consuming and expensive, and one may perform only at a few pressures for a given gas and oil composition (Ahmadi and Johns 2011). Slim-tube experimental results may be affected by the packing material used and asphaltene precipitation (Elsharkawy et al. 1996). For some oil displacements, a "knee" in the recovery curve is also not always evident because of a smearing miscible front by dispersion (Johns et al. 2002). For three-phase displacements, the oil recovery curve can bend gradually or abruptly with pressure or gas enrichment (Bhambri and Mohanty 2008, Okuno et al. 2011, Pedersen et al. 2012). The slim-tube MMP is usually not unique because there are multiple criteria for determining the MMP in the presence of dispersion

(Holm and Josendal 1974, Yellig and Metcalfe 1980, Creek and Sheffield 1993, Negahban and Kremesec 1992).

Dispersion-free analytical methods based on the method of characteristic (MOC) have been used for the traditional oil displacement involving two hydrocarbon phases (Helfferich 1981, Dumore et al. 1984, Johns 1992, Orr 2007). The MOC-based methods can give thermodynamic MMPs quickly and accurately only when the fluid characterization with a cubic EOS is reliable. MOC-based analytical solution for injection of a mixture of gas can be complicated when multiple tie-lines satisfy the geometric construction for material balance (Yuan and Johns 2005, Ahmadi et al. 2011). For example, analytical solutions for two-phase displacements with complex phase behavior that bifurcates into L_1-L_2 and/or L_1-V regions (similar to three-phase systems) have not yet been extended to displacements with more than three components.

LaForce et al. (2008ab, 2009) developed analytical solutions with MOC for partially miscible three-phase flow in four-component systems for CO_2 WAG. They later confirmed the validity of their analytical solutions by comparison to experimental results (LaForce et al. 2010). There are no analytical solutions, however, for three-phase displacements with more than four components (Li et al. 2015).

Ahmadi and Johns (2011) developed a simple and practical two-phase multiple-mixing-cell method with an Excel spreadsheet (PennPVT Toolkit 2010) to determine the MMP for oil displacements with any number of components. Their two-phase multiple mixing-cell method tracks the key tie lines that form in a series of mixing cells from the injector to the producer. Then, a MMP is determined as the pressure at which any of the mixing cells gives a critical tie-line, following the definition of thermodynamic MMP. Egwuenu et al. (2008) showed a fluid characterization method in which the MMP

estimated by an EOS was adjusted to the slim tube MMP available. Rezaveisi et al. (2014) used the multiple-mixing-cell method to determine tie-lines for improvement in computational time and robustness of two-phase flash calculations in EOS compositional simulation.

One proposal was recently made by Li et al. (2015) to estimate MMP for three-hydrocarbon-phase flow. Their method is based on the two-phase mixing-cell method of Ahmadi and Johns (2011), which relies on repeated contacts of fluid phases from neighboring cells, and finding the minimum pressure at which one of the tie lines in any cell becomes zero length. Their method starts with mixing oil and gas with a given ratio (e.g., 50 : 50 as used in their paper) in the first contact and flashing the resulting mixture. Two or three equilibrium phases may result from this first contact. The equilibrium phases and the initial gas and oil compositions are then ordered from upstream to downstream before the next contact on the basis solely of their proximity to the initial oil and injection gas compositions. After the phases are ordered, tie line lengths are calculated to determine if a miscibility is reached. Zero tie line length is used as the criterion to identify miscibility. If such miscibility is not achieved, a new contact at a new trial pressure is made and the procedure mentioned above is repeated.

One of the key assumptions in the mixing-cell method applied for three phases by Li et al. (2015) is that the movement of fluids from cell to cell is independent of three-phase relative permeability. This made their procedure also independent of phase labeling (i.e., identities of phases). The assumption has been used for the conventional thermodynamic MMP, which is by definition independent of fractional flow. However, three-hydrocarbon-phase flow unlikely develops complete miscibility, a tri-criticality, at operating reservoir conditions in gas floods.

178

An MMP was calculated for the West Sak oil by use of PVTsim NOVA (version 2.2, Calsep 2016) and a two-phase mixing-cell method. The injection gas consists of two gaseous mixtures: the rich-gas mixture of 35 mol% ethane, 34 mol% propane, and 31 mol% n-butane, and the lean-gas mixture of 84 mol% methane, 9 mol% ethane, 6 mol% propane, and 1 mol% n-butane. The injection gas contains 71.43% lean-gas mixture and 28.57% rich-gas mixture, resulting in 60% methane concentration in the injection gas. The reservoir temperature is 65°F. The properties of West Sak oil and enriched gas were given in Okuno and Xu (2014a).

Figure 5.1a shows the pressure-solvent-mole-fraction (P-x) diagram for the West Sak oil and the injection gas with 60% methane concentration at 65°F. Three phases are present at high solvent concentrations. The L_1 and L_2 phases become critical at approximately 8700 psia when solvent mole fraction is 0.94.

Figure 5.1b shows the pressure-temperature (P-T) diagram for the West Sak oil and the injection gas with 60% methane concentration. The critical point of the reservoir oil is calculated at 1059.55°F and 1029.6 psia by use of the PR EOS, and the critical point of the injection gas is calculated at 111.4°F and 1397.7 psia by use of the PR EOS. At the reservoir temperature of 65°F, the bubble point of the reservoir oil is 1198.5 psia.

The pressure at which L_1 and L_2 phases become critical is approximately 8700 psia (see Figure 5.1a). The measured slim-tube MMP is 1500 psia, at which 91% oil recovery was achieved (DeRuiter et al. 1994). PVTsim NOVA (version 2.2, Calsep 2016) was not able to calculate MMP for this displacement likely because a composition path was not solved for three phases. The MMP obtained by use of a two-phase mixing-cell method is 3219 +/− 111.5 psia. However, DeRuiter et al. (1994) observed a high displacement efficiency of 91% at 1500 psia in their experiment.

Figure 5.2 is the P-T diagram for the North Ward Estes (NWE) oil and the injection gas of CO_2. The reservoir temperature is 83°F. The properties of the components used were given in Kumar and Okuno (2016). Three phases coexist when CO_2 mole fraction is high. L_1/L_2 immiscibility persists at high pressures.

The slim-tube MMP is 935 psia, at which more than 95% oil recovery was achieved (Winzinger et al. 1991). PVTsim NOVA (version 2.2, Calsep 2016) was not able to calculate MMP for this displacement. A two-phase mixing-cell method gave a MMP of 1248 +/− 0.3 psia. The predicted tie line length at the calculated MMP, however, was not close to zero, which is not a thermodynamic MMP. The two examples given above indicate that available existing methods tend to overestimate a pressure required for efficient oil displacement. The fundamental question here is under what conditions three-hydrocarbon-phase flow can achieve a high displacement efficiency.

Okuno and Xu (2014ab) investigated mass transfer on multiphase transitions between two and three phases for three-hydrocarbon-phase flow. They studied the condition for a L_1 phase to be completely displaced by a non-L_1 phase in the presence of another immiscible phase. For example, the condition was observed in the multicontact miscibility developed during CO_2 WAG injection, in which L_1 phase is completely displaced by V phase in the presence of W phase, as studied in detail by a series of publications by LaForce and her co-workers (LaForce and Orr 2008ab, 2009, LaForce and Jessen 2010, LaForce et al. 2010, and LaForce 2012). Okuno and Xu (2014b) studied the MCM developed between L_1 and L_2 phases for the cases where L_1 phase is completely displaced by L_2 phase in the presence of V phase.

It is important to note a difference between the MCM condition studied in Okuno and Xu (2014ab) and that studied in the context of thermodynamic MMP. The former is

concerned with the multicontact miscibility between the L_1 phase and a non-L_1 phase (e.g., L_2), which yields complete displacement of the L_1 phase by the displacing non-L_1 phase in the presence/absence of other phases. This MCM is identical with the conventional miscibility concept used for thermodynamic MMP, only for the traditional oil displacement by gas involving only two hydrocarbon phases. The MCM defined by Okuno and Xu (2014ab) is more general in that it is not limited to oil displacements with two hydrocarbon phases as evident in its applicability to CO_2 WAG (LaForce and Orr 2008ab, 2009, LaForce and Jessen 2010, LaForce et al. 2010, and LaForce 2012) and three-hydrocarbon-phase flow (Okuno and Xu 2014ab). The traditional MCM concept is concerned with a single-phase condition developed between the injection gas and reservoir oil compositions, and its limitation is that single-phase flow does not always occur in oil displacements, for example in CO_2 WAG and low-temperature solvent injection. Therefore, the term "MMP" is not used in this chapter to avoid any confusion associated with the difference described here.

Okuno and Xu (2014a) derived two conditions for the multiphase transitions that yield high local displacement efficiency by three hydrocarbon phases. The derivation is based on a mass conservation generalized for a multiphase transition in 1D gas injection. They concluded that two non-oleic phases can collectively achieve high displacement efficiency if two conditions (i.e., two distance parameters) are satisfied on phase transition between two and three phases.

Their calculations of distance parameters use equations 2.9 and 2.10. The parameter Γ used determines the relative location of the N_P-phase tie simplex and an intersection involved in the phase transition. Once the tie line and tie triangle involved in a phase transition are given, the intersection between them can be calculated as explained

in their paper. The calculation of the intersection was necessary in their calculation of distance parameters because they used UTCOMP to obtain a composition path, with which the term v_D changes in time and space because of volume change of mixing. Their calculations of distance parameters by use of equations 2.9 and 2.10 are indirect and subject to the numerical accuracy of the located intersection between the tie line and the tie triangle involved in the phase transition of interest. In particular, distance parameters at a leading edge of a three-hydrocarbon-phase region sometimes fluctuated for highly miscible displacements. In such a case, the leading-edge distance parameter was not a good indicator to quantify local displacement efficiency in the presence of numerical dispersion, as explained in their paper. This is likely because the intersection obtained is sensitive to a small concentration change when the angle between the tie line and tie triangle is very small, for example, at near-miscibility conditions.

Okuno and Xu (2014a) successfully used their distance parameters to explain the non-monotonic oil recovery at a given throughput with respect to gas enrichment in quaternary displacements and the West Sak oil displacements reported in the literature (e.g., DeRuiter et al. 1994, Mohanty et al. 1995). They also applied the research method to analyze the interphase mass transfer when MCM between the L_1 phase and a non-L_1 phase is developed in the presence of another immiscible phase. Quaternary and multicomponent cases demonstrated the applicability of the derived conditions.

One way to improve the accuracy in calculation of distance parameters for a given composition path is to use equations 2.7 and 2.8, where v_D can be fixed. Use of equations 2.7 and 2.8 results in direct calculation of distance parameters, not requiring to find the intersection of a tie line and triangle as in Okuno and Xu (2014ab). It is believed that this is a simpler and more direct validation of the utility of the distance parameters to

182

quantify displacement efficiency in three-phase flow. **Table 5.1** summarizes main differences among two groups of prior publications and the current research.

Another minor advantage of the current research is that this formulation (i.e., 1D convective-only flow equations, equation 2.2) does not require solving the pressure equation; hence, it is computationally more efficient and robust, although the assumption of no volume change on mixing affects the composition path obtained. Sensitivity analyses will be conducted in terms of the effect of relative permeability and numerical dispersion on the displacement efficiency quantified by distance parameters (equations 2.7 and 2.8).

5.2 METHODOLOGY

Quantification of local displacement efficiency by using a characterized fluid model generally requires the following steps:

Step 1. Fluid characterization using an EOS

Step 2. Calculation of a composition path from the injection gas to the reservoir oil in composition space at the reservoir temperature for a given displacement pressure

Step 3. Calculate a relevant parameter that quantifies the efficiency of local oil displacement.

As summarized in Table 5.1, the main difference between this research and Okuno and Xu (2014ab) lies in Step 2, which has led to the difference in Step 3. The main difference between this research and Li et al. (2015) lies in the parameter used in Step 3. As discussed in the previous section, Li et al. (2015) determines a thermodynamic MMP by tracking tie line lengths. In this research and Okuno and Xu (2014ab), the quantification of oil displacement efficiency is based on a mass conservation equation applied to multiphase transitions.

183

An in-house 1D compositional simulator was developed to obtain composition paths to be used in calculation of distance parameters. The 1D convection-only flow equations are obtained by use of the assumption listed in section 2.3.1. The resulting form is given by equation 2.2. The simulation formulation used in this chapter follows chapter 2 in Orr (2007). However, different assumptions can be used to formulate the procedure to obtain composition path. For example, one can use an EOS-compositional simulator, such as UTCOMP, to obtain composition paths considering volume change of mixing as in Okuno and Xu (2014ab).

Reliable phase behavior calculations are important in the multiphase flow simulation; hence, the new PT flash algorithm presented in chapter 3 has been implemented in the simulator for robust and accurate multiphase behavior representation. The thermodynamic model used in multiphase behavior calculations is the PR EOS (Peng and Robinson 1976) with van der Waals mixing rules, although different EOSs can be used as long as they yield reliable multiphase representations (e.g., critical endpoints). Phase viscosity in this chapter is calculated by use of the Lohrenz-Bray-Clark correlation (Lohrenz et al. 1964). The three-phase relative permeability model used in the simulator is Corey's model. Different three-phase relative permeability models can also be used, e.g., the models of Stone I/II (1970, 1973), Delshad and Pope (1989), Jerauld (1997), and Yuan and Pope (2012).

The simulator solves 1D convective flow equations (equation 2.2) with no volume change of mixing by use of fully explicit scheme with one-point upstream weighting for the flux term, as described in Johns (1992) and Orr (2007) as following:

$$(C_i)_k^{n+1} = (C_i)_k^n + (\Delta t_D / \Delta x_D)[(F_i)_{k-1}^n - (F_i)_k^n], \qquad (5.1)$$

184

where superscript n is the time step index and subscript k is the grid block index. Δx_D and Δt_D are the grid block size and time step size, respectively, which are uniform in this research.

The traditional approach for phase identification given by Perschke et al. (1989) is used to identify phases in this research, as summarized in Xu and Okuno (2015). In the method of Perschke et al. (1989), when three equilibrium phases exist, the L_1 phase in a three-phase region of L_1-V-L_2 was the one with the highest concentration of the heaviest hydrocarbon component. The denser phase of the two remaining phases was labeled as L_2, and the less dense phase was V phase. For cases with only two equilibrium phases, in which L_1 phase was always assumed to exist, the other phase was labeled as either V or L_2 depending on the mass density of that phase compared to that of a threshold value. If the mass density of the phase was lower than a specified threshold value, it was labeled as V. Otherwise, it was labeled as L_2. Throughout this chapter, a trial-and-error approach is used to find a proper threshold for phase mass density for consistent phase identification for a given oil displacement.

A step-wise description is given below to explain how the simulator works.

Step 1. Calculate the overall composition of the first grid block close to the injector by use of

$$z_i = C_i \underline{\rho}_i / \sum_{i=1}^{N_C} C_i \underline{\rho}_i. \tag{5.2}$$

Step 2. Perform phase equilibrium calculations by use of the new PT flash algorithm developed in chapter 3 for the overall composition at a given grid block and time step.

185

Step 3. Calculate phase properties, such as saturation, molar density, mass density, and viscosity, by use of the results from step 2 (i.e., number of equilibrium phases and their compositions and amounts).

Step 4. Perform the phase identification of Perschke et al. (1989).

Step 5. Calculate phase relative permeabilities using Corey's model and phase fractional flow.

Step 6. Calculate the component overall volume fraction for the next grid block by use of equation 5.1.

Step 7. Calculate the overall composition for the next grid block by use of equation 5.2, and repeat steps 2 to 6 for all grid blocks. Calculate component recovery.

Step 8. Repeat steps 1 to 7 for the next time step until a specified simulation termination time.

In step 7, component recovery is calculated as a measurement for displacement efficiency as given below. Component recovery is calculated using

$$Q_i = C_i^{initial} + t_D F_i^{injected} - \int_0^1 C_i dx_D. \tag{5.3}$$

In equation 5.3, $C_i^{initial}$ is the amount of component i that initially exists in the reservoir, $t_D F_i^{injected}$ is the amount of component i that is injected into the reservoir, and $\int_0^1 C_i dx_D$ is the amount of component i that is currently present in the reservoir. Hence, Q_i is the amount of component i that is recovered.

The third term in equation 5.3 can be rewritten as

$$\int_0^1 C_i dx_D = \sum_{k=1}^{N_{GB}} C_i^k \Delta x_D^k, \tag{5.4}$$

where N_{GB} is for the number of grid blocks used in the simulation. Equation 5.4 can be used only when all grid blocks have a uniform size, as is the case in this chapter. Hence, component recovery is calculated as follows:

$$Q_i = C_i^{initial} + t_D F_i^{injected} - \sum_{k=1}^{N_{GB}} C_i^k \Delta x_D^k. \tag{5.5}$$

Once a composition path is calculated by the finite-difference simulation, equations 2.7 and 2.8 derived in chapter 2 are used to calculate distance parameters defined on the basis of volumetric information for the trailing and leading edges of the three-hydrocarbon-phase region. Three important features of distance parameters (equations 2.7 and 2.8) are summarized below.

Firstly, use of weak form of the 1D convective flow equations enables to take into account the effect of mixing on displacement efficiency through numerical dispersion. Secondly, three-phase relative mobilities are properly included in distance parameters (equations 2.7 and 2.8) through the parameter "γ". That is, the effect of relative permeability on oil displacement efficiency is taken into account, unlike the three-phase mixing-cell method of Li et al. (2015). Thirdly, use of volumetric information to calculate δ^L and δ^T defined in equations 2.7 and 2.8 avoids the mapping from volume space to composition space, which requires finding the intersection of the downstream two-phase tie line and upstream three-phase tie triangle. The intersection constructed by use of compositional information can be significantly affected if phase compositions change drastically at the phase transition, which often occurs at the leading edge of a three-phase region.

In the following case studies for the six three-hydrocarbon-phase reservoir oils, EOS fluid models are obtained from Kumar and Okuno (2016) for accurate three-phase behavior representations. Distance parameters are calculated by use of equations 2.7 and

2.8 at 0.4 PVI, at which saturation, concentration, and mass density profiles are given for a fixed pressure and a level of numerical dispersion. The distance parameters are then tested as a measure for quantification of local oil displacement efficiency. A sensitivity study is presented in terms of the effect of the relative permeability model used and the effect of numerical dispersion on oil displacement efficiency.

5.3 CASE STUDIES

This section gives the case studies by use of North Ward Estes (NWE) oil with pure CO_2 injection and ethane injection for Bakken oil displacement in the presence of water. Distance parameters are calculated at multiphase transition, and component recoveries are calculated at the breakthrough times for the leading and trailing edges of a three-phase region. High displacement efficiency is quantified for multiphase displacements for NWE oil and other five reservoir oils. Measured MMPs from slim tube experiments for all six three-hydrocarbon-phase reservoir oil displacements are compared with an optimal injection pressure (OIP) at which highest displacement efficiency is achieved. In all simulations, the ratio of the dimensionless time step size to the dimensionless grid block size is 0.1.

5.3.1 Displacement of North Ward Estes Oil by CO_2

This section presents the simulation results North Ward Estes (NWE) oil, a West Texas reservoir oil. NWE oil was characterized by Kumar and Okuno (2016) with the PR EOS and phase behavior data given in Winzinger et al. (1991). The properties of NWE oil are given in **Table 5.2**. The binary interaction parameters are given in **Table 5.3**. The oil gravity is calculated to be approximately 32ºAPI. The injection gas is pure CO_2.

188

Table 5.4 gives the parameters used in Corey's model for three-phase relative permeabilities (Khan 1992). These parameter values are used consistently for six three-hydrocarbon-phase oil displacements studied in this section. The number of grid blocks used is 250, unless otherwise stated.

5.3.1.1 Minimum Distance Conditions

Two conditions are used to quantify local displacement efficiency for this case. One condition is associated with the relation between the distance parameter calculated at the three-phase trailing edge and the PC1 recovery at breakthrough (BT) of the three-phase trailing edge. The other is the relation between the distance parameter calculated at the three-phase leading edge and the PC1 recovery at BT of the three-phase leading edge. The measured MMP with slim tube experiments is 937 psia (Winzinger et al. 1991), while the optimal injection pressure (OIP) for highest displacement efficiency by use of volumetric distance parameters (equations 2.7 and 2.8) is 935 psia.

Figure 5.3 shows the pressure-temperature (P-T) diagram calculated for NWE oil and injection gas by use of PVTsim Nova (version 2.2, Calsep 2016). The bubble point pressure at the reservoir temperature of 83ºF is 868.3 psia for the initial reservoir oil. The critical point of the initial oil is calculated to be 922ºF and 1534.8 psia by use PR EOS. **Figure 5.4** gives the pressure-solvent-mole-fraction (P-x) diagram calculated for mixtures of NWE oil and CO_2 at 83ºF by use of the new PT flash algorithm. Two immiscible liquid phases (L_1 and L_2) are present at CO_2 concentrations higher than 60% at the higher-pressure side of the three-phase (L_1, V, and L_2) region.

Simulations are performed at five pressures, 825 psia, 850 psia, 920 psia, 935 psia, and 1050 psia, at which three hydrocarbon phases are calculated. **Figure 5.5** presents the PC1 recovery at BT times of the leading and trailing edges of the three-phase

189

region at the five pressures. For NWE oil, PC1 is selected as the component to show component's recovery.

PC1 recoveries are 0.599, 0.709, 0.846, 0.877, and 0.546, at BTs of the leading edge of the three-phase region at 825 psia, 850 psia, 920 psia, 935 psia, and 1050 psia, respectively. The BTs of leading edge of the three-phase region are 1.745 PVI, 1.643 PVI, 1.513 PVI, 1.479 PVI, and 0.830 PVI at 825 psia, 850 psia, 920 psia, 935 psia, and 1050 psia, respectively.

Similarly, BTs of trailing edge of the three-phase region are 3.570 PVI, 6.072 PVI, 5.751 PVI, 5.669 PVI, 0.908 PVI, at 825 psia, 850 psia, 920 psia, 935 psia, and 1050 psia, respectively. PC1 recoveries are 0.614, 0.749, 0.915, 0.932, and 0.615, at 825 psia, 850 psia, 920 psia, 935 psia, and 1050 psia, respectively. Highest PC1 recovery is observed at 935 psia at BT of trailing edge of the three-phase region, and is 34.04% more efficient than that at 825 psia.

Figure 5.5 also indicates that the local displacement by three hydrocarbon phases becomes more efficient, and the propagation of three hydrocarbon phases becomes faster with increasing pressure for a pressure range between 850 psia and 935 psia. This results in the highest PC1 recovery at 935 psia than that at 850 psia.

At 1050 psia, although the BTs of the leading and trailing edges of the three-phase region are the fastest among the five pressures, the PC1 recovery is the lowest. This indicates that the faster propagation of three hydrocarbon phases does not balance the low efficiency of local oil displacement by three hydrocarbon phases, resulting in the lowest PC1 recovery at 1050 psia.

Figure 5.6 shows the distance parameters calculated at the trailing and leading edges of the three-phase region. The OIP (935 psia) is defined when distance parameters

190

are lowest ($\delta^T = 0.0041$ and $\delta^L = 0.0280$). At the three-phase trailing edge, the distance parameter is lower than that of the three-phase leading edge. It is likely because the concentrations' change at the three-phase leading edge is more drastic than that at the three-phase trailing edge. This makes the local level of mixing higher at the leading edge higher than that at the trailing edge.

The OIP is calculated in three steps in this chapter. Firstly, the minimum distance conditions are calculated for the three-phase trailing edge and the three-phase leading edge, respectively. Then, a turning point is identified on the minimum distance condition figures. After that, the same analyses as described above are performed for refined pressure conditions that bracket the turning point. This refining in pressure is to obtain a more precise OIP. Although not shown in the following analyses, this procedure to obtain an OIP has been applied for all six three-hydrocarbon-phase reservoir oils studied in this chapter. The OIP is defined as the pressure at which the distance parameters are the lowest and component recovery is the highest (i.e., recovery negatively correlates with δ^T and δ^L).

Figures 5.7 and 5.8 show PC1 component recoveries at BT of the three-phase leading edge and trailing edge with respect to the distance parameters calculated at the three-phase leading and trailing, respectively. For the NWE case, PC1 recovery is highest at the BTs of the leading and trailing edges at calculated OIP (935 psia).

NWE oil displacements by CO_2 at 83°F were also performed using UTCOMP. Reservoir and fluid properties were the same as in flow simulations given in the previous paragraphs (Tables 5.2, 5.3, and 5.4). **Figure 5.9** shows the oil recoveries at the BT of three-phase leading and trailing edges at the five pressures; that is, this figure shows the

oil displacement efficiency by the three-hydrocarbon-phase region at each pressure. At 935 psia, the highest oil displacement efficiency was calculated with UTCOMP.

Figure 5.10 shows the concentration profile at 0.4 PVI at 825 psia using the 1-D simulator developed in this research (Section 5.2). Because the pressure is below the bubble point pressure (868.3 psia, see Figure 5.1), the initial oil is in the $L_1 + V$ region. At the trailing edge of the three-phase region, the compositional distances between $L_1 + L_2$, $L_1 + V$, and $V + L_2$, are 0.129, 0.328, and 0.203, respectively. At the leading edge, the compositional distances between $L_1 + L_2$, $L_1 + V$, and $V + L_2$, are 0.074, 0.290, and 0.219, respectively.

Figures 5.11 and 5.12 show the profiles of phase saturation and phase mass densities at 0.4 PVI at 825 psia. The amount of L_1 phase does not exhibit significant decrease at the three-phase leading edge. This is because the injection gas (CO_2) cannot efficiently extract heavy components in the three-phase region (see Figure 5.10), resulting in low displacement efficiency. Figure 5.12 shows that the mass densities of L_1 and L_2 phases are close to each other at three-phase leading edge; however, these two phases are away from each other in composition space with a distance of 0.074.

Figures 5.13 to 5.15 show the concentration, phase saturation, and phase mass densities profiles at 0.4 PVI at 935 psia (the OIP). The same set of profiles at 0.4 PVI at 1050 psia are shown in **Figures 5.16 to 5.18**. The displacement of L_1 phase at the three-phase leading edge is least efficient at 1050 psia (Figure 5.17), and is the most efficient at 935 psia (Figure 5.14). Figures 5.15 and 5.18 also show that the miscibility level is highest at 935 psia.

At the three-phase leading edge, the composition distances between L_1 and L_2 phases are 0.074, 0.092, and 0.115, at 825 psia, 935 psia, and 1050 psia, respectively.

Although the composition distance between L_1 and L_2 phases is lowest at 825 psia, the PC1 recovery is not the highest (see Figure 5.5). This indicates that use of composition distance to identify MMP for three-phase flow is not always reliable, since displacement efficiency is affected by involved inter-phase mass transfer in three-phase flow.

At the OIP (935 psia), the L_1 phase in the downstream two-phase region splits into L_1 and L_2 phases in the three-phase region, and the L_2 and V phase in the three-phase region merge efficiently into L_2 phase in the upstream two-phase region. Hence, the PC1 recovery at BT of three-phase trailing edge is highest at 935 psia.

5.3.1.2 Effect of Numerical Péclet on OIP

In this section, the sensitivity of the displacement efficiency to the numerical Péclet number is studied. Component recovery and distance parameters are calculated by use of the same approaches as in the previous section. Lantz (1970) showed that numerical dispersion arises in numerical solutions because of truncation errors, which is often described by Péclet number. For two immiscible phases, the Péclet number for 1D displacements is written as

$$N_{Pe}^{-1} = \frac{\Delta x_D}{2} \frac{df_g}{dS_g}\left(1 - \frac{\Delta t_D}{\Delta x_D} \frac{df_g}{dS_g}\right),$$ (5.6)

where f_g is the fractional flow of gaseous phase and S_g is the saturation of gaseous phase. When the dimensionless time steps are small in comparison with the grid block size and the fractional flow derivative is approximated as 1.0, equation 5.6 is simplified to

$$N_{Pe} = \frac{2}{\Delta x_D}.$$ (5.7)

Equation 5.7 was used to represent the level of dispersion for single-point upstream weighting by Stalkup (1998) and Solano et al. (2001). Equation 5.7 is used in this section to approximate the level of numerical dispersion in all simulations by varying the number of grid blocks (GBs) used. In all simulations presented, a dimensionless time

193

step size is one-tenth of the dimensionless grid block size so that the time step little contributes to numerical dispersion.

Five different numbers of grid blocks are used in flow simulations; $N_{GB} = 50, 250, 500, 1000,$ and 2000. The resulting Péclet numbers for 1D displacements are approximately 100, 500, 1000, 2000, and 4000. **Figure 5.19** shows the relation between PC1 recovery at BT of the trailing edge with respect to distance parameter at the trailing edge at five N_{Pe} numbers. **Figure 5.20** shows the relation between PC1 recovery at BT of the leading edge with respect to distance parameter at the leading edge at five N_{Pe} numbers. Minimum distance conditions are used to identify the OIP as used in previous section. The minimum distance condition states that at the OIP, the distance parameter is a minimum and the component's recovery is a maximum. The OIP calculated is 935 psia for all five pressures with five N_{Pe} for NWE oil by use of the minimum distance conditions defined in this research.

Figures 5.19 and 5.20 illustrate that recoveries initially increase as the pressure approaches to the OIP (935 psia) for NWE oil. A maximum in the recoveries is eventually reached, after which the recoveries decrease (at 1050 psia). Both figures also show that recoveries at a greater level of dispersion (i.e., a smaller number of GBs) are smaller than those with a lower level of numerical dispersion (i.e., a larger number of GBs).

The most obvious increase in displacement efficiency due to a lower level of dispersion is observed at 1050 psia (see Figures 5.17 and **5.21**). The L_1 phase almost remains undisplaced by injecting CO_2 in the entire three-phase region with the use of N_{GB} = 250 (see Figure 5.17). Use of $N_{GB} = 2000$ shows significant L_1 phase amount decrease in downstream side of three-phase region. At the three-phase leading edge, L_1 phase

194

amount decreases from 0.831 to as low as 0.002. This is reflected by the distance parameters (see Figures 5.19 and 5.20). When 250 GBs are used, the distance parameters at the three-phase trailing and leading edges are 1.082477 and 1.531852, respectively. Use of 2000 GBs reduces the distance parameters to 0.000935 and 0.012513, respectively.

At the OIP (935 psia), Figure 5.14 (N_{GB} = 250) shows that L_1 phase saturation exhibits decreasing-increasing-decreasing trend near three-phase leading edge. However, use of 2000 GBs clearly diminishes the unfavorable increasing of L_1 phase amount at three-phase leading edge (see **Figure 5.22**). The distance parameters at three-phase trailing and leading edges with 250 GBs are 0.004156 and 0.028066, respectively. They are reduced to 0.000277 and 0.001650, respectively, when 2000 GBs are used.

At 825 psia with 250 GBs, L_1 phase was left behind the three-phase region with a saturation of 0.638 at the three-phase trailing edge, higher than that at the three-phase leading edge (see Figure 5.11). This indicates that oil displacement is not efficient. However, increasing N_{GB} to 2000 clearly increases displacement efficiency, especially at the three-phase trailing edge, as shown in **Figure 5.23**. The distance parameters at the three-phase trailing and leading edges with 250 GBs are 0.040236 and 0.828008, respectively. They are reduced to 0.003400 and 0.204596, respectively, with 2000 GBs.

In what follows, the effect of numerical Péclet number on minimum distance conditions is presented. Individual terms in distance parameter calculations at the OPI (935 psia) and 1.0 PVI with N_{GB} of 250 and 1000 are calculated.

Figure 5.24 shows the fractional flow curves with respect to dimensionless distance with N_{GB} of 250 and 1000. At the leading edge of the three-phase region, f_{L_1} and f_V fluctuate, as can be seen from Figures 5.24a and 5.24b. **Figures 5.25, 5.26, and**

5.27 show the compositions for L_1, V, and L_2 phases, respectively, with N_{GB} of 250. **Figures 5.28, 5.29, and 5.30** show the compositions for L_1, V, and L_2 phases, respectively, with N_{GB} of 1000. At the three-phase leading edge, CO_2 concentrations in L_2 phase exhibit significant increase from downstream side to upstream side.

Figure 5.31 shows the saturation profiles with N_{GB} of 250 and 1000. L_1 phase saturation is reduced from 0.7630 to 0.0377 with N_{GB} of 250. The decrease in L_1 phase saturation is 0.7253. When N_{GB} is 1000, L_1 phase saturation is reduced from 0.7646 to 0.0249, resulting in L_1 phase saturation decrease of 0.7397. Hence, more efficient displacement occurs at a lower level of dispersion (i.e., larger N_{GB}).

In the calculations of distance parameters, the term γ_j ($j = 1, 2, \ldots, N_P$) is required and calculated using $\gamma_j = (v_D S_j - f_j)/(v_D - 1)$ (equation 2.6). Hence, the fluctuations of fractional flow are also reflected in γ_j. **Figure 5.32** shows the γ_j used in distance parameter calculations (equation 2.6) with N_{GB} of 250 and 1000. The fluctuations of γ_j at the three-phase leading edge become smoother, when larger N_{GB} is used in simulations.

Detailed analysis of influential factors has indicated that the observed fluctuation with 250 grid blocks occurs because the level of mixing affects not all physical parameters in the current simulator. In particular, relative permeability parameters (Table 5.4) are assumed to be constant with phase compositions, which are affected substantially by the mixing near the displacement fronts. With 1000 grid blocks, the level of mixing is smaller (numerical N_{Pe} is larger), and therefore, the partial impact of mixing on simulation results is less obvious (Figure 5.32b).

The γ_j ($j = 1, 2, \ldots, N_P$) parameters determine the relative location of the N_P-phase tie simplex and an intersection involved in the phase transition (chapter 2). The intersection is calculated for a given set of the tie line and tie triangle involved in a phase

196

transition; for example, a downstream-side tie line and a upstream-side tie triangle. The location of the intersection relative to the downstream-side tie line gives the γ_j ($j = L_1$ and V) parameters on the tie line extension. Thus, $\underline{c}_{int} = \gamma_{L_1}^D \underline{c}_{L_1}^D + \gamma_V^D \underline{c}_V^D$, where $\gamma_{L_1}^D + \gamma_V^D =$ 1.0 and $\underline{c}_{int}$ is the intersection composition. Similarly, the location of the same intersection relative to the upstream-side tie triangle gives the γ_j ($j = L_1$, L_2, and V) parameters on the tie triangle extension. Thus, $\underline{c}_{int} = \gamma_{L_1}^U \underline{c}_{L_1}^U + \gamma_{L_2}^U \underline{c}_{L_2}^U + \gamma_V^U \underline{c}_V^U$, where $\gamma_{L_1}^U + \gamma_{L_2}^U + \gamma_V^U = 1.0$.

When N_{GB} is 250, at the three-phase leading edge, $\gamma_{L_1}^U$, $\gamma_{L_2}^U$, and γ_V^U are -0.0190, 0.8936, and 0.1254, respectively. The $\gamma_{L_1}^D$ and γ_V^D are 0.9073 and 0.0927, respectively. The composition calculated at the intersection is (0.0001, 0.7827, 0.0565, 0.0096, 0.0087, 0.0089, 0.0087, 0.0076, 0.0509, 0.0358, 0.0224, 0.0083).

At the three-phase leading edge, the composition distance between the intersection and upstream L_1 phase is 0.1956, and the composition distance between the intersection and upstream L_2 phase is 0.0201. The distance parameter calculated at the three-phase leading edge is 0.0295.

Similarly, at the three-phase trailing edge, $\gamma_{L_1}^D$, $\gamma_{L_2}^D$, and γ_V^D are -0.0413, 1.4440, and -0.4027, respectively. The $\gamma_{L_1}^U$ and $\gamma_{L_2}^U$ are -0.0447 and 1.0447, respectively. The composition of the intersection is calculated at (0.0000, 0.9541, 0.0000, 0.0000, 0.0000, 0.0000, 0.0000, 0.0000, 0.0055, 0.0100, 0.0135, 0.0168). The compositions for N_2, CH_4, C_2H_6, C_3H_8, C_4H_{10}, C_5H_{12}, and C_6H_{14} are zero at the three-phase trailing edge because the concentrations of these components are zero (Figures 5.25, 5.26, and 5.27).

The composition distance between the intersection and downstream V phase is 0.0298 at the three-phase trailing edge. The composition distance between the

197

intersection and downstream L_2 phase is 0.0178. The distance parameter calculated at three-phase trailing edge is 0.0024.

When N_{GB} is 1000, at the three-phase leading edge, $\gamma_{L_1}^U$, $\gamma_{L_2}^U$, and γ_V^U are −0.0145, 0.1601, and 0.8544, respectively. The $\gamma_{L_1}^D$ and γ_V^D are 0.1176 and 0.8824, respectively. The composition calculated at the intersection at the three-phase leading edge is (0.0000, 0.8364, 0.1122, 0.0154, 0.0064, 0.0043, 0.0029, 0.0018, 0.0093, 0.0062, 0.0039, 0.0013).

The composition distance between the intersection and upstream L_1 phase is 0.2623 at the three-phase leading edge. The composition distance between the intersection and upstream L_2 phase is 0.1304. Compared to the composition distances between the intersection and upstream L_1 and L_2 phases with N_{GB} of 250, the composition distances become greater with N_{GB} of 1000. The distance parameter calculated at the three-phase leading edge is reduced to 0.0109 by increasing N_{GB} to 1000.

At the three-phase trailing edge, the values of $\gamma_{L_1}^D$, $\gamma_{L_2}^D$, and γ_V^D are −0.0300, −0.0313, and 1.0612, respectively. The $\gamma_{L_1}^U$ and $\gamma_{L_2}^U$ are −0.0302 and 1.0302, respectively. The intersection involved at the three-phase trailing edge is calculated at the composition (0.0000, 0.9729, 0.0000, 0.0000, 0.0000, 0.0000, 0.0000, 0.0000, 0.0031, 0.0074, 0.0078, 0.0088). Zero concentrations of components N_2, CH_4, C_2H_6, C_3H_8, C_4H_{10}, C_5H_{12}, and C_6H_{14} result in zero values in the compositions of the intersection (see Figures 5.28, 5.29, and 5.30).

At the three-phase trailing edge, the composition distance between the intersection and downstream V phase is 0.0512. The composition distance between the intersection and downstream L_2 phase is 0.0257. The distance parameter calculated at the three-phase trailing edge is reduced to 0.0016 by increasing N_{GB} to 1000.

198

5.3.1.3 Effect of Relative Permeability Model Used on OIP

As explained in preceding section, three-phase relative mobilities are properly included in distance parameters (equations 2.7 and 2.8) through the parameter "γ", unlike the three-phase mixing-cell method of Li et al. (2015). In order to evaluate the effect of the relative permeability model used on the calculated OIP, a new set of parameters used in Corey's model for the three-phase relative permeabilities is given in **Table 5.5**.

Simulations are performed at five pressure conditions; 825 psia, 850 psia, 900 psia, 935 pisa, and 1000 psia. Three-phase displacements are not observed for the pressures below 825 psia and above 1000 psia. The number of GBs used in this section is 250.

Figure 5.33 and 5.34 show the minimum distance conditions for the three-phase trailing and leading edges with the use of the new relative permeability model given in Table 5.5. The calculated OIP is 1000 psia, at which the distance parameters are the minimum and the PC1 recoveries are the highest.

With the new relative permeability parameters, the distance parameters at the three-phase trailing edge are 0.0565, 0.0192, 0.0059, 0.0021, and 0.0008, at 825 psia, 850 psia, 900 psia, 935 pisa, and 1000 psia, respectively. The distance parameters at the three-phase leading edge are 0.0798, 0.0872, 0.0630, 0.0282, and 0.0112, at 825 psia, 850 psia, 900 psia, 935 pisa, and 1000 psia, respectively. The BTs of the three-phase trailing and leading edges and the PC1 recoveries at BTs of the three-phase trailing and leading edges are also affected by the relative permeability model used in the simulation.

To see the effect of relative permeability used on minimum distance conditions, individual terms used in distance parameter calculations are calculated. **Figure 5.35** shows the γ_j used in distance parameter calculations with the new set of relative

permeability model (Table 5.5) at 935 psia. Figure 5.32a presents the γ_j used in distance parameter calculations with the relative permeability model of Khan et al. (1992) (Table 5.4) at 935 psia. The fluctuations of γ_{L1} and γ_V are also reflected in fractional flow curves (see **Figure 5.36**).

In the new set of relative permeability model, the exponents used for all phases are doubled and the endpoint of V phase becomes significantly greater than that of L_1 and L_2 phases. The propagation of the three-phase leading edge becomes slower with the new set of relative permeability model.

Figure 5.37 shows the saturation profile with the new set of relative permeability model (Table 5.5) at 935 psia. The saturation profile obtained at 935 psia with the relative permeability model of Khan et al. (1992) is presented in Figure 5.31a. Because of the change made for the exponent and endpoint for V phase in the new relative permeability model, V phase travels slower. With a slower propagation of the three-phase leading edge, the reduction of L_1 phase saturation is from 0.5565 to 0.0425. That is, the decrease of L_1 phase saturation is 0.5140. Figure 5.31a shows that the reduction of L_1 phase saturation is 0.7253.

Figure 5.38 compares the CO_2 concentration profiles obtained with two sets of relative permeability models (see Tables 5.4 and 5.5). With the new set of relative permeability, CO_2 concentrations are higher than that with the model of Khan et al. (1991), although three-phase leading edge propagates slower.

The γ_j (j = 1, 2, .., N_P) parameters involved in multiphase transitions are calculated. With the new set of relative permeability model, at the three-phase leading edge, $\gamma_{L_1}^U$, $\gamma_{L_2}^U$, and γ_V^U are -0.0214, 0.8196, and 0.2018, respectively. The $\gamma_{L_1}^D$ and γ_V^D are 0.5059 and 0.4941, respectively. The intersection involved at the three-phase leading

edge is calculated at the composition (0.0000, 0.9357, 0.0048, 0.0035, 0.0036, 0.0027, 0.0023, 0.0022, 0.0126, 0.0117, 0.0108, 0.0100). The composition distance between the intersection and upstream L_1 phase is 0.5325, and the composition distance between the intersection and upstream L_2 phase is 0.0216. The distance parameter calculated at three-phase leading edge is 0.0282.

Similarly, the intersection involved at three-phase trailing edge is calculated with $\gamma_{L_1}^D$ of -0.0399, $\gamma_{L_2}^D$ of -0.1035, and γ_V^D of 1.1434. The composition distance between the intersection and downstream V phase is 0.0607 at the three-phase trailing edge. The composition distance between the intersection and downstream L_2 phase is 0.0638. The distance parameter calculated at three-phase trailing edge is 0.0021.

The difference in CO_2 propagation owing to the relative permeability models for this oil displacement is clear in Figure 5.38. Analysis of various parameters involved in the distance parameters may clarify what affects the in-situ propagation of the injected solvent in gas floods.

5.3.1.4 Robustness of the New Simultaneous PT Flash Algorithm in Simulation

The conventional sequential use of phase-split/-flash is also tested for NWE oil displacement at the calculated OIP (935 psia), for which millions of three-phase flash calculations are performed. Solutions from the conventional flash at each grid block are found to be the same as those obtained with the new algorithm in this case. **Figure 5.39** compares the number of iterations required for convergence with the new algorithm and the conventional algorithm. In the new algorithm, the sampling compositions used consist of 24 compositions distributed using the systematic distribution scheme (Appendix C) and the compositions from the previous time step. N_{Smax} is set to be 24. In the conventional algorithm, 27 guesses are used in phase stability tests. With the new

algorithm, the maximum number of iterations required for convergence is 119; however, with the conventional algorithm, the maximum number of iterations required for convergence is 497.

The number of fugacity-coefficient calculations is one of the many measurements to quantify computational efficiency. **Figure 5.40** compares the number of fugacity-coefficient calculations with the new algorithm and that with the conventional algorithm. The maximum number of fugacity-coefficient calculations with the new algorithm is 436. It occurs when the number of iterations required for convergence is at its maximum with the new algorithm. However, with conventional algorithm, the maximum number of fugacity-coefficient calculations is 3437, which is 7 times more than that with the new algorithm. With the conventional algorithm, more than 90% of the fugacity vector calculations are performed in two- and three-phase stability tests.

Figure 5.41 shows N_P and N_U obtained with the new algorithm with respect to dimensionless distance at 0.4 PVI at 935 psia. Non-zero N_U ($N_U = 1$) is detected in the entire single L_1 phase region. The number of iterations required for convergence in the single L_1-phase region is all 10. This is because the L_1-phase region at 0.4 PVI is also single L_1-phase region at the previous time step. Hence, at 0.4 PVI, the initial sampling compositions are all the same for all grid blocks in the single L_1-phase region. The composition in set U at 0.4 PVI is close to one of the equilibrium phase (V phase) at the next time step. Hence, the new PT flash algorithm presented in chapter 3 can capture more information regarding the Gibbs free energy surface compared to that of with the conventional algorithm.

5.3.2 Summary of Five Other Reservoir Oils

Many simulation runs and the same analyses were performed for other five three-hydrocarbon-phase reservoir oils. They are oil B (Shelton and Yarborough 1977), West Sak oil (DeRuiter et al. 1994), JEMA (Khan et al. 1992), oil G (Creek and Sheffield 1993), and BSB oil (Khan et al. 1992).

For oil B (Shelton and Yarborough 1977), the measured MMP is 1450 psia, and the calculated OIP is 1475 psia. For West Sak oil (DeRuiter et al. 1994), the measured MMP is 1500 psia, and the calculated OIP is 1500 psia. For JEMA (Khan et al. 1992), the measured MMP is 1250 psia, and the calculated OIP is 1200 psia. For oil G (Creek and Sheffield 1993), the measured MMP is 1035 psia, and the calculated OIP is 1075 psia. For BSB oil (Khan et al. 1992), the measured MMP is 1200 psia, and the calculated OIP is 1250 psia. Detailed figures for the minimum distance conditions for these five oil displacements are given in **Appendix F**.

5.3.3 Oil Displacement in the Presence of Water at Elevated Temperature

This section presents another case to validate the minimum distance conditions using a reservoir oil in the presence of water. The characteristics of this displacement are different from those presented in sections 5.3.1 and 5.3.2 in that this case involves water phase behavior.

Bakken shale reservoir oil is used (Nojabaei et al. 2013), along with the binary interaction parameters (BIPs) given in Siripatrachai et al. (2017). The properties of Bakken oil are given in **Tables 5.6**, and the BIPs are given in **Table 5.7**. The parameters used in Corey's model for three-phase relative permeabilities are given in **Table 5.8**. Reservoir temperature is 536°F. Injection gas is pure C_2. Component C_{22-80} is selected to

evaluate displacement efficiency. Flow simulations are performed for seven pressure conditions with a fixed number of GBs, 250.

Figure 5.42 shows the minimum distance condition for Bakken oil calculated at 0.4 PVI at seven pressures; 2000 psia, 2300 psia, 2600 psia, 2750 psia, 2900 psia, 3050 pisa, and 3200 psia. The distance parameter is calculated for multiphase transition between three and two phases. The efficiency of displacement of water by vapor is calculated at the BT of the multiphase transition. The lowest displacement efficiency is 0.9452 at 2000 psia, and the highest is 1.0 at 3050 psia and higher. Corresponding distance parameters calculated are 0.0085 and 0.0036 at 2000 psia and 3200 psia, respectively. The increase in the water-phase displacement efficiency is 5.8%. The decrease of distance parameter is 57.13%. This indicates that the distance parameter is able to capture a small increase in displacement efficiency in this case.

Another set of relative permeability is also tested for this case. The new set of relative permeability is obtained from Oak (1991) and is given in **Table 5.9**. **Figure 5.43** shows the minimum distance condition for Bakken oil calculated at 0.4 PVI at five pressures; 1800 psia, 2000 psia, 2300 psia, 2600 psia, and 2750 psia. The minimum distance parameter at multiphase transition is calculated at 1800 psia. The corresponding displacement efficiency is 98.17%. From the lowest pressure (1800 psia) to the highest pressure (2750 psia), distance parameter is reduced from 0.0282 to 0.0036. The decrease in displacement efficiency is from 0.9817 to 0.8860. Small increase in displacement efficiency can be properly captured by distance parameter calculated.

5.4 SUMMARY

This chapter presented the utility of the distance parameters for quantification of displacement efficiency for seven different displacement processes. Simulation cases

also showed the robustness and efficiency of the new simultaneous PT flash algorithm presented in chapter 3. Six cases are presented for displacement of L_1 phase by L_2 phase in the presence of V phase. The other case is the displacement of W phase by V phase in the presence of L_1 phase when the connate water evaporates as ethane is injected into an oil reservoir at an elevated temperature. Conclusions are as follows:

1. Efficient oil displacement can be achieved at substantially lower pressures in comparison with the MMP calculated with prior methods, as demonstrated for West Sak oil and North Ward Estes oil.

2. Distance parameters are calculated in volume space by use of equations 2.7 and 2.8 for a composition path obtained from the in-house 1D convection-only compositional simulator. Unlike Okuno and Xu (2014ab), it is not necessary to solve for the intersection between a tie line and a tie triangle when distance parameters are calculated on the volume basis. Hence, it is a simpler and more direct validation of the utility of the distance parameters to quantify the local displacement efficiency in three-phase flow.

3. Minimum distance conditions defined at a phase transition are used to calculate optimal injection pressure (OIP). Negative correlations between the distance parameter calculated at a phase transition and component recovery at BT of a phase transition are observed for all cases tested. This indicates that the highest displacement efficiency occurs when the distance parameters are the lowest.

4. Use of the weak form of the 1D convective compositional flow equations enables to take into account the effect of mixing on displacement efficiency through numerical dispersion. Use of a larger number of GBs results in lower distance parameters calculated at a phase transition. The recoveries at a greater level of dispersion

(i.e., a smaller number of GBs) are lower than those with a lower level of numerical dispersion (i.e., a larger number of GBs).

5. The effect of the relative permeability model used on displacement efficiency in three-phase flow is properly included in distance parameters (equations 2.7 and 2.8) through the parameter "γ". The cases tested showed that the relative permeability parameters may have a limited impact on simulated oil recovery when the miscibility level is high at OIP.

6. The robustness and efficiency of the new PT phase-stability/-split algorithm presented in chapter 3 were demonstrated in flow simulations for seven reservoir oil displacements. The new PT flash algorithm converges more rapidly than the conventional sequential algorithm in terms of the number of iterations required for convergence and the number of fugacity-coefficient calculations, except for the single-phase region. None of the tested cases showed convergence issues in phase behavior calculations.

7. The reliability of the OIP calculation in this research depends on the EOS fluid model used to represent multiphase behavior during the displacement process. The calculated OIPs for the cases are reasonably close to experimentally determined MMPs. This can be because the EOS fluid models obtained from Kumar and Okuno (2016) properly capture the three-phase behavior of the six reservoir oil cases tested.

Table 5.1. Summary of prior studies on quantification of local displacement efficiency in three-phase flow

	EOS model	Method to obtain composition path	MCM condition	Additional notes
Li et al. (2015)		1D mixing cell	Zero length for any of the key tie lines	The order of phase mobility is determined the compositional distance from the injection gas.
Okuno and Xu (2014ab)	PR EOS	1D convective flow with UTCOMP (volume change on mixing is modeled)	Mass conservation on multiphase transitions for L_1-phase completely displaced by non-L_1 phase	Indirect calculation of distance parameters requires obtaining an intersection between the extensions of upstream and downstream tie simplexes. The accuracy of the intersection can be sensitive to the angle between two tie simplexes at near-miscible conditions.
This research		1D convective flow simulator with no volume change of mixing		No volume change of mixing results in a composition path that is different from a more rigorous one from UTCOMP. Calculation of distance parameters in volume space is direct.

Table 5.2. Fluid properties of the NWE oil (Kumar and Okuno 2016)

Components	Oil	Gas	MW, g/mol	T_C, °F	P_C, psia	Acentric factor	V_C, ft³/lbm-mol
N_2	0.002	0.0	28.014	-232.510	492.258	0.040	1.438
CO_2	0.004	1.0	44.010	87.890	1069.798	0.225	1.506
CH_4	0.203	0.0	16.043	-116.590	667.174	0.008	1.586
C_2H_6	0.059	0.0	30.070	90.050	708.364	0.098	2.371
C_3H_8	0.059	0.0	44.097	205.970	615.830	0.152	3.252
C_4H_{10}	0.056	0.0	58.124	297.644	545.342	0.189	4.085
C_5H_{12}	0.049	0.0	72.151	377.078	490.083	0.239	4.870
C_6H_{14}	0.044	0.0	86.000	453.650	430.617	0.296	5.927
PC1	0.215	0.0	139.573	696.114	391.102	0.183	11.713
PC2	0.143	0.0	209.356	892.243	316.680	0.287	17.483
PC3	0.102	0.0	293.393	1093.827	265.882	0.407	24.908
PC4	0.064	0.0	472.233	1473.689	212.221	0.629	32.493

Table 5.3. Binary interaction parameters for the NWE oil given in Table 5.2
(Kumar and Okuno 2016)

	N_2	CO_2	CH_4	C_2H_6	C_3H_8	C_4H_{10}	C_5H_{12}	C_6H_{14}	PC1	PC2	PC3	PC4
N_2	0.000											
CO_2	0.000	0.000										
CH_4	0.100	0.100	0.000									
C_2H_6	0.100	0.145	0.042	0.000								
C_3H_8	0.100	0.132	0.042	0.040	0.000							
C_4H_{10}	0.100	0.125	0.042	0.040	0.030	0.000						
C_5H_{12}	0.100	0.119	0.042	0.040	0.030	0.012	0.000					
C_6H_{14}	0.100	0.116	0.042	0.040	0.030	0.016	0.006	0.000				
PC1	0.130	0.042	0.052	0.042	0.033	0.042	0.027	0.000	0.000			
PC2	0.130	0.089	0.056	0.042	0.036	0.056	0.046	0.000	0.000	0.000		
PC3	0.130	0.116	0.062	0.043	0.042	0.065	0.062	0.000	0.000	0.000	0.000	
PC4	0.130	0.134	0.073	0.044	0.058	0.075	0.082	0.000	0.000	0.000	0.000	0.000

Table 5.4. Parameters used in Corey model for three-phase relative permeabilities
(Khan 1992)

Residual oil saturation	0.2	Residual gas saturation	0.05
Endpoint for L_1 phase	0.48	Endpoint for V phase	0.687
Exponent for L_1 phase	2.5	Exponent for V phase	2.7
Parameters for L_2 phase are the same as used for V phase.			

Table 5.5. New set of parameters used in Corey model for three-phase relative permeabilities

Residual oil saturation	0.2	Residual gas saturation	0.05
Endpoint for L_1 phase	0.3	Endpoint for V phase	0.9
Exponent for L_1 phase	5	Exponent for V phase	5.4
Residual L_2 saturation	0.05		
Endpoint for L_2 phase	0.3	Exponent for L_2 phase	5.4

Table 5.6. Fluid properties of the Bakken oil (Nojabaei et al. 2013)

Components	Oil	Gas	MW, g/mol	T_C, ºF	P_C, psia	Acentric factor	V_C, ft^3/lbm-mol
C_1	0.142	0.0	16.535	-124.334	655.020	0.010	1.580
C_2	0.057	1.0	30.433	90.299	721.990	0.103	2.340
C_3	0.036	0.0	44.097	206.300	615.760	0.152	3.250
C_4	0.022	0.0	58.124	299.538	546.460	0.189	4.110
C_{5-6}	0.025	0.0	78.295	415.809	461.290	0.268	5.390
C_{7-12}	0.061	0.0	120.562	593.580	363.340	0.429	8.810
C_{13-21}	0.028	0.0	220.716	872.425	249.610	0.720	15.190
C_{22-80}	0.014	0.0	443.518	1384.821	190.120	1.016	36.000
Water	0.614	0.0	18.015	705.470	3203.728	0.344	0.897

Table 5.7. Binary interaction parameters for the Bakken oil given in Table 5.6 (Nojabaei et al. 2013)

	C_1	C_2	C_3	C_4	C_{5-6}	C_{7-12}	C_{13-21}	C_{22-80}	Water
C_1	0.000								
C_2	0.005	0.000							
C_3	0.004	0.003	0.000						
C_4	0.004	0.003	0.000	0.000					
C_{5-6}	0.004	0.003	0.000	0.000	0.000				
C_{7-12}	0.003	0.003	0.000	0.000	0.000	0.000			
C_{13-21}	0.003	0.003	0.000	0.000	0.000	0.000	0.000		
C_{22-80}	0.003	0.003	0.000	0.000	0.000	0.000	0.000	0.000	
Water	0.731	0.697	0.666	0.636	0.595	0.516	0.370	0.242	0.000

Table 5.8. Parameters used in Corey model for three-phase relative permeabilities
(Siripatrachai et al. 2017)

Residual oil saturation	0.1	Residual gas saturation	0.05
Endpoint for L_1 phase	0.95	Endpoint for V phase	0.9
Exponent for L_1 phase	2	Exponent for V phase	4
Residual water saturation	0.2		
Endpoint for W phase	0.95	Exponent for W phase	2

Table 5.9. Parameters used in Corey model for three-phase relative permeabilities
(Oak 1991)

Residual oil saturation	0.3	Residual gas saturation	0.08
Endpoint for L_1 phase	0.02	Endpoint for V phase	0.4
Exponent for L_1 phase	2	Exponent for V phase	3.8
Residual water saturation	0.2		
Endpoint for W phase	0.03	Exponent for W phase	3.2
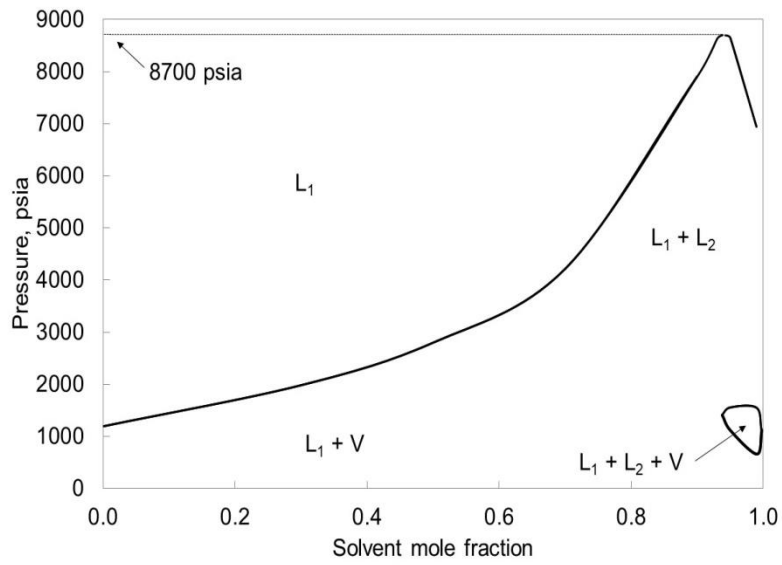
(a)
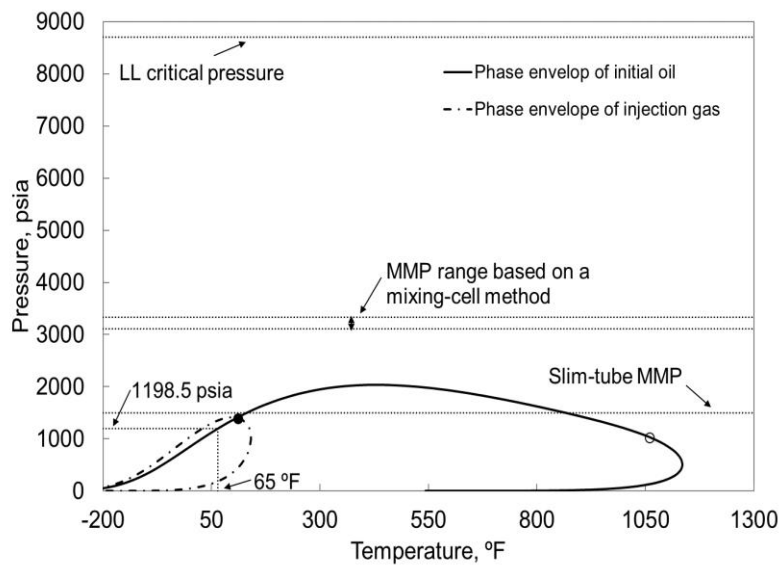
(b)

Figure 5.1. P-x and P-T diagrams for the West Sak oil and the injection gas with 60% methane concentration. The properties of components used were given in Okuno and Xu (2014a). The reservoir temperature is 65°F. (a) P-x diagram. (b) P-T diagram.

211
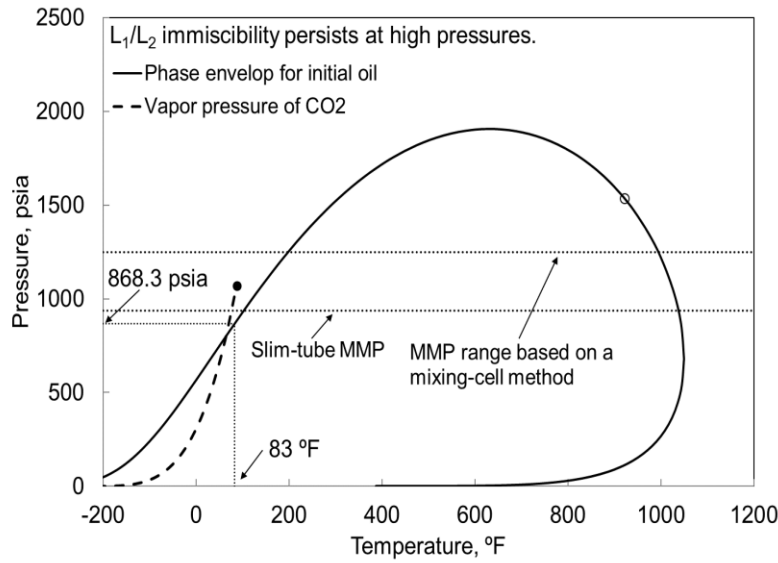
Figure 5.2. P-T diagram for the North Ward Estes (NWE) oil and the injection gas of CO_2. The properties of components used were given in Kumar and Okuno (2016).
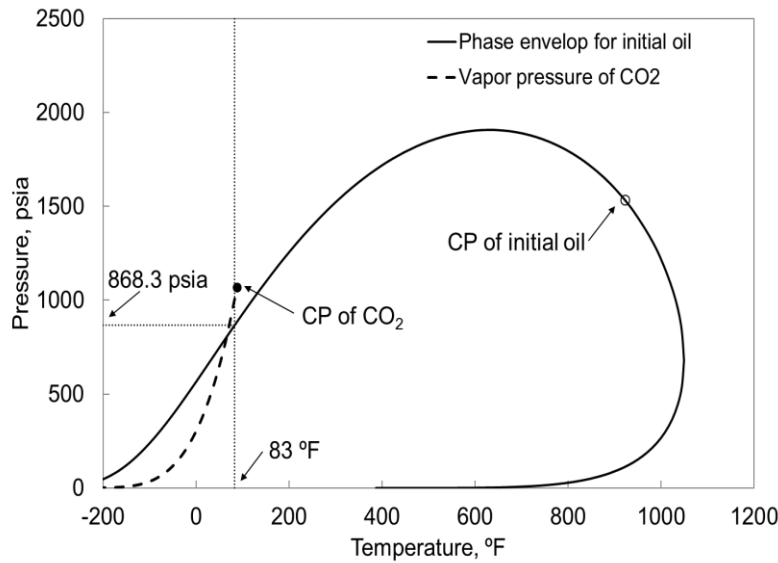
Figure 5.3. P-T diagram of the NWE oil and injection gas (CO_2). The properties of components used are given in Table 5.2. The binary interaction parameters are given in Table 5.3. The oil gravity is calculated to be approximately 32ºAPI. The bubble point pressure at the reservoir temperature of 83ºF is 868.3 psia for the initial oil. The critical point of the initial oil is calculated to be 922ºF and 1534.8 psia.

212
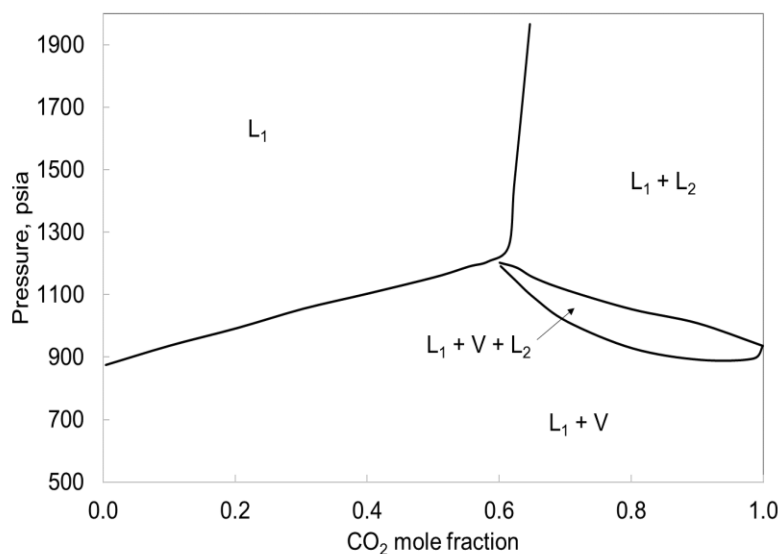
Figure 5.4. Pressure-solvent-mole-fraction (P-x) diagram calculated for mixtures of NWE Oil and CO_2 at 83ºF by use of the new PT flash algorithm presented in chapter 3. The properties of components used are given in Table 5.2. The binary interaction parameters are given in Table 5.3. Two immiscible liquid phases (L_1 and L_2) are present from 60.05% CO_2 concentration to 99.95% CO_2 concentration. Three phases (L_1, V, and L_2) exist between the L_1 + V and L_1 + L_2 regions.
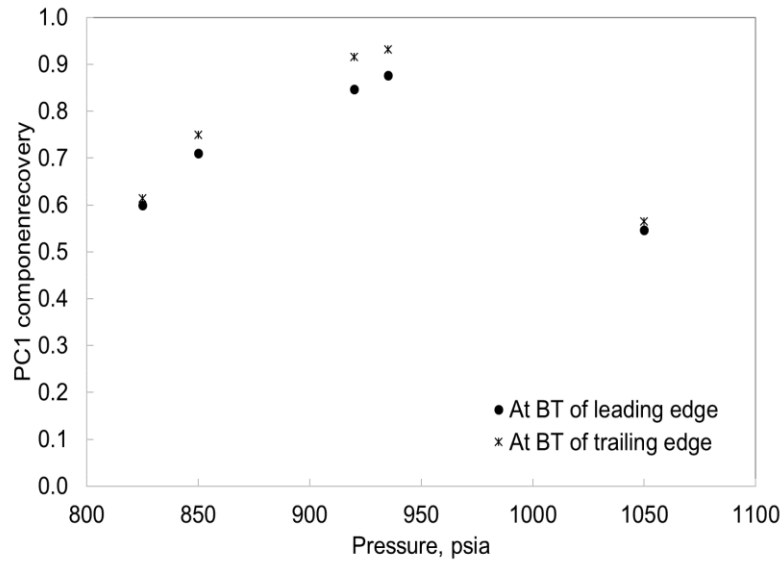
Figure 5.5. PC1 recovery at breakthrough (BT) times of the leading and trailing edges of the three-phase region at the five pressures at 83ºF. The number of GBs used is 250. PC1 recoveries are 0.599, 0.709, 0.846, 0.877, and 0.546, at BTs of the leading edge of the three-phase region at 825 psia, 850 psia, 920 psia, 935 psia, and 1050 psia, respectively. PC1 recoveries at BTs of the trailing edge of the three-phase region are 0.614, 0.749, 0.915, 0.932, and 0.615, at 825 psia, 850 psia, 920 psia, 935 psia, and 1050 psia, respectively. Highest PC1 recovery is observed at 935 psia at BT of trailing edge of the three-phase region, and is 34.04% more efficient than that at 825 psia.

214
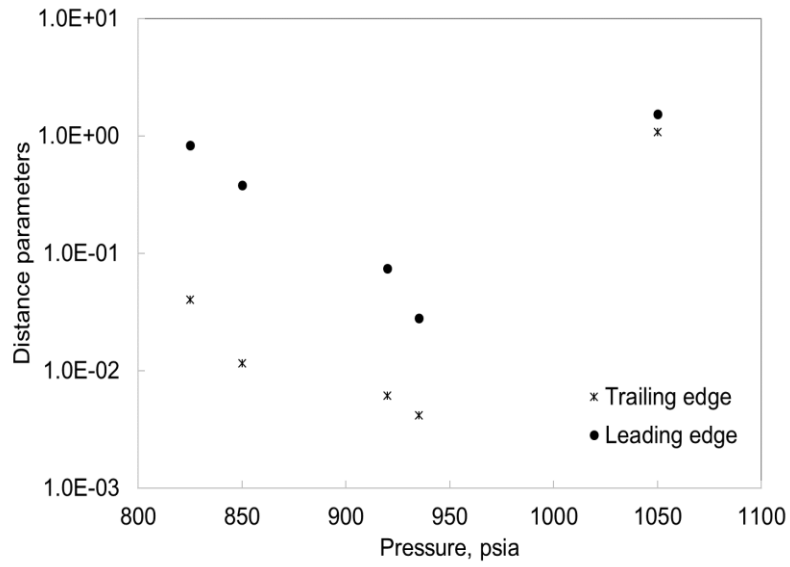
Figure 5.6. Distance parameters at the three-phase trailing and leading edges for NWE oil at the five different pressures at 83ºF.   The number of GBs used is 250. The OIP (935 psia) is defined when distance parameters are lowest ($\delta^T = 0.0041$ and $\delta^L = 0.0280$). At the three-phase trailing edge, the distance parameter is lower than that of the three-phase leading edge. It is likely because the concentrations' change at the three-phase leading edge is more drastic than that at the three-phase trailing edge.
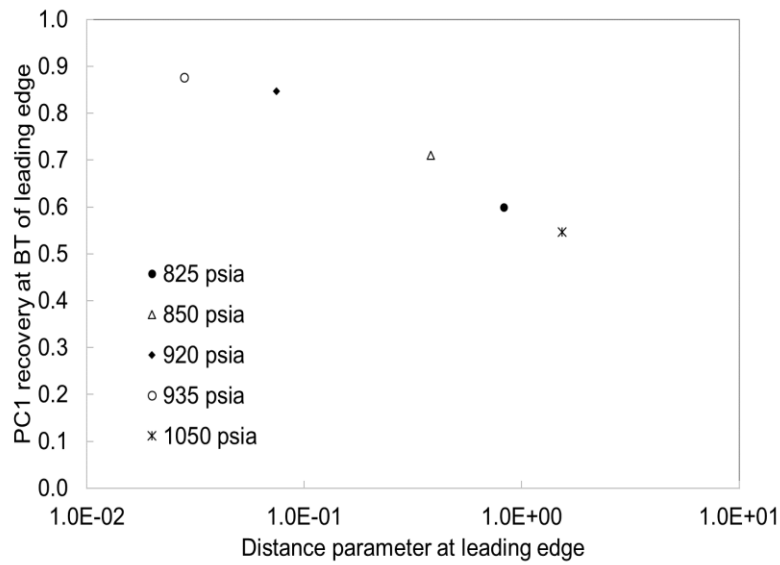
Figure 5.7. PC1 component recoveries at BT of the three-phase leading edge with respect to the distance parameters calculated at the three-phase leading edge for the NWE oil displaced by CO_2 at 83°F. The number of GBs used is 250. PC1 recovery is highest at the BTs of the leading edge at calculated OIP (935 psia).
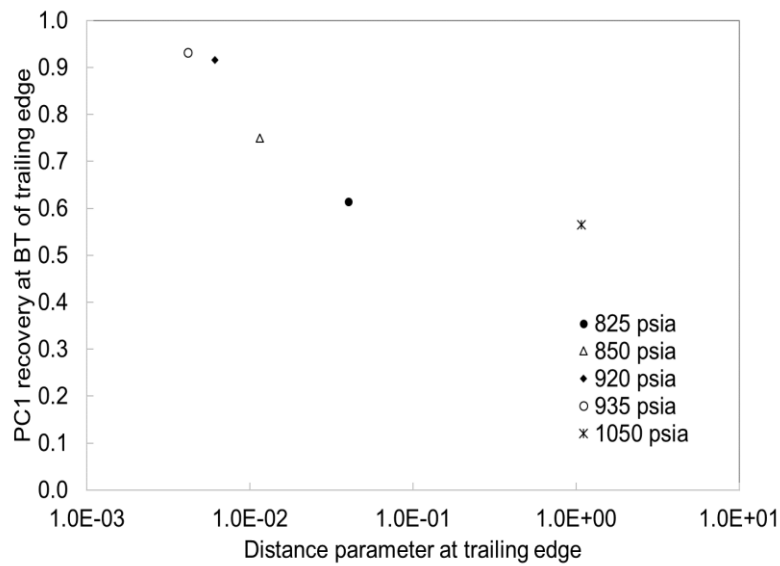
Figure 5.8. PC1 component recoveries at BT of the three-phase trailing edge with respect to the distance parameters calculated at the three-phase trailing edge for the NWE oil displaced by CO_2 at 83°F. The number of GBs used is 250. PC1 recovery is highest at the BTs of the trailing edge at calculated OIP (935 psia).

216
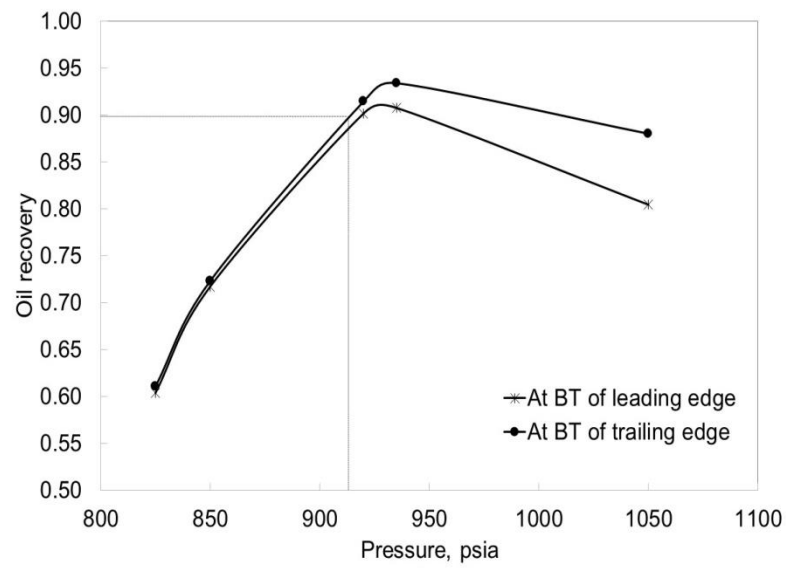
Figure 5.9. Oil recoveries at the BT of three-phase leading and trailing edges at the five pressures obtained by UTCOMP.
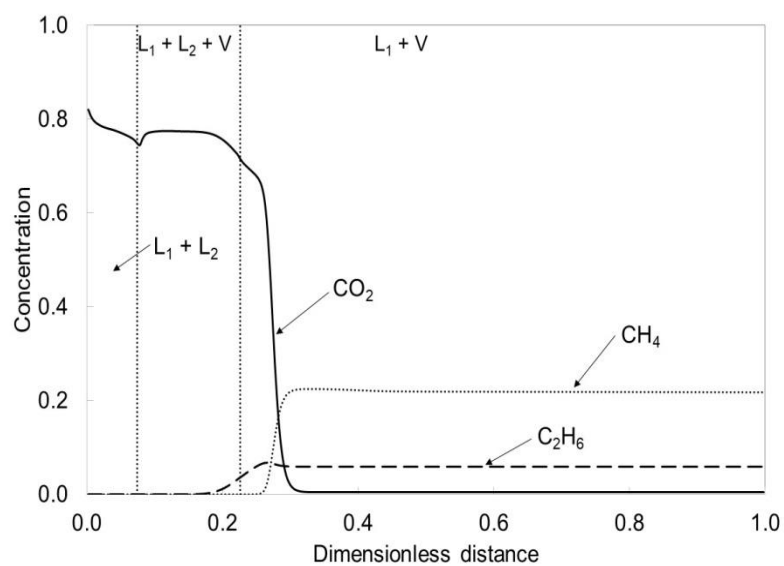
(a)
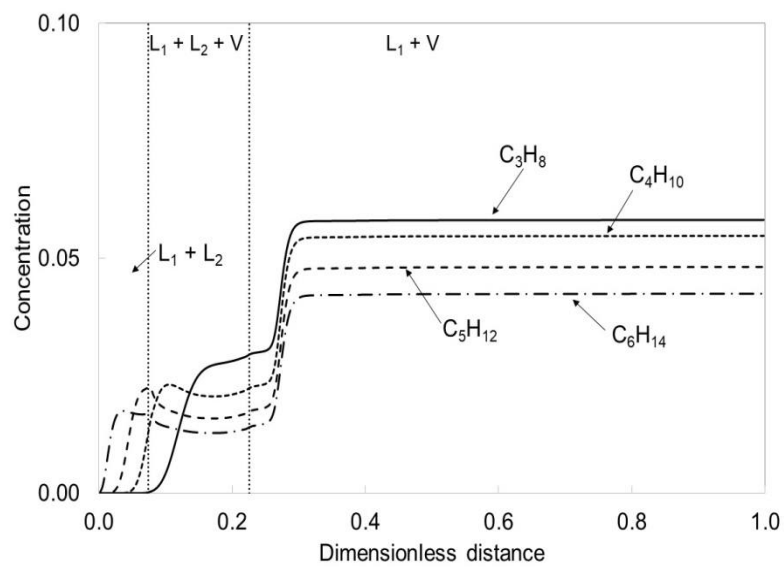
(b)

Figure 5.10. (Continued below)

(c)

Figure 5.10. Concentration profiles at 0.4 PVI at 825 psia for NWE oil displaced by CO_2 at 83°F. The properties of components used are given in Table 5.2. The binary interaction parameters are given in Table 5.3. The number of GBs used is 250. Because the pressure is below the bubble point pressure (868.3 psia, see Figure 5.3), the initial oil is in the $L_1 + V$ region. (a) Concentrations of CO_2, CH_4, and C_2H_6. (b) Concentrations of C_3H_8, C_4H_{10}, C_5H_{12}, and C_6H_{14}. (c) Concentrations of PC1, PC2, PC3, and PC4.

Figure 5.11. Phase saturation profile at 0.4 PVI at 825 psia for NWE oil displaced by CO_2 at 83°F. The properties of components used are given in Table 5.2. The binary interaction parameters are given in Table 5.3. The number of GBs used is 250. The amount of L_1 phase does not exhibit significant decrease at the three-phase leading edge.

220

Figure 5.12. Phase mass densities profile at 0.4 PVI at 825 psia for NWE oil displaced by CO_2 at 83°F. The properties of components used are given in Table 5.2. The binary interaction parameters are given in Table 5.3. The number of GBs used is 250. The mass densities of L_1 and L_2 phases are close to each other at three-phase leading edge; however, these two phases are away from each other in composition space with a distance of 0.074.

221

(a)

(b)

Figure 5.13. (Continued below)
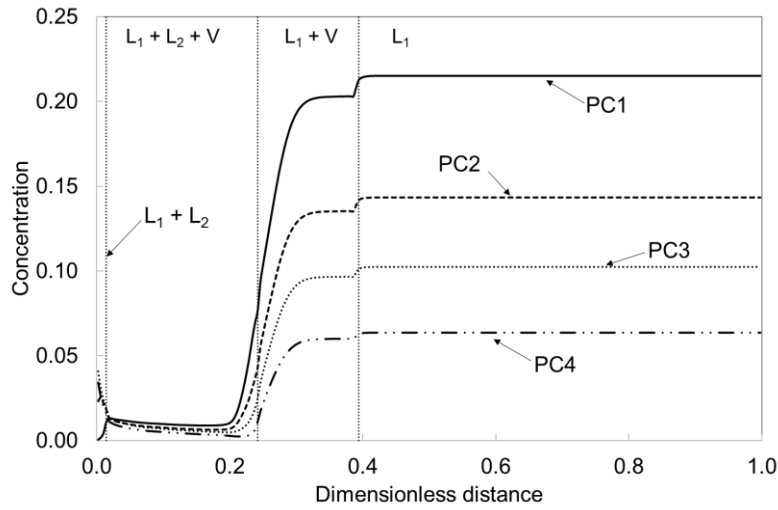
(c)

Figure 5.13. Concentration profiles at 0.4 PVI at 935 psia for NWE oil displaced by CO_2 at 83°F. The properties of components used are given in Table 5.2. The binary interaction parameters are given in Table 5.3. The number of GBs used is 250. Because the pressure is above the bubble point pressure (868.3 psia, see Figure 5.3), the initial oil is in the L_1 region. (a) Concentrations of CO_2, CH_4, and C_2H_6. (b) Concentrations of C_3H_8, C_4H_{10}, C_5H_{12}, and C_6H_{14}. (c) Concentrations of PC1, PC2, PC3, and PC4.

Figure 5.14. Phase saturation profile at 0.4 PVI at 935 psia for NWE oil displaced by CO_2 at 83°F. The properties of components used are given in Table 5.2. The binary interaction parameters are given in Table 5.3. The number of GBs used is 250.
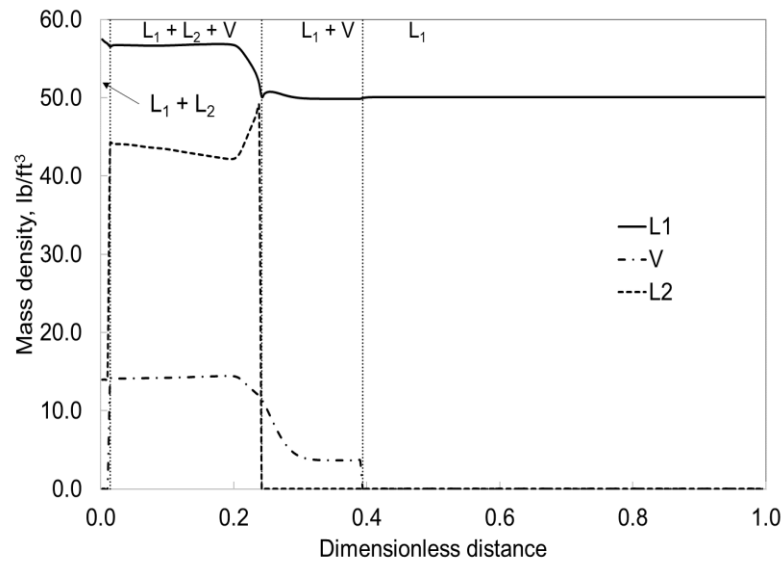
Figure 5.15. Phase mass densities profile at 0.4 PVI at 935 psia for NWE oil displaced by CO_2 at 83°F. The properties of components used are given in Table 5.2. The binary interaction parameters are given in Table 5.3. The number of GBs used is 250.

224

(a)

(b)

Figure 5.16. (Continued below)

(c)

Figure 5.16. Concentration profiles at 0.4 PVI at 1050 psia for NWE oil displaced by CO_2 at 83°F. The properties of components used are given in Ta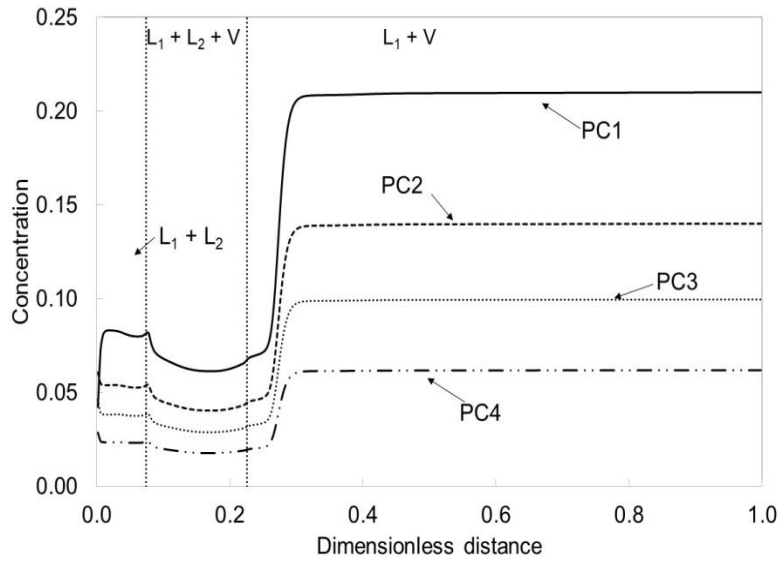ble 5.2. The binary interaction parameters are given in Table 5.3. The number of GBs used is 250. (a) Concentrations of CO_2, CH_4, and C_2H_6. (b) Concentrations of C_3H_8, C_4H_{10}, C_5H_{12}, and C_6H_{14}. (c) Concentrations of PC1, PC2, PC3, and PC4.

Figure 5.17. Phase saturation profile at 0.4 PVI at 1050 psia for NWE oil displaced by CO_2 at 83°F. The properties of components used are given in Table 5.2. The binary interaction parameters are given in Table 5.3. The number of GBs used is 250.
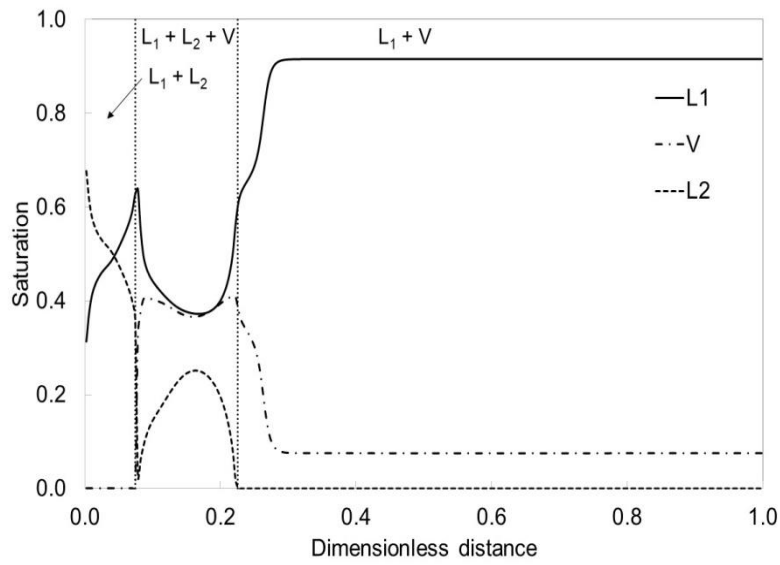

Figure 5.18. Phase mass densities profile at 0.4 PVI at 1050 psia for NWE oil displaced by CO_2 at 83°F. The properties of components used are given in Table 5.2. The binary interaction parameters are given in Table 5.3. The number of GBs used is 250.

227
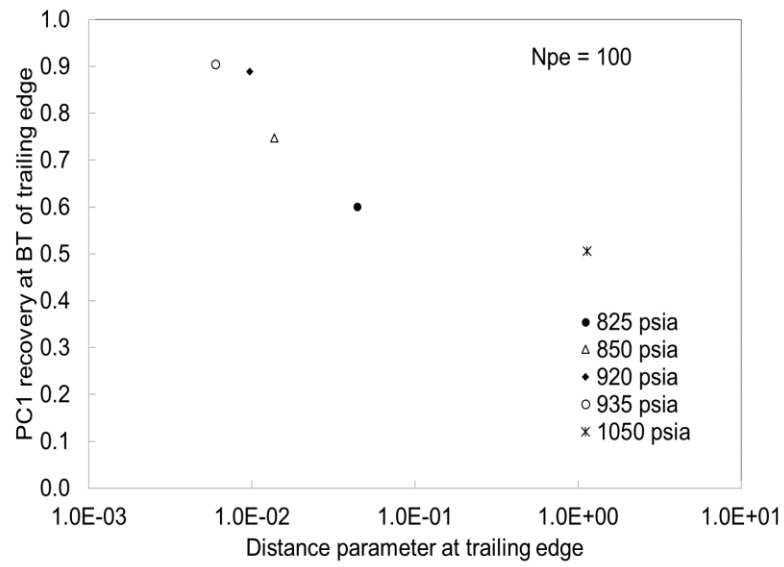
(a)
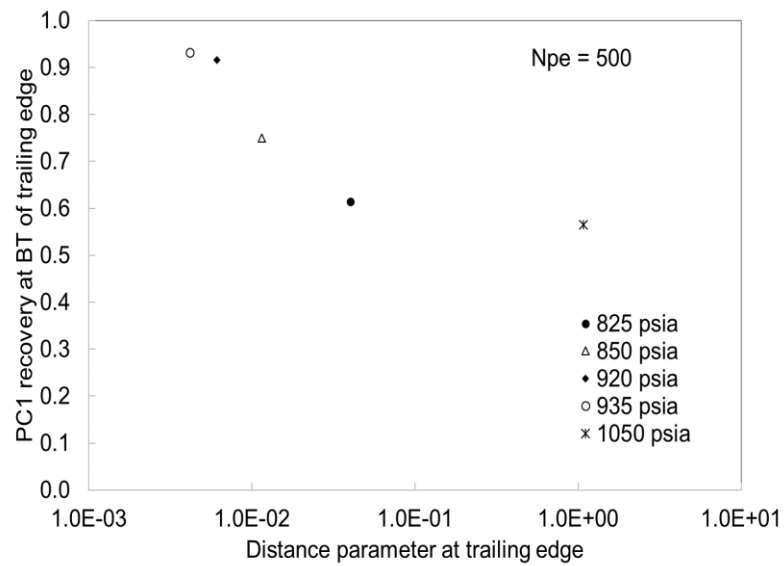
(b)

Figure 5.19. (Continued below)

(c)

(d)

Figure 5.19. (Continued below)
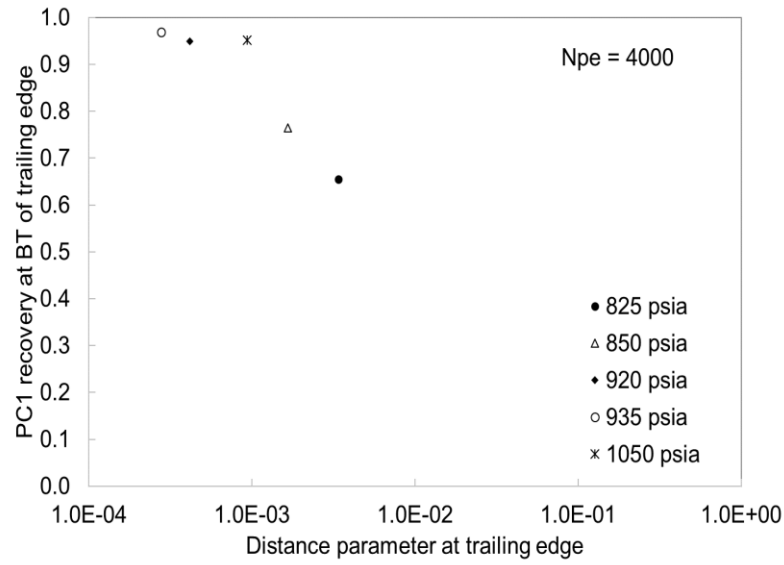
(e)

Figure 5.19. Minimum distance condition at the three-phase trailing edge at five N_{Pe} numbers for NWE oil displaced by CO_2 at 0.4 PVI at 83°F. The properties of components used are given in Table 5.2. The binary interaction parameters are given in Table 5.3. (a) $N_{Pe} = 100$. (b) $N_{Pe} = 500$. (c) $N_{Pe} = 1000$. (d) $N_{Pe} = 2000$. (e) $N_{Pe} = 4000$. Recoveries initially increase as the pressure approaches to the OIP (935 psia). A maximum in the recoveries is eventually reached, after which the recoveries decrease (at 1050 psia).
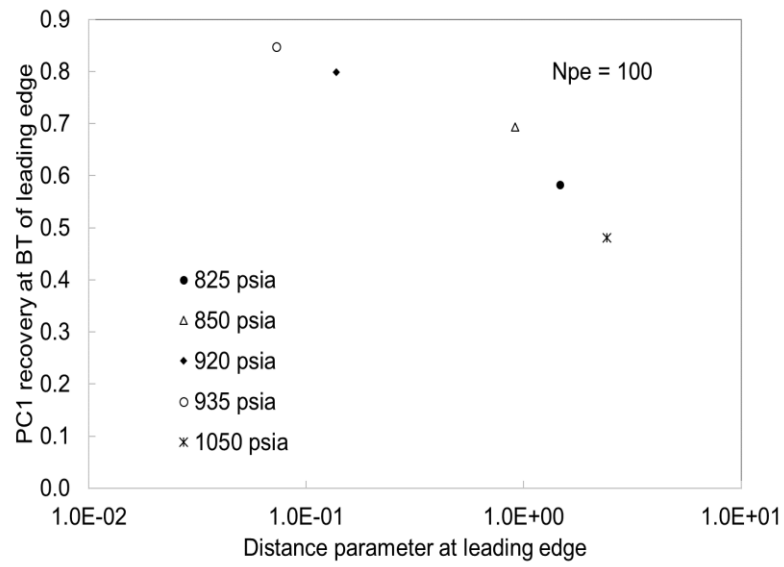
(a)
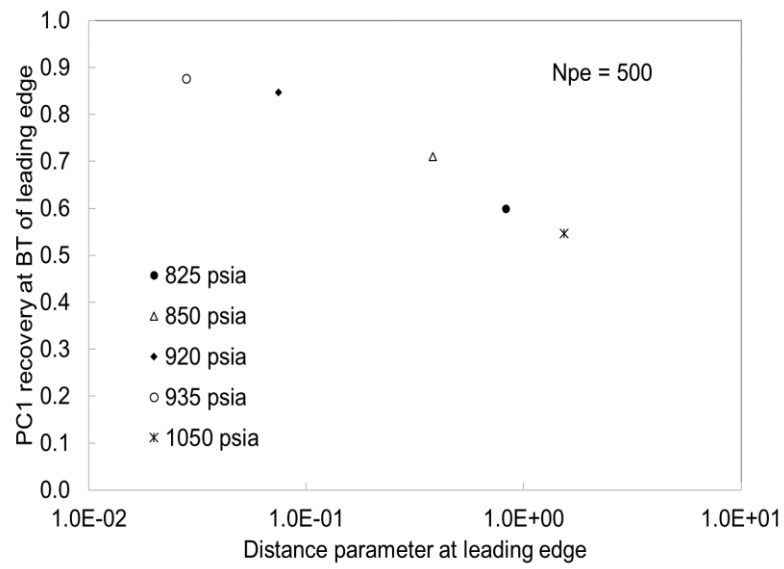
(b)

Figure 5.20. (Continued below)
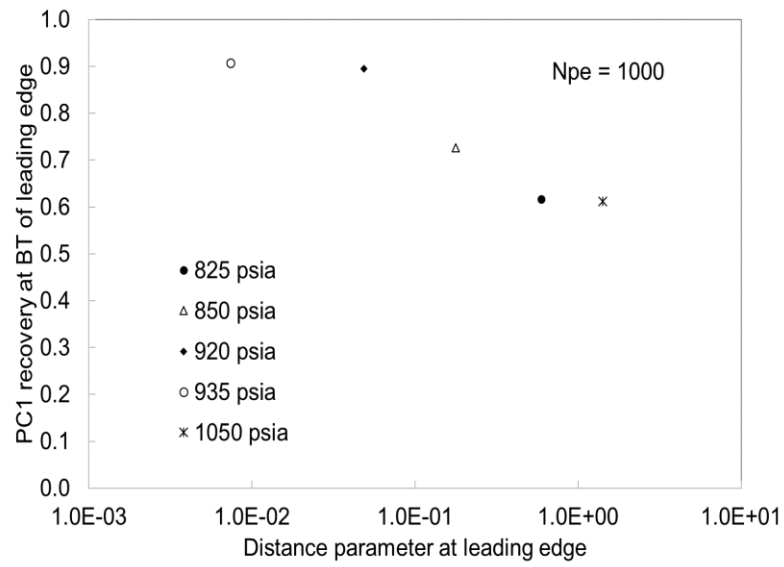
(c)
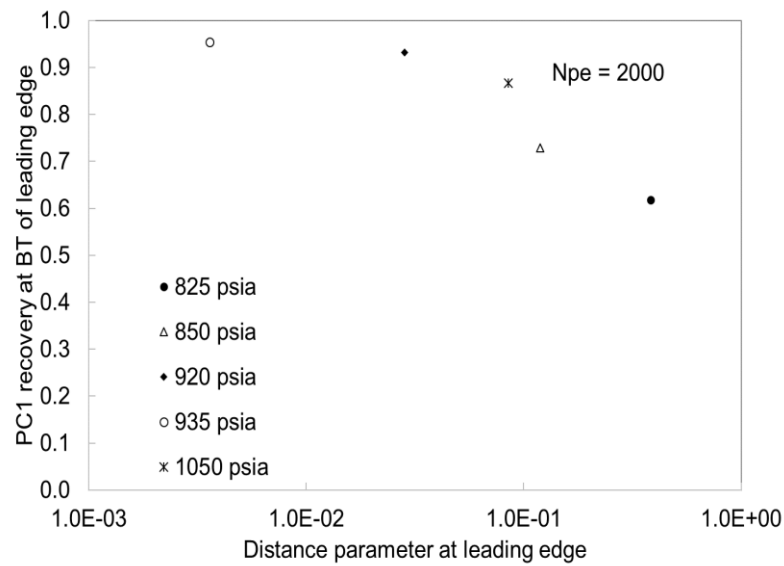
(d)

Figure 5.20. (Continued below)
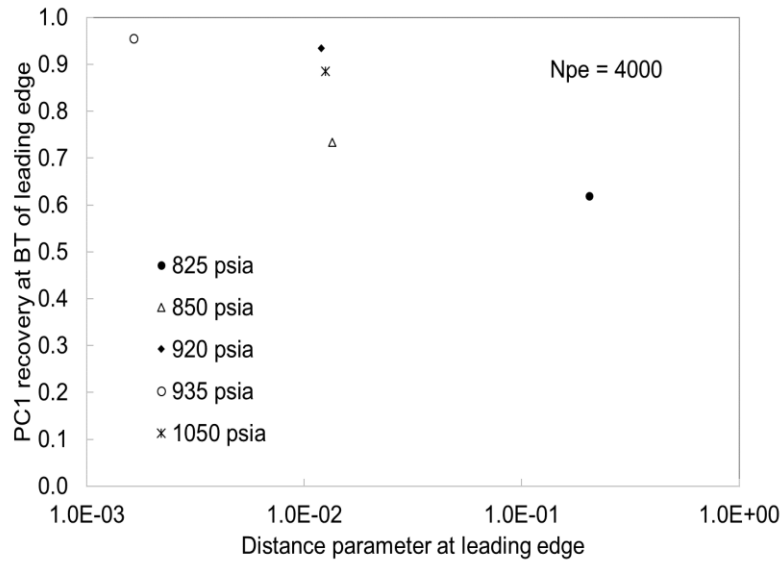
(e)

Figure 5.20. Minimum distance condition at the three-phase leading edge at five N_{Pe} numbers for NWE oil displaced by CO_2 at 0.4 PVI at 83°F. The properties of components used are given in Table 5.2. The binary interaction parameters are given in Table 5.3. (a) $N_{Pe} = 100$. (b) $N_{Pe} = 500$. (c) $N_{Pe} = 1000$. (d) $N_{Pe} = 2000$. (e) $N_{Pe} = 4000$. Recoveries initially increase as the pressure approaches to the OIP (935 psia). A maximum in the recoveries is eventually reached, after which the recoveries decrease (at 1050 psia).
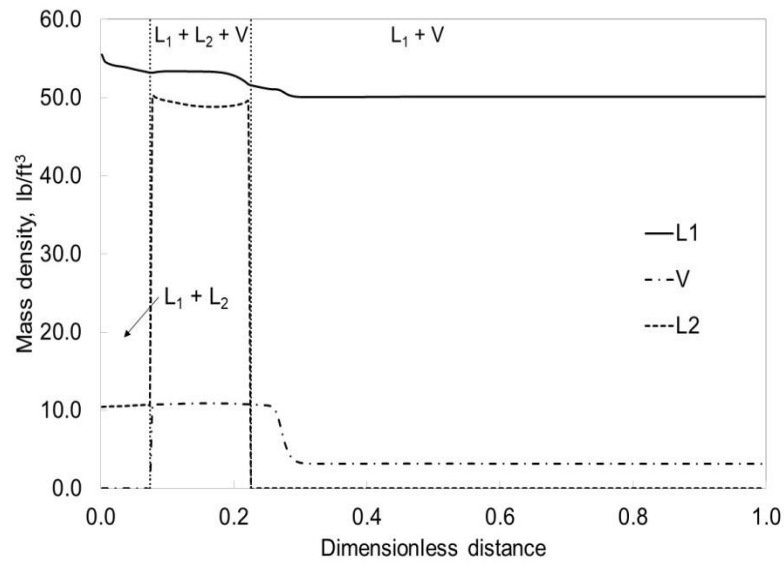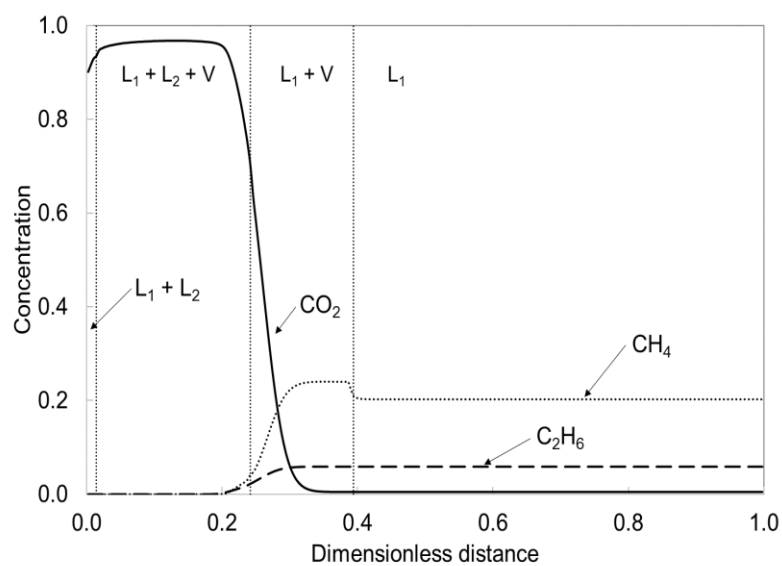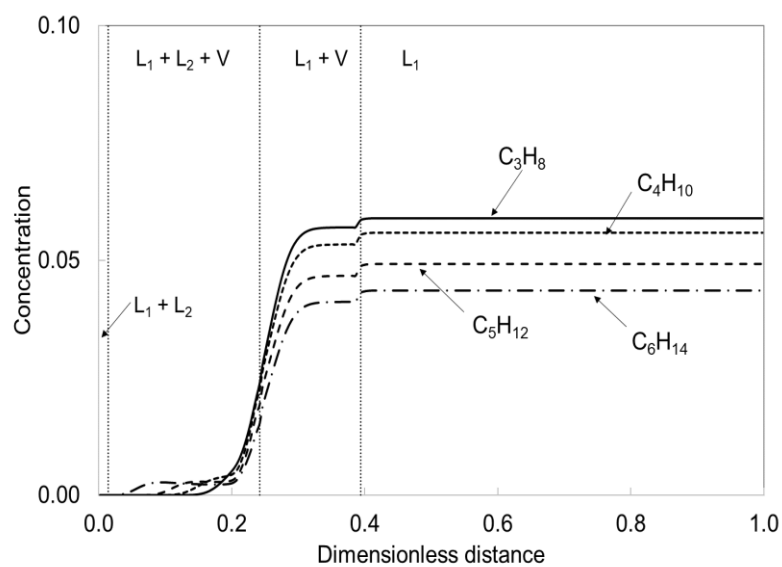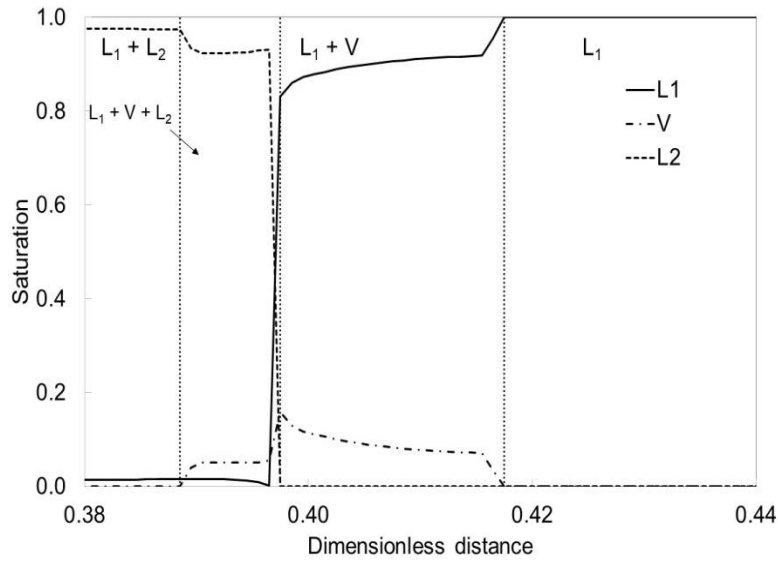
Figure 5.21. Phase saturation profile at 0.4 PVI at 1050 psia for NWE oil displaced by CO_2 at 83°F. The properties of components used are given in Table 5.2. The binary interaction parameters are given in Table 5.3. The number of GBs used is 2000. Use of $N_{GB} = 2000$ shows significant L_1 phase amount decrease in downstream side of three-phase region. At the three-phase leading edge, L_1 phase amount decreases from 0.831 to as low as 0.002.

234
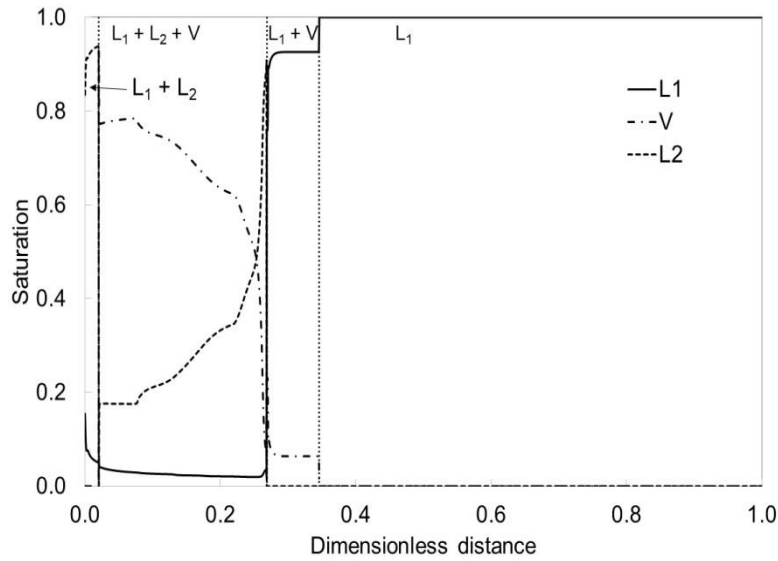
Figure 5.22. Phase saturation profile at 0.4 PVI at 935 psia for NWE oil displaced by CO_2 at 83°F. The properties of components used are given in Table 5.2. The binary interaction parameters are given in Table 5.3. The number of GBs used is 2000. Use of 2000 GBs clearly diminishes the unfavorable increasing of L_1 phase amount at three-phase leading edge.
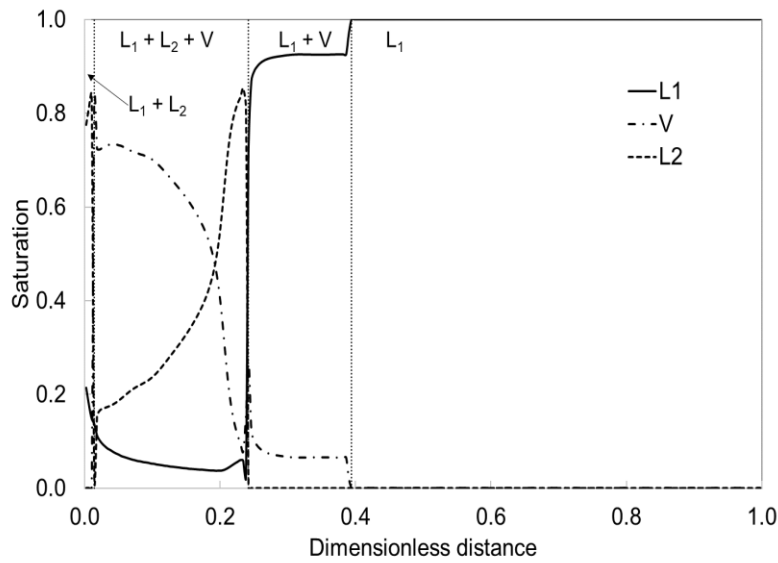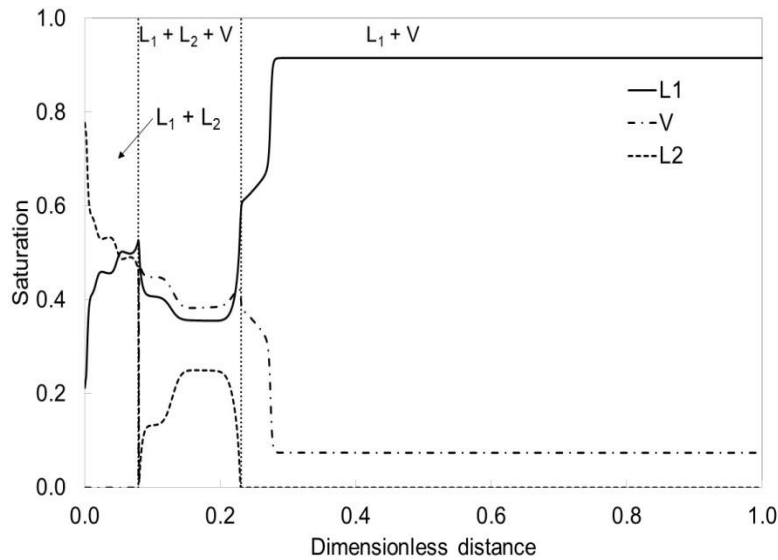

Figure 5.23. Phase saturation profile at 0.4 PVI at 825 psia for NWE oil displaced by CO_2 at 83°F. The properties of components used are given in Table 5.2. The binary interaction parameters are given in Table 5.3. The number of GBs used is 2000.

235
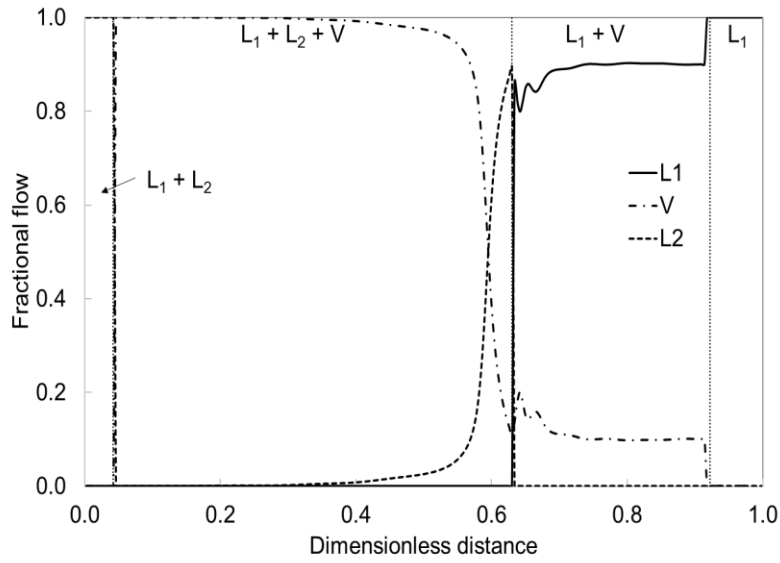
(a)
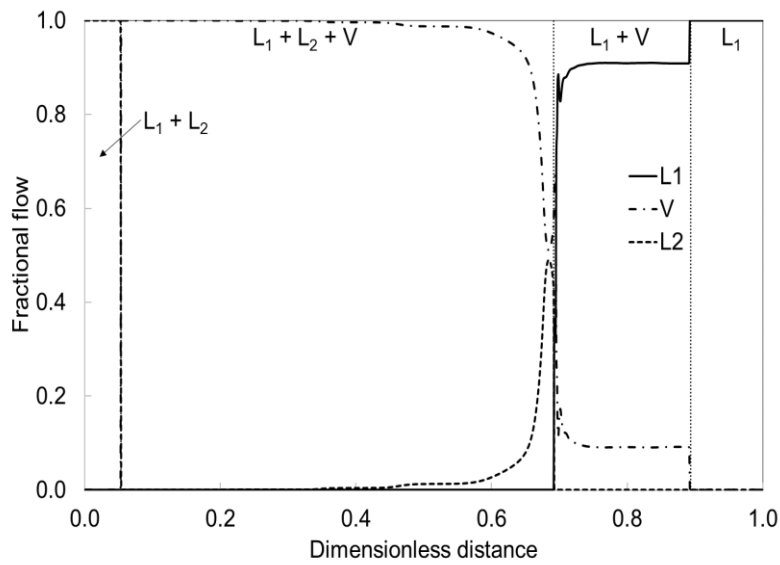
(b)

Figure 5.24. Fractional flow profile at 1.0 PVI at 935 psia for NWE oil displaced by CO_2 at 83 °F. The properties of components used are given in Table 5.2. The binary interaction parameters are given in Table 5.3. (a)The number of GBs used is 250. (b)The number of GBs used is 1000.
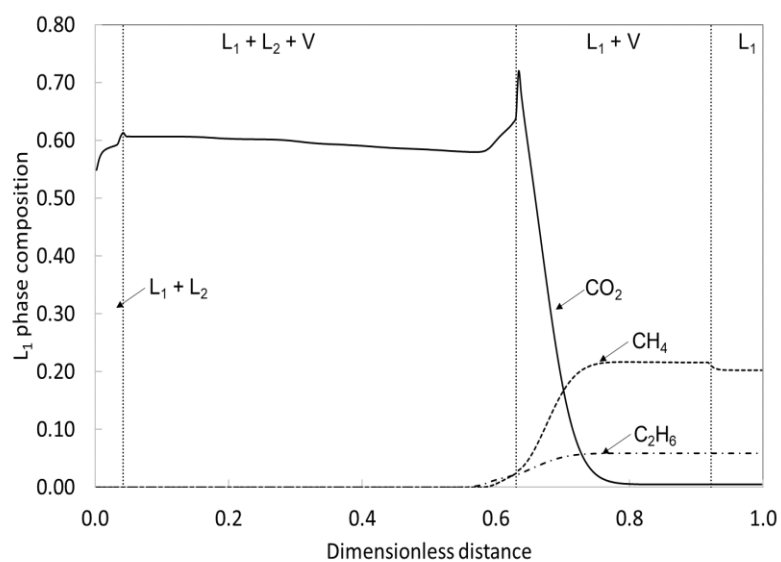
(a)
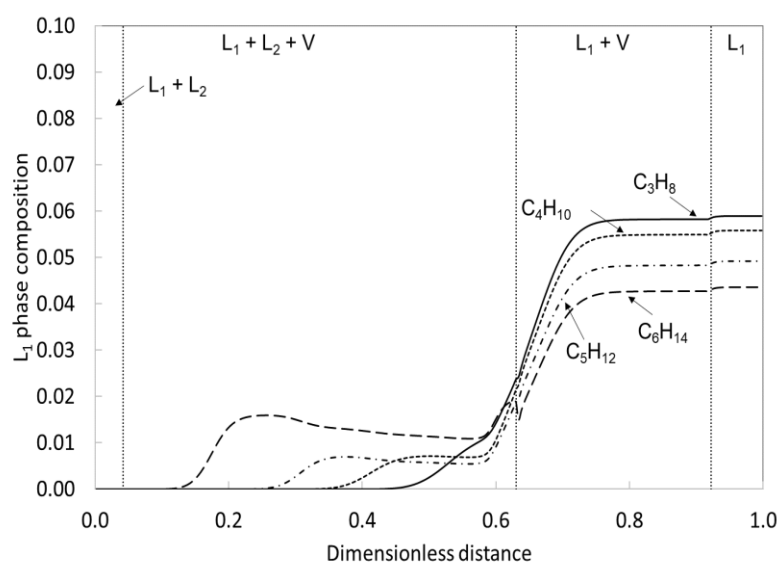
(b)

Figure 5.25. (Continued below)

237
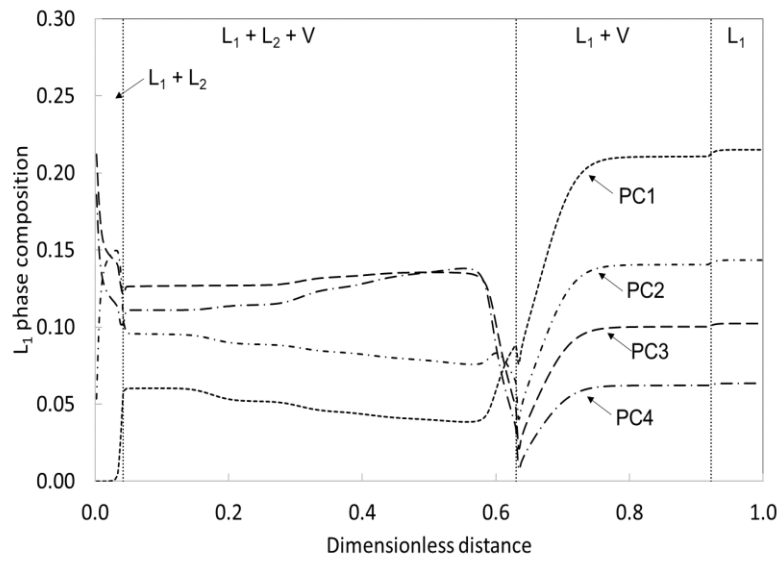
(c)

Figure 5.25. L_1 phase composition profile at 1.0 PVI at 935 psia for NWE oil displaced by CO_2 at 83 °F. The properties of components used are given in Table 5.2. The binary interaction parameters are given in Table 5.3.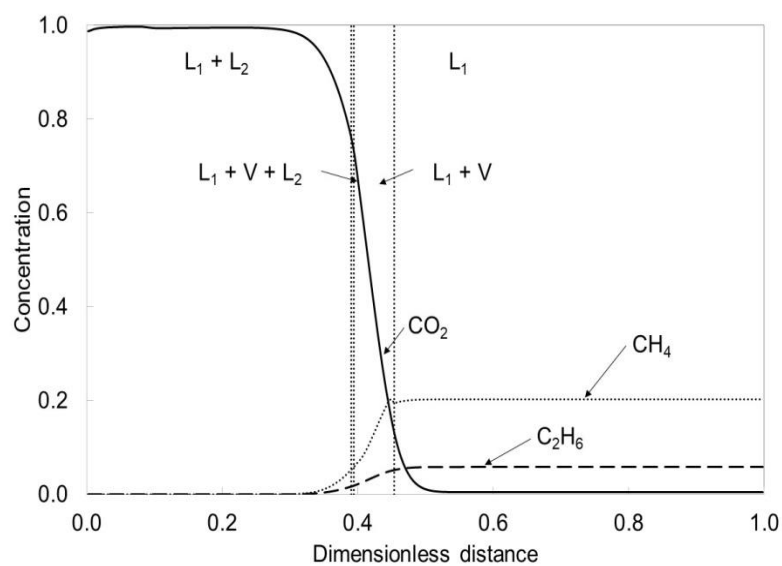 The number of GBs used is 250. (a) CO_2, CH_4, and C_2H_6. (b) C_3H_8, C_4H_{10}, C_5H_{12}, and C_6H_{14}. (c) PC1, PC2, PC3, and PC4.

238
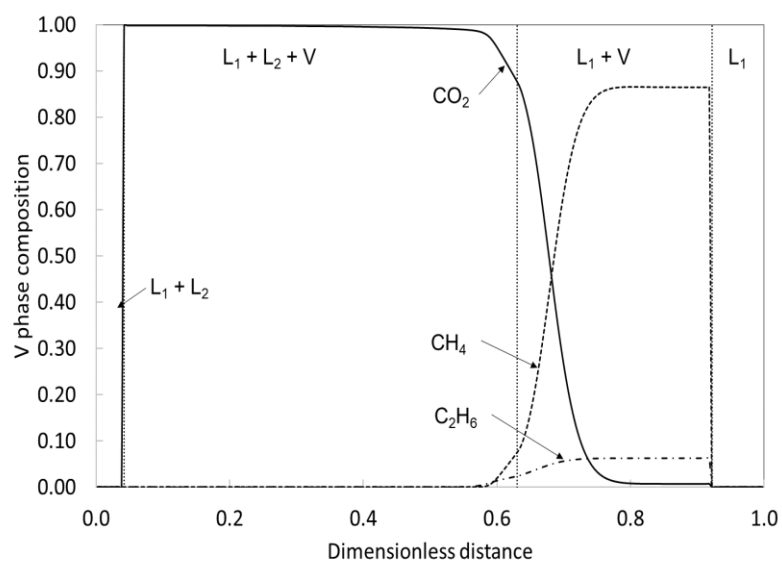
(a)
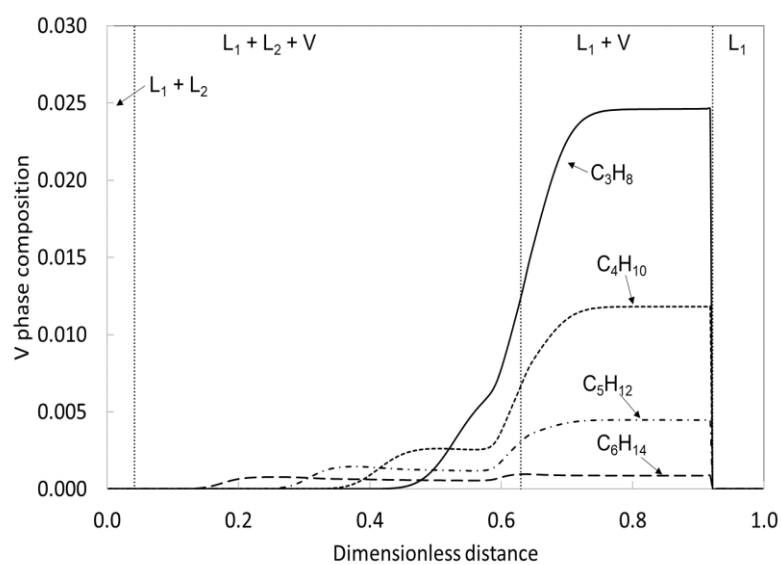
(b)

Figure 5.26. (Continued below)
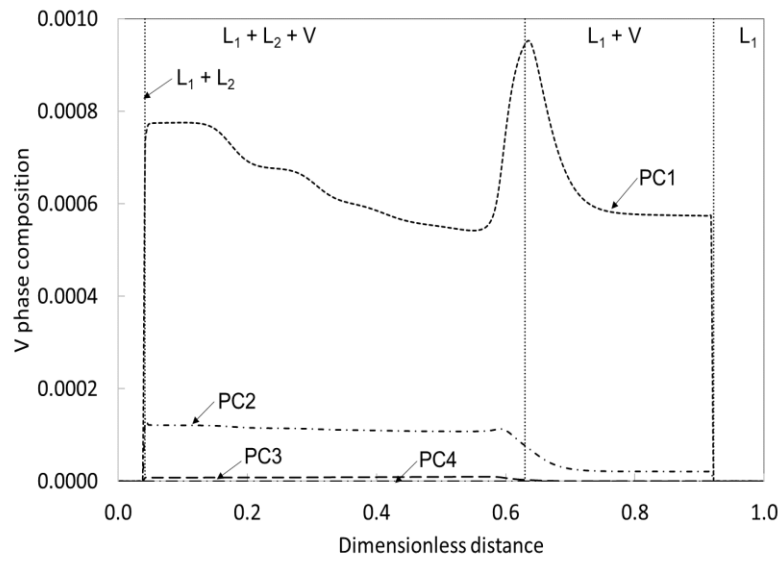
(c)

Figure 5.26. V phase composition profile at 1.0 PVI at 935 psia for NWE oil displaced by CO_2 at 83 °F. The properties of components used are given in Table 5.2. The binary interaction parameters are given in 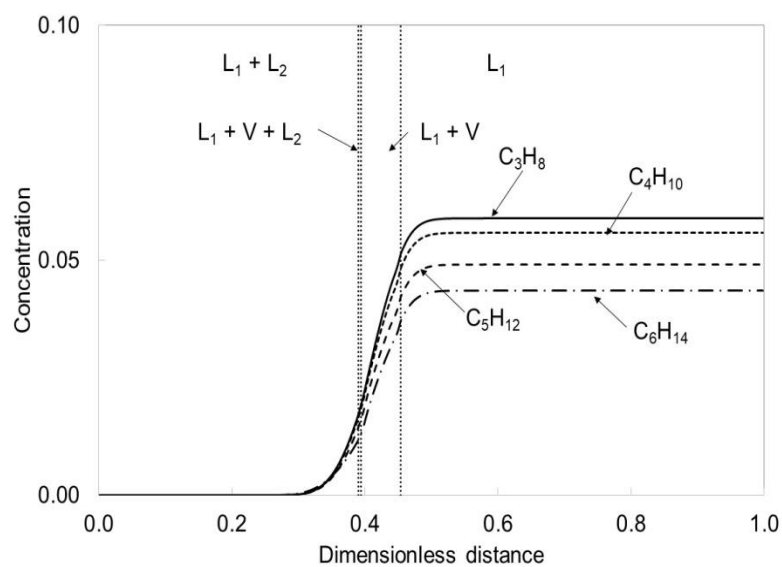Table 5.3. The number of GBs used is 250. (a) CO_2, CH_4, and C_2H_6. (b) C_3H_8, C_4H_{10}, C_5H_{12}, and C_6H_{14}. (c) PC1, PC2, PC3, and PC4.
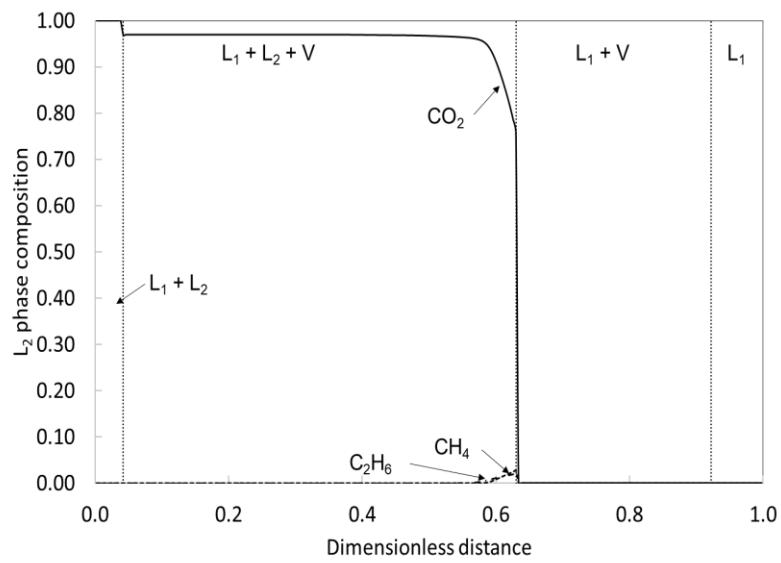
(a)
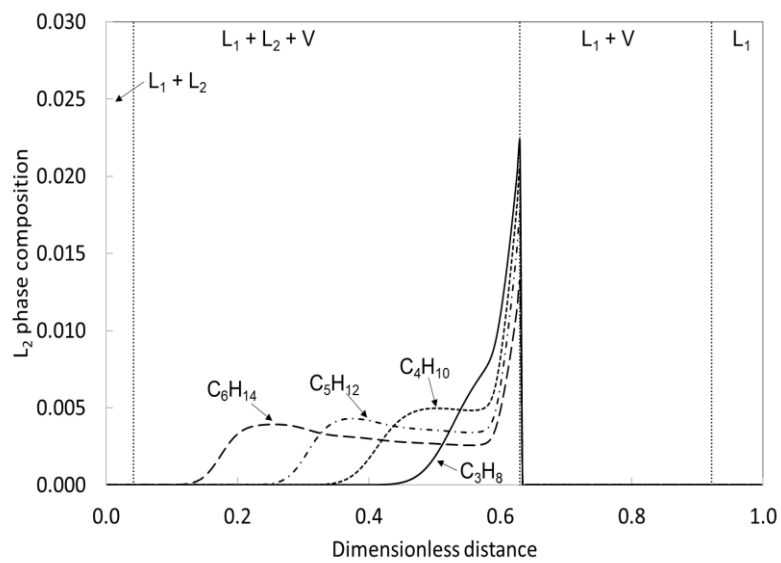
(b)

Figure 5.27. (Continued below)

241
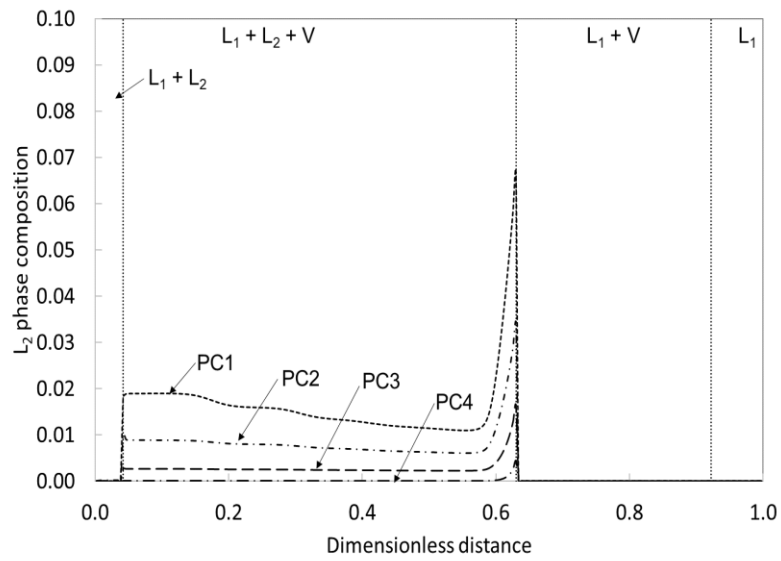
(c)

Figure 5.27. L_2 phase composition profile at 1.0 PVI at 935 psia for NWE oil displaced by CO_2 at 83 °F. The properties of components used are given in Table 5.2. The binary interaction parameters are given in Tab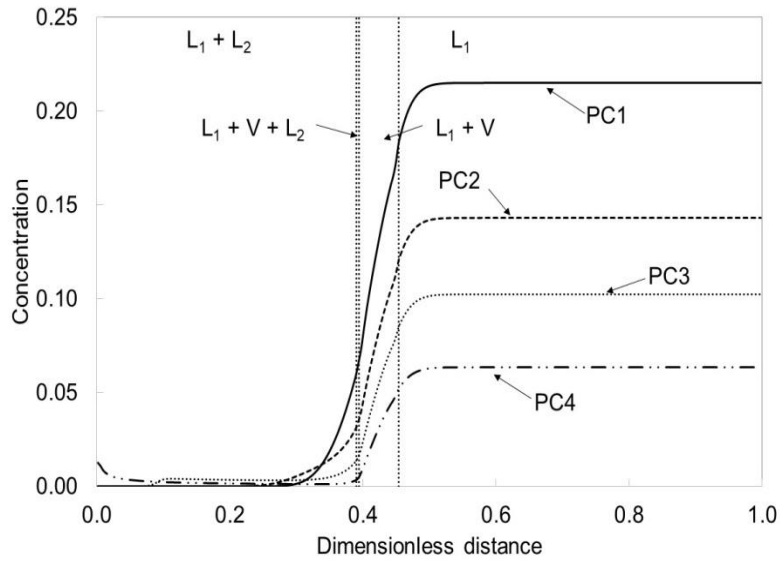le 5.3. The number of GBs used is 250. (a) CO_2, CH_4, and C_2H_6. (b) C_3H_8, C_4H_{10}, C_5H_{12}, and C_6H_{14}. (c) PC1, PC2, PC3, and PC4.
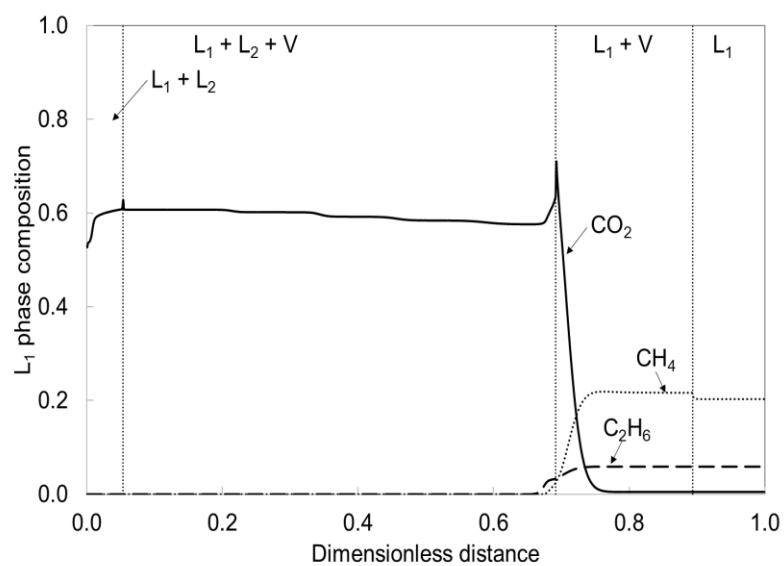
(a)
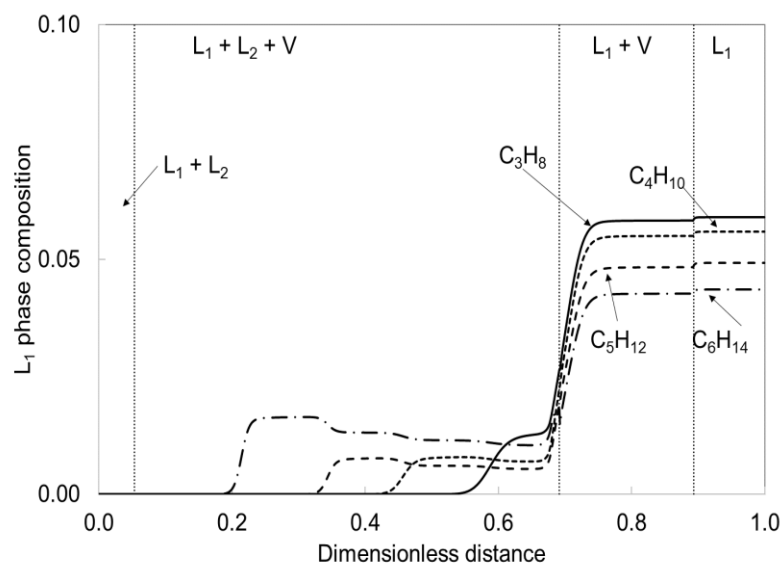
(b)

Figure 5.28. (Continued below)
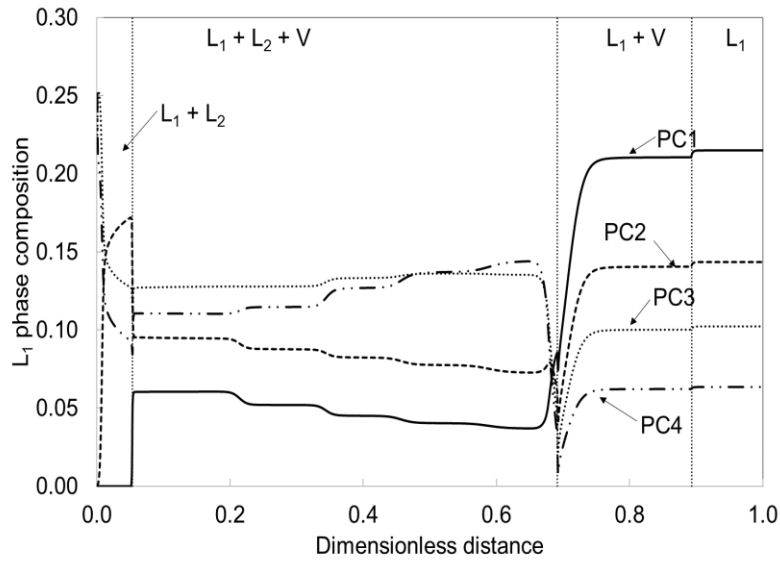
(c)

Figure 5.28. L_1 phase composition profile at 1.0 PVI at 935 psia for NWE oil displaced by CO_2 at 83 °F. The properties of components used are given in Table 5.2. The binary interaction parameters are given in Table 5.3. The number of GBs used is 1000. (a) CO_2, CH_4, and C_2H_6. (b) C_3H_8, C_4H_{10}, C_5H_{12}, and C_6H_{14}. (c) PC1, PC2, PC3, and PC4.
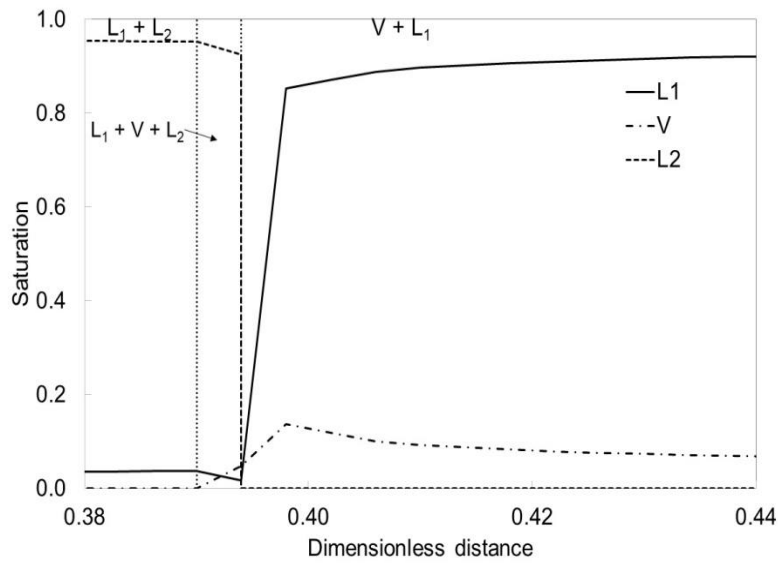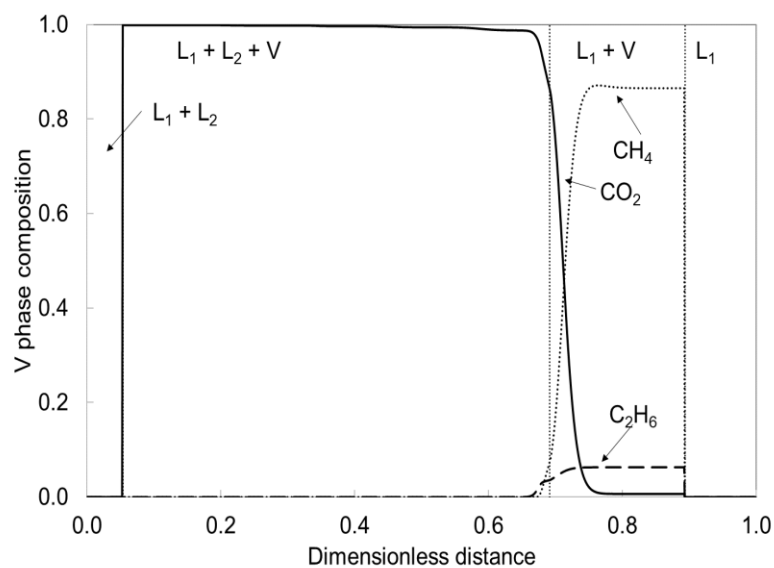
(a)
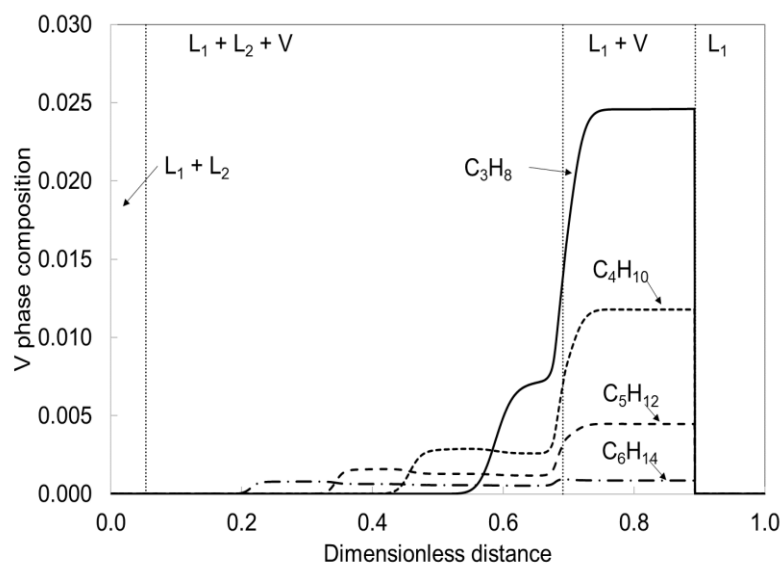
(b)

Figure 5.29. (Continued below)
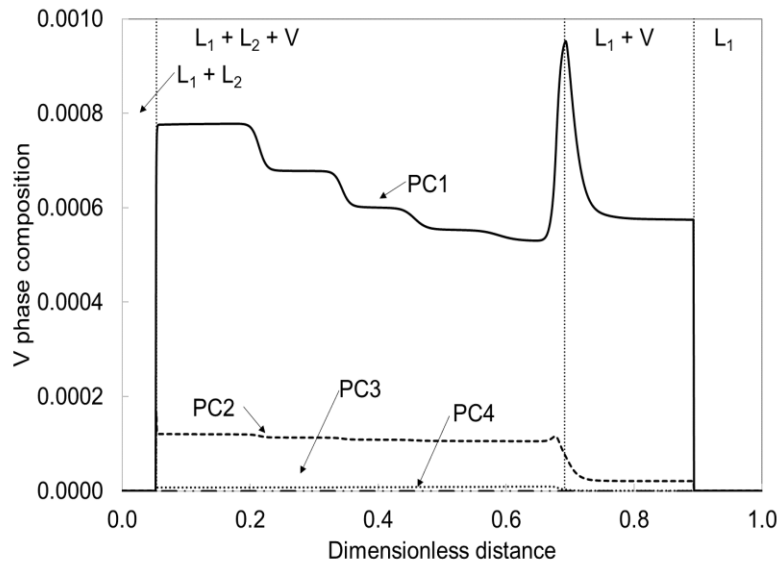
(c)

Figure 5.29. V phase composition profile at 1.0 PVI at 935 psia for NWE oil displaced by CO_2 at 83 °F. The properties of components used are given in Table 5.2. The binary interaction par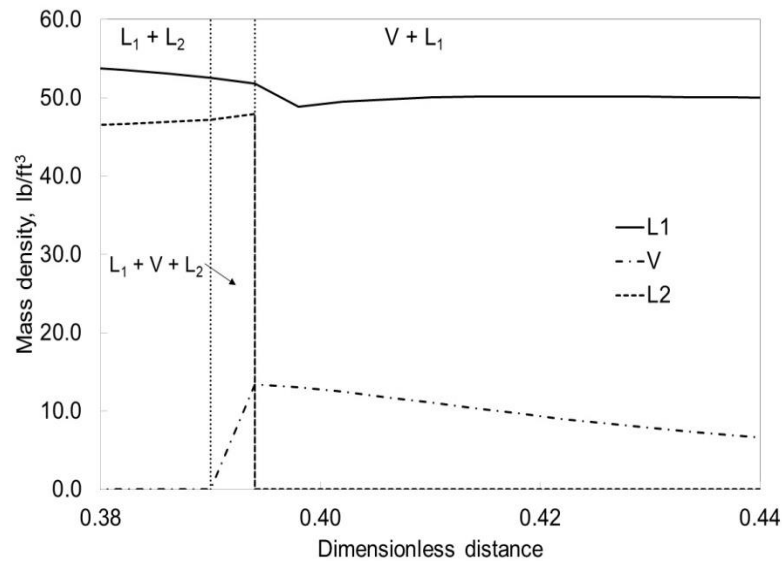ameters are given in Table 5.3. The number of GBs used is 1000. (a) CO_2, CH_4, and C_2H_6. (b) C_3H_8, C_4H_{10}, C_5H_{12}, and C_6H_{14}. (c) PC1, PC2, PC3, and PC4.
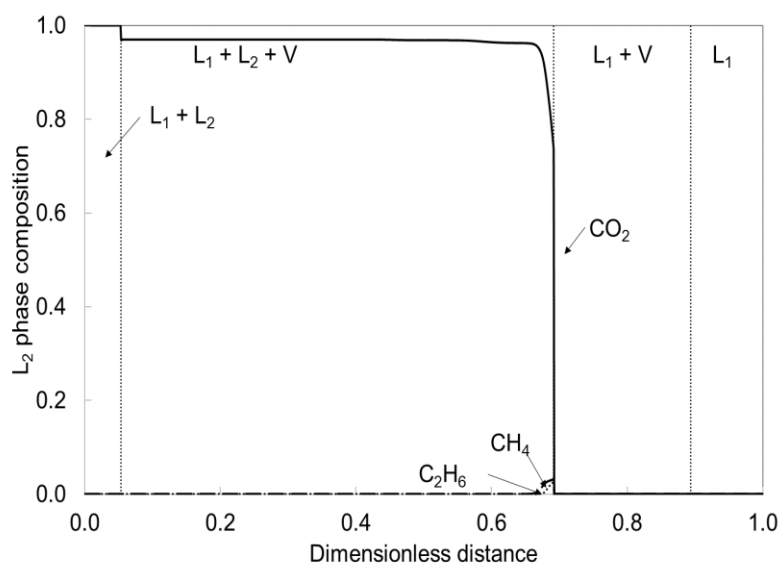
(a)
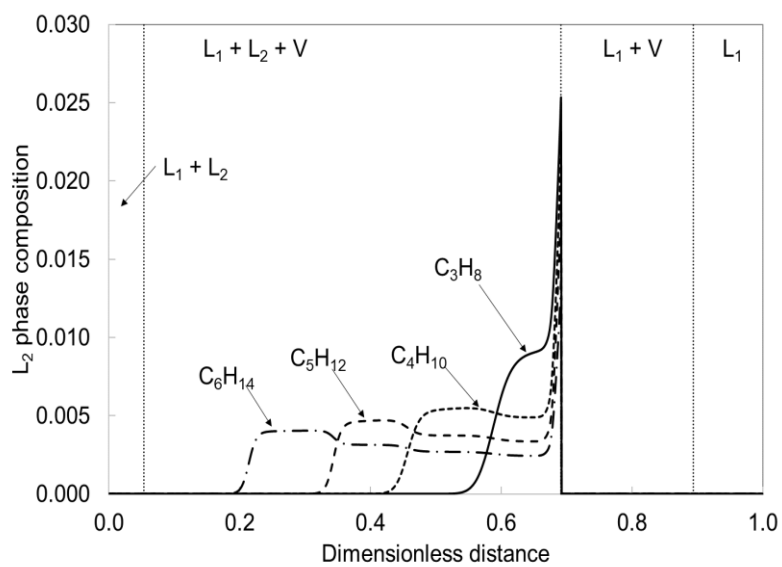
(b)

Figure 5.30. (Continued below)

247
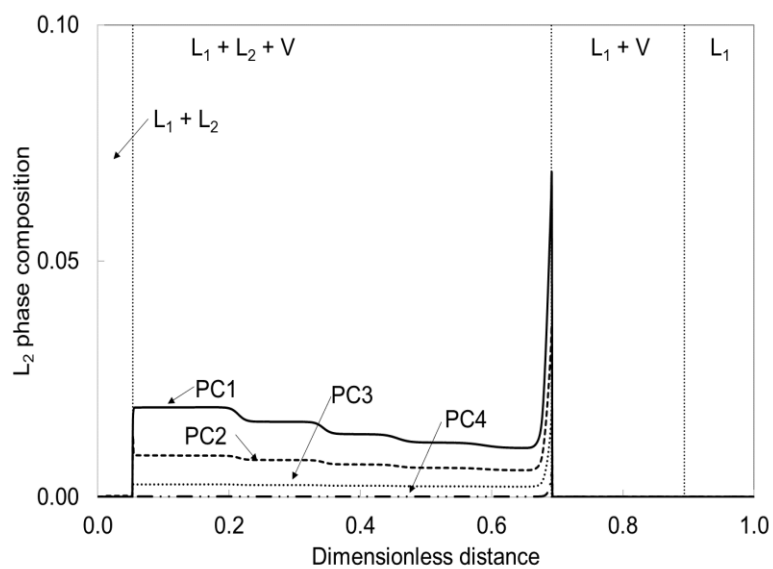
(c)

Figure 5.30. L_2 phase composition profile at 1.0 PVI at 935 psia for NWE oil displaced by CO_2 at 83 °F. The properties of components used are given in Table 5.2. The binary interaction parameters are given in Table 5.3. The number of GBs used is 1000. (a) CO_2, CH_4, and C_2H_6. (b) C_3H_8, C_4H_{10}, C_5H_{12}, and C_6H_{14}. (c) PC1, PC2, PC3, and PC4.
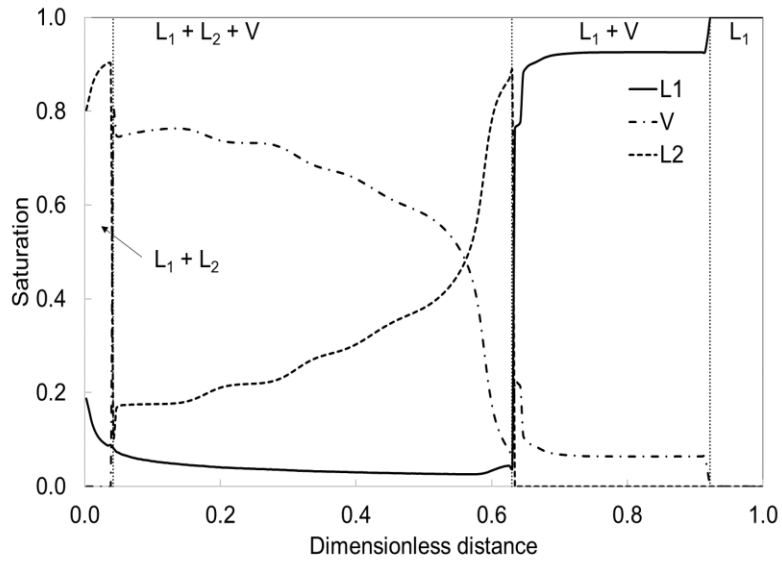
(a)
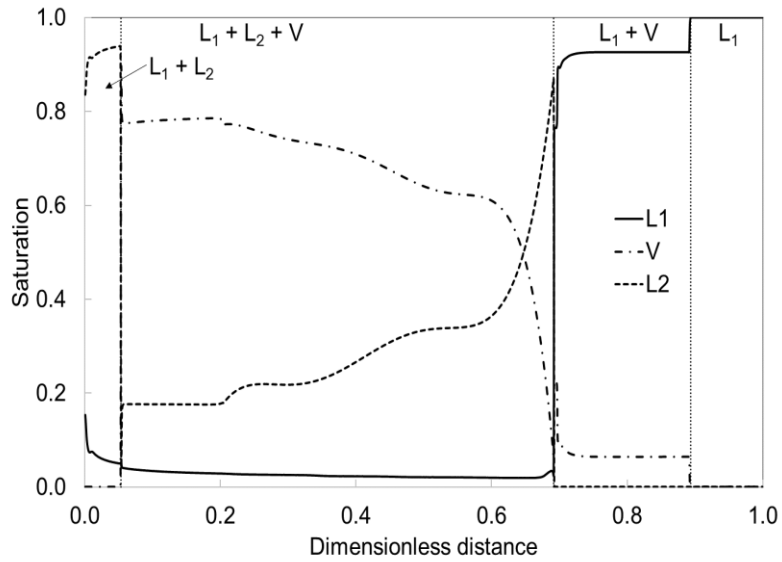
(b)

Figure 5.31. Saturation profile at 1.0 PVI at 935 psia for NWE oil displaced by CO_2 at 83 °F. The properties of components used are given in Table 5.2. The binary interaction parameters are given in Table 5.3. (a)The number of GBs used is 250. (b)The number of GBs used is 1000.
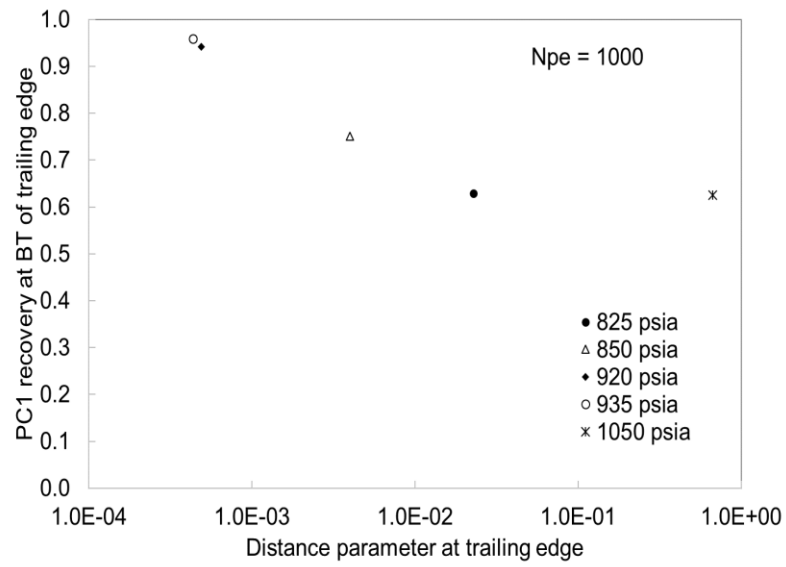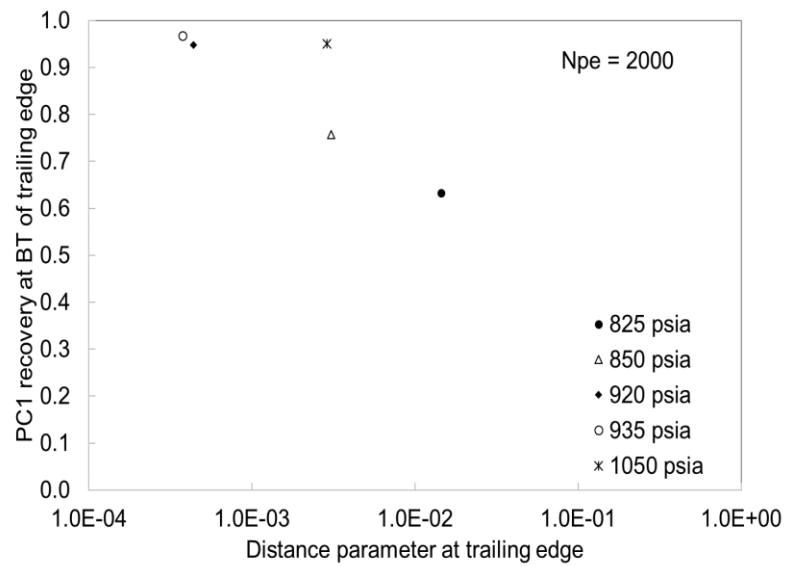
249

(a)

(b)
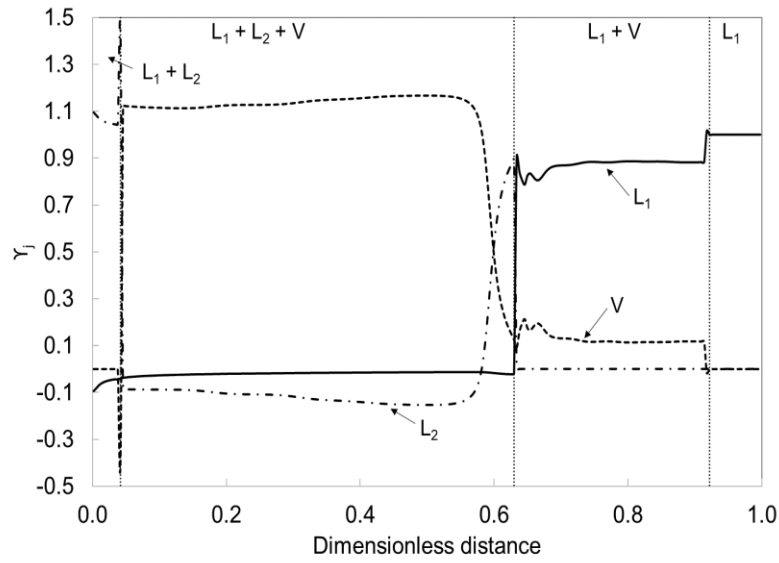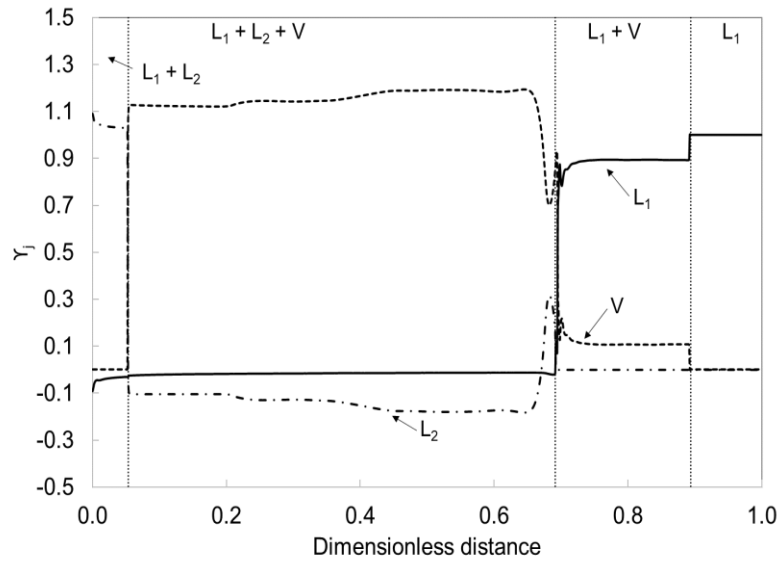
Figure 5.32. γ profile at 1.0 PVI at 935 psia for NWE oil displaced by CO_2 at 83 °F. The properties of components used are given in Table 5.2. The binary interaction parameters are given in Table 5.3. (a)The number of GBs used is 250. (b)The number of GBs used is 1000.

250
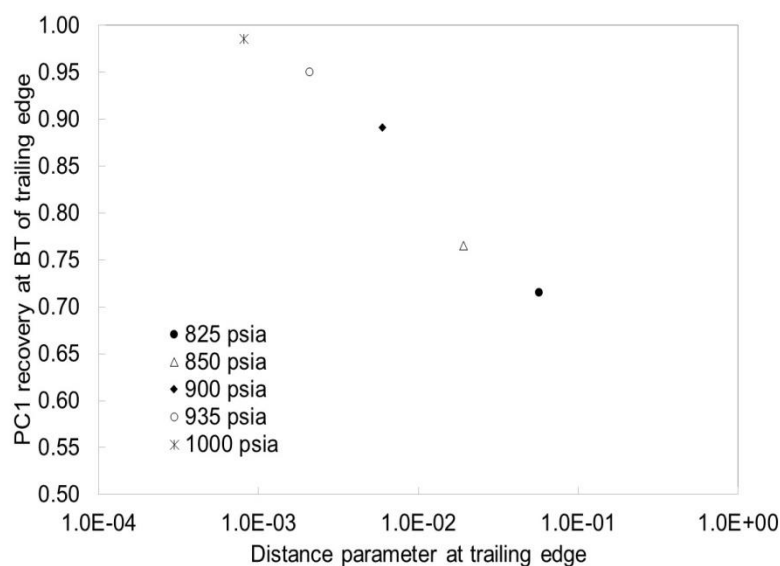
Figure 5.33. Minimum distance condition at the three-phase trailing edge for the NWE oil displaced by CO2 at 83°F. The number of GBs used is 250. The relative permeability model used is given in Table 5.5. PC1 recovery is highest at the BTs of the trailing edge at calculated OIP (1000 psia).
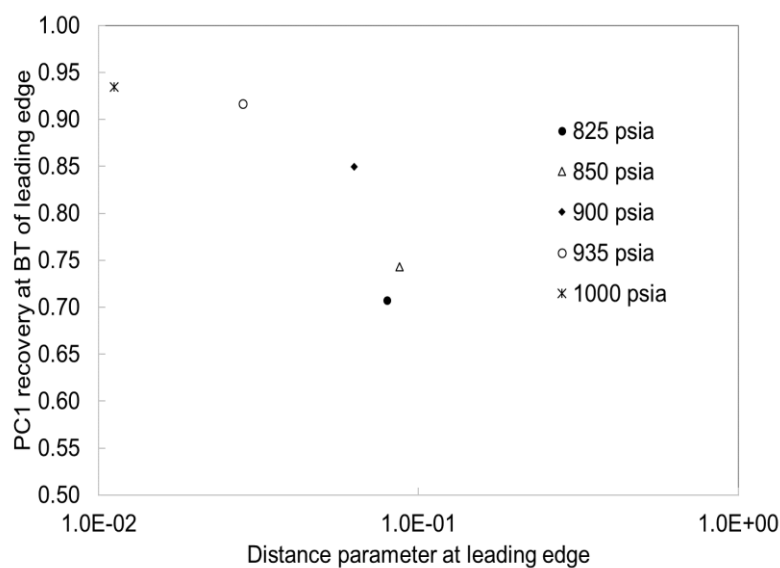
Figure 5.34. Minimum distance condition at the three-phase leading edge for the NWE oil displaced by CO2 at 83°F. The number of GBs used is 250. The relative permeability model used is given in Table 5.5. PC1 recovery is highest at the BTs of the leading edge at calculated OIP (1000 psia).

251
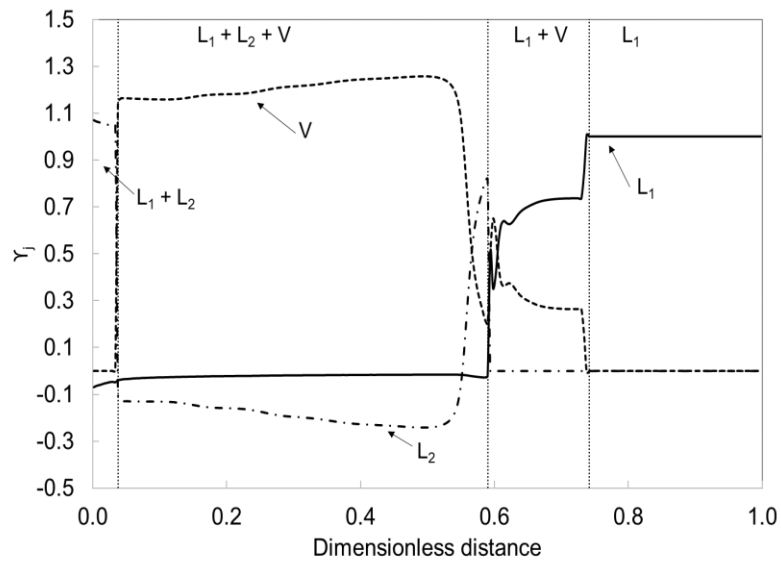
Figure 5.35. γ profile at 1.0 PVI at 935 psia for NWE oil displaced by CO_2 at 83 °F. The properties of components used are given in Table 5.2. The relative permeability model used is given in Table 5.5.
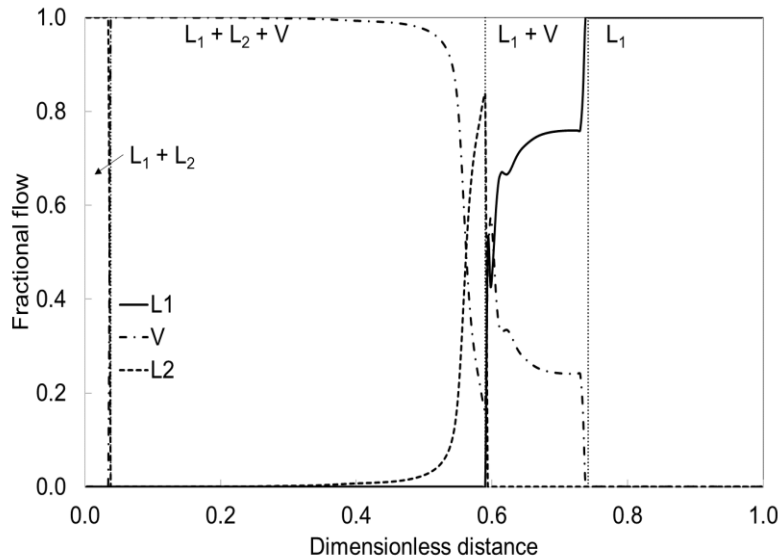
Figure 5.36. Fractional flow profile at 1.0 PVI at 935 psia for NWE oil displaced by CO_2 at 83 °F. The properties of components used are given in Table 5.2. The relative permeability model used is given in Table 5.5.

252
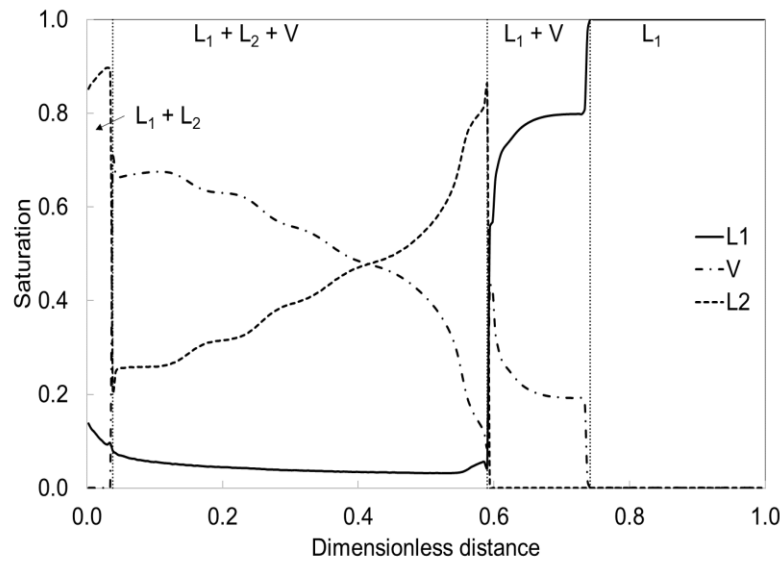
Figure 5.37. Saturation profile at 1.0 PVI at 935 psia for NWE oil displaced by CO_2 at 83 °F. The properties of components used are given in Table 5.2. The relative permeability model used is given in Table 5.5.
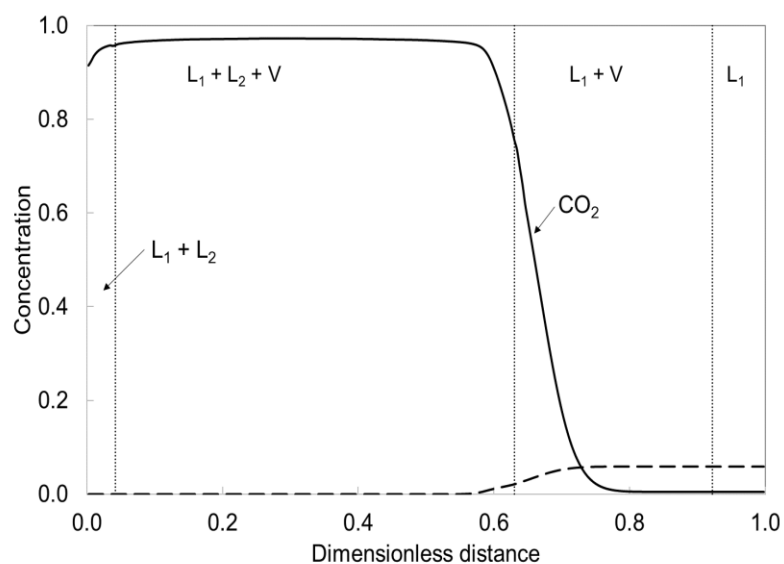
(a)
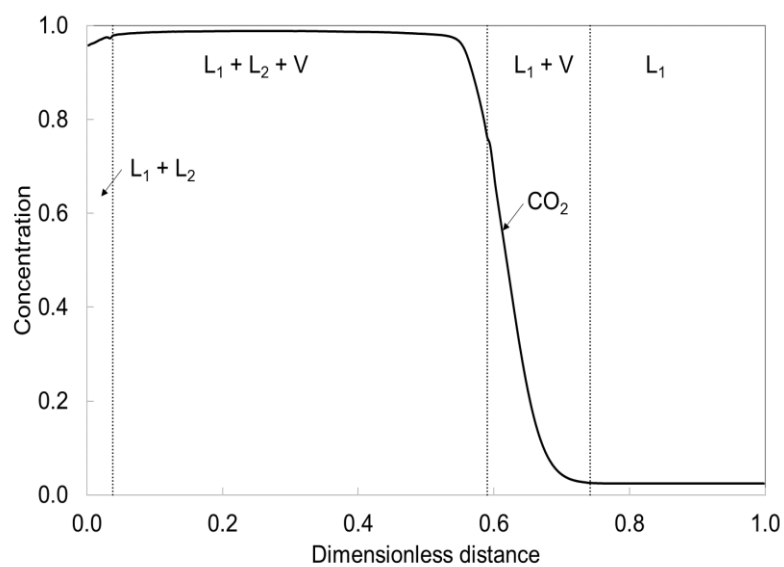
(b)

Figure 5.38. CO_2 concentration profiles at 1.0 PVI at 935 psia for NWE oil displaced by CO_2 at 83 °F. The properties of components used are given in Table 5.2. (a) The relative permeability model used is given in Table 5.4. (b) The relative permeability model used is given in Table 5.5.

254
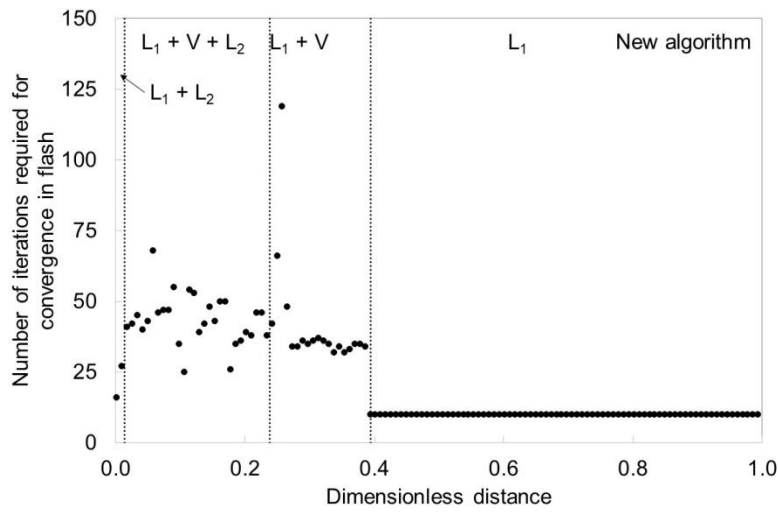
(a)
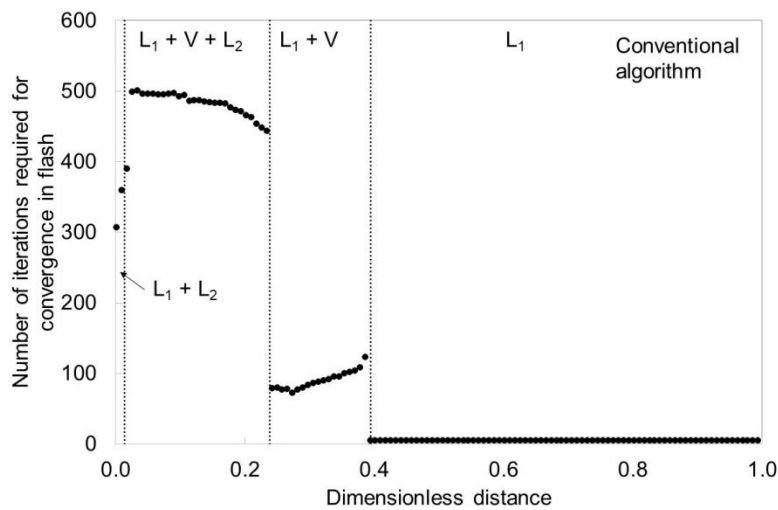
(b)

Figure 5.39. Number of iterations required for convergence with respect to dimensionless distance for the NWE oil displaced by CO_2 at 83°F at 0.4 PVI at OIP (935 psia). (a) With the new algorithm. (b) With conventional algorithm.

255
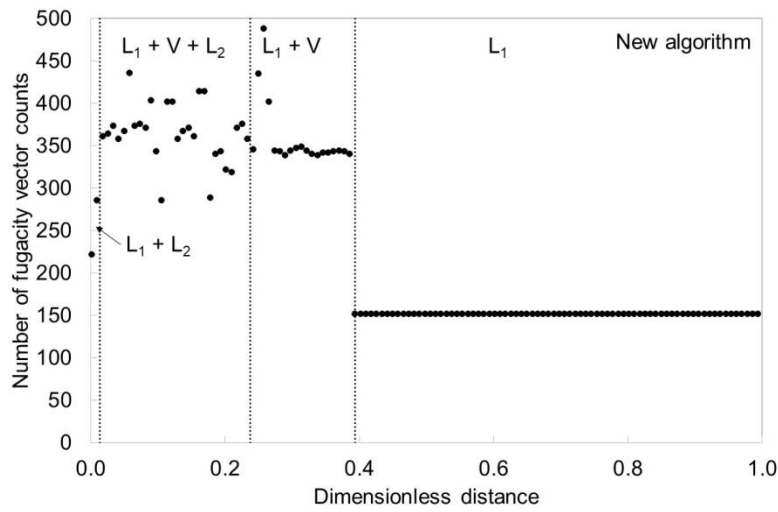
(a)
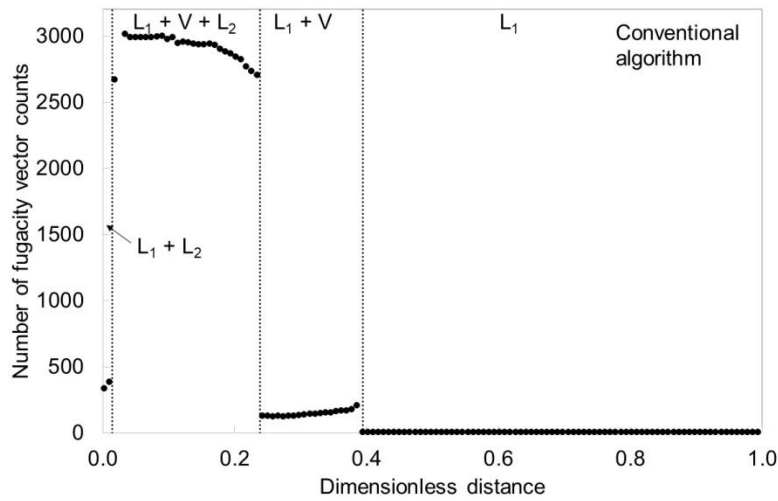
(b)

Figure 5.40. Number of fugacity-coefficient calculations with respect to dimensionless distance for the NWE oil displaced by CO_2 at 83°F at 0.4 PVI at OIP (935 psia). (a) With the new algorithm. (b) With conventional algorithm.

256
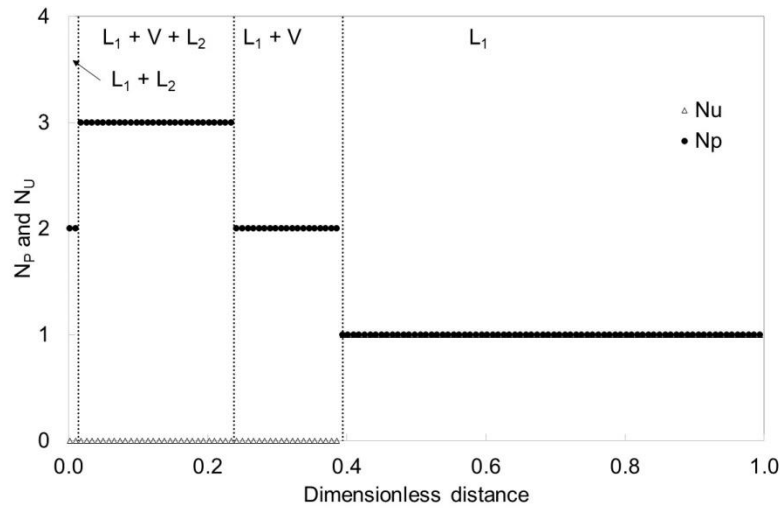
Figure 5.41. Number of compositions in set P (N_P) and number of compositions in set U (N_U) obtained with the new algorithm upon convergence with respect to dimensionless distance for the NWE oil displaced by CO_2 at 83°F at 0.4 PVI at OIP (935 psia). Non-zero N_U ($N_U = 1$) is detected in the entire single L_1 phase region. The number of iterations required for convergence in the single L_1-phase region is all 10. The composition in set U at 0.4 PVI is close to one of the equilibrium phase (V phase) at the next time step.
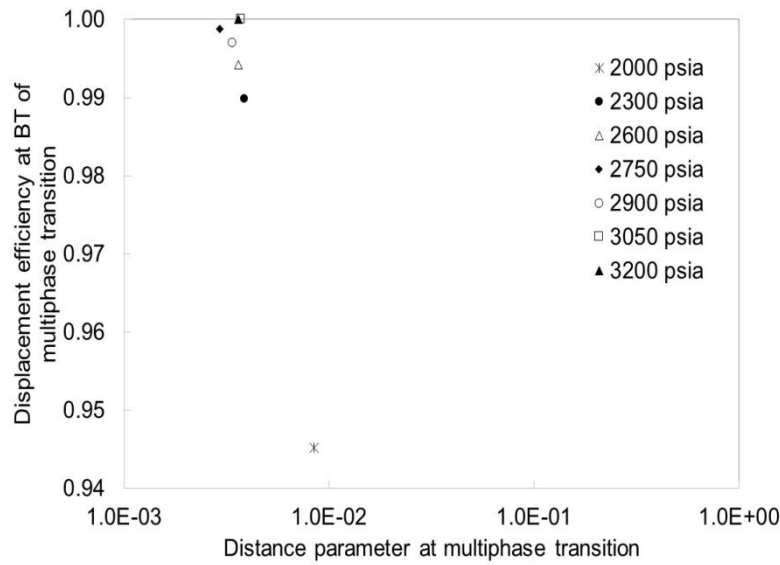
Figure 5.42. Minimum distance condition for Bakken oil displaced by C_2 at 0.4 PVI at seven pressures; 2000 psia, 2300 psia, 2600 psia, 2750 psia, 2900 psia, 3050 pisa, and 3200 psia. The properties of Bakken oil are given in Tables 5.6, and the BIPs are given in Table 5.7. The parameters used in Corey's model for three-phase relative permeabilities are given in Table 5.8. Reservoir temperature is 536°F. The number of GBs used is 250. The distance parameter is calculated for multiphase transition between three and two phases. The efficiency of displacement of water by vapor is calculated at the BT of the multiphase transition.
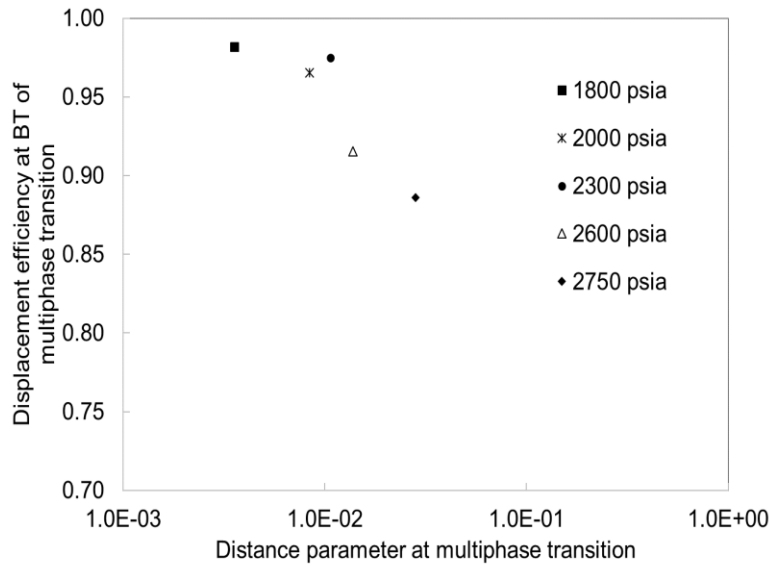
Figure 5.43. Minimum distance condition for Bakken oil displaced by C_2 at 0.4 PVI at five pressures; 1800 psia, 2000 psia, 2300 psia, 2600 psia, and 2750 psia. The properties of Bakken oil are given in Tables 5.6, and the BIPs are given in Table 5.7. The parameters used in Corey's model for three-phase relative permeabilities are given in Table 5.9. Reservoir temperature is 536°F. The number of GBs used is 250. The distance parameter is calculated for multiphase transition between three and two phases. The efficiency of displacement of water by vapor is calculated at the BT of the multiphase transition.

259

CHAPTER 6: Conclusions and Recommendations for Future Research

In this dissertation, two main types of research questions were addressed regarding multiphase behavior in solvent injection: robust multiphase flash calculation and the efficiency of local oil displacement in multiphase flow.

For the first topic, isobaric-isothermal multiphase flash calculation was reformulated by using the tangent-plane distance equations that integrate phase-split and phase-stability calculations in Chapter 3. The main advantage of this new algorithm over the conventional algorithms is that it is not necessary to assume a certain number of phases prior to calculation. The robustness of the new algorithm was demonstrated for complex multiphase mixtures, which tend to exhibit many local minima of the Gibbs free energy in composition space. The algorithm is also expected to be useful for other thermodynamic specifications, in which pressure or temperature is part of the flash solution. As an example, Chapter 4 presented an application of the algorithm to multiphase isenthalpic flash, in which temperature changes during the iteration process.

For the second topic, local displacement efficiency in multiphase flow was studied on the basis of the recent research that gave a detailed explanation of the complex mechanism for high displacement efficiency in low-temperature solvent injection. A simple condition was derived for multicontact miscibility that is developed between a displaced phase and a displacing phase in the presence/absence of other phases. A parameter derived from a general mass conservation upon phase transition, which is called the distance parameter, tends to diminishes as the multicontact miscibility is developed for a displaced phase and a displacing phase. Chapter 5 demonstrated the applicability of the distance parameter to quantify the local displacement efficiency for various displacement cases. An in-house 1D compositional simulator was developed by

using the robust flash algorithm presented in Chapter 3, and it was successfully used to solve for a composition path for a given displacement.

Conclusions are summarized in section 6.1. Recommendations for future research are described in section 6.2.

6.1 CONCLUSIONS

Conventional method for multiphase flash is the sequential usage of phase-stability/-split calculations, in which multiple false solutions are obtained in phase-split calculations and corrected in phase-stability analysis. Improvement of the robustness and efficiency of multiphase flash is important for compositional flow simulation with complex phase behavior. In chapter 3, we presented a new algorithm for isothermal-isobaric flash for an arbitrary number of phases. The unified formulation developed for simultaneous phase-stability/split calculation is based on the classical criterion of phase equilibrium, as explained in Baker et al. (1982). The correct set of equations is solved with successive substitution for stationary points of the tangent plane distance defined at a reference phase composition. Although the main focus of this chapter was on robust solution of multiphase flash, the new algorithm can be used also to initialize a 2nd-order convergent method in the vicinity of a solution. The conclusions on the new simultaneous PT flash calculations are as following:

1.   The number of equilibrium phases is part of the solution in the new algorithm, in contrast to the sequential stability/flash approach. It is not necessary to find false solutions and correct them for robust multiphase flash with the new algorithm. The advantage of the new algorithm in terms of robustness is more pronounced for more

complex phase behavior, in which multiple local minima of the Gibbs free energy are present.

      2.   The new algorithm can be initialized even when no reliable information is available about the equilibrium phases of the fluid of interest.   In the method used for initializing the algorithm, NC sampling compositions are distributed near compositional vertices, and the others are systematically distributed around the overall composition specified.   No K-value correlation is necessary to initialize the new algorithm.   This also yields the flexibility that the new algorithm offers in terms of robustness and efficiency.   For example, one can initialize the algorithm with more sampling compositions for enhanced robustness by capturing more information regarding the Gibbs free energy during the iteration.   If reasonable estimates are available for equilibrium phases (e.g., correlations, the solution from the previous time step in flow simulation, and tie-simplex tabulation), one can use them to reduce the number of equations to be solved.

      3.   The new algorithm does not use the stability equations of Gupta et al. (1991) because they are not necessary with the formulation presented in this research. Consequently, there is no need to solve the augmented Jacobian matrix that must be solved at each iteration in the algorithm of Gupta et al. (1991).   Also, the new algorithm does not exhibit the convergence problems that are associated with the stability equations of Gupta et al. (1991).

      4.   Case studies showed that the new algorithm finds more stable solutions (lower Gibbs free energy) for the complex cases tested, for which the conventional method only finds local minima.   It was shown that the new algorithm can find non-tangent stationary points of the tangent-plane-distance function, if present, in addition to equilibrium phases.

5.   The iteration scheme of the new algorithm is the traditional successive substitution, of which convergence behavior has been studied in the literature (e.g., Michelsen 1982a, Mehra et al. 1983, Ammar and Renon 1987, Kaul 1992).   The new algorithm can be used to initialize a 2nd-order convergent method as demonstrated in case 4.   It is expected to be more difficult for the algorithm to converge for mixtures that exhibit a large negative deviation from an ideal solution, according to the analysis of Heidemann and Michelsen (1995).

In Chapter 4, we presented a detailed analysis for narrow-boiling behavior and its effects on the direct substitution (DS) isenthalpic flash for two and three phases.   A modified DS algorithm was then developed based on the analysis.   This chapter also presented a new algorithm for multiphase PH flash integrated with stability analysis. The correct set of equations is solved for stationary points on the tangent-plane-distance function that is defined at an adaptively selected reference composition.   We also analyzed narrow-boiling behavior on the basis of the multiphase PH-flash equations, where energy and phase behavior equations are coupled through the temperature dependency of K values.   Cases were presented to demonstrate the robustness of the developed algorithms and the narrow-boiling conditions derived.   The conclusions on the new PH flash calculations are as following:

1.   Narrow-boiling behavior is characterized by the enthalpy behavior that is substantially sensitive to temperature.   The total enthalpy for a fixed overall composition and pressure becomes sensitive to temperature when at least one of the phase compositions drastically changes with a small change in temperature so that the phase mole fractions significantly change.   The mechanistic understanding of the narrow-boiling behavior was presented using the Gibbs free energy surfaces in binary composition space at different temperatures.

2.	The prior DS algorithms (e.g., Michelsen 1987, Agarwal et al. 1991) have convergence issues when narrow-boiling behavior is involved. The fundamental reason is that the system of equations solved in the algorithms becomes degenerate for narrow-boiling fluids. The prior DS algorithms use temperature oscillation as an indicator for narrow-boiling fluids. However, temperature oscillation in these algorithms is a consequence of, not the reason for, the narrow-boiling behavior. That is, it is not a good indicator that improves the robustness.

3.	The modified DS algorithm developed in this chapter adaptively switches between Newton's iteration step and the bisection algorithm depending on the DS Jacobian condition number that offers an unambiguous criterion regarding the computational accuracy and robustness in the DS algorithm. The bisection algorithm solves for temperature based solely on the enthalpy constraint when narrow-boiling behavior is identified by a large condition number of the Jacobian matrix. This decoupling of temperature from the other variables is plausible when the system of equations is degenerate.

4.	The new simultaneous PH flash algorithm can robustly solve PH flash for narrow-boiling fluids. It does not require a special treatment for one degree of freedom, for which the total enthalpy is discontinuous in temperature. This is because the algorithm does not require to fix the number of equilibrium phases in the iteration. The advantage of the proposed algorithm is pronounced when the fluid of interest exhibits complex phase appearance/disappearance, and/or when narrow-boiling behavior is involved, as in thermal compositional flow simulation.

5.	The initialization of new simultaneous PH flash algorithm is possible even when no reliable information is available about the equilibrium phases of the fluid of interest. No K-value correlation is necessary to initialize the new algorithm.

6.   The new simultaneous PH flash algorithm offers the flexibility in terms of robustness and efficiency depending on the number of sampling compositions (N_S) used. It becomes more robust with increasing N_S at the expense of computational efficiency. As N_S increases, the algorithm becomes more robust because the possibility of finding all stationary points of the tangent-plane distance function increases.   However, the number of iterations required tends to increase with increasing N_S because the algorithm with more sampling compositions may take more iterations when merging and adding some of the sampling compositions.

7.   The general condition for narrow-boiling behavior is that the interplay between the energy and phase behavior equations is significant.   Two subsets of the narrow-boiling condition were derived by analyzing the convex function whose gradient vectors consist of the RR equations; (i) the overall composition is near an edge of composition space, and (ii) the solution conditions (temperature, pressure, and overall composition) are near a critical point, including a critical endpoint.   A special case of the first specific condition is the fluids with one degree of freedom, for which enthalpy is discontinuous in temperature space.

8.   The analysis of the RR convex function gave the clear limiting conditions toward which the tendency of narrow-boiling behavior increases.   Narrow-boiling behavior tends to occur in thermal compositional simulation likely because water is by far the most dominant component in the fluid systems formed in the simulation.

In Chapter 5, we presented the utility of the distance parameters for quantification of displacement efficiency for seven different displacement processes.   Simulation cases also showed the robustness and efficiency of the new simultaneous PT flash algorithm presented in chapter 3.   Six cases are presented for displacement of L_1 phase by L_2 phase in the presence of V phase.   The other case is the displacement of W phase by V

phase in the presence of L_1 phase when the connate water evaporates as ethane is injected into an oil reservoir at an elevated temperature. Conclusions on the quantification of displacement efficiency in multiphase oil displacement are as follows:

1.   Efficient oil displacement can be achieved at substantially lower pressures in comparison with the MMP calculated with prior methods, as demonstrated for West Sak oil and North Ward Estes oil.

2.   Distance parameters are calculated in volume space by use of equations 2.7 and 2.8 for a composition path obtained from the in-house 1D convection-only compositional simulator. Unlike Okuno and Xu (2014ab), it is not necessary to solve for the intersection between a tie line and a tie triangle when distance parameters are calculated on the volume basis. Hence, it is a simpler and more direct validation of the utility of the distance parameters to quantify the local displacement efficiency in three-phase flow.

3.   Minimum distance conditions defined at a phase transition are used to calculate optimal injection pressure (OIP). Negative correlations between the distance parameter calculated at a phase transition and component recovery at BT of a phase transition are observed for all cases tested. This indicates that the highest displacement efficiency occurs when the distance parameters are the lowest.

4.   Use of the weak form of the 1D convective compositional flow equations enables to take into account the effect of mixing on displacement efficiency through numerical dispersion. Use of a larger number of GBs results in lower distance parameters calculated at a phase transition. The recoveries at a greater level of dispersion (i.e., a smaller number of GBs) are lower than those with a lower level of numerical dispersion (i.e., a larger number of GBs).

266

5.   The effect of the relative permeability model used on displacement efficiency in three-phase flow is properly included in distance parameters (equations 2.7 and 2.8) through the parameter "γ".   The cases tested showed that the relative permeability parameters may have a limited impact on simulated oil recovery when the miscibility level is high at OIP.

6.   The robustness and efficiency of the new PT phase-stability/-split algorithm presented in chapter 3 were demonstrated in flow simulations for seven reservoir oil displacements.   The new PT flash algorithm converges more rapidly than the conventional sequential algorithm in terms of the number of iterations required for convergence and the number of fugacity-coefficient calculations, except for the single-phase region.   None of the tested cases showed convergence issues in phase behavior calculations.

7.   The reliability of the OIP calculation in this research depends on the EOS fluid model used to represent multiphase behavior during the displacement process.   The calculated OIPs for the cases are reasonably close to experimentally determined MMPs. This can be because the EOS fluid models obtained from Kumar and Okuno (2016) properly capture the three-phase behavior of the six reservoir oil cases tested.

6.2 RECOMMENDATIONS FOR FUTURE RESEARCH

Compositional reservoir simulations require accurate modeling of complex phase behaviors.   The advantage of the new PT flash algorithm developed in chapter 3 in terms of robustness is more pronounced for more complex phase behavior, in which multiple local minima of the Gibbs free energy are present.   The main novelty lies in the unified usage of the TPD equation for PT multiphase flash for an arbitrary number of iterative compositions.   The fundamental structure of the current algorithm broadly

follows the traditional SS algorithm.   Although the SS algorithm is more robust, a 2nd-order convergent method should be investigated to accelerate the convergence rate in the vicinity of a solution based on the new formulation.

The new PT flash algorithm developed in chapter 3 can find many, if not all, stationary points of the TPD function defined at one of equilibrium phases upon convergence.   It is recommended to conduct further research on the number of stationary points of complex reservoir fluids with the new PT flash algorithm. Preliminary studies were performed for 24 simple mixtures available in the literature, for which results were given in Appendix C.   If we have prior knowledge on the number of stationary points of reservoir fluids, it is possible that we can optimize the initial sampling compositions distributed (N_S) to reduce the number of equations to be solved with the new algorithm.

Upon convergence of the new PT flash algorithm, the sampling compositions in set P correspond to equilibrium phases.   Those in set U, if any, correspond to stationary points of the converged TPD function, at which D_R values are positive.   In other words, the converged sampling compositions in set P are tangent stationary points, and those in set U, if any, are non-tangent stationary points.   Set U captures additional information regarding the Gibbs free energy during the iterations; however, it is currently unclear how useful the set U is in flow simulations with the current implementation.

The formulation developed in chapter 3 is applicable with any EOSs, although only the PR EOS was used in this research.   A limitation of cubic EOSs is that they are not originally designed to represent complex phase behavior associated with polar components (e.g., water and asphaltene) that commonly exist in viscous-oil reservoirs. With this limitation, asphaltene precipitation, water-asphaltene emulsion, and water dissolution may not be accurately captured (Jia and Okuno 2017).   More sophisticated

EOSs, such as cubic-plus-association (CPA) EOS, can be tested to widen the application of the current formulation.

The formulation used for the new PT flash algorithm was extended to non-isothermal conditions, for which temperature is part of the solution (chapter 4). It is conceivable that the formulation can be extended to model multiphase equilibrium under capillary pressures for tight reservoirs. For such flash calculations, pressures of non-wetting phases are part of the solution, and the number of phases cannot be specified prior to the calculation.

Robust isenthalpic (PH) flash is important in compositional simulation of steam injection, which involves at least three phases consisting of the oleic, gaseous, and aqueous phases. Chapter 4 addressed two long existing issues associated with standalone PH flash calculations. Further investigation should be made to demonstrate the robustness and efficiency of the simultaneous PH flash algorithm developed in chapter 4.

Robust phase identification approach should be further investigated. The phase identification used in chapter 5 is the traditional method developed by Perschke et al. (1989). A trial-and-error approach was used to define a threshold mass density to identify phases for each displacement case. Mohanty et al. (1995), Li et al. (2014) and Beygi et al. (2014) reported the use of a fixed mass density threshold for phase labeling in a two-phase region in three-hydrocarbon-phase flow simulation. For the cases tested in this dissertation, none of the cases showed computational failures associated with incorrect assignment of equilibrium phases identities. It is currently unclear why such failures have not been observed in chapter 5. A possible reason is that prior reports on phase identification problems may have come partly from convergence issues in flash

calculations.   The new PT flash algorithm used in this research did not show any convergence issue for the simulation cases tested.

During CO_2 injection and coinjection of steam and solvent for heavy-oil/bitumen recovery, asphaltene precipitation/deposition occurs (Gauter et al. 199, Qin et al. 2000, Mohebbinia et al. 2014).   For such as process, at least four phases exist; L_1, L_2, V and an asphaltene phase.   Application of the distance parameter for four-phase displacements is to be explored.

APPENDIX A: Enthalpy and Jacobian Matrix in DS Algorithm

Appendix A presents the calculations for enthalpy and its associated derivatives and the Jacobian matrix used in DS algorithm for PH flash.

Appendix A-1: ENTHALPY AND ASSOCIATED DERIVATIVES

It is important to use temperature and enthalpy of a dimensionless form in PH flash. Dimensionless temperature and pressure are defined as

$$T_D = T/T_{ref} \tag{A-1.1}$$

$$\underline{H}_{Dj} = \underline{H}_j/\underline{H}_{spec}, \tag{A-1.2}$$

where T_D is the dimensionless temperature, and $\underline{H}_{Dj}$ is the dimensionless molar enthalpy of phase j. T_{ref} is some reference value to make temperature better scaled in PH flash. For example, T_{ref} can be a temperature near the original reservoir temperature in thermal oil recovery processes (e.g., 300 K). Note that some of the prior PH-flash algorithms in the literature did not use dimensionless temperature and enthalpy.

The dimensionless total molar enthalpy ($\underline{H}_D^t$) of N_P phases is

$$\underline{H}_D^t = \sum_{j=1}^{N_P} \beta_j \underline{H}_{Dj} = \sum_{j=1}^{N_P} \beta_j \left(\underline{H}_{Dj}^{IGM} + \underline{H}_{Dj}^{dep} \right). \tag{A-1.3}$$

The molar phase enthalpy ($\underline{H}_{Dj}$) can be calculated as the summation of the molar ideal-gas-mixture enthalpy ($\underline{H}_{Dj}{}^{IGM}$) and the molar enthalpy departure ($\underline{H}_{Dj}{}^{dep}$). The dimensionless molar enthalpy of phase j as an ideal gas mixture, $\underline{H}_{Dj}{}^{IGM}$, is

$$\underline{H}_{Dj}^{IGM} = \underline{H}_j^{IGM}/\underline{H}_{spec} = \sum_{i=1}^{N_C} x_{ij} \underline{H}_i^{IG}/\underline{H}_{spec}. \tag{A-1.4}$$

$\underline{H}_i^{IG}$ is the molar ideal-gas enthalpy for component i and calculated using the following fourth-order polynomial correlation:

$$\underline{H}_i^{IG} = C_{P1i}^0(T - T_0) + C_{P2i}^0(T^2 - T_0^2)/2$$
$$+ C_{P3i}^0(T^3 - T_0^3)/3 + C_{P4i}^0(T^4 - T_0^4)/4, \tag{A-1.5}$$

where C_{P1i}^0, C_{P2i}^0, C_{P3i}^0, and C_{P4i}^0 are coefficients for component i, and T_0 is 273.15 K.

The dimensionless molar enthalpy departure for phase j is

$$\underline{H}_{Dj}^{dep} = \left\{\left[\left(RT^2\frac{\partial A_{mj}}{\partial T} + RTA_{mj}\right)\Big/2\sqrt{2}B_{mj}\right]\ln\left[\frac{Z_j+(1+\sqrt{2})B_{mj}}{Z_j+(1-\sqrt{2})B_{mj}}\right]\right.$$

$$\left.+RT(Z_j-1)\right\}\Big/\underline{H}_{spec} \tag{A-1.6}$$

on the basis of the PR EOS.

Now, the sensitivity of $\underline{H}_D{}^t$ to T_D is analyzed using equation A-1.3,

$$\frac{\partial \underline{H}_D^t}{\partial T_D} = \sum_{j=1}^{N_P}\frac{\partial \beta_j}{\partial T_D}\underline{H}_{Dj} + \sum_{j=1}^{N_P}\frac{\partial \underline{H}_{Dj}}{\partial T_D}\beta_j. \tag{A-1.7}$$

The partial derivative of $\underline{H}_{Dj}$ with respect to T_D can be calculated as follows:

$$\frac{\partial \underline{H}_{Dj}}{\partial T_D} = \sum_{i=1}^{N_C}\frac{\partial \underline{H}_{Dj}}{\partial \underline{H}_j}\frac{\partial \underline{H}_j}{\partial x_{ij}}\frac{\partial x_{ij}}{\partial \beta_j}\frac{\partial \beta_j}{\partial T}\frac{\partial T}{\partial T_D}, \tag{A-1.8}$$

where $\partial \underline{H}_{Dj}/\partial \underline{H}_j = 1/\underline{H}_{spec}$ and $\partial T/\partial T_D = T_{ref}$.

The partial derivative of $\underline{H}_j$ with respect to x_{ij} in equation A-1.8 is

$$\frac{\partial \underline{H}_j}{\partial x_{ij}} = \frac{1}{2\sqrt{2}B_{mj}^2}\left[\left(RT^2\frac{\partial^2 A_{mj}}{\partial T\,\partial x_{ij}} + RT\frac{\partial A_{mj}}{\partial x_{ij}}\right)B_{mj} - \left(RT^2\frac{\partial A_{mj}}{\partial T} + RTA_{mj}\right)\frac{\partial B_{mj}}{\partial x_{ij}}\right]\times$$

$$\ln\left[\frac{Z_j+(1+\sqrt{2})B_{mj}}{Z_j+(1-\sqrt{2})B_{mj}}\right] + \left[\left(RT^2\frac{\partial A_{mj}}{\partial T} + RTA_{mj}\right)\Big/B_{mj}\right]\times$$

$$\frac{[Z_j(\partial B_{mj}/\partial x_{ij})-B_{mj}(\partial Z_j/\partial x_{ij})]}{[Z_j+(1+\sqrt{2})B_{mj}][Z_j+(1-\sqrt{2})B_{mj}]} + RT\left(\frac{\partial Z_j}{\partial x_{ij}}-1\right) + \frac{\partial \underline{H}_j^{IGM}}{\partial x_{ij}}, \tag{A-1.9}$$

where $\dfrac{\partial B_{mj}}{\partial x_{ij}} = \dfrac{P}{RT}\dfrac{\partial b_{mj}}{\partial x_{ij}} = B_i$

$\dfrac{\partial A_{mj}}{\partial x_{ij}} = \dfrac{P}{(RT)^2}\dfrac{\partial a_{mj}}{\partial x_{ij}} = \sum_{i=1}^{N_C}2x_{ij}A_{ik}$

$\dfrac{\partial Z_j}{\partial x_{ij}} = \dfrac{(\partial A_{mj}/\partial x_{ij})(B_{mj}-Z_j)+(\partial B_{mj}/\partial x_{ij})[A_{mj}-2B_{mj}-3B_{mj}^2+2(3B_{mj}+1)Z_j-Z_j^2]}{3Z_j^2-2Z_j(1-B_{mj})+(A_{mj}-3B_{mj}^2-2B_{mj})}$

$\dfrac{\partial^2 A_{mj}}{\partial T\,\partial x_{ij}} = \dfrac{P}{(RT)^2}\dfrac{\partial^2 a_{mj}}{\partial T\,\partial x_{ij}} - \dfrac{2}{T}\dfrac{\partial A_{mj}}{\partial x_{ij}}$

$\dfrac{\partial^2 a_{mj}}{\partial T\,\partial x_{ij}} = \sum_{i=1}^{N_C}2(RT)^2(1-k_{ii})\left[\dfrac{\partial x_{ij}}{\partial T}A_i + x_{ij}\left(\dfrac{\partial A_i}{\partial T} + \dfrac{2}{T}A_i\right)\right]\Big/P.$

$\dfrac{\partial^2 a_i}{\partial T_D^2} = -0.45724\dfrac{R^2 T_{Ci}^{1.5}\kappa_i}{P_{Ci}}T_{ref}^2\left[\dfrac{-\kappa_i\sqrt{T}}{2T_{Ci}^2} - \dfrac{1+\kappa_i[1-(T/T_{Ci})^{0.5}]}{2T^{1.5}}\right]$

$\dfrac{\partial^2 a_{mj}}{\partial T_D^2} = T_{ref}^2\sum_{i=1}^{N_C}\sum_{k=1}^{N_C}-x_{ij}x_{kj}(a_ia_k)^{-1.5}\left(a_i\dfrac{\partial a_k}{\partial T} + a_k\dfrac{\partial a_i}{\partial T}\right)^2(1-k_{ik})$

$\qquad + T_{ref}^2\sum_{i=1}^{N_C}\sum_{k=1}^{N_C}\dfrac{x_{ij}x_{kj}}{2}(a_ia_k)^{-0.5}\times$

$\qquad\left(2\dfrac{\partial a_k}{\partial T}\dfrac{\partial a_i}{\partial T} + a_i\dfrac{\partial^2 a_k}{\partial T^2} + a_k\dfrac{\partial^2 a_i}{\partial T^2}\right)(1-k_{ik})$

$$\frac{\partial^2 A_{mj}}{\partial T_D^2} = T_{ref}^2 \left[\frac{-2P}{R^2 T^3} \frac{\partial a_{mj}}{\partial T} + \frac{P}{(RT)^2} \frac{\partial^2 a_{mj}}{\partial T^2} - \frac{2[T(\partial A_{mj}/\partial T) - A_{mj}]}{T^2} \right]$$

Phase composition x_{ij} is calculated as follows:

$$x_{ij} = K_{ij} z_i / t_i, \tag{A-1.1}$$

where $t_i = 1 + \sum_{j=1}^{N_P - 1} \beta_j (K_{ij} - 1)$ for $i = 1, 2, \ldots, N_C$. The partial derivative of x_{ij} with respect to β_j in equation A-1.8 is

$$\frac{\partial x_{ij}}{\partial \beta_j} = -K_{ij} z_i (K_{ij} - 1) / t_i^2. \tag{A-1.11}$$

The partial derivative of x_{ij} with respect to T in equation A-1.9 is

$$\frac{\partial x_{ij}}{\partial T} = \left\{ z_i \frac{\partial K_{ij}}{\partial T} t_i - z_i K_{ij} \sum_{j=1}^{N_P - 1} [\frac{\partial \beta_j}{\partial T}(K_{ij} - 1) + \beta_j \frac{\partial K_{ij}}{\partial T}] \right\} / t_i^2. \tag{A-1.12}$$

The partial derivative of $\underline{H}_{Dj}$ with respect to T_D can be obtained by substituting equations A-1.9 and A-1.11 into equation A-1.8. Consequently, the sensitivity of $\underline{H}_D^t$ to T_D can be expressed as

$$\frac{\partial \underline{H}_D^t}{\partial T_D} = \sum_{i=1}^{N_C} \sum_{j=1}^{N_P} \ln \left[\frac{Z_j + (1+\sqrt{2})B_{mj}}{Z_j + (1-\sqrt{2})B_{mj}} \right] \frac{K_{ij} z_i R T^2}{2\sqrt{2} B_{mj} t_i^2} \sum_{j=1}^{N_P - 1}(K_{ij} - 1)\beta_j \times$$

$$\left[\sum_{i=1}^{N_C} \frac{2 z_i A_i (1 - k_{ii})}{t_i^2} \beta_j \frac{\partial K_{ij}}{\partial T} \right] \frac{1}{\underline{H}_{spec}} + \sum_{j=1}^{N_P} \underline{H}_j \frac{T_{ref}}{\underline{H}_{spec}} \frac{\partial \beta_j}{\partial T}$$

$$+ \sum_{i=1}^{N_C} \sum_{j=1}^{N_P} \ln \left[\frac{Z_j + (1+\sqrt{2})B_{mj}}{Z_j + (1-\sqrt{2})B_{mj}} \right] \frac{-K_{ij} z_i R T^2}{2\sqrt{2} B_{mj} t_i^2} \sum_{j=1}^{N_P - 1}(K_{ij} - 1)\beta_j \times$$

$$\left[\sum_{i=1}^{N_C} \frac{2 z_i A_i (1 - k_{ii})}{t_i} \frac{\partial K_{ij}}{\partial T} + \sum_{i=1}^{N_C} 2 x_{ij}(1 - k_{ii}) \left(\frac{\partial A_i}{\partial T} + \frac{2 A_i}{T} \right) \right] \frac{T_{ref}}{\underline{H}_{spec}} \frac{\partial \beta_j}{\partial T}$$

$$+ \sum_{i=1}^{N_C} \sum_{j=1}^{N_P} \ln \left[\frac{Z_j + (1+\sqrt{2})B_{mj}}{Z_j + (1-\sqrt{2})B_{mj}} \right] \frac{-K_{ij} z_i R T}{2\sqrt{2} B_{mj}^2 t_i^2} \sum_{j=1}^{N_P - 1}(K_{ij} - 1)\beta_j \times$$

$$\left[B_{mj} \frac{\partial A_{mj}}{\partial x_{ij}} - \left(T \frac{\partial A_{mj}}{\partial T} + A_{mj} \right) \frac{\partial B_{mj}}{\partial x_{ij}} \right] \frac{T_{ref}}{\underline{H}_{spec}} \frac{\partial \beta_j}{\partial T}$$

$$+ \sum_{i=1}^{N_C} \sum_{j=1}^{N_P} \left(T \frac{\partial A_{mj}}{\partial T} + A_{mj} \right) \left(Z_j \frac{\partial B_{mj}}{\partial x_{ij}} - B_{mj} \frac{\partial Z_j}{\partial x_{ij}} \right) \times$$

$$\frac{-RT K_{ij} z_i}{t_i^2 B_{mj}[Z_j + (1+\sqrt{2})B_{mj}][Z_j + (1-\sqrt{2})B_{mj}]} \sum_{j=1}^{N_P - 1}(K_{ij} - 1)\beta_j \frac{T_{ref}}{\underline{H}_{spec}} \frac{\partial \beta_j}{\partial T}$$

$$+ \sum_{i=1}^{N_C} \sum_{j=1}^{N_P} \frac{-K_{ij} z_i R T}{t_i^2} \sum_{j=1}^{N_P - 1}(K_{ij} - 1)\beta_j \left(\frac{\partial Z_j}{\partial x_{ij}} - 1 \right) \frac{T_{ref}}{\underline{H}_{spec}} \frac{\partial \beta_j}{\partial T}$$

$$+ \sum_{i=1}^{N_C} \sum_{j=1}^{N_P} \frac{-K_{ij} z_i \underline{H}_i^{IG}}{t_i^2} \sum_{j=1}^{N_P - 1}(K_{ij} - 1)\beta_j \frac{T_{ref}}{\underline{H}_{spec}} \frac{\partial \beta_j}{\partial T}$$

$$+\sum_{i=1}^{N_C}\sum_{j=1}^{N_P}\ln\left[\frac{Z_j+(1+\sqrt{2})B_{mj}}{Z_j+(1-\sqrt{2})B_{mj}}\right]\frac{K_{ij}z_iRT^2}{2\sqrt{2}B_{mj}t_i^2}\sum_{j=1}^{N_P-1}(K_{ij}-1)\beta_j\times$$

$$\left[\sum_{i=1}^{N_C}\frac{2z_iA_i(1-k_{ii})}{t_i^2}(K_{ij}-1)\right]\frac{T_{ref}}{\underline{H}_{spec}}\left(\frac{\partial\beta_j}{\partial T}\right)^2 \qquad\text{(A-1.13)}$$

In the conventional two-phase notation for oleic (L) and gaseous (V) phases, the L phase is the reference phase in equation A-1.13; thus, for a two-phase system, the sensitivity of $\underline{H}_D{}^t$ to T_D can be expressed as follows:

$$\frac{\partial\underline{H}_D^t}{\partial T_D}=\alpha_1(T_D)\left(\frac{\partial\beta_V}{\partial T_D}\right)^2+\alpha_2(T_D)\frac{\partial\beta_V}{\partial T_D}+\alpha_3(T_D), \qquad\text{(A-1.14)}$$

where $\alpha_1(T_D)=\sum_{i=1}^{N_C}\ln\left[\frac{Z_V+(1+\sqrt{2})B_{mV}}{Z_V+(1-\sqrt{2})B_{mV}}\right]\frac{RT^2K_iz_i(K_i-1)\beta_V}{2\sqrt{2}B_{mV}t_i^2}\left[\sum_{i=1}^{N_C}\frac{2z_iA_i(1-k_{ii})(K_i-1)}{t_i^2}\right]\frac{T_{ref}}{\underline{H}_{spec}}+$

$\qquad\sum_{i=1}^{N_C}\ln\left[\frac{Z_L+(1+\sqrt{2})B_{mL}}{Z_L+(1-\sqrt{2})B_{mL}}\right]\frac{RT^2z_i(K_i-1)\beta_V}{2\sqrt{2}B_{mL}t_i^2}\left[\sum_{i=1}^{N_C}\frac{2z_iA_i(1-k_{ii})(K_i-1)}{t_i^2}\right]\frac{T_{ref}}{\underline{H}_{spec}}$

$\alpha_2(T_D)=\underline{H}_V\frac{T_{ref}}{\underline{H}_{spec}}-\underline{H}_L\frac{T_{ref}}{\underline{H}_{spec}}+\sum_{i=1}^{N_C}\ln\left[\frac{Z_V+(1+\sqrt{2})B_{mV}}{Z_V+(1-\sqrt{2})B_{mV}}\right]\frac{-K_iz_iRT^2(K_i-1)\beta_V}{2\sqrt{2}B_{mV}t_i^2}\times$

$\qquad\left[\sum_{i=1}^{N_C}\frac{2z_iA_i(1-k_{ii})}{t_i}\frac{\partial K_i}{\partial T}+\sum_{i=1}^{N_C}2y_i(1-k_{ii})\left(\frac{\partial A_i}{\partial T}+\frac{2A_i}{T}\right)\right]\frac{T_{ref}}{\underline{H}_{spec}}$

$\qquad-\sum_{i=1}^{N_C}\ln\left[\frac{Z_L+(1+\sqrt{2})B_{mL}}{Z_L+(1-\sqrt{2})B_{mL}}\right]\frac{-z_iRT^2(K_i-1)\beta_V}{2\sqrt{2}B_{mL}t_i^2}\sum_{i=1}^{N_C}2x_i(1-k_{ii})\times$

$\qquad\left(\frac{\partial A_i}{\partial T}+\frac{2A_i}{T}\right)\frac{T_{ref}}{\underline{H}_{spec}}+\sum_{i=1}^{N_C}\ln\left[\frac{Z_V+(1+\sqrt{2})B_{mV}}{Z_V+(1-\sqrt{2})B_{mV}}\right]\frac{-K_iz_iRT(K_i-1)\beta_V}{2\sqrt{2}B_{mV}{}^2t_i^2}\times$

$\qquad\left[B_{mV}\frac{\partial A_{mV}}{\partial y_i}-\left(T\frac{\partial A_{mV}}{\partial T}+A_{mV}\right)\frac{\partial B_{mV}}{\partial y_i}\right]\frac{T_{ref}}{\underline{H}_{spec}}$

$\qquad-\sum_{i=1}^{N_C}\ln\left[\frac{Z_L+(1+\sqrt{2})B_{mL}}{Z_L+(1-\sqrt{2})B_{mL}}\right]\frac{-z_iRT(K_i-1)\beta_V}{2\sqrt{2}B_{mL}{}^2t_i^2}\frac{T_{ref}}{\underline{H}_{spec}}\times$

$\qquad\left[B_{mL}\frac{\partial A_{mL}}{\partial x_i}-\left(T\frac{\partial A_{mL}}{\partial T}+A_{mL}\right)\frac{\partial B_{mL}}{\partial x_i}\right]$

$\qquad+\sum_{i=1}^{N_C}\left(T\frac{\partial A_{mV}}{\partial T}+A_{mV}\right)\left(Z_V\frac{\partial B_{mV}}{\partial y_i}-B_{mV}\frac{\partial Z_V}{\partial y_i}\right)\times$

$\qquad\frac{-RTK_iz_i(K_i-1)\beta_V}{t_i^2B_{mV}[Z_V+(1+\sqrt{2})B_{mV}][Z_V+(1-\sqrt{2})B_{mV}]}\frac{T_{ref}}{\underline{H}_{spec}}$

$\qquad-\sum_{i=1}^{N_C}\left(T\frac{\partial A_{mL}}{\partial T}+A_{mL}\right)\left(Z_L\frac{\partial B_{mL}}{\partial x_i}-B_{mL}\frac{\partial Z_L}{\partial x_i}\right)\frac{T_{ref}}{\underline{H}_{spec}}$

$\qquad\frac{-RTz_i(K_i-1)\beta_V}{t_i^2B_{mL}[Z_L+(1+\sqrt{2})B_{mL}][Z_L+(1-\sqrt{2})B_{mL}]}$

$\qquad+\sum_{i=1}^{N_C}\frac{-K_iz_iRT}{t_i^2}(K_i-1)\beta_V\left(\frac{\partial Z_V}{\partial y_i}-1\right)\frac{T_{ref}}{\underline{H}_{spec}}-$

$\qquad\sum_{i=1}^{N_C}\frac{-z_iRT}{t_i^2}(K_i-1)\beta_V\left(\frac{\partial Z_L}{\partial x_i}-1\right)\frac{T_{ref}}{\underline{H}_{spec}}$

$\qquad+\sum_{i=1}^{N_C}\frac{-K_{iV}z_i\underline{H}_i^{IG}}{t_i^2}(K_i-1)\beta_V\frac{T_{ref}}{\underline{H}_{spec}}-\sum_{i=1}^{N_C}\frac{-z_i\underline{H}_i^{IG}}{t_i^2}(K_i-1)\beta_V\frac{T_{ref}}{\underline{H}_{spec}}$

$\alpha_3(T_D)=\sum_{i=1}^{N_C}\ln\left[\frac{Z_V+(1+\sqrt{2})B_{mV}}{Z_V+(1-\sqrt{2})B_{mV}}\right]\frac{K_iz_iRT^2(K_i-1)\beta_V}{2\sqrt{2}B_{mV}t_i^2}\left[\sum_{i=1}^{N_C}\frac{2z_iA_i(1-k_{ii})}{t_i^2}\beta_V\frac{\partial K_i}{\partial T}\right]\frac{1}{\underline{H}_{spec}}$

$$+\sum_{i=1}^{N_C} \ln\left[\frac{Z_L+(1+\sqrt{2})B_{mL}}{Z_L+(1-\sqrt{2})B_{mL}}\right]\frac{z_i RT^2(K_i-1)\beta_V}{2\sqrt{2}B_{mL}t_i^2}\left[\sum_{i=1}^{N_C}\frac{2z_i A_i(1-k_{ii})}{t_i^2}\beta_V\frac{\partial K_i}{\partial T}\right]\frac{1}{\underline{H}_{spec}}.$$

In equation A-1.14, $t_i = 1 + (K_i - 1)\beta_V$. Particularly, $\partial\beta_V/\partial T_D$ helps understand the physical meaning of narrow-boiling, where the amount of the V phase (i.e., β_V) rapidly increases with a small change in temperature (T_D). That is, a narrow-boiling system exhibits a large value for $|\partial\beta_V/\partial T_D|$.

Appendix A-2: JACOBIAN MATRIX IN DS ALGORITHM

The elements of the Jacobian matrix used in the DS algorithm for a N_C-component N_P-phase system are

$$\frac{\partial g_j}{\partial T_D} = -T_{ref}\sum_{i=1}^{N_C}\frac{z_i}{t_i^2}\left[t_i K_{ij}\frac{\partial \ln K_{ij}}{\partial T} - (K_{ij}-1)\sum_{k=1}^{N_P-1}\beta_k K_{ik}\frac{\partial \ln K_{ik}}{\partial T}\right]$$

$$\text{for } j = 1, 2, \dots, N_P - 1, \qquad\qquad\qquad (A\text{-}2.1)$$

$$\frac{\partial g_j}{\partial \beta_k} = \sum_{i=1}^{N_C}\frac{z_i}{t_i^2}(1-K_{ij})(1-K_{ik})$$

$$\text{for } j, k = 1, 2, \dots, N_P - 1, \qquad\qquad\qquad (A\text{-}2.2)$$

$$\frac{\partial g_{N_P}}{\partial T_D} = T_{ref}\sum_{j=1}^{N_P}\beta_j\left(\sum_{i=1}^{N_C}\frac{\partial x_{ij}}{\partial T}\frac{H_i^{IG}}{\underline{H}_{spec}} + \sum_{i=1}^{N_C}\frac{x_{ij}}{\underline{H}_{spec}}\frac{\partial H_i^{IG}}{\partial T} + \frac{\partial H_{Dj}^{dep}}{\partial T}\right), \qquad (A\text{-}2.3)$$

$$\frac{\partial g_{N_P}}{\partial \beta_k} = \left(\underline{H}_{Dk}^{IGM} + \underline{H}_{Dk}^{dep}\right) - \left(\underline{H}_{DN_P}^{IGM} + \underline{H}_{DN_P}^{dep}\right)$$

$$\text{for } k = 1, 2, \dots, N_P - 1, \qquad\qquad\qquad (A\text{-}2.4)$$

where $t_i = 1 - \sum_{j=1}^{N_P-1}(1-K_{ij})\beta_j$ for $i = 1, 2, \dots, N_C$, $g_j = \sum_{i=1}^{N_C}(1-K_{ij})z_i/t_i = 0$ for $j = 1, 2, \dots, (N_P - 1)$, and $g_{N_P} = (\underline{H}^t - \underline{H}_{spec})/\underline{H}_{spec} = 0$.

The Jacobian matrix of $N_P \times N_P$ can be written in the matrix form as follows:

$$J = \begin{bmatrix} \dfrac{\partial g_{N_P}}{\partial T_D} & \dfrac{\partial g_{N_P}}{\partial \beta_1} & \cdots & \dfrac{\partial g_{N_P}}{\partial \beta_{N_P-1}} \\ \dfrac{\partial g_1}{\partial T_D} & \dfrac{\partial g_1}{\partial \beta_1} & \cdots & \dfrac{\partial g_1}{\partial \beta_{N_P-1}} \\ \vdots & \vdots & \ddots & \vdots \\ \dfrac{\partial g_{N_P-1}}{\partial T_D} & \dfrac{\partial g_{N_P-1}}{\partial \beta_1} & \cdots & \dfrac{\partial g_{N_P-1}}{\partial \beta_{N_P-1}} \end{bmatrix} = \begin{bmatrix} J_{11} & J_{12} & \cdots & J_{1N_P} \\ J_{21} & J_{22} & \cdots & J_{2N_P} \\ \vdots & \vdots & \ddots & \vdots \\ J_{N_P 1} & J_{N_P 2} & \cdots & J_{N_P N_P} \end{bmatrix}$$

$$= \begin{bmatrix} J_{11} & P^{1\times(N_P-1)} \\ Q^{(N_P-1)\times 1} & R^{(N_P-1)\times(N_P-1)} \end{bmatrix}, \qquad\qquad\qquad (A\text{-}2.5)$$

where J_{11} is equation A-2.3, $Q^{(N_P - 1) \times 1}$ consists of equations A-2.1, $P^{1 \times (N_P - 1)}$ consists of equations A-2.4, and $R^{(N_P - 1) \times (N_P - 1)}$ is the Hessian matrix of F consisting of equations A-2.2.

Gaussian elimination for $Q^{(N_P - 1) \times 1}$ yields

$$J' = \begin{bmatrix} J_{11} & P^{1 \times (N_P - 1)} \\ 0^{(N_P - 1) \times 1} & R'^{(N_P - 1) \times (N_P - 1)} \end{bmatrix}, \tag{A-2.6}$$

where $R' = \dfrac{1}{J_{11}} \begin{bmatrix} J_{22} J_{11} - J_{12} J_{21} & \cdots & J_{2N_P} J_{11} - J_{1N_P} J_{21} \\ \vdots & \ddots & \vdots \\ J_{2N_P} J_{11} - J_{12} J_{N_P 1} & \cdots & J_{N_P N_P} J_{11} - J_{1N_P} J_{N_P 1} \end{bmatrix}. \tag{A-2.7}$

Equation A-2.6 clearly indicates that the system of equations tend to be degenerate with increasing J_{11}, regardless of the curvature of the RR convex function.

Also, matrix J is singular, when R is not of full rank. To see this, consider matrix J when the pth and q^{th} phases are critical ($p \neq q$). As described in Okuno et al. (2010), $J_{mp} = J_{mq}$, where m = 2, 3, …, N_P, for such a case. $J_{1p} = J_{1q}$ when the compositions of the two phases are identical. Therefore, the pth and q^{th} columns of matrix J are identical when R is not of full rank.

APPENDIX B: DS Algorithms of Michelsen (1987) and

Agarwal et al. (1991)

Appendix B presents the step wise descriptions and flow charts of the DS algorithms for PH flash of Michelsen (1987) and Agarwal et al. (1991).

Appendix B-1: Ds Algorithm of Michelsen (1987)

This section presents a step-wise description for the two-phase DS algorithm of Michelsen (1987), and then gives the flow chart of his algorithm.

Step 1. Specify $\underline{H}_{spec}$, P, and z_i, along with model parameters such as critical temperature T_C, critical pressure P_C, acentric factor ω, and $N_C \times N_C$ binary interaction parameters (BIPs).

Step 2. Input an initial guess for temperature, $T^{(1)}$, where the number in the bracket represents the iteration-step number $k = 1$. Calculate initial guesses for K values based on Wilson's correlation (1969).

Step 3. Solve RR equations for the phase mole fraction $\beta_V^{(k)}$ for the kth iteration step so that $|g_1^{(k)}| < \varepsilon_1$ (e.g., $\varepsilon_1 = 10^{-10}$). Calculate the corresponding $x_i^{(k)}$ and $y_i^{(k)}$.

Step 4. Calculate the residual of the enthalpy constraint ($g_2^{(k)}$). If $| g_2^{(k)}|$ is less than the tolerance ε_2, stop (e.g., $\varepsilon_2 = 10^{-10}$). Otherwise, continue to step 5.

Step 5. Calculate $\ln\varphi_{ij}^{(k)}$, $(\partial\ln\varphi_{ij}/\partial T)^{(k)}$, and phase heat capacities ($C_{Pj}^{(k)}$) for $j = V$ and L.

Step 6. Calculate K values using one SS step (i.e., $\ln K_i^{(k)} = (\ln\varphi_{iL} - \ln\varphi_{iV})^{(k)}$), $(\partial\ln K_i/\partial T)^{(k)}$, and $g_1^{(k)}$.

Step 7. Construct the 2×2 Jacobian matrix (see Appendix A).

Step 8. Perform one Newton's iteration step to obtain $\beta_V^{(k+1)}$ and $T^{(k+1)}$.

Step 9. Calculate $f_O = |T^{(k+1)} - T^{(i)}|$, where $i = 1, 2, \ldots, k$, to check for temperature oscillation. Continue to step 10 if f_O is greater than ε_O; $\varepsilon_O = \min_i(|T^{(i)} - T^{(i+1)}|)/C$, where $i = 1, 2, \ldots, (k - 1)$ and C (e.g., 10^2) is a constant that defines the investigation radius around $T^{(k+1)}$. Otherwise, temperature is considered to be oscillating. Then, go to step 4 with $\beta_V^{(k)} = 0.5$ and $x_i^{(k)} = y_i^{(k)} = z_i$ only for the first time the oscillation is detected.

Step 10. Update K values; $\ln K_i^{(k+1)} = \ln K_i^{(k)} + (\partial \ln K_i / \partial T)^{(k)}(T^{(k+1)} - T^{(k)})$. Go to step 3 after increasing the iteration-step number by one; $k = k + 1$.

The DS algorithm of Michelsen (1987) performs one Newton's iteration step to obtain β_V and T in step 8; however, note that its convergence behavior is linear as can be seen in the K-value updates in composition (step 6) and T (step 10). Also, the only stopping criterion is that $|g_2|$ be less than ε_2 in step 4. The other residual for g_j has been satisfied in step 3. These are also true for the DS algorithm of Agarwal et al. (1991).

In step 5, phase compressibility factors are selected so that the resulting Gibbs free energy is minimized among the possible root selections (Evelein et al. 1976). This conventional root selection, however, is not applied when step 9 detects temperature oscillation associated with narrow-boiling behavior. For such a case, Michelsen (1987) suggested that the oscillating single-phase system be split into two phases of initially equal amounts and compositions (i.e., $\beta_V = 0.5$ and $x_i = y_i = z_i$) only for the first time the oscillation is detected. Then, the maximum compressibility factor is chosen for the V phase and the minimum for the L phase for this iteration step and also the subsequent iterations. However, this scheme does not always resolve the temperature oscillation issue.

How to detect temperature oscillations was not explained in Michelsen (1987) and Agarwal et al. (1991). In our implementation of their DS algorithms, it has been

observed that the temperature oscillations occur between two distinct temperature ranges in a quite regular manner. Based on the observation, temperature oscillations are detected using the procedure given in step 9. The definition of temperature oscillation becomes stricter if a greater value is used for the C constant.

The flow chart of his algorithm is given below.

Flowchart boxes:

- Specify $\underline{H}_{spec}$, P, z_i, T_c, P_c, ω and BIP
- k=1, Input $T^{(1)}$. Calculate initial guesses for K values based on Wilson's correlation
- Solve RR equations for $\beta_V^{(k)}$ such that $|g_1^{(k)}| < \varepsilon_1$ and calculate $x_i^{(k)}$ and $y_i^{(k)}$
- $|g_2^{(k)}| < \varepsilon_2$? — YES → Output $\beta_V^{(k)}$, $x_i^{(k)}$ and $y_i^{(k)}$
- NO ↓
- Calculate $\ln\varphi_{ij}^{(k)}$, $(\partial\ln\varphi_{ij}/\partial T)^{(k)}$ and $C_{Pj}^{(k)}$ for j = V and L
- Calculate $\ln K_i^{(k)} = (\ln\varphi_{iL} - \ln\varphi_{iV})^{(k)}$, $(\partial\ln K_i/\partial T)^{(k)}$ and $g_1^{(k)}$
- Construct the 2×2 Jacobian matrix
- Perform one Newton's iteration step to obtain $\beta_V^{(k+1)}$ and $T^{(k+1)}$
- T oscillates ? — YES → Assume $\beta_V^{(k)} = 0.5$, $x_i^{(k)} = y_i^{(k)} = z_i$
- NO ↓
- (k = k + 1) Calculate $\ln K_i^{(k+1)} = \ln K_i^{(k)} + (\partial\ln K_i/\partial T)^{(k)}(T^{(k+1)} - T^{(k)})$

1. Details of the check of temperature oscillation:
   Calculate $f_o = |T^{(k+1)}-T^{(i)}|$, where i=1, 2, ..., k. If $f_o \leq \varepsilon_o = \min_i(|T^{(i)}-T^{(i+1)}|)/C$, where i=1, 2, ..., (k-1) and C (e.g., 10^2) is a constant that defines the investigation radius around $T^{(k+1)}$, temperature is considered to be oscillating.

2. Compressibility factor selection approach:
   Before detecting temperature oscillation, phase compressibility factors are selected so that the resulting Gibbs free energy is minimized among the possible roots selections.
   After detecting temperature oscillation, the oscillating single-phase system will be split into two phases with the assumption $\beta_V^{(k)} = 0.5$ and $x_i^{(k)} = y_i^{(k)} = z_i$, only for the first time the oscillation is detected. Then, the maximum compressibility factor is chosen for the V phase and the minimum for the L phase for this iteration step and subsequent iterations.

279

Appendix B-2: DS ALGORITHM OF AGARWAL ET AL. (1991)

This section presents a step-wise description for the two-phase DS algorithm of Agarwal et al. (1991), and then gives the flow chart of their algorithm.

The main modification of the DS algorithm made by Agarwal et al. (1991) was that a quasi-Newton step was used for a preliminary update of K values before constructing the Jacobian matrix. The quasi-Newton step used was based on Nghiem (1983) and Nghiem and Li (1984), and referred to as QNSS. Steps 1-4 are not presented below as they are the same as in previous section.

Step 5. Calculate $\ln\varphi_{ij}^{(1)}$ and phase heat capacities $(C_{Pj}^{(1)})$ for $j = V$ and L.

Step 6. Calculate the residuals of the fugacity equations $(f_i^{(1)})$.

Step 7. $T^{(2)} = T^{(1)} - g_2^{(1)}/(\sum_j\beta_jC_{Pj})^{(1)}$.

Step 8. Solve RR equstions for the vapor phase mole fraction $\beta_V^{(k)}$ for the kth iteration step so that $|g_1^{(k)}| < \varepsilon_1$. Calculate the corresponding $x_i^{(k)}$ and $y_i^{(k)}$.

Step 9. Calculate the residual of the enthalpy constraint $(g_2^{(k)})$. If $|g_2^{(k)}|$ is less than the tolerance ε_2, stop. Otherwise, continue to step 10.

Step 10. Calculate the residuals of the fugacity equations $(f_i^{(k)})$.

Step 11. Perform a QNSS step for intermediate K values, $K_i^{(k+0.5)}$;

$$\ln\vec{K}^{(k+0.5)} = \ln\vec{K}^{(k)} + \frac{\left(\ln\vec{K}^{(k)} - \ln\vec{K}^{(k-1)}\right)^T \vec{f}^{(k-1)}}{\left(\ln\vec{K}^{(k)} - \ln\vec{K}^{(k-1)}\right)^T (\vec{f}^{(k)} - \vec{f}^{(k-1)})}\vec{f}^{(k)},$$

where $\vec{K}$ and $\vec{f}$ are vectors consisting of N_C K values and N_C residuals of the fugacity equations, respectively.

Step 12. Calculate $x_i^{(k+0.5)}$ and $y_i^{(k+0.5)}$ based on $\beta_V^{(k)}$ and $K_i^{(k+0.5)}$.

Step 13. Construct the 2×2 Jacobian matrix based on $x_i^{(k+0.5)}$ and $y_i^{(k+0.5)}$.

Step 14. Perform one Newton's iteration step to obtain $\beta_V^{(k+1)}$ and $T^{(k+1)}$.

Step 15. Calculate $f_O = |T^{(k+1)} - T^{(i)}|$, where $i = 1, 2, \ldots, k$, to check for temperature oscillation. Continue to step 16 if f_O is greater than ε_O; $\varepsilon_O = \min_i(|T^{(i)} - T^{(i+1)}|)/C$, where $i = 1, 2, \ldots, (k - 1)$ and C (e.g., 10^2) is a constant that defines the investigation radius around $T^{(k+1)}$. Otherwise, temperature is considered to be oscillating. Then, go to step 9 with $\beta_V^{(k)} = 0.5$ and $x_i^{(k)} = y_i^{(k)} = z_i$ only for the first time the oscillation is detected.

Step 16. Update K values; $\ln K_i^{(k+1)} = \ln K_i^{(k)} + (\partial \ln K_i/\partial T)^{(k)}(T^{(k+1)} - T^{(k)})$. Go to step 8 after increasing the iteration-step number by one; $k = k + 1$.

In steps 5 and 10, phase compressibility factors are selected so that the resulting Gibbs free energy is minimized among the possible root selections. As in previous section, this conventional root selection is not used when step 15 detects temperature oscillation. For such a case, the procedure of Michelsen (1987) described before is followed. The maximum compressibility factor is chosen for the V phase and the minimum for the L phase in step 10 of the subsequent iterations.

The flow chart of his algorithm is given below.

Specify $\underline{H}_{spec}$, P, z_i, T_c, P_c, ω and BIP

k=1, Input $T^{(1)}$
Calculate initial guesses for K values based on Wilson's correlation

Solve RR equations for $\beta_V^{(k)}$ such that $|g_1^{(k)}| < \varepsilon_1$ and calculate $x_i^{(k)}$ and $y_i^{(k)}$

$|g_2^{(k)}| < \varepsilon_2$?

YES → Output $\beta_V^{(k)}$, $x_i^{(k)}$ and $y_i^{(k)}$

NO

Calculate $\ln\varphi_{ij}^{(1)}$ and $C_{Pj}^{(1)}$ for j = V and L

Calcuate $f_i^{(1)}$ from fugacity equations

Calculate $T^{(2)} = T^{(1)} - g_2^{(1)}/(\sum_j \beta_j C_{Pj})^{(1)}$

Solve RR equations for $\beta_V^{(k)}$ such that $|g_1^{(k)}| < \varepsilon_1$ and calculate $x_i^{(k)}$ and $y_i^{(k)}$

The check procedure of temperature oscillation and the compressibility factor selection approach are the same as presented in the DS algorithm by Michelsen.

$|g_2^{(k)}| < \varepsilon_2$?

YES → Output $\beta_V^{(k)}$, $x_i^{(k)}$ and $y_i^{(k)}$

NO

Calcuate $f_i^{(k)}$ from fugacity equations

Perform a QNSS step for intermediate K values
$$\ln\vec{K}^{(k+0.5)} = \ln\vec{K}^{(k)} + \frac{\left(\ln\vec{K}^{(k)} - \ln\vec{K}^{(k-1)}\right)^T \vec{f}^{(k-1)}}{\left(\ln\vec{K}^{(k)} - \ln\vec{K}^{(k-1)}\right)^T \left(\vec{f}^{(k)} - \vec{f}^{(k-1)}\right)} \vec{f}^{(k)}$$

Calculate $x_i^{(k+0.5)}$ and $y_i^{(k+0.5)}$ based on $\beta_V^{(k)}$ and $K_i^{(k+0.5)}$

Construct the 2 ×2 Jacobian matrix based on $x_i^{(k+0.5)}$ and $y_i^{(k+0.5)}$

Perform one Newton's iteration step to obtain $\beta_V^{(k+1)}$ and $T^{(k+1)}$

T oscillates ?

YES → Assume $\beta_V^{(k)} = 0.5$
$x_i^{(k)} = y_i^{(k)} = z_i$

NO

(k = k + 1)

Calculate $\ln K_i^{(k+1)} = \ln K_i^{(k)} + (\partial \ln K_i/\partial T)^{(k)}(T^{(k+1)} - T^{(k)})$

APPENDIX C: Flow Chart and Initialization Scheme of the Unified Phase-Stability/-Split Algorithm for Multiphase PT Flash

Appendix C presents the flow chart and initialization scheme of the unified phase-stability/-split algorithm for multiphase PT flash given in Chapter 3.   A sample input file of case 3.1 used in chapter 3 is given.   At last, a summary of the number of stationary points obtained with the new simultaneous PT flash algorithm for 24 cases available in the literature is given at last.

Appendix C-1: FLOW CHART

This section presents the flow chart of the unified phase-stability/-split algorithm for multiphase PT flash given in Chapter 3.
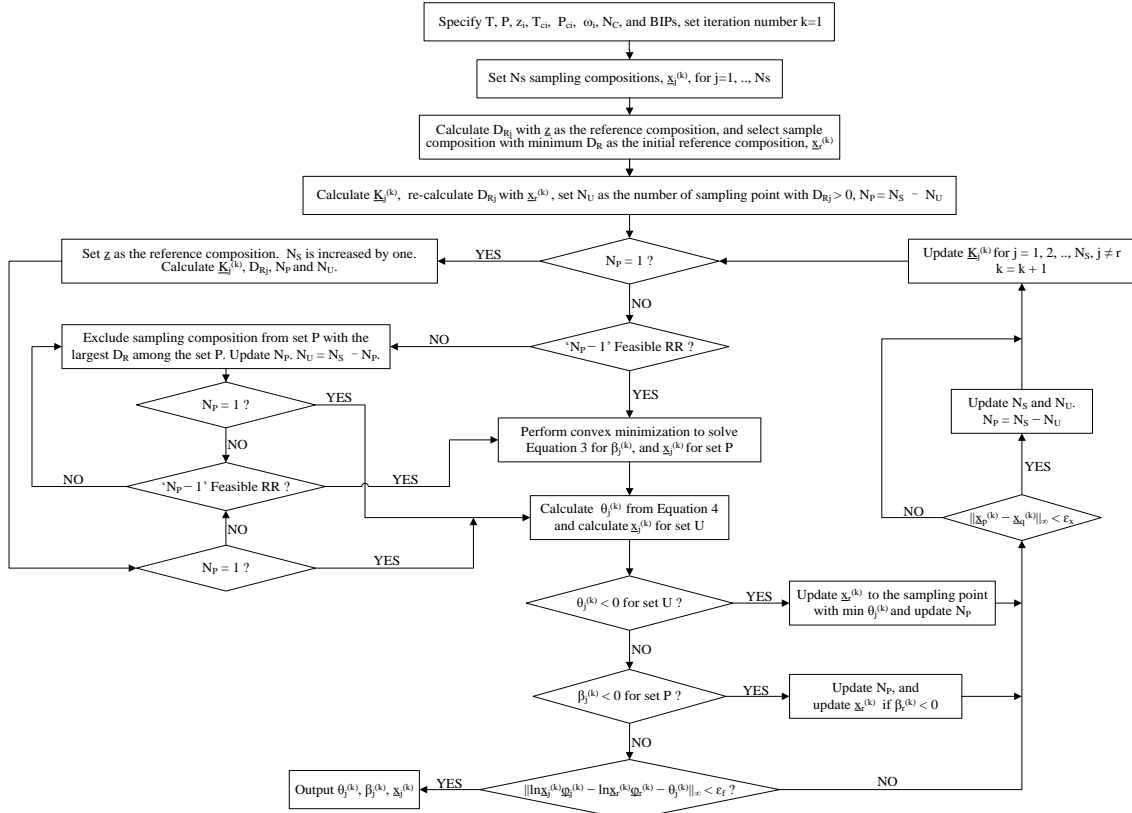
Appendix C-2: INITIALIZATION SCHEME

This section presents the initialization scheme used for the unified phase-stability/-split algorithm for multiphase PT flash given in Chapter 3.

The algorithm developed in this research attempts to find stationary points of TPD that give the global minimum of the Gibbs free energy for the fluid under consideration with a specified $\underline{z}$, P, and T. One of the most important factors that affect global convergence of the algorithm is how iterative sampling compositions are distributed in composition space. If no reliable information is available regarding equilibrium phase compositions for the fluid of interest at specified conditions, sampling compositions should be distributed in composition space in a certain systematic manner. Ideally, they are expected to find all stationary points of TPD. Such a possibility is generally expected to increase as more sampling compositions are used, unless they are placed close to each other.

This appendix C-2 presents the procedure used in this paper to distribute sampling compositions uniformly with respect to the specified $\underline{z}$, for the initialization of the algorithm developed. First, N_C sampling compositions are placed near the N_C vertices of composition space. If more sampling compositions are desired, the composition space is divided into N_C different regions that have the overall composition $\underline{z}$ as the common vertex. Each of the N_C regions is defined by this common vertex $\underline{z}$ and the other ($N_C -$ 1) vertices among N_C vertices of pure components. Then, a systematic procedure is applied to distribute sampling compositions around the central point for each of the N_C regions. The number of sampling compositions placed in each region can be defined individually, or correlated with the relative size of that region to the entire composition space, as described later. A stepwise description is given below.

284

Step 1. Distribute N_C sampling compositions near the N_C vertices of composition space (e.g., 99.9% that component and 0.1% the equimolar mixture of the other components).

Step 2. If more sampling compositions are desired, the composition space is divided into N_C different regions (R_i for i = 1, 2,… N_C) that have the overall composition $\underline{z}$ as the common vertex. Each of the N_C regions is defined by $\underline{z}$ and the other ($N_C - 1$) vertices among N_C vertices of pure components. Then, define the number of sampling compositions $N_{Si} \geq 1$ (i = 1, 2,… N_C) for R_i (i = 1, 2,… N_C). Set i to be 1.

Step 3. For the ith region R_i, calculate the arithmetic mean of the N_C compositions, $\underline{z}$ and ($N_C - 1$) pure components. This corresponds to the central point in R_i, and becomes a sampling composition. Then, connect the central point with the N_C vertices of R_i. This results in N_C lines in R_i.

Step 4. For R_i, evenly divide each of the N_C lines obtained from step 3 into r_{1i} segments ($r_{1i} \geq 1$). This results in ($r_{1i} - 1$)N_C sampling compositions within R_i.

Step 5. If $r_{1i} \geq 2$, construct ($r_{1i} - 1$)$N_C(N_C - 1)/2$ lines that are parallel to edges of composition space by connecting sampling compositions obtained from step 4.

Step 6. Evenly divide the ($r_{1i} - 1$)$N_C(N_C - 1)/2$ lines obtained from step 5 into r_{2i} segments ($r_{2i} \geq 1$). This results in ($r_{1i} - 1$)($r_{2i} - 1$)$N_C(N_C - 1)/2$ sampling compositions within R_i.

Step 7. Repeat steps 3 – 6 for the next region until sampling compositions are distributed for all N_C regions defined in step 2. That is, increase i by one, where i $\leq N_C$. Go back to step 3.

The first step gives N_C sampling compositions. Step 3 gives one sampling composition at the center for each region; hence, N_C sampling compositions in the N_C regions. Steps 4 and 6 give ($r_{1i} - 1$)N_C and ($r_{1i} - 1$)($r_{2i} - 1$)$N_C(N_C - 1)/2$ sampling

compositions, respectively, for each region. Therefore, the total number of sampling compositions distributed by use of the procedure given above is $N_C + \Sigma_i[1 + (r_{1i} - 1)N_C + (r_{1i} - 1)(r_{2i} - 1)N_C(N_C - 1)/2]$ for $N_C \geq 2$. The minimum N_S is $2N_C$ ($N_C \geq 2$) when $r_1 = 1$ for all regions; i.e., N_C compositions from step 1 and N_C compositions from step 3.

In step 2, N_{Si} (≥ 1) for R_i ($i = 1, 2,\ldots N_C$) can be correlated with the size of R_i relative to the entire composition space as follows:

2.1. Calculate $n_{Si} = \left(z_i^n / \sum_{i=1}^{N_C} z_i^n\right)(N_{S\,max} - N_C)$, where N_{Smax} is the maximum number of initial sampling compositions specified by the user. The exponent n can be also specified.

2.2. Solve $n_{Si} = (r_1 - 1)N_C + (r_1 - 1)(r_2 - 1)N_C(N_C - 1)/2$ for r_1 and r_2 subject to a certain constraint regarding r_1 and/or r_2, such as $r_2 = r_1 - 1$ that is used in this paper.

2.3. Round down r_1 and r_2 to make them integers, r_{1i} and r_{2i}. Calculate $N_{Si} = 1 + (r_{1i} - 1)N_C + (r_{1i} - 1)(r_{2i} - 1)N_C(N_C - 1)/2$. Note that $N_S = N_C + \sum_{i=1}^{N_C} N_{Si} \leq N_{Smax}$ due to the rounding of r_1 and r_2.

As an example, **Figure C.1** shows the sampling compositions distributed by use of the above procedure for $N_C = 3$, $N_{Smax} = 100$, and $n = 1$ along the constraint $r_2 = r_1 - 1$. The resulting N_S is 81, which consists of 3 compositions near the pure components, 3 at the centers of three regions, and 75 in the largest region defined by $\underline{z}$ and components 2 and 3.

This is merely one of many possible procedures to systematically distribute sampling compositions; it is not the purpose of this appendix to single out a procedure that yields rapid convergence of the algorithm. When reasonable estimates are available for potential phase compositions, they can be used to initialize the algorithm.
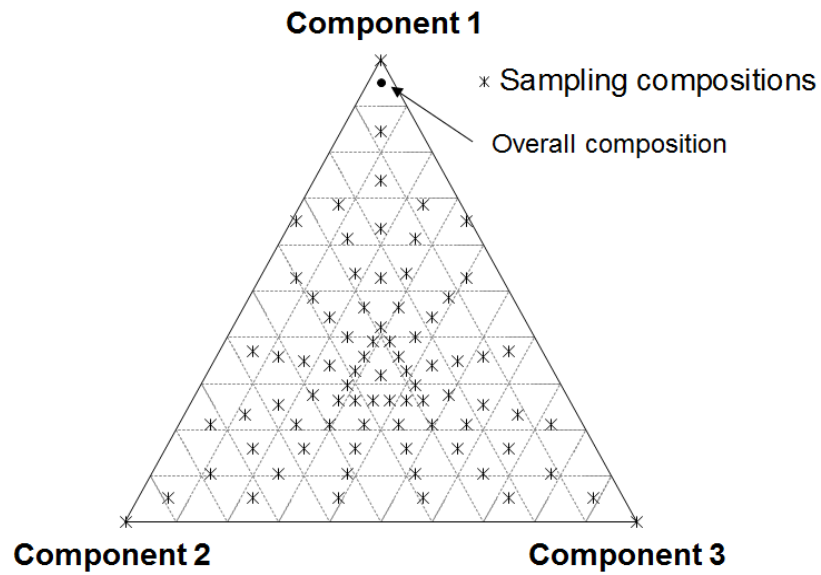
Figure C.1 Sampling compositions distributed for $N_C = 3$ by use of the procedure given in Appendix C. The resulting N_S is 81 with $N_{Smax} = 100$, n = 1.0, and constraint $r_2 = r_1 - 1$.

Appendix C-3: SAMPLE INPUT FILE OF CASE 3.1 USED IN CHAPTER 3

'Nc'

3

'Pres in bars'

65.0D0

'Tres in K'

560.0D0

'Tol'

1.0D-10

'maxiter'

15000

'Nsmax'

6

'expo'

1.0

'Zint'

0.75D0

0.15D0

0.10D0

'Tc in K '

647.30D0

369.80D0

717.00D0

'Pc in bars '

220.89D0

42.460D0

14.190D0

'w'

0.344D0

0.152D0

0.742D0

'kij'

0.0000D0 0.6841D0 0.3583D0

0.6841D0 0.0000D0 0.0000D0

0.3583D0 0.0000D0 0.0000D0

Appendix C-4: SUMMARY OF NUMBERS OF STATIONARY POINTS FOR 24 CASES

The table below summarizes the studies on the numbers of stationary points of the TPD function for 24 cases taken from the literature. All calculations are performed using the initialization scheme presented in Appendix C-2 for the new PT flash algorithm. The number of initial sampling compositions is $2N_C$. Obviously, different results will be obtained with different initialization methods.

		Number of stationary points reported in the literature	Number of stationary points obtained using new PT flash algorithm (chapter 3)
$C_1 + H_2S$ at 190 K and 40.53 bars		3	3 ($N_U = 1$ and $N_P = 2$)
Reference: Nagarajan et al. (1991)			
$N_2 + C_2$ at 270 K and 76 bars	Overall composition is (0.1, 0.9)	1	1
	Overall composition is (0.18, 0.82)	2	2
	Overall composition is (0.3, 0.7)	2	2
	Overall composition is (0.44, 0.56)	2	2
	Overall composition is (0.6, 0.4)	1	1
Reference: Hua et al. (1998), Nichita et al. (2002), Sofyan et al. (2003), Nichita and Gomez (2009), Ivanov et al. (2013)			
$CO_2 + C_1$ at 220 K and 60.8 bars	Overall composition is (0.1, 0.9)	1	1
	Overall composition is (0.2, 0.8)	2	2
	Overall composition is (0.3, 0.7)	2	2
	Overall composition is (0.43, 0.57)	2	2
	Overall composition is (0.6, 0.4)	1	1
Reference: Hua et al. (1998), Sofyan et al. (2003), Ivanov et al. (2013)			

$N_2 + C_1 + C_2$ at 270 K and 76 bars	Overall composition is (0.3, 0.1, 0.6)	2	2
	Overall composition is (0.15, 0.3, 0.55)	2	2
	Overall composition is (0.08, 0.38, 0.54)	1	1
	Overall composition is (0.05, 0.05, 0.9)	1	1
Reference: Hua et al. (1998), Harding and Floudas (2000), Sofyan et al. (2003), Corazza et al. (2007), Saber and Shaw (2008), Nichita and Gomez (2009), Ivanov et al. (2013)			
$C_1 + CO_2 + H_2S$ with overall composition of (0.4989, 0.0988, 0.4023)	T = 208.5 K and P = 55.1 bars	4	3 (N_U = 1 and N_P = 2)
	T = 210.5 K and P = 57.5 bars	2	3 (N_U = 1 and N_P = 2)
	T = 227.55 K and P = 48.6 bars	2	2
Reference: Sun and Seider (1995), Sofyan et al. (2003), Corazza et al. (2007), Nichita and Gomez (2009)			
$C_1 + CO_2 + H_2S$ with overall composition of (0.48, 0.12, 0.4)	T = 208.5 K and P = 55.1 bars	4	3 (N_U = 1 and N_P = 2)
Reference: Sun and Seiider (1995), Sofyan et al. (2003), Corazza et al. (2007), Nichita and Gomez (2009)			
Eight-component case at 353 K and 358 bars		2	2
Reference: Nagarajan et al. (1991), Sun and Seider (1995), Saber and Shaw (2008), Ivanov et al. (2013), Henderson et al. (2014)			
Twelve-component case at 240 K and 60 bars		2	2
Reference: Ivanov et al. (2013), Henderson et al. (2014)			
$C_7H_8 + H_2O + H_2$ at 473.15 K and 100 bars	Overall composition is (0.2, 0.5, 0.3)	3	3
	Overall composition is (0.79, 0.2, 0.01)	3	2
Reference: Bünz et al. (1991), Sun and Seider (1995)			
$C_3 + CO_2 + nC_{16}$ at 294 K and 54 bars	Overall composition is (0.112, 0.84, 0.048)	4	3 (N_U = 1 and N_P = 2)
Reference: Sun and Seider (1995)			

APPENDIX D: Motions of Sampling Compositions in the Unified Phase-Stability/-Split Algorithm for Multiphase PT Flash

Appendix D presents the motions of the sampling compositions in the unified phase-stability/-split algorithm for multiphase PT flash for cases 3.1 and 3.2 given in chapter 3.   The EOS parameters and solutions for these cases were discussed in the case studies section in chapter 3.

Appendix D-1: MOTIONS OF SAMPLING COMPOSITIONS FOR CASE 3.1 IN CHAPTER 3

Case 1 was a ternary mixture consisting of H_2O, C_3, and $n\text{-}C_{16}$ at 560 K and 65 bars (Tables 3.1 and 3.2).   The convergence behavior of the new algorithm was presented in Figure 3.4.   **Figure D-1.1** shows the movement of sampling compositions at selected iteration steps.   In this figure, a star represents the overall composition. Solid squares represent the sampling compositions in set U.   The reference composition in set P is shown by a solid diamond, and the other sampling compositions in set P are hollow squares.   This symbolic notation is used throughout this appendix.

After the initialization, six sampling compositions are distributed in composition space, in which three are located near compositional vertices and the other three are in the central points of each area, as can be seen in Figure D-1.1a.   All six sampling compositions are updated significantly after the 1st iteration, where three sampling compositions are set U with positive θ values.   Figures D-1.1b and D-1.1c show that the six compositions do not merge (i.e., N_S remains 6) during the 2nd and 3rd iterations, but the reference composition is adaptively selected on the basis of step 7 of the new algorithm.   That is, the composition with negative θ value is selected as the reference composition during the iterations.

After the 4th iteration, a composition in set U merges into a composition in set P, resulting in N_P of five and N_U of zero (see Figure D-1.1e). The reference composition used from iteration step 4 until the final convergence is located in the vicinity of the equilibrium L_1 phase. Two compositions merge during iteration step 5, resulting in N_S of three. The correct N_S, two (i.e., N_P of two and N_U of zero), is identified at the 7th iteration. As can be seen in Figures D-1.1g and D-1.1h, the compositions in set P at the 7th iteration are in the vicinity of the final equilibrium compositions. The converged compositions in set P are connected by the tie line in Figure D-1.1h.

Figure D-1.2 shows the motion of the sampling compositions by use of a triangular prism, where each horizontal cross section represents the ternary diagram at a certain iteration step. The same iteration steps as Figure D-1.1 are presented. The merging of sampling compositions can be seen at the 4th, 5th, and 7th iteration steps.

(a) After the initialization ($N_U = 4$ and $N_P = 2$)

(b) After the 1st iteration ($N_U = 3$ and $N_P = 3$)
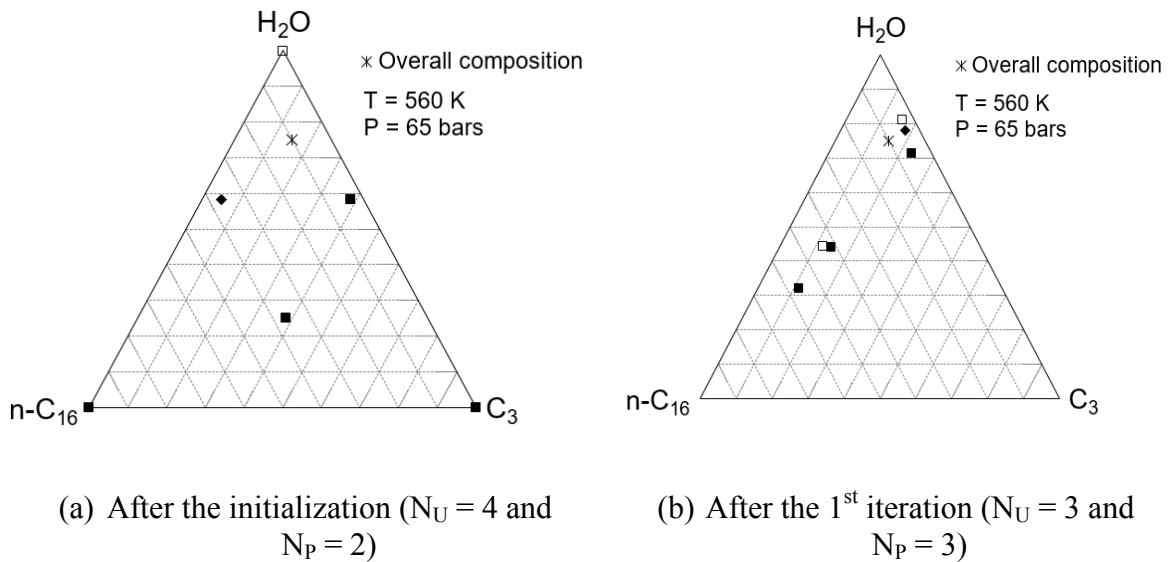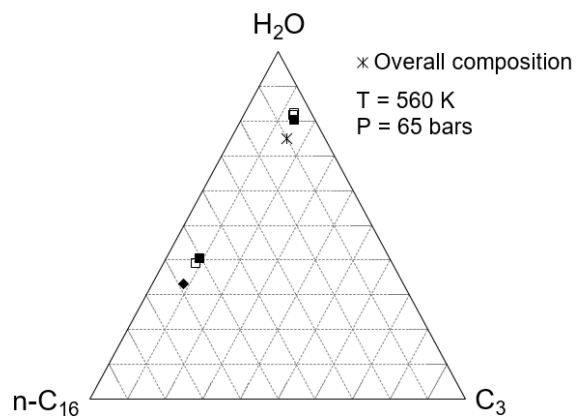
(c) After the 2nd iteration ($N_U = 2$ and $N_P = 4$)
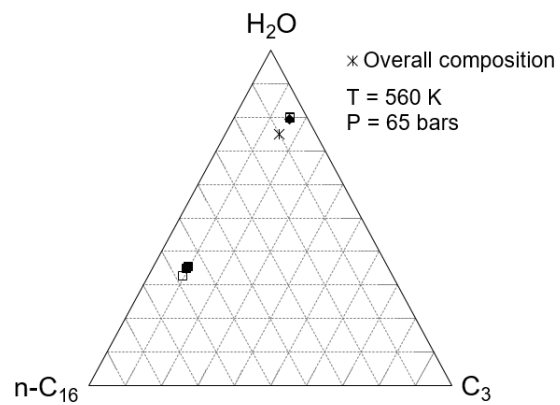
(d) After the 3rd iteration ($N_U = 2$ and $N_P = 4$)
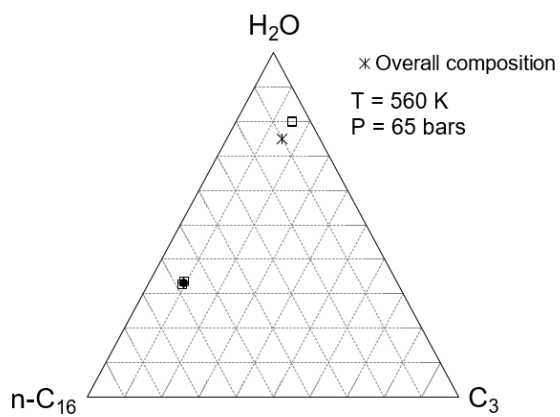
(e) After the 4th iteration ($N_U = 0$ and $N_P = 5$)
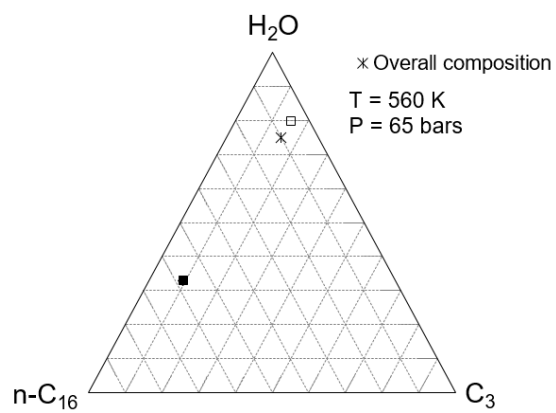
(f) After the 5th iteration ($N_U = 1$ and $N_P = 2$)
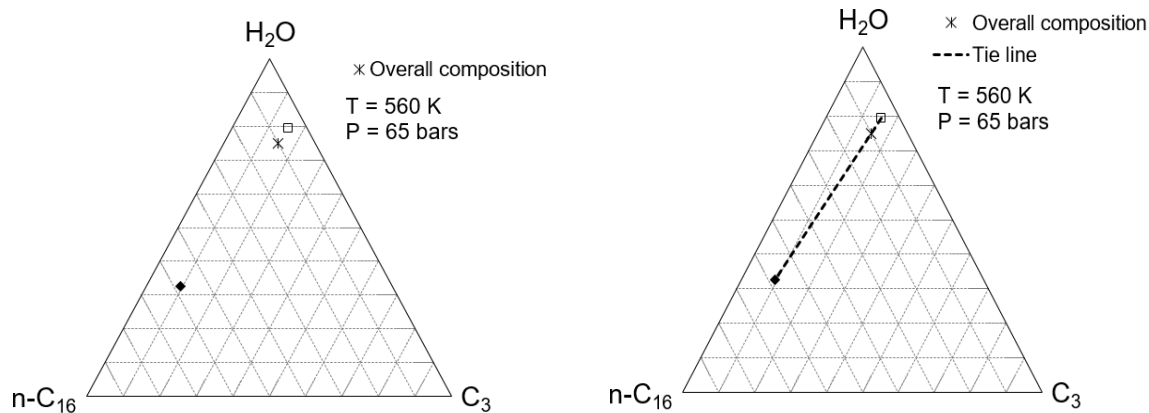
(g) After the 7th iteration ($N_U = 0$ and $N_P = 2$)

(h) After the 21st iteration ($N_U = 0$ and $N_P = 2$)

Figure D-1.1. Movement of sampling compositions for case 3.1 in chapter 3. A star represents the overall composition. Solid squares represent the sampling compositions in set U. The reference composition in set P is shown by a solid diamond, and the other sampling compositions in set P are hollow squares.
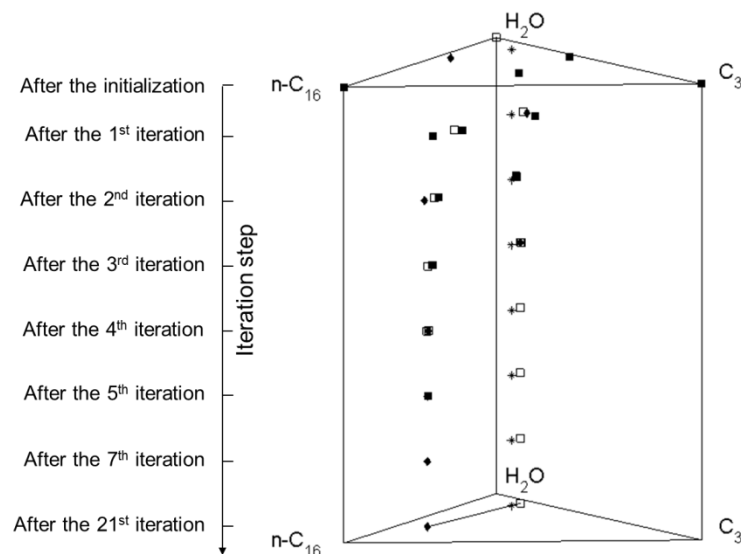
Figure D-1.2. Triangular prism to present sampling compositions at selected iteration steps for case 3.1 in chapter 3.

294

Appendix D-2: MOTIONS OF SAMPLING COMPOSITIONS FOR CASE 3.2 IN CHAPTER 3

Figure D-2.1 presents the motion of sampling compositions for the binary mixture consisting of 97% C_1 and 3% H_2S at 190 K and 40.53 bars (Tables 3.3 and 3.4). The convergence behavior was presented in Figure 3.6.

N_S of five is identified after initialization. Early in the iteration, compositions often switch between sets P and U, while smoothly changing their compositions. From the 7th iteration on, the compositions in set U move towards the L_1-like composition (the left lobe in Figure 3.5). The number of sampling compositions in set U, N_U, reduces from 3 to 2 to 1 at iteration steps 7, 10, and 31, respectively. From the 31st iteration on, the correct N_S, three (= N_P of two and N_U of one), is maintained until the final convergence at the 92nd iteration.
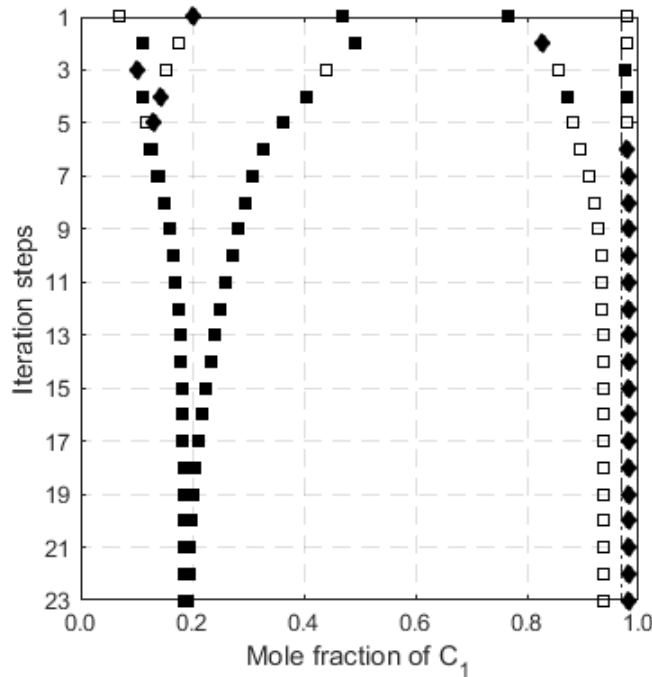
(a) Iteration steps from 1 through 23
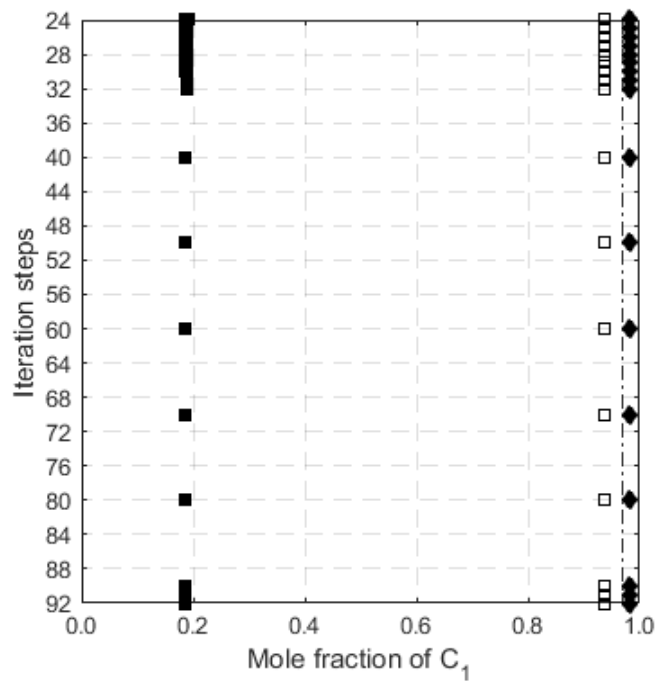
(b) Iteration steps from 24 through 92

Figure D-2.1. Movement of sampling compositions for case 3.2 in chapter 3. The vertical dashed line shows the location of the overall composition. Solid squares represent the sampling compositions in set U. The reference composition in set P is shown by a solid diamond, and the other sampling compositions in set P are hollow squares.

APPENDIX E: Stepwise Description and Flow Chart of Multiphase Isenthalpic Flash Integrated with Stability Analysis

Appendix E presents the stepwise description and the flow chart of the multiphase PH flash integrated with stability analysis given in Chapter 4.

Appendix E-1: STEPWISE DESCRIPTION

Step 1. Specify $\underline{H}_{spec}$, P, and overall composition $\underline{z}$, along with model parameters, such as critical temperature T_C, critical pressure P_C, acentric factor ω, and $N_C \times N_C$ binary interaction parameters (BIPs). Input an initial guess for dimensionless temperature, $T_D^{(1)}$, where the number in the bracket represents the iteration-step number $k = 1$.

Step 2. Set N_S sampling compositions $\underline{x}_j^{(k)}$ for $j = 1, 2,\ldots, N_S$.

Step 3. Calculate D_j (equation 3.1) with $\underline{z}$ as the reference composition for $j = 1, 2, \ldots, N_S$. Select the sampling composition that has the minimum D value as the reference composition $\underline{x}_r^{(k)}$. Calculate K values, $\underline{K}_j^{(k)}$, by use of $\ln Kij = \ln\varphi ir - \ln\varphi ij$ for $j = 1, 2, \ldots, N_S$ and $j \neq r$, which is derived from equations 4.17 and 4.18. Recalculate D_j with the selected reference composition. Set N_U as the number of sampling compositions that have positive D values. $N_P = N_S - N_U$. If $N_P = 1$, go to step 7. Otherwise, go to step 4.

Step 4. Check to see if the feasible region for the RR equations (set P) is bounded (Okuno et al. 2010b). If so, go to step 6. Otherwise, go to step 5.

Step 5. Exclude from set P as many sampling compositions as required until the feasibility is satisfied for the given RR problem. The exclusion is conducted in the descending order in terms of D within set P. Then, update N_P. If $N_P = 1$, go to step 7. Otherwise, continue to step 6.

Step 6. Solve the RR equations (equation 3.5) for set P to obtain $\beta_j^{(k)}$ and $\underline{x}_j^{(k)}$ for j = 1, 2,…, N_P.

Step 7. Calculate $\theta_j^{(k)}$ and $\underline{x}_j^{(k)}$ for set U, where j = (N_P + 1), (N_P + 2)…, N_S.

Step 8. If $\theta_j^{(k)} > 0$ for j = (N_P + 1), (N_P + 2)…, N_S, go to step 9. Otherwise, set $\theta_j^{(k)} = 0$, and select the sampling composition that has the minimum θ_j value, as the reference composition. Then, update N_P and K values with the new reference composition. Go to step 11.

Step 9. If $0 < \beta_j^{(k)} < 1$ for j = 1, 2,…, N_P, go to step 10. Otherwise, set $\beta_j^{(k)} = 0$ and $\theta_j^{(k)} \neq 0$, and select the sampling composition with $0 < \beta_j < 1$ as the reference composition. Then, update N_P and K values with the new reference composition. Go to step 11.

Step 10. Stop, if $\left\| \underline{f}_j^{(k)} \right\|_\infty < \varepsilon_f$ (e.g., $\varepsilon f = 10^{-10}$) and $|g_{NP}^{(k)}| < \varepsilon_h$ (e.g., $\varepsilon_h = 10^{-10}$) for j = 1, 2,…, N_S (r ≠ j). Otherwise, go to step 11.

Step 11. Check for merging compositions. If $\left\| \underline{x}_j^{(k)} - \underline{x}_q^{(k)} \right\|_\infty < \varepsilon_x$ (e.g., $\varepsilon_x = 10^{-3}$) for j, q = 1, 2,…, N_S, and j ≠ q, delete the jth sampling composition. Add a new sampling composition, and update the reference composition. Then, go to step 12.

Step 12. Update K values in composition space for sets P and U by use of $\ln K_{ij} = \ln \varphi_{ir} - \ln \varphi_{ij}$ for j = 1, 2, …, N_S and j ≠ r. If N_P = 1, go to step 7. Otherwise, go to step 13.

Step 13. Construct the $N_P \times N_P$ Jacobian matrix only for set P, and calculate its condition number. If the condition number is greater than ξ (e.g., 10^6), go to step 16. Otherwise, perform one Newton's iteration step to obtain $\beta_j^{(k+1)}$ and $T_D^{(k+1)}$ for j = 1, 2,…, N_P.

298

Step 14. Check to see if $T_D^L < T_D^{(k+1)} < T_D^U$. If so, continue to step 15. Otherwise, update $T_D^{(k+1)}$ using the Regula Falsi method (Zhu and Okuno 2014b).

Step 15. Update K values in temperature space for sets P and U: $\ln K_{ij}^{(k+1)} = \ln K_{ij}^{(k)} + [T_D^{(k)}(T_D^{(k+1)} - T_D^{(k)})/T_D^{(k+1)}](\partial \ln K_{ij}/\partial T_D)^{(k)}$. Go to step 4 after increasing the iteration-step number by one: $k = k + 1$.

Step 16-1. Set t_L to the highest temperature between T_D^L and $T_D^{(k)}$ that gives a negative g_{NP}. Set t_U to the lowest temperature between T_D^U and $T_D^{(k)}$ that gives a positive g_{NP}.

Step 16-2. $T_D^{(k+1)} = 0.5(t_L + t_U)$.

Step 16-3. Perform PT flash at $T_D^{(k+1)}$ to calculate $\beta_j^{(k+1)}$, $\theta_j^{(k+1)}$ and $\underline{x}_j^{(k+1)}$ such that $\left\| \underline{f}_j^{(k+1)} \right\|_\infty < \varepsilon_f$ for $j = 1, 2, \ldots, N_S$, and $r \neq j$.

Step 16-4. Calculate the condition number of the Jacobian matrix. If it is greater than ξ, continue to step 16-5. Otherwise, go to step 4.

Step 16-5. Calculate $g_{NP}^{(k+1)}$. If $|g_{NP}^{(k+1)}|$ is less than ε_h, stop. Otherwise, $t_L = T_D^{(k+1)}$ for $g_{NP}^{(k+1)} < 0$, and $t_U = T_D^{(k+1)}$ for $g_{NP}^{(k+1)} > 0$. Then, go to step 16-2 after increasing the iteration-step number by one; $k = k + 1$.

In Step 3, a reference composition is initialized to define equation 4.17. First, function D with the overall composition as the reference is used to calculate D_j (equation 3.1) at N_S sampling compositions ($j = 1, 2, \ldots, N_S$). Then, the initial reference composition is defined at which D is the minimum among the N_S sampling compositions. This procedure is also used when a new reference composition is to be selected during the iterations. Note that D values are used only for the initialization of sampling compositions.

In Step 11, the sampling composition to be added is taken from the previous iteration in this research.   The composition that has a greater distance from that of the merged sampling composition is added.   The purpose of adding a sampling composition in step 11 is to keep the original Ns, which should be always equal to or greater than the number of stationary points on the tangent plane distance function.   It has been observed that this step is crucial for PH flash for water/solvent/bitumen mixtures, in which the number and identities of phases can change frequently with temperature for a given overall composition and pressure.

Appendix E-2: FLOW CHART

This section presents the flow chart of the multiphase PH flash integrated with stability analysis given in Chapter 4.

Specify $\underline{H}_{spec}$, P, $\underline{z}$, T_c, P_c, ω, and BIPs. Set iteration number k = 1 and input $T_D^{(k)}$

Set N_S sampling compositions $\underline{x}_j^{(k)}$ for j = 1, 2, ..., N_S

Calculate D_j with $\underline{z}$ as the reference composition, and select the sampling composition with the minimum D value as the reference composition $\underline{x}_r^{(k)}$

Initialize K values, $\underline{K}_j^{(k)}$, and recalculate D_j with the selected reference composition. Set N_U as the number of sampling compositions with positive D values. $N_P = N_S - N_U$

$N_P = 1$?　　　YES

NO

'$N_P - 1$' Feasible RR?　　　NO

YES

Set $\beta^{(k)} = 0$ and $\theta^{(k)} \neq 0$ for the sampling composition that has maximum D value within set P

Update N_P

Solve RR equations to obtain $\beta_j^{(k)}$ and $\underline{x}_j^{(k)}$ for j = 1, 2, ..., N_P

$N_P = 1$?　　　YES

NO

'$N_P - 1$' Feasible RR?　　　NO

YES

Calculate $\theta_j^{(k)}$ and $\overline{x}_j^{(k)}$ for j = (N_P + 1), (N_P + 2), ..., N_S

Update reference composition and K values

Update N_P　　Update reference composition and K values　　NO　　$\theta_j^{(k)} > 0$ for j = (N_P + 1), (N_P + 2), ..., N_S?

YES

Update N_P　　Update reference composition and K values　　NO　　$0 < \beta_j^{(k)} < 1$ for j = 1, 2, ..., N_P?

YES

Output $\underline{x}_j^{(k)}$, $\beta_j^{(k)}$, $\theta_j^{(k)}$ and $T_D^{(k)}$　　YES　　$\|\underline{f}_j^{(k)}\|_\infty < \varepsilon_f$ and $|g_{NP}^{(k)}| < \varepsilon_h$?

NO

Delete the jth sampling point if $\theta_j^{(k)} > 0$　　YES　　$\|\underline{x}_j^{(k)} - \underline{x}_q^{(k)}\|_\infty < \varepsilon_f$ for j, q = 1, 2, ..., N_S, j ≠ q?

Add a new sampling point $\underline{x}_j^{(k)}$ and update reference composition

NO

Update K values in composition space for j = 1, 2, ..., N_S

$N_P = 1$?　　　YES

NO

Construct the $N_P \times N_P$ Jacobian matrix

Let $t_L = \max\{T_D^{(k)}, T_D^L\}$ for $g_{NP} < 0$, $t_U = \min\{T_D^{(k)}, T_D^U\}$ for $g_{NP} > 0$

Jacobian condition number < ξ ?　　　NO

YES

Calculate $T_D^{(k+1)} = 0.5(t_L + t_U)$

Perform PT flash at $T_D^{(k+1)}$ to calculate $\beta_j^{(k+1)}$, $\theta_j^{(k+1)}$, and $\underline{x}_j^{(k+1)}$, such that $\|\underline{f}_j^{(k+1)}\|_\infty < \varepsilon_f$ for j = 1, 2, ..., N_S, and j ≠ r

Jacobian condition number < ξ ?　　　YES

Output $\underline{x}_j^{(k+1)}$, $\beta_j^{(k+1)}$, $\theta_j^{(k+1)}$ and $T_D^{(k+1)}$

NO

$|g_{NP}^{(k+1)}| < \varepsilon_h$?　　　YES

NO

Let $t_L = T_D^{(k+1)}$ for $g_{NP}^{(k+1)} < 0$, and $t_U = T_D^{(k+1)}$ for $g_{NP}^{(k+1)} > 0$　　(k = k + 1)

Perform one Newton's iteration step to obtain $\beta_j^{(k+1)}$ and $T_D^{(k+1)}$ for j = 1, 2, ..., N_P

$T_D^L < T_D^{(k+1)} < T_D^U$?　　　NO　　Update $T_D^{(k+1)}$ using Regula Falsi method

YES

(k = k + 1)　　Calculate $\ln K_{ij}^{(k+1)} = \ln K_{ij}^{(k)} + [T_D^{(k)}(T_D^{(k+1)} - T_D^{(k)})/T_D^{(k+1)}](\partial \ln K_{ij}/\partial T_D)^{(k)}$ for j = 1, 2, ..., N_S

301

APPENDIX F: Minimum Distance Conditions for Five Reservoir Oils

Appendix F presents a summary of the minimum distance conditions for five other reservoir oils given in Chapter 5.　The five oils are oil B (Shelton and Yarborough 1977), West Sak oil (DeRuiter et al. 1994), JEMA (Khan et al. 1992), oil G (Creek and Sheffield 1993), and BSB oil (Khan et al. 1992).

Appendix F-1: Oil B (Shelton and Yarborough 1977)

Figures F-1.1 presents the minimum distance conditions at the three-phase trailing edge at two N_{Pe} numbers for oil B (Shelton and Yarborough 1977) displaced by CO_2 at 0.4 PVI at 94°F.　Figure F-1.2 presents the minimum distance conditions at the three-phase leading edge at two N_{Pe} numbers for oil B (Shelton and Yarborough 1977) displaced by CO_2 at 0.4 PVI at 94°F.　The measured MMP is 1450 psia, and the calculated OIP is 1475 psia.
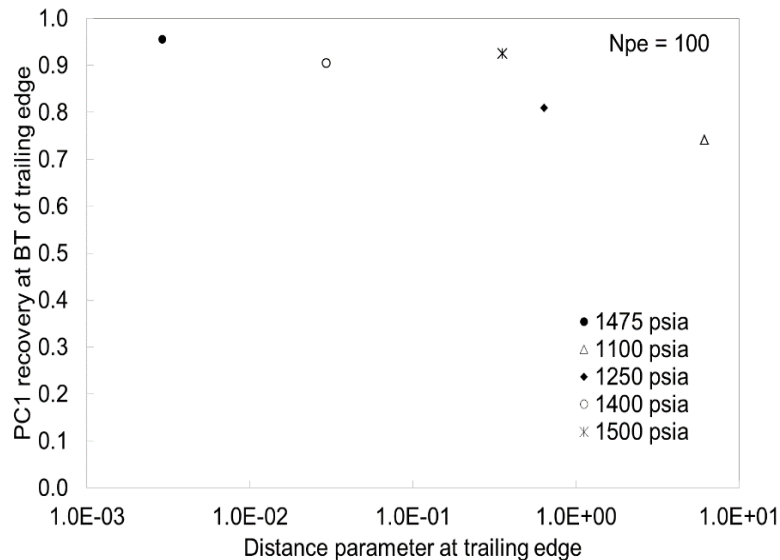
(a)

Figure F-1.1 (Continued below)

(b)

Figure F-1.1. Minimum distance condition at the three-phase trailing edge at two N_{Pe} numbers for oil B displaced by CO_2 at 0.4 PVI at 94 ℉.   The properties of components used can be found in Kumar (2016). (a) N_{Pe} = 100.   (b) N_{Pe} = 4000.

(a)

Figure F-1.2 (Continued below)

(b)

Figure F-1.2. Minimum distance condition at the three-phase trailing edge at two N_{Pe} numbers for oil B displaced by CO_2 at 0.4 PVI at 94 °F. The properties of components used can be found in Kumar (2016). (a) $N_{Pe} = 100$. (b) $N_{Pe} = 4000$.

Appendix F-2: West Sak Oil (DeRuiter et al. 1994)

Figure F-2.1 presents the minimum distance conditions at the three-phase trailing edge at two N_{Pe} numbers for West Sak Oil (DeRuiter et al. 1994) displaced by enriched gas at 0.4 PVI at 65°F. Figure F-2.2 presents the minimum distance conditions at the three-phase leading edge at two N_{Pe} numbers for West Sak Oil (DeRuiter et al. 1994) displaced by enriched gas at 0.4 PVI at 65°F. The measured MMP is 1500 psia, and the calculated OIP is 1500 psia.

(a)

(b)

Figure F-2.1. Minimum distance condition at the three-phase trailing edge at two N_{Pe} numbers for West Sak Oil displaced by enriched gas at 0.4 PVI at 65 ℉. The properties of components used can be found in Kumar (2016). (a) $N_{Pe} = 100$. (b) $N_{Pe} = 4000$.

305

(a)

(b)

Figure F-2.2. Minimum distance condition at the three-phase leading edge at two N_{Pe} numbers for West Sak Oil displaced by enriched gas at 0.4 PVI at 65 ℉.   The properties of components used can be found in Kumar (2016). (a) N_{Pe} = 100.   (b) N_{Pe} = 4000.

Appendix F-3: JEMA Oil (Khan et al. 1992)

Figure F-3.1 presents the minimum distance conditions at the three-phase trailing edge at two N_{Pe} numbers for JEMA Oil (Khan et al. 1992) displaced by CO_2 at 0.4 PVI at 110°F. Figure F-3.2 presents the minimum distance conditions at the three-phase leading edge at two N_{Pe} numbers for for JEMA Oil (Khan et al. 1992) displaced by CO_2 at 0.4 PVI at 110°F. The measured MMP is 1250 psia, and the calculated OIP is 1200 psia.
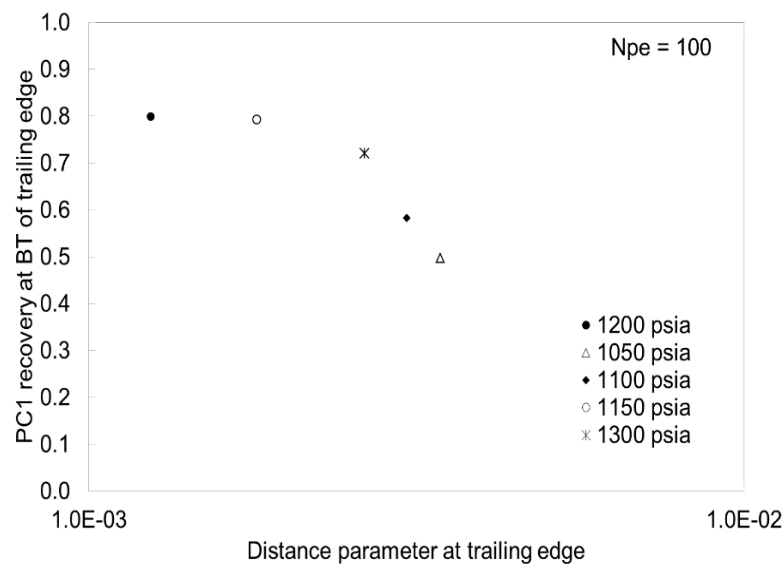
(a)

Figure F-3.1 (Continued below)
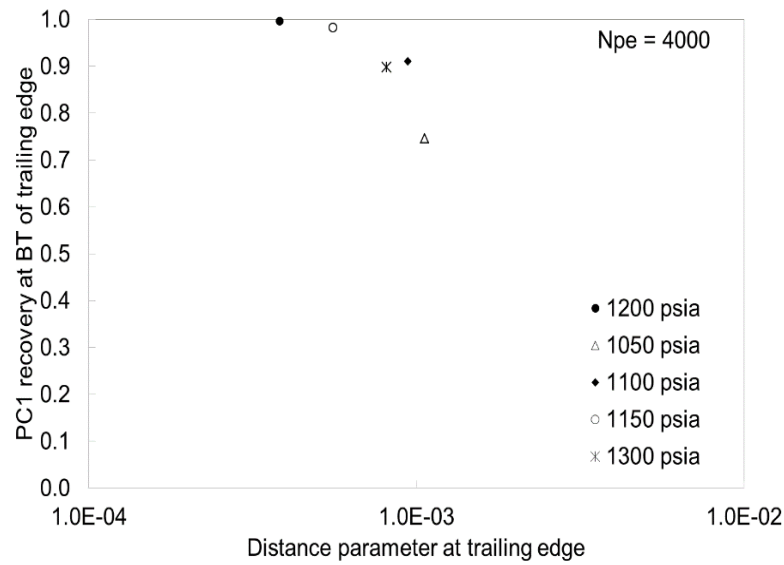
(b)

Figure F-3.1. Minimum distance condition at the three-phase trailing edge at two N_{Pe} numbers for JEMA Oil displaced by CO_2 at 0.4 PVI at 110 °F. The properties of components used can be found in Kumar (2016). (a) $N_{Pe} = 100$. (b) $N_{Pe} = 4000$.

(a)

Figure F-3.2 (Continued below)

The figure shows a scatter plot with "PC1 recovery at BT of leading edge" on the y-axis (ranging from 0.0 to 1.0) and "Distance parameter at leading edge" on the x-axis (from 1.0E-02 to 1.0E-01). Legend: • 1200 psia, △ 1050 psia, ◆ 1100 psia, ○ 1150 psia, ✳ 1300 psia. Npe = 4000.

(b)

Figure F-3.2. Minimum distance condition at the three-phase leading edge at two N_{Pe} numbers for JEMA Oil displaced by CO_2 at 0.4 PVI at 110 °F. The properties of components used can be found in Kumar (2016). (a) $N_{Pe} = 100$. (b) $N_{Pe} = 4000$.

Appendix F-4: Oil G (Creek and Sheffield)
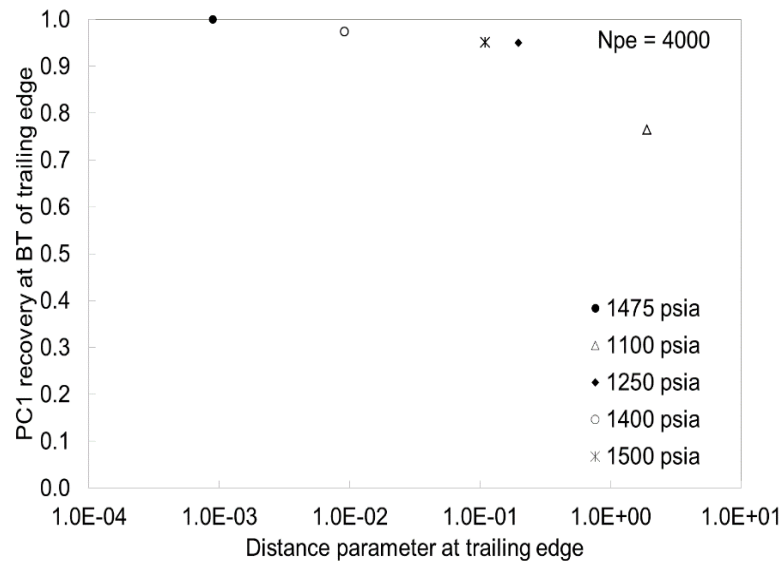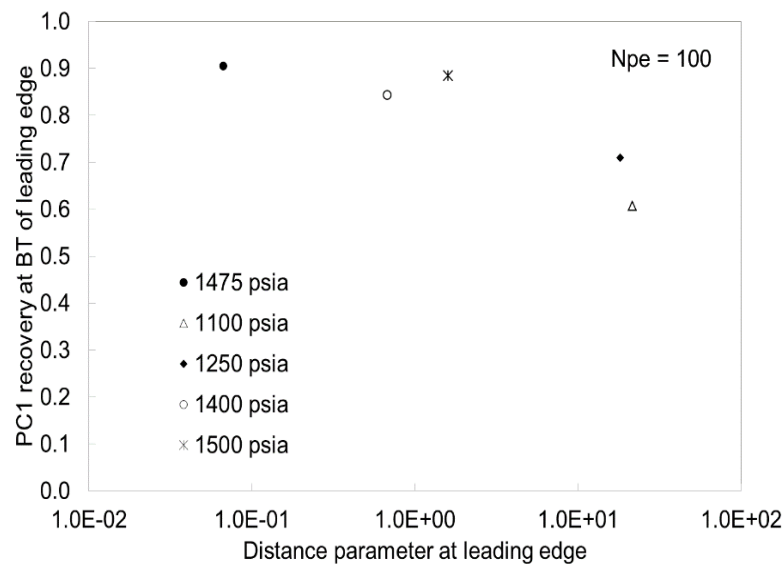
Figure F-4.1 presents the minimum distance conditions at the three-phase trailing edge at two N_{Pe} numbers for Oil G (Creek and Sheffield) displaced by CO_2 at 0.4 PVI at 94°F. Figure F-4.2 presents the minimum distance conditions at the three-phase leading edge at two N_{Pe} numbers for Oil G (Creek and Sheffield) displaced by CO_2 at 0.4 PVI at 94°F. The measured MMP is 1035 psia, and the calculated OIP is 1075 psia.
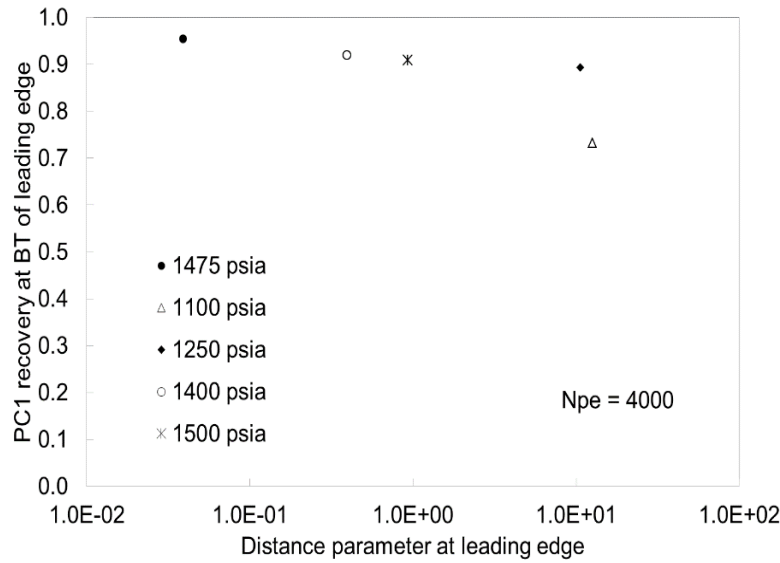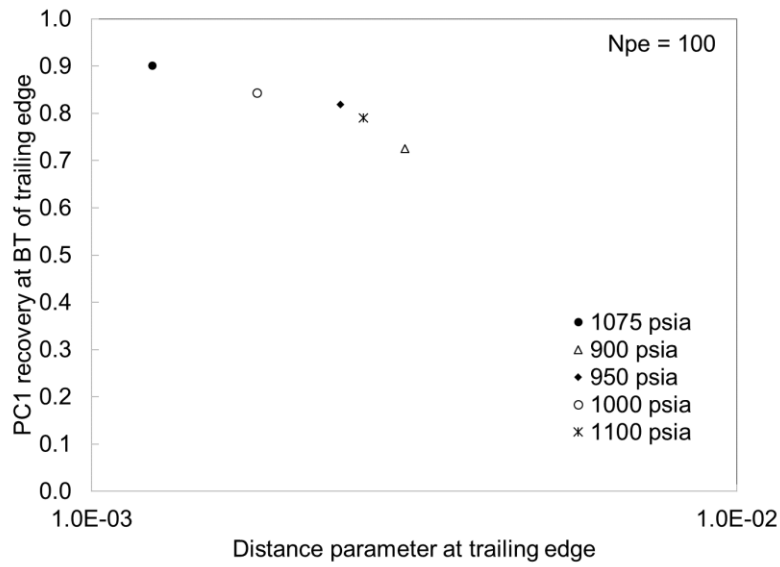
(a)
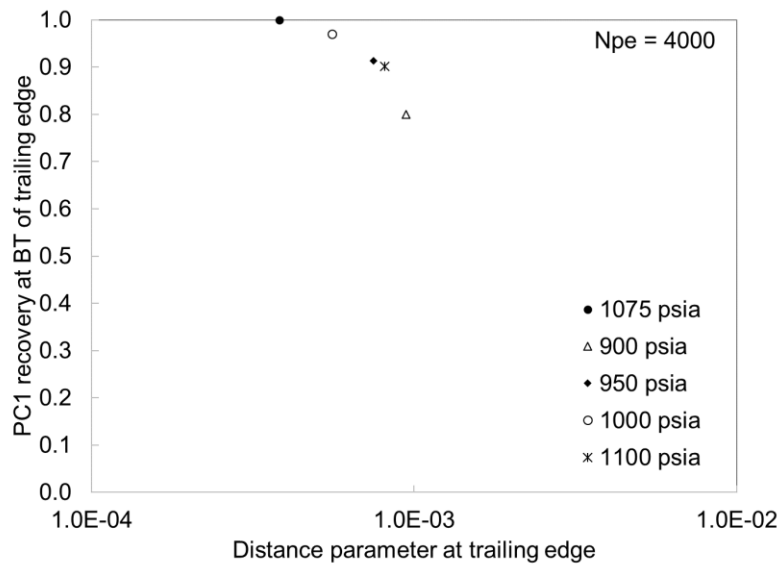
(b)

Figure F-4.1. Minimum distance condition at the three-phase trailing edge at two N_{Pe} numbers for Oil G displaced by CO_2 at 0.4 PVI at 94 ℉.   The properties of components used can be found in Kumar (2016). (a) $N_{Pe} = 100$.   (b) $N_{Pe} = 4000$.
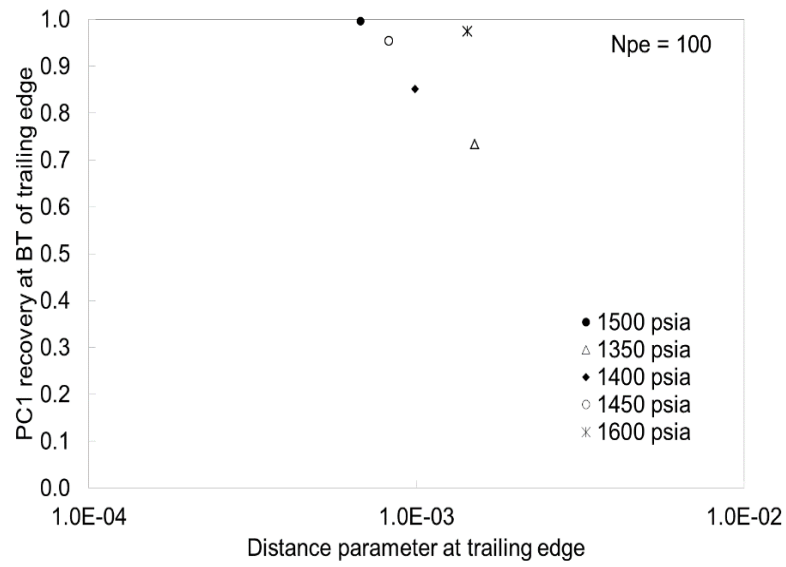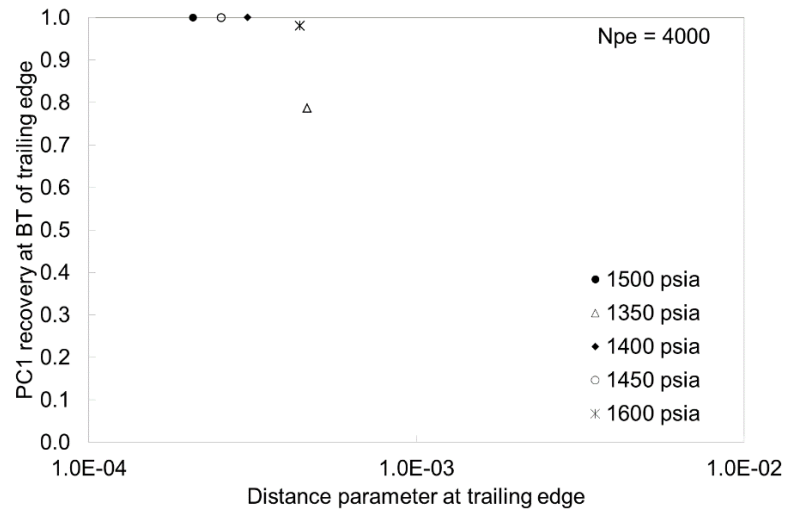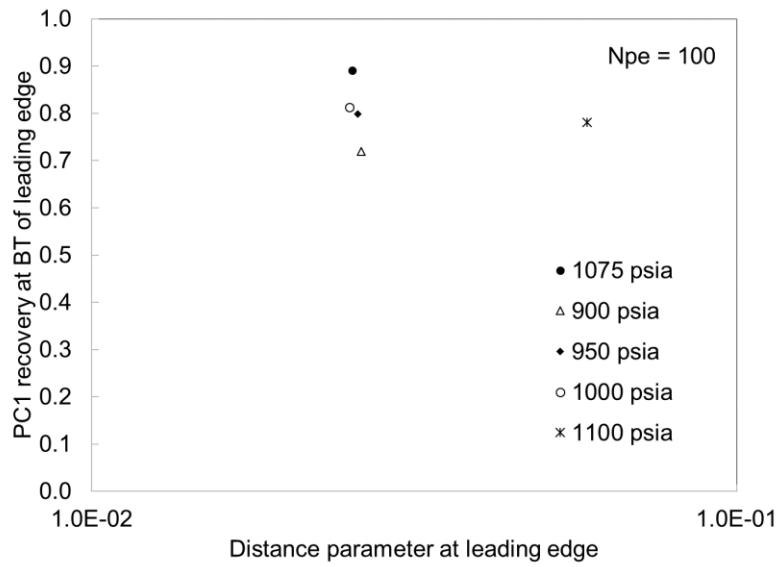
(a)
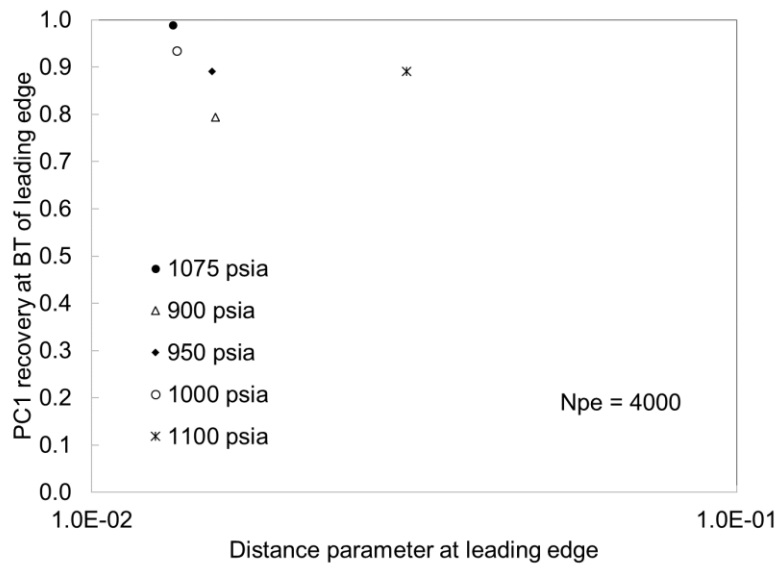
(b)

Figure F-4.2. Minimum distance condition at the three-phase trailing edge at two N_{Pe} numbers for Oil G displaced by CO_2 at 0.4 PVI at 94 °F. The properties of components used can be found in Kumar (2016). (a) $N_{Pe} = 100$. (b) $N_{Pe} = 4000$.

311

Appendix F-5: BSB Oil (Khan et al. 1992)

Figure F-5.1 presents the minimum distance conditions at the three-phase trailing edge at two N_{Pe} numbers for BSB oil (Khan et al. 1992) displaced by CO_2 at 0.4 PVI at 105°F. Figure F-5.2 presents the minimum distance conditions at the three-phase leading edge at two N_{Pe} numbers for BSB oil (Khan et al. 1992) displaced by CO_2 at 0.4 PVI at 105°F. The measured MMP is 1200 psia, and the calculated OIP is 1250 psia.

Npe = 100

- 1250 psia
△ 1050 psia
◆ 1100 psia
○ 1200 psia
✳ 1300 psia
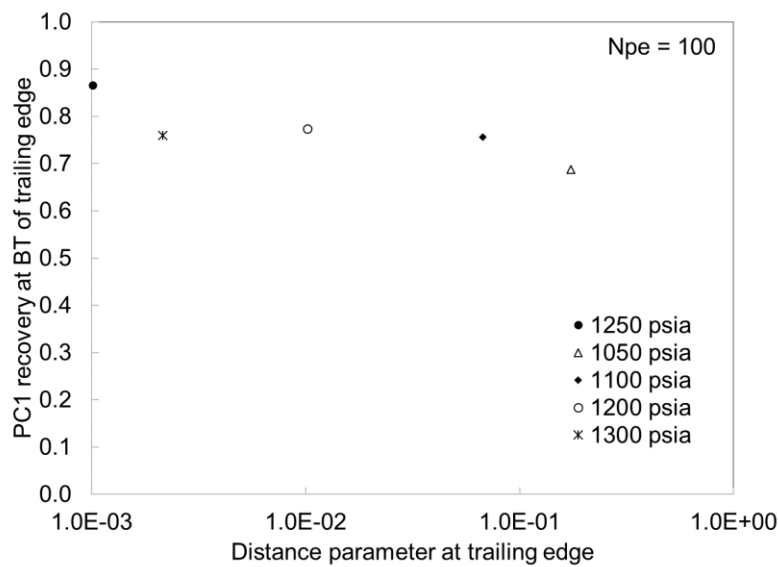
(a)

Figure F-5.1 (Continued below)
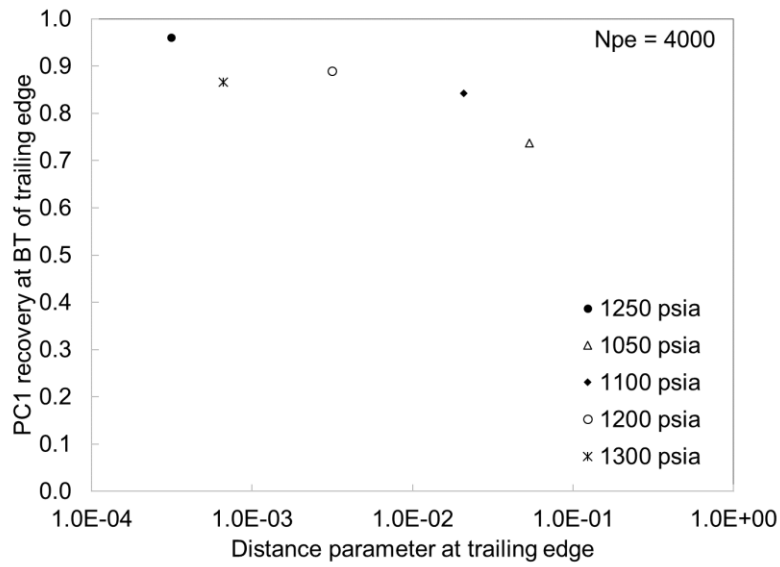
(b)

Figure F-5.1. Minimum distance condition at the three-phase trailing edge at two N_{Pe} numbers for BSB oil displaced by CO_2 at 0.4 PVI at 105 °F. The properties of components used can be found in Kumar (2016). (a) $N_{Pe} = 100$. (b) $N_{Pe} = 4000$.
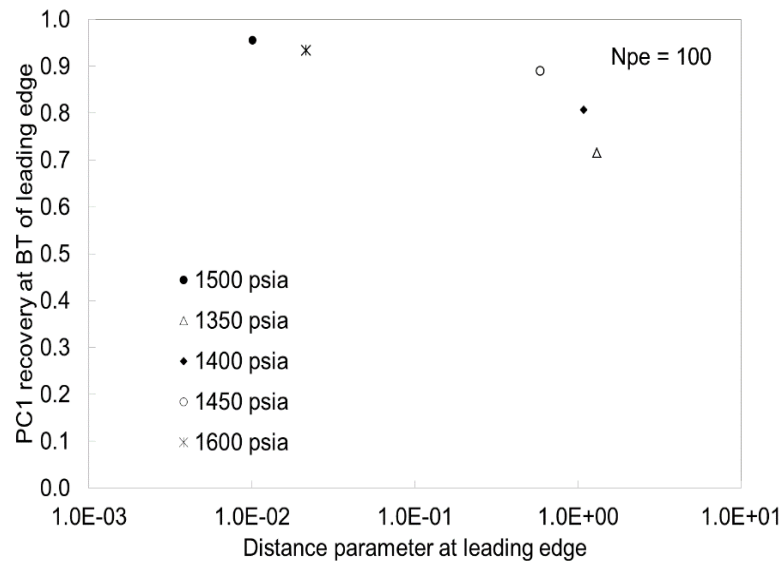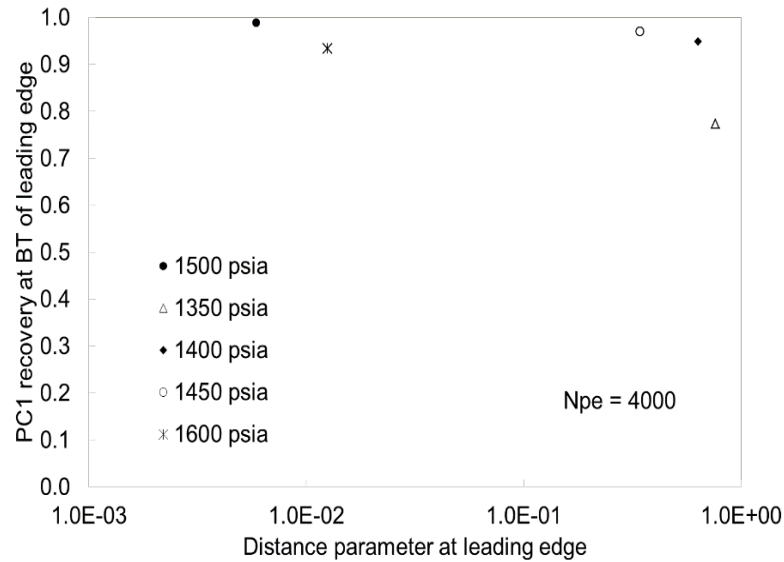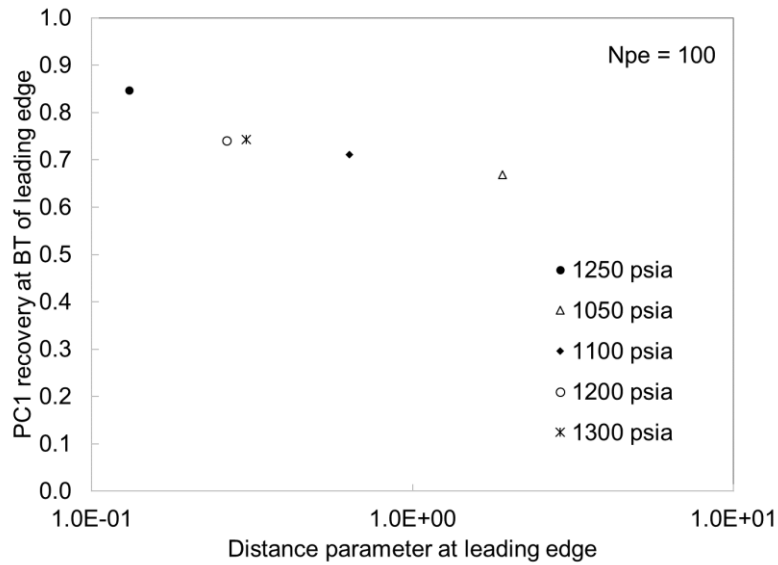

(a)

Figure F-5.2 (Continued below)
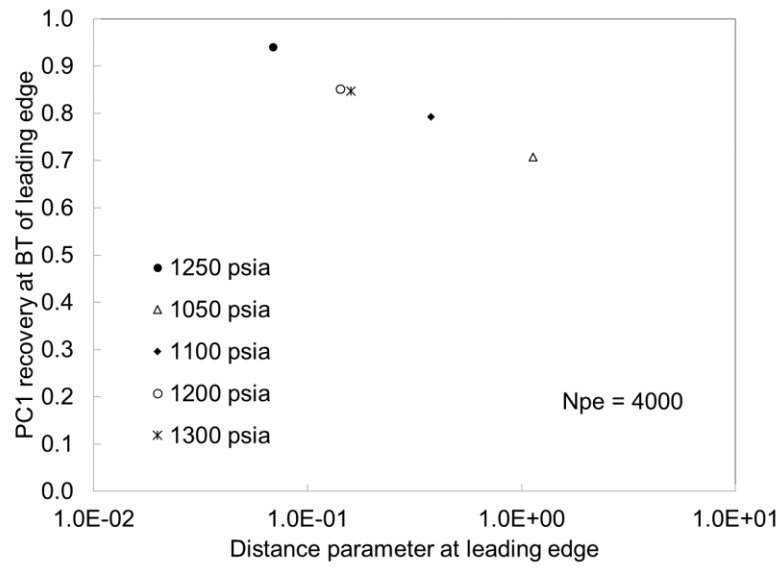
(b)

Figure F-5.2. Minimum distance condition at the three-phase leading edge at two N_{Pe} numbers for BSB oil displaced by CO_2 at 0.4 PVI at 105 °F. The properties of components used can be found in Kumar (2016). (a) $N_{Pe} = 100$. (b) $N_{Pe} = 4000$.

Glossary
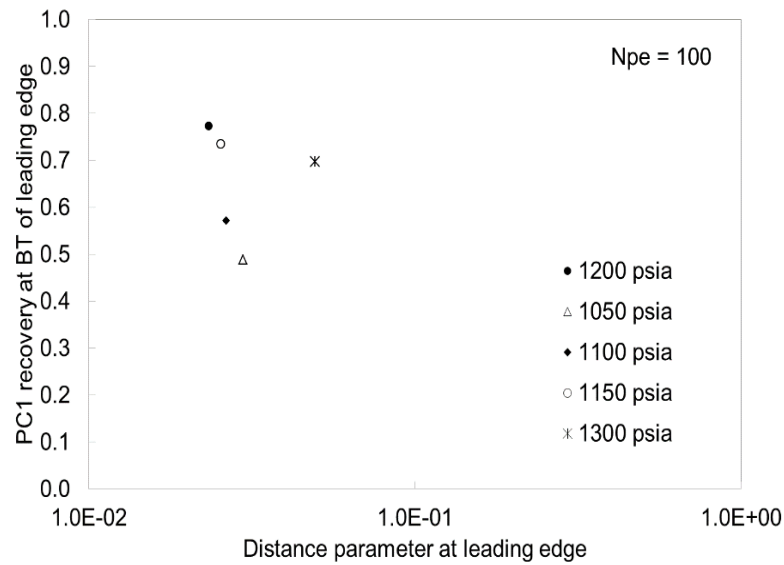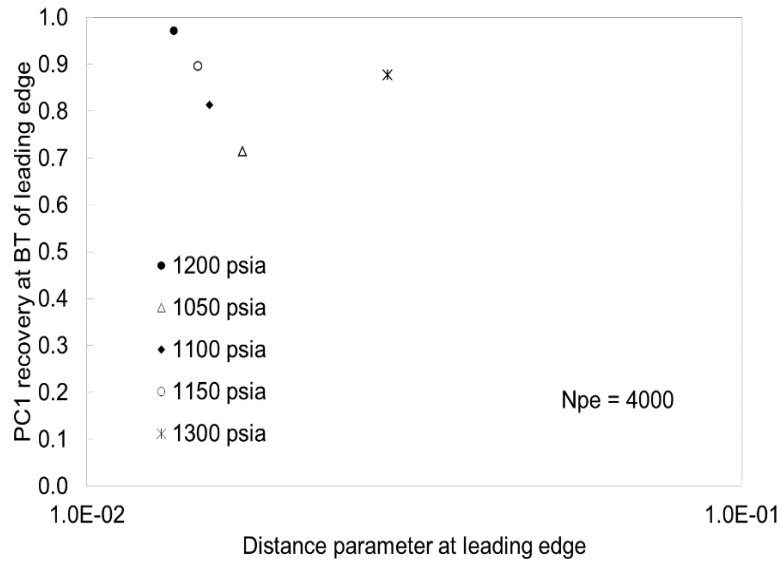
Roman Symbols

a	Attraction parameter defined in equation 2.51
A	Dimensionless attraction parameter for a cubic equation of state
b	Co-volume parameter defined in equation 2.51
B	Dimensionless co-volume parameter for a cubic equation of state
c_{ij}	Volumetric fraction of component i in phase j
$\underline{c}_j$	Vector consisting of c_{ij} as defined in equation 2.6
C	Constant defined for temperature oscillation check
C_i	Overall volume fraction of component i
$C_{Pi}{}^0$	Coefficients of component i defined in equation A-1.5
C_{Pj}	Heat capacity of phase j
$\bar{\bar{D}}$	Diagonal matrix defined in equation 2.12
D	Tangent plane distance defined in equation 2.22 or Diagonal matrix defined in equation 4.5
D_R	Dimensionless tangent plane distance defined in equation 2.23
f_{ij}	Fugacity of component i in phase j, or residual of fugacity equations defined in equation 3.3
f_j	Fractional flow of phase j
$\vec{f}$	Vector consisting of N_C residuals of the fugacity equations
F	Non-monotonic convex function defined in equation 4.3
F_i	Overall fractional flow of component i
g_j	Residuals of material balance equations defined in equation 2.49
g_{NP}	Residual of the enthalpy constraint defined in equation 2.50
GB	Grid block
G_R	Dimensionless Gibbs free energy defined in equation 2.40
$\underline{G}$	Molar Gibbs free energy
$\bar{\underline{G}}$	Partial molar Gibbs free energy
H	Enthalpy or the Hessian matrix defined in equation 4.5
$\underline{H}$	Molar enthalpy
J	Jacobian matrix
k_{ij}	Binary interaction parameter between components i and j
K_i	K value of component i for a two-phase system defined in equation 2.29
K_{ij}	K value of component i in phase j
$\underline{K}_j$	Vector consisting of N_C K values for phase j
$\vec{\vec{K}}_{ij}$	Dispersion tensor for component i in phase j
L_1	Oleic phase
L_2	Solvent-rich liquid phase
n	Exponent used in distribution in Appendix C-2
N_C	Number of components

N_{GB}	Number of grid blocks used in simulations
N_P	Number of phases or Number of sampling compositions in set P
N_{Pe}	Péclet number defined in equation 5.7
N_S	Number of sampling compositions
N_{Si}	Number of sampling compositions distributed in R_i defined in Appendix C-2
N_{Smax}	Maximum number of initial sampling compositions used in distribution in Appendix C-2
N_U	Number of sampling compositions in set U
P	Pressure
P_C	Critical pressure
P_R	Reduced pressure
Q_i	Recovery of component i
r_{1i}	Number of segments used in step 4 in Appendix C-2
r_{2i}	Number of segments used in step 6 in Appendix C-2
R	Universal gas constant
R_i	Region defined in step 2 in Appendix C-2
S_j	Saturation of phase j
$\underline{S}$	Molar entropy
t_D	Dimensionless time in pore volumes
t_i	Parameter defined in equation 2.49
T	Temperature or tangent plane defined in equation 2.21
T_C	Critical temperature
T_D	Dimensionless Temperature
T_0	273.15 K defined in equation A-1.5
T_R	Reduced temperature
$\vec{u}_j$	Flux of phase j
V	Vapor phase
V_C	Critical volume
V_D	Dimensionless velocity defined in equation 2.6
$\underline{V}$	Molar volume
W	Aqueous phase
x_D	Dimensionless distance from the injector
x_i	Mole fraction of component i in the L phase for a L-V two-phase system
x_{ij}	Mole fraction of component i in phase j
$\underline{x}_j$	Vector consisting of x_{ij}
X_i	Parameter defined in equation 2.27
y_i	Mole fraction of component i in the V phase for a L-V two-phase system
Y	Matrix defined in equation 4.5
z_i	Overall mole fraction of component i
Z_j	Compressibility factor of phase j

Greek Symbols

$\underline{\rho}_i$	Molar density of component i
α	Coefficients defined in in equation A-1.14
$\boldsymbol{\beta}$	Vector of independent mole fractions β_j for $j = 1, 2, \ldots, (N_P - 1)$
β_j	Mole fraction of phase j
γ:	Parameter defined in equation 2.6
δ:	Distance parameters defined in equations 2.7, 2.8, 2.9, and 2.10
ε	Convergence or merging criterion or small values used in equations 2.7, 2.8, 2.9, and 2.10
ε_o	Constant used for temperature oscillation check
θ_j	Parameter defined in equation 3.3 or Parameter for phase j calculated by equation 3.6
$\underline{\rho}_j$	Molar density of phase j
ϕ	Porosity
φ_{ij}	Fugacity coefficient of component i in phase j
ω	Acentric factor
Γ	Parameter defined in equations 2.9, and 2.10

Subscripts

C	Critical property
D	Dimensionless property
f	Fugacity equations
h	Enthalpy constraint
i	Component index
ini	Initial condition
int	Intersection
j	Phase index
k	Grid block index
m	Mixture or material balance
r	Reference composition
ref	Reference value
sol	Solution condition
spec	Specified value
V	Vapor phase
W	Aqueous phase
w	Water component
x	Composition

Superscripts

D	Downstream used in equation 2.5
dep	Departure
IG	Ideal gas
IGM	Ideal gas mixture

k	Iteration step number
L	Lower bound used in equation 4.16 or leading edge
n	Time step index
t	Total property
T	Transpose or trailing edge
U	Upper bound used in equation 4.16
U	Upstream used in equation 2.5
vap	Vapor pressure

Abbreviations

1D	One-dimensional
2D	Two-dimensional
3D	Three-dimensional
BIP	Binary interaction parameter
BSB	Bob Slaughter Block
BSBQ	Quaternary model of Bob Slaughter Block oil
BT	Breakthrough
C_B	Bitumen
CEP	Critical endpoint
CN	Carbon number
CP	Critical point
DS	Direct substitution
EOS	Equation of state
FCM	First-contact miscibility
GFE	Gibbs free energy
LCEP	Lower critical endpoint
MCM	Multi-contact miscibility
MMP	Minimum miscibility pressure
MOC	Method of characteristics
MW	Molecular weight
NWE	North Ward Estes
OIP	Optimal injection pressure
PC	Pseudo-component
PDE	partial differential equation
PH	Isenthalpic
PR	Peng-Robinson
PT	Isobaric-isothermal
P-T-x	Pressure-temperature-composition
PVI	Pore volume injected
PVT	pressure-volume-temperature
P-x	Pressure-composition
QNSS	Quasi-Newton successive substitution
RR	Rachford-Rice

SA	Stability analysis
SRK	Soave-Redlich-Kwong
SS	Successive substitution
SVD	Singular value decomposition
TPD	Tangent plane distance
UCEP	Upper critical endpoint
UTCOMP	Three-dimensional equation-of-state compositional reservoir simulator
WAG	Water-alternating-gas

References

Abdel-Ghani, R.M. 1995. *EOS Mixing Rules for Multi-Phase Behaviour*. MSc thesis, the University of Calgary, Calgary.

Abhvani, A.S. and Beaumont, D.N. 1987. Development of an Efficient Algorithm for the Calculation of Two-Phase Flash Equilibria. *SPE Reservoir Engineering* **2**(4): 695- 702.

Agarwal, R.K., Li, Y.K. Nghiem, L.X., and Coombe, D.A. 1991. Multiphase Multicomponent Isenthalpic Flash Calculations. *Journal of Canadian Petroleum Technology* **30**(3): 69-75.

Ahmadi, K. and Johns, R.T. 2011. Multiple-Mixing-Cell Method for MMP Calculations. *SPE Journal* **16**(4): 733-742.

Alsaifi, N.M. and Englezos, P. 2011. Prediction of Multiphase Equilibrium Using the PC-SAFT Equation of State and Simultaneous Testing of Phase Stability. *Fluid Phase Equilibria* **302**(1-2): 169-178.

Amani, M.J., Gray, M.R., and Shaw, J.M. 2013a. Phase Behavior of Athabasca Bitumen Water Mixtures at High Temperature and Pressure. *The Journal of Supercritical Fluids* **77**: 142-152.

Amani, M.J., Gray, M.R. and Shaw, J.M. 2013b. Volume of Mixing and Solubility of Water in Athabasca Bitumen at High Temperature and Pressure. *Fluid Phase Equilibria* **358**: 203-211.

Ammar, M.N. and Renon, H. 1987. The Isothermal Flash Problem: New Methods for Phase Split Calculations. *AIChE Journal* **33**(6): 926-939.

Baker, L.E., Pierce, A.C., and Luks, K.D. 1982. Gibbs Energy Analysis of Phase Equilibria. *SPE Journal* **22**(5): 731-742.

Belkadi, A., Yan, W., Moggia, E., Michelsen, M.L., Stenby, E.H., Aavatsmark, I., Vignati, E., and Cominelli, A. 2013. Speeding Up Compositional Reservoir Simulation through an Efficient Implementation of Phase Equilibrium Calculation. Paper presented at the SPE Reservoir Simulation Symposium, February 18-20, Woodlands, Texas.

Bhambri, P. and Mohanty, K.K. 2008. Two-and Three-Hydrocarbon Phase Streamline-Based Compositional Simulation of Gas Injections. *Journal of Petroleum Science and Engineering* **62**(1): 16-27.

Brantferger, K.M. 1991. *Development of a Thermodynamically Consistent, Fully Implicit, Compositional, Equation-of-State, Steamflood Simulator*. PhD dissertation, the University of Texas at Austin, Austin, Texas.

Brantferger, K.M., Pope, G.A., and Sepehrnoori, K. 1991. Development of a Thermodynamically Consistent, Fully Implicit, Equation-of-State, Compositional Steamflood Simulator. Paper presented at the SPE Symposium on Reservoir Simulation, February 17-20, Anaheim, California.

Bryant, D.W. and Monger, T.G. 1988. Multiple-Contact Phase Behavior Measurement and Application with Mixtures of CO_2 and Highly Asphaltic Crude. *SPE Reservoir Engineering* **3**(2): 701-710.

Bünz, A.P., Dohrn, R., and Prausnitz, J.M. 1991. Three-Phase Flash Calculations for Multicomponent Systems. *Computers and Chemical Engineering* **15**(1): 47-51.

Burgos-Solórzano, G.I., Brennecke, J.F., and Stadtherr, M.A. 2004. Validated Computing Approach for High-Pressure Chemical and Multiphase Equilibrium. *Fluid Phase Equilibria* **219**(2): 245-255.

Calsep. 2016. PVTsim Nova, Version 2.2. Lyngby, Denmark: Calsep International Consultants. www.pvtsim.com.

Castier, M. 2009. Solution of the Isochoric–Isoenergetic Flash Problem by Direct Entropy Maximization. *Fluid Phase Equilibria* **276**(1): 7-17.

Chaikunchuensakun, S., Stiel, L.I., and Baker, E.L. 2002. A Combined Algorithm for Stability and Phase Equilibrium by Gibbs Free Energy Minimization. *Industrial and Engineering Chemistry Research* **41**(16): 4132–4140.

Chang, Y.-B. 1990. *Development and Application of an Equation of State Compositional Simulator*. PhD dissertation, the University of Texas at Austin, Austin, Texas.

Chang, Y.-B., Pope, G.A., and Sepehrnoori, K. 1990. A Higher-Order Finite-Difference Compositional Simulator. *Journal of Petroleum Science and Engineering* **5**(1): 35-50.

Chien, M.C.H., Yardumian, H.E., Chung, E.Y., and Todd, W.W. 1989. The Formulation of a Thermal Simulation Model in a Vectorized, General Purpose Reservoir Simulator. Paper presented at the SPE Symposium on Reservoir Simulation, February 6-8, Houston, Texas.

Christiansen, R.L. 1986. *Method of Determining the Minimum Level of Enrichment for a Miscible Gas Flood*. United States Patent: 4610160.

Corazza, M.L., Corazza, F.C., Cardozo Filho, L., and Dariva, C. 2007. A Subdivision Algorithm for Phase Equilibrium Calculations at high Pressures. *Brazilian Journal of Chemical Engineering* **24**(4): 611-622.

Creek, J.L. and Sheffield, J.M. 1993. Phase Behavior, Fluid Properties, and Displacement Characteristics of Permian Basin Reservoir Fluid/CO_2 Systems. *SPE Reservoir Engineering* **8**(1): 34-42.

Danesh, A. 1998. P*VT and Phase Behaviour of Petroleum Reservoir Fluids*, New York: Elsevier.

Davenport, A.J., Rowlinson, J.S., and Saville, G. 1966. Solutions of Three Hydrocarbons in Liquid Methane. *Transactions of the Faraday Society* **62**: 322-327.

Deiters, U. and Schneider, G.M. 1976. Fluid Mixtures at High Pressures. Computer Calculations of the Phase Equilibria and the Critical Phenomena in Fluid Binary Mixtures

from the Redlich-Kwong Equation of State. *U. Deiters and G. M. Schneider: Fluid Mixtures at High Pressures etc.* **80**(12): 1316-1321.

Deiters, U.K. and Pegg, I.L. 1989. Systematic Investigation of the Phase Behavior in Binary Fluid Mixtures. I. Calculations Based on the Redlich-Kwong Equation of State. *Journal of Chemical Physics* **90**(11): 6632-6641.

Delshad, M. and Pope, G.A. 1989. Comparison of the Three-Phase Oil Relative Permeability Models. *Transport in Porous Media* **4**(1): 59-83.

Dennis, Jr. J.E. and Schnabel, R.B. 1996. *Numerical Methods for Unconstrained Optimization and Nonlinear Equations*. SIAM, Philadelphia, Pennsylvania.

DeRuiter, R.A., Nash, L.J., and Singletary, M.S. 1994. Solubility and Displacement Behavior of a Viscous Crude with CO_2 and Hydrocarbon Gases. *SPE Reservoir Engineering* **9**(2): 101-106.

Dickson, J.L., Clingman, S., Dittaro, L.M., Jaafar, A.E., Yerian, J.A., and Perlau, D.L. 2011. Design Approach and Early Field Performance for a Solvent-Assisted SAGD Pilot at Cold Lake, Canada. Paper presented at the SPE Heavy Oil Conference and Exhibition, December12-14, Kuwait City, Kuwait.

Dindoruk, B. 1992. *Analytical Theory of Multiphase, Multicomponent Displacement in Porous Media*. PhD dissertation, Stanford University, Stanford, CA.

Dumore, J.M., Hagoort, J., and Risseeuw, A.S. 1984. An Analytical Model for One-Dimensional, Three-Component Condensing and Vaporizing Gas Drives. *SPE Journal* **24**(2): 169-179.

Economou, I.G., Heidman, J.L., Tsonopoulos, C., and Wilson, G.M. 1997. Mutual Solubilities of Hydrocarbons and Water: III. 1-Hexene, 1-Octene, C_{10}-C_{12} Hydrocarbons. *AIChE Journal* **43**(2): 535-546.

Egwuenu, A. M., Johns, R. T., and Li, Y. 2008. Improved Fluid Characterization for Miscible Gas Floods. *SPE Reservoir Evaluation and Engineering* **11** (4): 655–665.

Elsharkawy, A.M., Poettmann, F.H., and Christiansen, R.L. 1992. Measuring Minimum Miscibility Pressure: Slim-Tube or Rising-Bubble Method? Paper presented in SPE/DOE Enhanced Oil Recovery Symposium, April22-24, Tulsa, Oklahoma.

Enick, R., Holder, G.D., and Morsi, B.I. 1985. Critical and Three Phase Behavior in the Carbon Dioxide/Tridecane System. *Fluid Phase Equilibria* **22**(2): 209-224.

Fulco, G.J. 1999. January. Case History of Miscible Gas Flooding in the Powder River Basin North Buck Draw Unit. Paper presented in SPE Rocky Mountain Regional Meeting , May15-18, Gillette, Wyoming.

Galindo, A. and Blas, F.J. 2002. Theoretical Examination of the Global Fluid Phase Behavior and Critical Phenomena in Carbon Dioxide + n-Alkane Binary Mixtures. *Journal of Physical Chemistry B* **106**(17): 4343-4564.

Garcáa-Sánchez, F., Schwartzentruber, J., Ammar, M.N., and Renon, H. 1996. Modeling of Multiphase Liquid Equilibria for Multicomponent Mixtures. *Fluid Phase Equilibria* **121**(1-2): 207-225.

Gardner, J.W., Orr, Jr., F.M., and Patel, P.D. 1981. The Effect of Phase Behavior on CO_2-Flood Displacement Efficiency. *Journal of Petroleum Technology* **33**(11): 2067-2081.

Gautam, R. and Seider, W.D. 1979. Computation of Phase and Chemical Equilibrium. *AIChE Journal* **25**(6): 991-1007.

Gauter, K. 1999. *Fluid Multiphase Behavior in Ternary Systems of Near-Critical CO_2*. PhD dissertation, the Technical University of Berlin, Berlin, Germany.

Gauter, K., Heidemann, R.A., and Peters, C.J. 1999. Modeling of Fluid Multiphase Equilibria in Ternary Systems of Carbon Dioxide as the Near-Critical Solvent and Two Low-Volatile Solutes. *Fluid Phase Equilibria* **158-160**: 133-141.

Gernert, J., Jäger, A., and Span, R. 2014. Calculation of Phase Equilibria for Multi-Component Mixtures Using Highly Accurate Helmholtz Energy Equations of State, *Fluid Phase Equilibria* **375**: 209-218.

Gill, P.E. and Murray, W. 1974. Newton-Type Methods for Unconstrained and Linearly Constrained Optimization. *Mathematical Programming* **7**(3): 311-350.

Glandt, C.A. and Chapman, W.G. 1995. Effect of Water Dissolution on Oil Viscosity. *SPE Reservoir Engineering* **10**(1): 59-64.

Glaso, O. 1990. Miscible Displacement: Recovery Tests with Nitrogen. *SPE Reservoir Engineering* **5**(1): 61 - 68.

Godbole, S.P., Thele, K.J., and Reinbold, E.W. 1995. EOS Modeling and Experimental Observations of Three-Hydrocarbon-Phase Equilibria. *SPE Reservoir Engineering* **10**(2): 101-108.

Grabowski, J.W., Vinsome, P.K., Lin, R.C., Behie, G.A., and Rubin, B. 1979. A Fully Implicit General Purpose Finite-Difference Thermal Model for In Situ Combustion and Steam. Paper presented at the SPE Annual Technical Conference and Exhibition, September 23-26, Las Vegas, Nevada.

Gregorowicz, J. and de Loos, Th.W. 1996. Modeling of the Three Phase LLV Region for Ternary Hydrocarbon Mixtures with the Soave-Redlich-Kwong Equation of State. *Fluid Phase Equilibria* **118**(1): 121-132.

Griswold, J. and Kasch, J.E. 1942. Hydrocarbon-Water Solubilities at Elevated Temperatures and Pressures. *Industrial and Engineering Chemistry* **34**(7): 804-806.

Guler, B., Wang, P., Delshad, M., Pope, G.A., and Sepehrnoori, K. 2001. Three- and Four- Phase Flow Compositional Simulations of CO_2/NGL EOR. Paper presented at

Annual Technical Conference and Exhibition, September 30-October 3, New Orleans, Louisiana.

Gupta, A.K. 1990. *Steady State Simulation of Chemical Process*. PhD dissertation, University of Calgary, Calgary, Alberta.

Gupta, A.K., Bishnoi, P.R., and Kalogerakis, N. 1990. Simultaneous Multiphase Isothermal/Isenthalpic Flash and Stability Calculations for Reacting/Non-Reacting Systems. *Gas Separation and Purification* **4**: 215-222.

Gupta, S.C. and Gittins, S.D. 2006. Christina Lake Solvent Aided Process Pilot. *Journal of Canadian Petroleum Technology* **45**(9): 1-11.

Gupta, S.C., Gittins, S., and Picherack, P. 2005. Field Implementation of Solvent Aided Process. *Journal of Canadian Petroleum Technology* **44**(11): 8-13.

Han, G. and Rangaiah, G.P. 1998. A Method for Multiphase Equilibrium Calculations, *Computers and Chemical Engineering* **22**(7-8): 897-911.

Harding, S.T. and Floudas, C.A. 2000. Phase Stability with Cubic Equations of State: Global Optimization Approach. *AIChE Journal* **46**(7): 1422-1440.

Haugen, K.B. and Beckner, B. 2013. A Critical Comparison of Reduced and Conventional EOS Algorithms. *SPE Journal* **18**(02): 378-388.

Heidari, M., Nghiem, L.X., and Maini, B.B. 2014. Improved Isenthalpic Multiphase Flash Calculations for Thermal Compositional Simulators. Paper presented at the SPE Heavy Oil Conference-Canada, June 10-12, Calgary, Alberta.

Heidemann, R.A. and Michelsen, M.L. 1995. Instability of Successive Substitution. *Industrial and Engineering Chemistry Research* **34**(3): 958-966.

Heidman, J.L., Tsonopoulos, C., Brady, C.J., and Wilson, G.M. 1985. High-Temperature Mutual Solubilities of Hydrocarbons and Water. Part II: Ethylbenzene, Ethylcyclohexane, and n-Octane. *AIChE Journal* **31**(3): 376-384.

Helfferich, F.G. 1981. Theory of Multicomponent, Multiphase Displacement in Porous Media. *SPE Journal* **21**(1): 51-62.

Henderson, N., Sartori, J., and F. Sacco, W. 2014. Phase Stability Analysis Using a Polarization Technique and the Randomness of a Stochastic Method in an Unconstrained Optimization Framework. *Industrial and Engineering Chemistry Research* **53**(8): 3342-3352.

Henry, R.L. and Metcalfe, R.S. 1983. Multiple-Phase Generation During Carbon Dioxide Flooding. *SPE Journal* **23**(4): 595-601.

Higham, N.J. 2002. *Accuracy and Stability of Numerical Algorithms*, Second edition. SIAM, Philadelphia, Pennsylvania.

Holm, L.W. and Josendal, V.A. 1974. Mechanisms of Oil Displacement by Carbon Dioxide. *Journal of Petroleum Technology* **26**(12): 1427-1438.

Hornbrook, M.W., Dehghani, K., Qadeer, S., Ostermann R.D., and Ogbe, D.O. 1991. Effects of CO2 Addition to Steam on Recovery of West Sak Crude Oil. *SPE Reservoir Engineering* **6**(3): 278-286.

Horn, L.D.V. and Kobayashi, R. 1967. Vapor-Liquid Equilibria of Light Hydrocarbons at Low Temperatures and Elevated Pressures in Hydrocarbon Solvents. Methane-Propane-n-Heptane, Methane-Ethane-n-Heptane, and Methane-Propane-Toluene Systems. *Journal of Chemical and Engineering Data* **12**(3): 294-303.

Hoteit, H. and Firoozabadi, A. 2006. Compositional Modeling of Discrete-Fractured Media without Transfer Functions by the Discontinuous Galerkin and Mixed Methods. *SPE Journal* **11**(03): 341-352.

Hottovy, J.D., Luks, K.D., and Kohn, J.P. 1981. Three-Phase Liquid-Liquid-Vapor Equilibria Behavior of Certain Binary CO_2-n-Paraffin Systems. *Journal of Chemical and Engineering Data* **26**(3): 256-258.

Hua, J.Z., Brennecke, J.F., and Stadtherr, M.A. 1996. Reliable Prediction of Phase Stability Using an Interval Newton Method. *Fluid Phase Equilibria* **116**(1): 52-59.

Hua, J.Z., Brennecke, J.F., and Stadtherr, M.A. 1998a. Reliable Computation of Phase Stability Using Interval Analysis: Cubic Equation of State Models. *Computers and Chemical Engineering* **22**(9): 1207-1214.

Hua, J.Z., Brennecke, J.F., and Stadtherr, M.A. 1998b. Enhanced Interval Analysis for Phase Atability: Cubic Equation of State Models. *Industrial and Engineering Chemistry Research* **37**(4): 1519-1527.

Hudgins, D., Llave, F., and Chung, F. 1990. Nitrogen Miscible Displacement of Light Crude Oil: A Laboratory Study. *SPE Reservoir Engineering* **5**(1): 100 - 106.

Iranshahr, A., Voskov, D.V., and Tchelepi, H.A. 2010. Tie-Simplex Parameterization for EOS-Based Thermal Compositional Simulation. *SPE Journal* **15**(2): 545-556.

Ishimoto, K., Pope, G.A., and Sepehrnoori, K. 1987. An Equation of State Steam Simulator. *In Situ* **11**(1): 1-37.

Ivanov, B.B., Galushko, A.A., and Stateva, R.P. 2013. Phase Stability Analysis with Equations of State: A Fresh Look from a Different Perspective. *Industrial and Engineering Chemistry Research* **52**(32): 11208-11223.

Jacobson, H., 1972. Acid Gases and Their Contribution to Miscibility. *Journal of Canadian Petroleum Technology* **11**(2): 1-5.

Jarrell, P.M., Fox, C.E., Stein, M.H., and Webb, S.L. 2002. *Practical Aspects of CO_2 Flooding.* (Volume 22). Richardson, TX: Society of Petroleum Engineers.

Jerauld, G.R., 1997. General Three-Phase Relative Permeability Model for Prudhoe Bay. *SPE Reservoir Engineering* **12**(04): 255-263.

Jia, W. and Okuno, R. 2017. Modeling of the Interaction Between Asphaltene and Water for Multiphase Reservoir Fluids by Use of Cubic-Plus-Association Equation of State. Paper presented at the SPE Annual Technical Conference and Exhibition, October 9-11, San Antonio, Texas.

Johns, R.T. 1992. *Analytical Theory of Multicomponent Gas Drives with Two-Phase Mass Transfer*. PhD dissertation, Stanford University, Stanford, CA.

Johns, R.T., Dindoruk, B., and Orr, Jr., F.M. 1993. Analytical Theory of Combined Condensing/Vaporizing Gas Drives. *SPE Advanced Technology Series* **1**(2): 7-16.

Johns, R.T., Sah, P., and Solano, R. 2002. Effect of Dispersion on Local Displacement Efficiency for Multicomponent Enriched-Gas Floods above the Minimum Miscibility Enrichment. *SPE Reservoir Evaluation and Engineering* **5**(1): 4-10.

Kaul, P.K. 1992. *A New and Efficient Approach for Two Phase Equilibrium Prediction Using Cubic Equations of State*. MSc thesis, Mississippi State University, Mississippi State, Mississippi.

Khan, S.A. 1992. *An Expert System to Aid in Compositional Simulation of Miscible Gas Flooding*. PhD dissertation, the University of Texas at Austin, Austin, Texas.

Khan, S.A., Pope, G.A., and Sepehrnoori, K. 1992. Fluid Characterization of Three-Phase CO_2/Oil Mixtures. Paper presented at the SPE/DOE Enhanced Oil Recovery Symposium, April 22-24, Tulsa, Oklahoma.

Kumar, A. and Okuno, R. 2016. A New Algorithm for Multiphase-Fluid Characterization for Solvent Injection. *SPE Journal* **21**(05):1688-1704.

LaForce, T.C. 2012. Insight from Analytical Solutions for Improved Simulation of Miscible WAG Flooding in One Dimension. *Computational Geoscience* **16**: 1007-1020.

LaForce, T.C. and Johns, R.T. 2005a. Analytical Solutions for Surfactant-Enhanced Remediation of Nonaqueous Phase Liquids. *Water Resourced Research* **41**: 1-14.

LaForce, T.C. and Johns, R.T. 2005b. Composition Routes for Three-Phase Partially Miscible Flow in Ternary Systems. *SPE Journal* **10**(2): 161-174.

LaForce, T.C. and Orr, Jr., F.M. 2008. Development of Gas/Oil Miscibility in Water and Gas Injection. Paper presented at the SPE Annual Technical Conference and Exhibition, September 21-24, Denver, Colorado.

LaForce, T.C. and Orr, Jr., F.M. 2009. Four-Component Gas/Water/Oil Displacements in One Dimension: Part III. Development of Miscibility. *Transport in Porous Media* **79**: 225-247.

LaForce, T.C., Jessen, K., and Orr, Jr., F.M. 2008a. Four-Component Gas/Water/Oil Displacements in One Dimension: Part I. Structure of the Conservation Law. *Transport in Porous Media* **71**: 199-216.

LaForce, T.C., Jessen, K., and Orr, Jr., F.M. 2008b. Four-Component Gas/Water/Oil Displacements in One Dimension: Part II. Example Solutions. *Transport in Porous Media* **72**: 83-96.

Lake, L.W., Johns, R.T., Rossen, B., and Pope, G. 2014. *Fundamentals of Enhanced Oil Recovery*, Society of Petroleum Engineers.

Lantz, R.B. 1971. Quantitative Evaluation of Numerical Diffusion (Truncation Error). *SPE Journal* **11**(3): 315-320.

Larson, L.L., Silva, M.K., Taylor, M.A., and Orr Jr., F.M. 1989. Temperature Dependence of L1/L2/V Behavior in CO2/Hydrocarbon Systems. *SPE Reservoir Engineering* **4**(1): 105-114.

Li, D. Kumar, K., and Mohanty, K.K. 2003. Compositional Simulation of WAG Process for a Viscous Oil. Paper presented at Annual Technical Conference and Exhibition, 5-8 October, Denver, Colorado.

Li, L., Khorsandi, S., Johns, R.T., and Ahmadi, K. 2015. Multiple-Mixing-Cell Method for Three-Hydrocarbon-Phase Displacements. *SPE Journal* **20**(6): 1-339.

Li, Z., and Firoozabadi, A. 2012. General Strategy for Stability Testing and Phase-Split Calculation in Two and Three Phases. *SPE Journal* **17**(4): 1096-1107.

Litvak, M.L. 1994. New Procedure for Phase-Equilibrium Computations in Compositional Reservoir Simulators. *SPE Advanced Technology Series* **2**(2): 113-121.

Liu, K., Subramanian, G., Dratler, D.I., Lebel, J.P., and Yerian, J.A. 2009. A General Unstructured-Grid, Equation-of-State-Based, Fully Implicit Thermal Simulator for Complex Reservoir Processes. *SPE Journal* **14**(2): 355-361.

Llave, F.M., Luks, K.D. and Kohn, J.P. 1987. Three-Phase Liquid-Liquid-Vapor Equilibria in the Nitrogen-Methane-Ethane and Nitrogen-Methane-Propane Systems. *Journal of Chemical and Engineering Data* **32**(1): 14-17.

Lohrenz, J., Bray, B.C., and Clark, C.R. 1964. Calculating Viscosities of Reservoir Fluids from Their Compositions. *Journal of Petroleum Technology* **16**(10): 1171-1176.

Lucia, A., Bonk, B.M., Waterman, R.R., and Roy, A. 2012. A Multi-Scale Framework for Multiphase Equilibrium Flash. *Computers and Chemical Engineering* **36**: 79-98.

Lucia, A. and Liu, D. 1998. An Acceleration Method for Dogleg Methods in Simple Singular Regions. *Industrial and Engineering Chemistry Research* **37**(4): 1358-1363.

Lucia, A. and Yang F. 2003. Multivariable Terrain Methods. *AIChE Journal* **49**(10): 2553-2563.

Lucia, A. and Macchietto, S. 1983. New Approach to Approximation of Quantities Involving Physical Properties Derivatives in Equation-Oriented Process Design. *AIChE Journal* **29**(5): 705-712.

Lucia, A., Miller, D.C., and Kumar, A. 1985. Thermodynamically Consistent Quasi-Newton Formulae. *AIChE Journal* **31**(8): 1381-1388.

Lucia, A., Padmanabhan, L., and Venkataraman, S. 2000. Multiphase Equilibrium Flash Calculations. *Computers and Chemical Engineering* **24**(12): 2557-2569.

Luo, S. and Barrufet, M.A. 2005. Reservoir Simulation Study of Water-in-Oil Solubility Effect on Oil Recovery in Steam Injection Process. *SPE Reservoir Evaluation and Engineering* **8**(6): 528-533.

McDonald, C.M. and Floudas, C.A. 1997. GLOPEQ: A New Computational Tool for the Phase and Chemical Equilibrium Problem. *Computers and Chemical Engineering* **21**(1): 1-23.

Malik, Q.M. and Islam, M.R. 2000. CO_2 Injection in the Weyburn Field of Canada: Optimization of Enhanced Oil Recovery and Greenhouse Gas Storage with Horizontal Wells. Paper presented at the SPE/DOE Improved Oil Recovery Symposium, April 3-5, Tulsa, Oklahoma.

Mallison, B.T., Gerritsen, M.G., Jessen, K., and Orr, Jr., F.M. 2005. High-Order Upwind Schemes for Two-Phase, Multicomponent Flow. *SPE Journal* **10**(3): 297-311.

McGarry, J. 1983. Correlation and Prediction of the Vapor Pressures of Pure Liquids over Large Pressure Ranges. *Industrial and Engineering Chemistry Process Design and Development* **22**(2): 313-322.

McGuire, P.L., Spence, A.P., and Redman, R.S. 2001. Performance Evaluation of a Mature Miscible Gasflood at Prudhoe Bay. *SPE Reservoir Evaluation and Engineering* **4**(4): 318-326.

Mehra, R.K., Heidemann, R.A., and Aziz, K. 1982. Computation of Multiphase Equilibrium for Compositional Simulation. *SPE Journal* **22**(1): 61-68.

Mehra, R.K., Heidemann, R.A., and Aziz, K. 1983. An Accelerated Successive Substitution Algorithm. *Canadian Journal of Chemical Engineering* **61**(4): 590-596.

Menzie, D.E. and Nielsen, R.F. 1963. A Study of the Vaporization of Crude Oil by Carbon Dioxide Repressuring. *Journal of Petroleum Technology* **15**(11): 1247-1252.

Metcalfe, R.S. and Yarborough, L. 1979. The Effect of Phase Equilibria on the CO_2 Displacement Mechanism. *SPE Journal* **19**(4): 242-252.

Michelsen, M.L. 1982a. the Isothermal Flash Problem. Part I. Stability. *Fluid Phase Equilibria* **9**(1): 1-19.

Michelsen, M.L. 1982b. The Isothermal Flash Problem. Part II. Phase-Split Calculation. *Fluid Phase Equilibria* **9**(1): 21-40.

Michelsen, M.L. 1987. Multiphase Isenthalpic and Isentropic Flash Algorithms. *Fluid Phase Equilibria* **33**(1-2): 13-27.

Michelsen, M.L. 1993. Phase Equilibrium Calculations. What is Easy and What is Difficult? *Computers and Chemical Engineering* **17**(5-6): 431-439.

Michelsen, M.L. 1998. Speeding Up the Two-Phase PT-Flash, with Applications for Calculation of Miscible Displacement. *Fluid Phase Equilibria* **143**(1-2): 1-12.

Michelsen, M.L. 1999. State Function Based Flash Specifications. *Fluid Phase Equilibria* **158-160**: 617-626.

Michelsen, M.L. and Mollerup, J.M. 2004. *Thermodynamic Models: Fundamentals and Computational Aspects*. Tie-Line Publications. Holte, Denmark.

Mizenko, G.J. 1992. North Cross (Devonian) Unit CO_2 Flood: Status Report. Paper SPE 24210 presented at the SPE/DOE Enhanced Oil Recovery Symposium, April 22-24, Tulsa, Oklahoma.

Mohanty, K.K., Masino Jr., W.H., Ma, T.D., and Nash, L.J. 1995. Role of Three-Hydrocarbon-Phase Flow in a Gas-Displacement Process. *SPE Reservoir Engineering* **10**(3): 214-221.

Mohebbinia, S. 2013. *Advanced Equation of State Modeling for Compositional Simulation of Gas Floods*. PhD dissertation, the University of Texas at Austin, Austin, Texas.

Mushrif, S.H. 2004. Determining Equation of State Binary Interaction Parameters Using K- and L-Points. Master thesis, the University of Saskatchewan, Saskatoon.

Nagarajan, N.R., Cullick, A.S., and Griewank, A. 1991. New Strategy for Phase Equilibrium and Critical Point Calculations by Thermodynamic Energy Analysis. Part I. Stability analysis and flash. *Fluid phase equilibria* **62**(3): 191-210

Negahban, S. and Kremesec Jr, V.J. 1992. Development and Validation of Equation-of-State Fluid Descriptions for CO_2/Reservoir-Oil Systems. *SPE Reservoir Engineering* **7**(3): 363-368.

Néron, A., Lantagne, G., and Marcos, B. 2012. Computation of Complex and Constrained Equilibria by Minimization of the Gibbs Free Energy, *Chemical Engineering Science* **82**: 260-271.

Neshat, S.S. 2016. *Compositional Three-Phase Relative Permeability and Capillary Pressure Models Using Gibbs Free Energy*. MSc thesis. The University of Texas at Austin, Austin, Texas.

Nghiem, L.X. 1983. A New Approach to Quasi-Newton Methods with Application to Compositional Modeling. Paper presented at the SPE Reservoir Simulation Symposium, November 15-18, San Francisco, California.

Nghiem, L.X., Aziz, K., and Li, Y.K. 1983. A Robust Iterative Method for Flash Calculations Using the Soave-Redlich-Kwong or the Peng-Robinson Equation of State. *SPE Journal* **23**(3): 521-530.

Nghiem, L.X. and Heidemann, R.A. 1982. General Acceleration Procedure for Multiphase Flash Calculation with Application to Oil-Gas-Water Systems. Paper presented at the 2nd European Symposium on Enhanced Oil Recovery, November 8-10, Paris, France.

Nghiem, L. X. and Li, Y.K. 1984. Computation of Multiphase Equilibrium Phenomena with an Equation of State. *Fluid Phase Equilibria* **17**(1): 77-95.

Nghiem, L.X. and Li, Y.K. 1986. Effect of Phase Behavior on CO_2 Displacement Efficiency at Low Temperatures: Model Studies with an Equation of State. *SPE Reservoir Engineering* **1**(4): 414-422.

Nichita, D.V. and Gomez, S. 2009. Efficient Location of Multiple Global Minima for the Phase Stability Problem. *Chemical Engineering Journal* **152**(1): 251-263.

Nichita, D.V., Gomez, S., and Luna, E. 2002. Multiphase Equilibria Calculation by Direct Minimization of Gibbs Free Energy with a Global Optimization Method. *Computers and Chemical Engineering* **26**(12): 1703-1724.

Nojabaei, B., Johns, R.T., and Chu, L. 2013. Effect of Capillary Pressure on Phase Behavior in Tight Rocks and Shales. *SPE Reservoir Evaluation and Engineering* **16**(03): 281-289.

Oak, M.J. 1991. Three-Phase Relative Permeability of Intermediate-Wet Berea Sandstone. Paper presented at the SPE Annual Technical Conference and Exhibition, 6-9 October, Dallas, Texas.

Ohanomah, M.O. and Thompson, D.W. 1984. Computation of Multicomponent Phase Equilibria-Part I. Vapor-Liquid Equilibria. *Computers and Chemical Engineering* **8**(3-4): 147-156.

Okuno, R. 2009. *Modeling of Multiphase Behavior for Gas Flooding Simulation*. PhD dissertation, the University of Texas at Austin, Austin, Texas.

Okuno, R., Johns, R.T., and Sepehrnoori, K. 2010. A New Algorithm for Rachford-Rice for Multiphase Compositional Simulation. *SPE Journal* **15**(2): 313-325.

Okuno, R., Johns, R.T., and Sepehrnoori, K. 2011. Mechanisms for High Displacement Efficiency of Low-Temperature CO_2 Floods. *SPE Journal* **16**(4): 751-767.

Okuno, R. and Xu, Z. 2014a. Efficient Displacement of Heavy Oil by Use of Three Hydrocarbon Phases. *SPE Journal* **19**(5): 956-973.

Okuno, R. and Xu, Z. 2014b. Mass Transfer on Multiphase Transitions in Low-Temperature Carbon Dioxide Floods. *SPE Journal* **19**(6): 1005-1023.

Okuyiga, M.O. 1992. Equation of State Characterization and Miscibility Development in a Multiple Phase Hydrocarbon System. Paper presented at Annual Technical Conference and Exhibition, October 4-7, Washington, D.C., USA.

Orr, Jr., F.M. 2007. *Theory of Gas Injection Processes*. Tie-Line Publications, Holte, Denmark.

Orr, Jr., F.M. and Jessen, C.M. 1984. Interpretation of Pressure-Composition Phase Diagrams for CO_2/Crude-Oil Systems. *SPE Journal* **24**(5): 485-497.

Orr, Jr., F.M., Johns, R.T., and Dindoruk, B. 1993. Development of Miscibility in Four-Component CO_2 Floods. *SPE Reservoir Engineering* **8**(2)135-142.

Orr Jr, F.M., Silva, M.K., and Lien, C.L. 1983. Equilibrium Phase Compositions of CO_2/crude Oil Mixtures-Part 2: Comparison of Continuous Multiple-Contact and Slim-Tube Displacement Tests. *SPE Journal* **23**(02): 281-291.

Orr, Jr., F.M., Silva, M.K., Lien, C.L., and Pelletier, M.T. 1982. Laboratory Experiments to Evaluate Field Prospects for CO_2 Flooding. *Journal of Petroleum Technology* **34**(4):888-898.

Pan, H. and Firoozabadi, A. 1998. Complex Multiphase Equilibrium Calculations by Direct Minimization of Gibbs Free Energy by Use of Simulated Annealing. *SPE Reservoir Engineering* **1**(1): 36-41.

Pan, H. and Firoozabadi, A. 2003. Fast and Robust Algorithm for Compositional Modeling: Part II-Two-Phase Flash Computations. *SPE Journal* **8**(4): 380-391.

Pan, H. and Tchelepi, H.A. 2011. Compositional Flow Simulation Using Reduced-Variables and Stability-Analysis Bypassing. Paper presented at the SPE Reservoir Simulation Symposium. February 21-23, Woodlands, Texas.

Peng, D.-Y. and Robinson, D.B. 1978. The Characterization of the Heptanes and Heavier Fractions for the GPA Peng-Robinson Programs. *Research report (Gas Processors Association),* RR-28.

Perschke, D.R. 1988. *Equation of State Phase Behavior Modeling for Compositional Simulation*. PhD dissertation, the University of Texas at Austin, Austin, Texas.

Perschke, D.R., Chang, Y.-B., Pope, G.A., and Sepehrnoori, K. 1989. Comparison of Phase Behavior Algorithms for an Equation-of-State Compositional Simulator. Paper SPE-19443-MS available from SPE.

Perschke, D.R., Pope, G.A., and Sepehrnoori, K. 1989. Phase Identification During Compositional Simulation. Paper SPE-19442-MS available from SPE.

Peters, C.J. 1994. Multiphase Equilibria in Near-Critical Solvents. in: E. Kiran and J.M.H. Levelt Sengers *Supercritical Fluids*, 117-145. Kluwer Academic Publishers.

Peters, C.J., De Roo, J.L., and de Swaan Arons, J. 1993. Phase Equilibria in Binary Mixtures of Propane and Hexacontane. *Fluid Phase Equilibria* **85**: 301-312.

Polishuk, I., Wisniak, J., and Segura, H. 2004. Estimation of Liquid-Liquid-Vapor Equilibria in Binary Mixtures of n-Alkanes. *Industrial and Engineering Chemistry Research* **43**(18): 5957-5964.

Rachford, Jr., H.H. and Rice, J.D. 1952. Procedure for Use of Electronic Digital Computers in Calculating Flash Vaporization Hydrocarbon Equilibrium. *Petroleum Transactions AIME* **195**: 327-328.

Rao, D.N. 1997. A New Technique of Vanishing Interfacial Tension for Miscibility Determination. *Fluid Phase Equilibria* **139**(1-2):311-324.

Reid, T. 1994. Study of Hydrocarbon Miscible Solvent Slug Injection Process for Improved Recovery of Heavy Oil from Schrader Bluff Pool, Milne Point Unit, Alaska. Annual Report for DE-FG22-93BC14864 submitted to U.S. Department of Energy.

Rezaveisi, M., Sepehrnoori, K., and Johns, R.T. 2014. Tie-Simplex-Based Phase-Behavior Modeling in an IMPEC Reservoir Simulator. *SPE Journal* **19**(2): 327-339.

Rodrigues, A.B. and Kohn, J.P. 1967. Three Phase Equilibria in the Binary Systems Ethane-n-Docosane and Ethane-n-Octacosane. *Journal of Chemical and Engineering Data* **12**(2): 191-193.

Roper, M. 1989. *An Experimental Study of CO_2/West-Sak-Crude-Oil Phase Behavior*. Master thesis, University of Alaska Fairbanks, Alaska.

Rowlinson, J.S. and Freeman, P.I. 1961. Lower Critical Solution Points in Hydrocarbon Mixtures. *Pure and Applied Chemistry* **2**(1-2): 329-334.

Rubin, B. and Buchanan, W.L. 1985. A General Purpose Thermal Model. *SPE Journal* **25**(2): 202-214.

Saber, N. and Shaw, J.M. 2008. Rapid and Robust Phase Behaviour Stability Analysis Using Global Optimization. *Fluid Phase Equilibria* **264**(1): 137-146.

Scott, R.L. and van Konynenburg, P.H. 1970. van der Waals and Related Models for Hydrocarbon Mixtures. *Discussions of the Faraday Society* **49**: 87-97.

Sharma, A.K., Patil, S.L., Kamath, V.A., and Sharma, G.D. 1989. Miscible Displacement of Heavy West Sak Crude by Solvents in Slim Tube. Paper presented at the SPE California Regional Meeting, April 5-7, Bakersfield, California.

Shelton, J.L. and Yarborough, L. 1977. Multiple Phase Behavior in Porous Media during CO2 or Rich-Gas Flooding. *Journal of Petroleum Technology* **29**(9):1171-1178.

Sheng, J. 2013. *Enhanced Oil Recovery Field Case Studies* (1st Edition). Gulf Professional Publishing.

Shu, W.R. and Hartman, K.J. 1988. Effect of Solvent on Steam Recovery of Heavy Oil. *SPE Reservoir Engineering* **3**(2): 457-465.

Siripatrachai, N., Ertekin, T., and Johns, R.T. 2017. Compositional Simulation of Hydraulically Fractured Tight Formation Considering the Effect of Capillary Pressure on Phase Behavior. *SPE Journal* **22**(4): 1046-1063.

Siu, A.L., Rozon, B.J., Li, Y.K., Nghiem, L.X., Acteson, W.H., and McCormack, M.E. 1991. A Fully Implicit Thermal Wellbore Model for Multicomponent Fluid Flows. *SPE Reservoir Engineering* **6**(3): 302-310.

Sofyan, Y., Ghajar, A.J., and Gasem, K.A.M. 2003. Multiphase Equilibrium Calculations Using Gibbs Minimization Techniques. *Industrial and Engineering Chemistry Research* **42**(16): 3786-3801.

Solano, R., Johns, R.T., and Lake, L.W. 2001. Impact of Reservoir Mixing on Recovery in Enriched-Gas Drives Above the Minimum Miscibility Enrichment. *SPE Reservoir Evaluation and Engineering* **4**(5): 358-365.

Stalkup, F.I. 1987. Displacement Behavior of the Condensing/Vaporizing Gas Drive Process, Paper presented at the SPE Annual Technical Conference and Exhibition, September 27–30, Dallas, TX.

Stalkup, F. 1998. Predicting the Effect of Continued Gas Enrichment above the MME on Oil Recovery in Enriched Hydrocarbon Gas Floods. Paper presented at the SPE Annual Technical Conference and Exhibition, September 27-30, New Orleans, Louisiana.

Stein, M.H., Frey, D.D., Walker, R.D., and Pariani, G.J. 1992. Slaughter Estate Unit CO_2 Flood: Comparison Between Pilot and Field-Scale Performance. *Journal of Petroleum Technology* **44**(9): 1026-1032.

Stone, H.L. 1970. Probability Model for Estimating Three-Phase Relative Permeability. *Journal of Petroleum Technology* **22**(02): 214-218.

Stone, H.L. 1973. Estimation of Three-Phase Relative Permeability and Residual Oil Data. *Journal of Petroleum Technology* **12**(4).

Sun, A.C. and Seider, W.D. 1995. Homotopy-Continuation Method for Stability Analysis in the Global Minimization of the Gibbs Free Energy. *Fluid Phase Equilibria* **103**(2): 213-249.

Tanner, C.S., Baxley, P.T., Crump III, J.G., and Miller, W.C. 1992. Production Performance of the Wasson Denver Unit CO_2 Flood. Paper presented at the SPE/DOE Enhanced Oil Recovery Symposium, April 22-24, Tulsa, Oklahoma.

Tchelepi, H.A. and Orr, Jr., F.M. 1994. Interaction of Viscous Fingering, Permeability Heterogeneity and Gravity Segregation in Three Dimensions. *SPE Reservoir Engineering* **9**(4): 266-271.

Teh, Y.S. and Rangaiah, G.P. 2002. A Study of Equation-Solving and Gibbs Free Energy Minimization Methods for Phase Equilibrium Calculations. *Chemical Engineering Research and Design* **80**(7): 745-759.

Tessier, S.R., Brennecke, J.F., and Stadtherr, M.A. 2000. Reliable Phase Stability Analysis for Excess Gibbs Energy Models. *Chemical Engineering Science* **55**(10): 1785-1796.

Trangenstein, J.A. 1985. Minimization of Gibbs Free Energy in Compositional Reservoir Simulation. Paper presented at the SPE Reservoir Simulation Symposium, February 10-13, Dallas, Texas.

Trangenstein, J.A. 1987. Customized Minimization Techniques for Phase Equilibrium Computations in Reservoir Simulation. *Chemical Engineering Science* **42**(12): 2847-2863.

Trangenstein, J.A. and Bell, J.B. 1989. Mathematical Structure of Compositional Reservoir Simulation. *SIAM Journal on Scientific and Statistical Computing* **10**(5): 817-845.

Tsonopoulos, C. 1999. Thermodynamic Analysis of the Mutual Solubilities of Normal Alkanes and Water. *Fluid Phase Equilibria* **156**(1): 21-33.

Tsonopoulos, C. and Wilson, G.M. 1983. High-Temperature Mutual Solubilities of Hydrocarbons and Water. Part I: Benzene, Cyclohexane and n-Hexane. *AIChE Journal* **29**(6): 990-999.

Turek, E.A., Metcalfe, R.S., and Fishback, R.E. 1988. Phase Behavior of Several CO_2/West Texas-Reservoir-Oil Systems. *SPE Reservoir Engineering* **3**(2): 505-516.

Uzunov, D.I. 1993. *Introduction to the Theory of Critical Phenomena*. World Scientific Publishing, Singapore.

van Konynenburg, P.H. 1968. *Critical Lines and Phase Equilibria in Binary Mixtures*. PhD dissertation, University of California, Los Angeles, California.

Van Odyck, D.E.A., Bell, J.B., Monmont, F., and Nikiforakis, N. 2009. The Mathematical Structure of Multiphase Thermal Models of Flow in Porous Media. *Proceedings of the Royal Society A: Mathematical, Physical and Engineering Science* **465**(2102): 523-549.

Varavei, A. and Sepehrnoori, K. 2009. An EOS-Based Compositional Thermal Reservoir Simulator. Paper presented at the SPE Reservoir Simulation Symposium, February 2-4, The Woodlands, Texas.

Varotsis, N., Stewart, G., Todd, A.C., and Clancy, M. 1986. Phase Behavior of Systems Comprising North Sea Reservoir Fluids and Injection Gases. *Journal of Petroleum Technology* **38**(12): 1221-1233.

Venkataraman, S. and Lucia, A. 1986. Exploiting the Gibbs-Duhem Equation in Separation Calculations. *AIChE Journal* **32**(7): 1057-1066.

Venkataraman, S. and Lucia, A. 1987. Avoiding Variable-Scaling Problems Using the Gibbs-Helmholtz Equation. *Computers and Chemical Engineering* **11**(1): 73-76.

Venkatramani, A. and Okuno, R. 2014. Modeling of Multiphase Behavior for Water/n-Alkane Mixtures by Use of the Peng-Robinson EOS, Paper presented at the SPE Heavy Oil Conference-Canada, June 10-12, Calgary, Alberta.

Venkatramani, A.V. 2014. *Modeling of Water-Containing Reservoir Oil for Steam Injection Simulation*. MSc thesis. the University of Alberta, Alberta.

Wagner, W. 1973. New Vapour Pressure Measurements for Argon and Nitrogen and a New Method for Establishing Rational Vapour Pressure Equations. *Cryogenics* **13**(8): 470-482.

Wagner, J.R., McCaffrey, D.S., and Kohn, J.P. 1968. Partial Miscibility Phenomena in the Ternary System Ethane-n-Hexadecane-n-Eicosane. *Journal of Chemical and Engineering Data* **13**(1): 22-24.

Walsh, B.W. and Orr Jr., F.M., 1990. Prediction of Miscible Flood Performance. The Effect of Dispersion on Composition Paths in Ternary Systems. *In Situ* **14**(1): 19-47.

Wang, P. and Stenby E.H. 1994. Non-Iterative Flash Calculation Algorithm in Compositional Reservoir Simulation. *Fluid Phase Equilibria* **94**: 93-108.

Wang, P., and Barker, J.W. 1995. Comparison of Flash Calculations in Compositional Reservoir Simulation. Paper presented at the SPE Annual Technical Conference and Exhibition, October 22-25, Dallas, Texas.

Wang, Y., Lin, C.-Y., Bidinger, C., Muralidharan, V., and Lee, S.-T. 2003. Compositional Modeling of Gas Injection with Three Hydrocarbon Phases for Schrader Bluff EOR. Paper presented at the SPE Annual Technical Conference and Exhibition, 5-8 October 2003, Denver, Colorado.

Whitson, C.H. and Michelsen, M.L. 1989. The Negative Flash. *Fluid Phase Equilibria* **53**: 51-71.

Winzinger, R., Brink, J.L, Patel, K.S., Davenport, C.B., Patel, Y.R., and Thakur, G.C. 1991. Design of a Major CO_2 Flood, North Ward Estes Field, Ward County, Texas. *SPE Reservoir Engineering* **6**(1): 11-16.

Wilson, G. 1969. A Modified Redlich-Kwong Equation of State, Application to General Physical Data Calculations. Paper presented at AIChE National Meeting, May 4-7, Cleveland, Ohio.

Xu, G., Brennecke, J.F., and Stadtherr, M.A. 2002. Reliable Computation of Phase Stability and Equilibrium from the SAFT Equation of State. *Industrial and Engineering Chemistry Research* **41**(5): 938-952.

Xu, G., Haynes, W.D., and Stadtherr, M.A. 2005. Reliable Phase Stability Analysis for Asymmetric Models. *Fluid Phase Equilibria* **235**(2): 152-165.

Xu, G., Scurto, A.M., Castier, M., Brennecke, J.F., and Stadtherr, M.A. 2000. Reliable Computation of High-Pressure Solid-Fluid Equilibrium. *Industrial and Engineering Chemistry Research* **39**(6): 1624-1636.

Xu, Z. and Okuno, R. 2015. Numerical Simulation of Three-Hydrocarbon-Phase Flow with Robust Phase Identification. Paper presented at SPE Reservoir Simulation Symposium, February 23-25, Houston, Texas, USA.

Yang, Q. 2006. *Automatic Development of Global Phase Diagrams for Binary Systems in Pressure-Temperature Space*. Master thesis, the University of Saskatchewan, Saskatoon.

Yellig, W.F. and Metcalfe, R.S. 1980. Determination and Prediction of CO_2 Minimum Miscibility Pressures. *Journal of Petroleum Technology* **32**(1): 160-168.

Yuan, H. and Johns, R. 2005. Simplified Method for Calculation of Minimum Miscibility Pressure or Enrichment. *SPE Journal* **10**(4): 416-425.

Yuan, C. and Pope, G. 2012. A New Method to Model Relative Permeability in Compositional Simulators to Avoid Discontinuous Changes Caused by Phase-Identification Problems. *SPE Journal* **17**(04):1221-1230.

Zaydullin, R., Voskov, D., and Tchelepi, H.A. 2012. Nonlinear Formulation Based on an Equation-of-State Free Method for Compositional Flow Simulation. *SPE Journal* **18**(2): 264-273.

Zaydullin, R., Voskov, D.V., James, S.C., Henley, H., and Lucia, A. 2014. Fully Compositional and Thermal Reservoir Simulation. *Computers and Chemical Engineering* **63**: 51-65.

Zick, A.A. 1986. A Combined Condensing/Vaporizing Mechanism in the Displacement of Oil by Enriched Gases, Paper presented at SPE Annual Technical Conference and Exhibition, October 5-8, New Orleans, LA.

Zhou, D. and Orr, Jr., F.M. 1998. An Analysis of Rising Bubble Experiments to Determine Minimum Miscibility Pressures. *SPE Journal* **3**(1): 19-25.

Zhu, D. and Okuno, R. 2014a. A Robust Algorithm for Isenthalpic Flash of Narrow-Boiling Fluids, *Fluid Phase Equilibria* **379**: 26-51.

Zhu, D. and Okuno, R. 2014b. A Robust Algorithm for Multiphase Isenthalpic Flash. Paper presented at SPE Heavy Oil Conference-Canada, June 10-12, Calgary, Alberta.

Zhu, D. and Okuno, R. 2015a. Analysis of Narrow-Boiling Behavior for Thermal Compositional Simulation. Paper presented at the SPE Reservoir Simulation Symposium, February 23-25, Houston, Texas.

Zhu, D. and Okuno, R. 2015b. Robust Isenthalpic Flash for Multiphase Water/Hydrocarbon Mixtures. *SPE Journal* **20**(6): 1350-1365.

Zhu, D. and Okuno, R. 2016. Multiphase Isenthalpic Flash Integrated with Stability Analysis, *Fluid Phase Equilibria* **423**: 203-219.

Zhu, D. Eghbali, S., Shekhar, C., and Okuno, R. 2017. A Unified Algorithm for Phase-Stability/Split Calculation for Multiphase PT Flash. SPE-175060-PA. Accepted for publication on SPE Journal on July 13th, 2017.

VITA

Di Zhu was born in Hubei province, China on June 21st, 1987, the daughter of Jianjun Zhu and Zhangfeng Sun. Di Zhu attended Jianghan Oil Field High School, Hubei, China. In 2005, she entered the Yangtze University, Hubei, China, where she received the degree of Bachelor of Engineering in Prospecting Techniques and Engineering in 2009. She then studied at the China University of Petroleum (East China) and obtained the degree of Master of Engineering in Geodetection and Information Technology in 2012. In September 2012, she entered the graduate school in the School of Mining and Petroleum Engineering at the University of Alberta to study for her PhD degree. Her PhD program at the University of Alberta was transferred to the Hildebrand Department of Petroleum and Geosystems Engineering at the University of Texas at Austin in January 2016.

E-mail address: dizhu@utexas.edu

This dissertation was typed by the author.